2.

Characterizing the Physical Oceanography of Coastal Waters Off Rhode Island, Part 1: Literature Review, Available Observations, and A Representative Model Simulation

Prepared for the Rhode Island Ocean Special Area Management Plan 2010

By

Daniel L. Codiga and David S. Ullman

University of Rhode Island, March 24, 2010

Executive Summary

In support of the Rhode Island Ocean Special Area Management Plan development process, the physical oceanography of coastal waters off Rhode Island is reviewed and summarized. The OSAMP area includes central and eastern Block Island Sound (BIS), all of Rhode Island Sound (RIS) except state waters along its northern and eastern boundaries, and an area of the continental shelf extending about 25 km offshore southward from each. A literature review, updated analyses of key observations, and results of a hydrodynamic simulation are used to provide an updated, integrated view of the physical oceanography of the system. The focus is on the geographic and vertical spatial structure, and seasonal evolution, of hydrographic (temperature, salinity, and density) and circulation (seasonal-mean and weather-band) features, and on characterizing tidal variations. Conditions are shaped by a complex interplay among wind-driven variability, tidal processes, and density gradients that arise from combined effects of interaction with adjacent estuaries, solar heating, and heat flux through the air-sea interface. BIS is mostly estuarine in character, with the lowest salinities, the strongest tidal currents, relatively constant density stratification year-round dominantly due to salinity, and strong and persistent seasonal-mean currents including bidirectional exchange flow at each of its three openings and a prominent estuarine outflow bounded by a front on the shelf to the south. In RIS and the offshore area, the seasonal cycle is more pronounced: in winter and fall the stratification is minimal and circulation is a weak upwelling pattern directed offshore at shallow depths and onshore near the seafloor; in spring and summer strong stratification develops due to an important temperature contribution, and a system of more distinct currents occurs. These include the southern New England shelf flow westward along the offshore area, which bifurcates in the east where a portion moves northward as the RIS Current, a narrow flow that proceeds counterclockwise around the perimeter of RIS likely in association with a tidal mixing front. In southwestern RIS the southward RIS Current strengthens, in association with sharpened density gradients of the outflow front, then merges south of Block Island with the estuarine outflow and joins the southern New England shelf flow to leave the area westward. Tidal currents are stronger than or comparable to these seasonal-mean flow patterns, as are weather-band current variations driven by the wind. The baseline knowledge of physical oceanography presented here forms a component of the ecological characterization of the area needed to support assessments of potential impacts of policy decisions regarding development and protection of ocean-based resources.

Table of Contents

List of Figures

List of Tables

List of Appendices

Abstract

An integrated view has been developed for the physical oceanography of coastal waters off Rhode Island, including central and eastern Block Island Sound (BIS), Rhode Island Sound (RIS), and an offshore area extending about 25 km to the south from them. Results are based on a comprehensive literature review of observational and modeling studies; updated observational analyses of (i) satellite sea surface temperatures, (ii) a hydrographic climatology constructed from archived conductivity-temperature-depth (CTD) casts, and (iii) HF radar surface currents; and output from a realistically configured and forced data-assimilative hydrodynamic model spanning a larger regional domain. Emphasis is on the geographic and vertical spatial structure, and seasonal evolution, of hydrographic (temperature, salinity, and density) and circulation (seasonal-mean and weather-band) features, and on characterizing tidal variations. The seasonal cycle in temperatures spans from about 3 ^{o}C to about 21 ^{o}C, as shaped mainly by heat fluxes across the air-sea interface and solar radiative heating, and hence is relatively uniform geographically except for a tendency for shallow inshore waters to be up to a few degrees colder due to enhanced tidal mixing there. In deeper areas surface temperatures exceed deep temperatures by about 5-6 ^{o}C in spring and up to 10-12 ^{o}C in summer, but only by about 1 ^{o}C or less in fall, and in winter the deep water can be warmer by up to a degree due to surface cooling. Salinity variations reflect the influence of interactions with surrounding estuarine systems, and range from about 31 to 33 PSU with the freshest water in and near BIS due to strong influence of Long Island Sound (LIS) exchange flow, and surface values persistently about 0.1 to 0.9 PSS fresher than at depth. Density stratification has pronounced seasonality in deeper areas, with a pycnocline in winter and fall that is about 30-40 m deep and weak (surface to seafloor difference $\Delta\sigma_t$ of about 0.1 kg m^{-3}; peak buoyancy frequency N^2 about 2-3x10^{-4} s^{-2}) due to surface cooling and strong winds, then about 10-20 m deep and stronger in spring ($\Delta\sigma_t$ about 1 kg m^{-3}; peak N^2 about 5-6 x10^{-4} s^{-2}) and summer ($\Delta\sigma_t$ about 2-2.5 kg m^{-3}; peak N^2 about 10-12 s^{-2}), when the temperature influence dominates. Stratification is strongest in BIS during the winter, due to LIS exchange flow, and weakest there in summer due to strong tidal currents. BIS has relatively strong (5-15 cm s^{-1}) seasonal-mean currents including bidirectional exchange flow at each of its three openings, and a prominent geostrophic estuarine outflow bounded by a hydrographic front that spans the water column on the shelf to the south. In RIS and the offshore area, seasonal-mean currents undergo a stronger seasonal cycle: in winter and fall there is a weak (~1-2 cm s^{-1}) upwelling pattern, and in spring and summer a system of more distinct currents. These include

the southern New England shelf flow (up to 10 cm s^{-1}) westward along the offshore area, which bifurcates in the east where a portion moves northward as the RIS Current, a narrow flow moving counterclockwise around the perimeter of the stratified interior of RIS at about 5 cm s^{-1} likely in association with geostrophic adjustment of the horizontal density gradient due to a tidal mixing front. In southwestern RIS the southward RIS Current strengthens to about 15-20 cm s^{-1}, in association with sharpened warm-season inshore-offshore density gradients, then merges south of Block Island with the estuarine outflow and joins the southern New England shelf flow to leave the area westward. The strengths of these seasonal-mean flow patterns are, at most, comparable to tidal and weather-band current fluctuations and generally much weaker than them. Tidal currents are dominantly semi-diurnal and sharply enhanced (up to 100 cm s^{-1}) in and near BIS due to the resonant response of LIS. Weather-band current variations are driven predominantly by the wind, decay modestly with depth except in summer when they are isolated in the upper layer by the strong pycnocline, and peak in winter at about 20-30 cm s^{-1} when they are dominantly parallel to the nearly east-west orientation of the larger regional coastline.

1 Purpose and Scope

The purpose of this report is to summarize the current state of understanding of the physical oceanography of coastal waters off Rhode Island. The region of interest is the Rhode Island Ocean Special Area Management Plan (OSAMP) domain (Figure 1), which can be broken in to three areas: (a) approximately the eastern half of Block Island Sound (BIS), (b) all of Rhode Island Sound (RIS) with the exception of an area extending up to several kilometers south from the entrances to the Narragansett Bay and Mount Hope Bay estuarine system, and excluding the Massachusetts state waters at its eastern end, and (c) an offshore region extending about 25-30 km southward from these two areas. Water depths are typically 10-35 m and reach up to about 70 m in the offshore area; a companion OSAMP report discusses the bathymetric features and terminal-moraine geologic history of the region in detail.

The focus here is primarily on gross attributes of hydrographic fields (temperature, salinity, density, and density stratification) and circulation characteristics (seasonal-mean flow, weather band variations, and tidal fluctuations), including their geographic variations and water column vertical structure. Companion OSAMP reports cover waves, sediment transport, and other water properties such as oxygen concentration, none of which are addressed here. Our three main aims are to (a) review relevant literature, (b) use available observations to characterize the area, and (c) describe the output from a representative regional numerical hydrodynamic simulation configured to model the system realistically using up-to-date techniques including data assimilation. In the companion Part 2 report, the findings of a new observational campaign will be presented.

2 Introduction

2.1 Regional Setting

The RI OSAMP region is an inshore temperate shelf sea on the inner portion of the southern New England continental shelf (Figure 1). The southern New England shelf lies south of Massachusetts, Rhode Island, and Long Island, New York, extending nominally from the Hudson Shelf Canyon in the west to Nantucket Shoals in the east; it is the northern half of the region between Cape Hatteras and Cape Cod known as the Middle Atlantic Bight. The physical oceanography of the broader southern New England shelf, which bounds the RI OSAMP region to the south (Figure 2), has received considerable attention and a solid baseline understanding has therefore been built up (see, e.g., reviews by Beardsley and Boicourt (1981), Ingham (1982),

Mountain (2003), and (Lentz 2008a, b)). The OSAMP area, in sharp contrast, been the focus of relatively little research; for example, in a recent review of Mid-Atlantic Bight observed mean circulation using all available archived moored current meter records, the OSAMP area forms a somewhat conspicuous gap in coverage (see Figure 1 of Lentz (2008a)).

Water on the southern New England shelf originates primarily from the Scotian Shelf to the north (Chapman and Beardsley 1989), and passes across Nantucket Shoals (adjacent the RI OSAMP region to the southeast), generally after having passed through the Gulf of Maine and around or across Georges Bank. The polar origins, together with the effects of river and estuarine contributions, lead to shelf waters that are generally cooler and fresher on the inshore side of the shelf break front than the adjacent deep ocean slope water conditions to the south. Shelf waters undergo a pronounced seasonal cycle in temperature, influenced largely by air-sea interaction. Seasonality in salinity, associated mainly with spring freshening due to episodic coastal runoff, is less regular than that of temperature, and commonly weaker than inter-annual variability. Stratification, the vertical gradient in density associated with horizontal layering of water such that less dense layers overlie denser layers, results from comparably important influences of river freshening and surface heating, and peaks in summer. Cold bottom water formed in the winter, referred to as a "cold pool", can persist in some areas throughout the summer heating period and subsequent fall overturning when winds increase.

The regional-scale long-term mean vertical-average general circulation of the southern New England shelf is alongshore to the southwest, increasing in strength with distance offshore to reach 10-15 cm/s in a jet centered near the shelf break (e.g., Lentz 2008a); it is typically strongest at the surface and weakens toward the seafloor without reversing direction. Spatial and temporal variability of non-tidal flow superposed on this broad mean circulation pattern is significant (typically 10 to 40 cm/s, but up to 80 cm/s) and results largely from wind fluctuations, coastal-origin flows emanating from rivers and estuaries, and, in some years to a limited extent, interactions with Gulf Stream rings or the influence of hurricanes.

Regional surface winds (described in detail in a companion OSAMP report) in winter average about 4-12 m/s East-Southeastward, and due to storms are highly variable with peak speeds up to about 25 m/s. Summer winds are much less variable and weaker, averaging 2.5-7.5 m/s, and oriented in the East-Northeastward direction. Although wind fluctuations drive much of the variability of the circulation, wind is of secondary importance to mean currents, which are driven primarily by a large-scale alongshore pressure gradient and oriented largely in the upwind

direction. In the across-shelf direction, deep flow on the shelf is weakly onshore throughout the region (Bumpus et al. 1973); this is consistent with both the upwelling-favorable sense of mean winds driving shallow water offshore by Ekman transport, and also with the influence of deep onshore limbs of bidirectional exchange flows at the mouths of numerous estuaries in the area. Regional tidal conditions (Moody et al. 1984) over the main shelf include dominance of semi-diurnal constituents, typical sea level amplitudes of about 0.5 to 1 m, and tidal currents of up to 5 cm/s. In inshore areas, these attributes can be modified by near resonance of estuaries, for example Long Island Sound, which can amplify currents to as much as 100 cm/s.

2.2 Influences of Immediately Adjacent Waters

In addition to the deeper shelf area to its south, numerous bodies of water bound the OSAMP domain (Figure 2). Moving clockwise from the west, these include (a) western BIS and the Long Island Sound (LIS); (b) the West Passage, East Passage, and Sakonnet Passage entrances to the Narragansett Bay (NB) and Mount Hope Bay (MHB) estuarine system; (c) the semi-enclosed embayment Buzzards Bay (BB); and (d) Vineyard Sound (VS), a tidal strait that connects at its eastern end to Nantucket Sound. Exchanges of water and water properties with the OSAMP domain occur at each of these boundaries. Estimates of long-term mean volume transport exhanges based on sparse available observations (Table 1) were compiled by Codiga (2009),

Table 1. Estimated long-term mean volume transport exchanges with adjacent waters.

Body of water	Transport ($1000\ m^3\ s^{-1}$)	Source of observations used
Long Island Sound	23 +/- 5	Codiga and Aurin (2007)
Narragansett Bay	1-3 +/- 2	Kincaid et al. (2003)
Buzzards Bay	1-2 +/- 2	Signell (1987), Butman et al. (1988)
Vineyard Sound	4 +/- 4	Geyer & Signell (1990), Beardsley et al. (2007)

who emphasized that interaction with LIS has the most important influence on the OSAMP region. This conclusion holds despite the large uncertainties in the transport estimates, including the possibility that the sampling on which the LIS estimate is based significantly overestimates the net exchange because it lies within a local recirculation. The dominance of LIS can be anticipated based on river inputs to each system; the long-term mean river runoff to LIS

(approximately 500 m^3/s, the large majority of which is from the Connecticut River, see Figure 2) is about 10 times as high as that entering NB/MHB, with even smaller amounts entering BB and VS; the bi-directional estuarine exchange flows for the LIS and NB/MHB estuarine systems are amplified relative to these river inputs by a factor of about 15-25.

3 Characterization Based on Observations

In this section, available observations from the OSAMP region are summarized. Previously analyzed field studies are described, and new analyses are presented for sea surface temperature (SST), archived historical conductivity-temperature-depth (CTD) casts, and surface currents measured by high-frequency (HF) radar. Hydrographic fields are taken up first, then currents, with a literature review at the start of each subsection; in these literature reviews and those that follow in later sections, an important resource is the comprehensive catalogue of publications gathered and described by Battelle (USACE 2002) as part of an Army Corps of Engineers dredged material disposal site assessment. Appendix A includes a complete listing (Table A1) of observation-oriented publications and Appendix B includes a complete listing (Table B1) of modeling-oriented publications.

3.1 Hydrographic Fields

3.1.1 Literature Review

Some of the earliest and still very pertinent scientific analyses of OSAMP waters consist of a series of 1950s publications by Gordon A. Riley and colleagues that focused primarily on LIS but encompassed BIS and, to a lesser extent, RIS as well. A view of the geographic patterns and seasonal cycle of temperatures and salinities was laid out in an analysis of a series of vessel-based CTD surveys completed in the late 1940s (Riley 1952) that included a small number of bathythermograph transects across BIS and RIS. For OSAMP area surface temperatures, they documented the seasonal range of surface temperatures from about 2-4 ^oC in winter to about 20 ^oC in summer. The tendency was noted for inshore temperatures to be a few degrees cooler during winter, and to a lesser extent warmer during summer, relative the offshore OSAMP area. Surface salinities were in the range of 29.5 to 32.5 parts per thousand (PPT), with a prominent gradient of increasingly lower values from western RIS through BIS towards LIS. Together with freshening towards BB and eastward in to VS, this was considered evidence of dilution of saltier ocean waters by river inputs, which was concluded to be the dominant process determining hydrographic conditions along with air-sea heating/cooling. In late fall and winter, temperature

increases with depth of up to about 1 ^{o}C were commonly observed, indicative of a lag between cooling of shallow and deeper waters. In other seasons, typical surface temperatures were about 1-2 ^{o}C higher than at the bottom in shallow areas, reaching 5 ^{o}C higher in deeper areas, and offshore of Block Island in summer there were decreases of about 10 ^{o}C across a distinct thermocline about 15 m deep. Vertical salinity gradients were reported as typically no more than 1 ppt. Results of a similar survey in 1951-1952 presented by Powers (1953), which included more complete measurements of the vertical structure of the water column and seafloor conditions, demonstrated very similar features. In these early surveys complex spatial structure of water properties on scales of about 1 to 10 km were prominent, and recognized to be transient features that varied in response to river flow, wind, and tidal conditions, but further diagnosis of related processes was not possible due to the short sampling duration.

In 1963-1964, a US Navy field program obtained CTD casts repeated about each 2-3 months along two onshore-offshore transects in western-central and eastern-central RIS (Shonting et al. 1966; Shonting and Cook 1970). The seasonal temperature ranges noted above were confirmed and a mid-depth thermocline, with temperature differences of about 5-6 ^{o}C in spring increasing to at least 10 ^{o}C in late summer, was noted to span most of the area and be replaced by nearly homogenous temperatures in fall and winter as a consequence of wind mixing. Salinity patterns included persistent freshening in the upper several meters within 10-20 km of the northern shore, which was attributed to outflow from NB, and vertical gradients over most of the area that sharpened to about 1 PPT in late spring and early summer but were essentially absent during the late fall and winter. The density anomaly sigma-t was shown to take values in the range of about 23.8 to 25.2 kg m^{-3}, with peak vertical differences of 1-1.5 kg m^{-3} in early summer when near-surface freshening contributed in the same sense of, and with comparable importance to, higher surface temperatures. As in earlier surveys, transient small-scale variability in both temperature and salinity, including large fluctuations in the thermocline depth within a single survey and from survey to survey, were prominent and could not be addressed by the short-term nature of the nearly synoptic sampling.

CTD casts along transects across BIS were sampled in the late 1960s and early 1970s (Ichiye 1967; Williams 1969; Hardy 1972; Hollman 1974). These studies revealed similarities of BIS hydrography to that of RIS, including comparable vertical gradients. There were also notable geographic variations, with water in the south and west of BIS generally the most fresh, by up to 1 PPT, and the least strongly stratified. This feature was interpreted as the signature of fresh

outflow from LIS that spans the entire water column and is concentrated along the coast of Long Island and rounds Montauk Point to exit BIS southward. The saltiest water in BIS was near the bottom toward the north. Tidal fluctuations in water properties were also resolved and quantified, and attributed to advection by strong BIS tidal currents oriented largely east-west along the large-scale salinity gradient.

In the early 1970s an intensive field campaign was undertaken by Raytheon (1975) to characterize waters of northeastern BIS, as motivated by their potential capability to accommodate heat from cooling towers of a proposed nuclear power facility near Ninigret Pond. CTD casts were collected nominally each 2 weeks from July 1975 through September 1976 at a rectangular 3 by 4 array of stations spanning an area about 4 km by 6 km in the northeastern portion of BIS. Analysis by Snooks et al. (1977) confirmed in greater detail many of the features described in previous studies: seasonal formation (April) and breakdown (September) of a mid-depth thermocline, across which temperatures decrease in depth by up to 8-12 ^{o}C; temperature increases of about 1 ^{o}C with depth during fall and winter; salinities with a weak annual cycle but strong and irregular variability on timescales of weeks to months in association with river runoff, and typical surface to bottom differences of about 0.5 PPT; and variations in density and stratification controlled both by temperature and salinity. Photographic-method thermographs were also mounted on moorings at shallow and deep depths and recorded temperatures each 15 minutes at two sites for more than a year (Raytheon 1975). These records showed that temperature changes occur primarily on several-day timescales in association with weather events, and how the spring and summer warming process is slow and gradual while the fall breakdown in the resulting stratification occurs abruptly over a few days or less.

Bowman and Esaias (1981) reported results of a one-week CTD survey in September 1978 that included several casts in BIS. Their analysis emphasized the geographic variations in stratification, using top to bottom density differences, and as in previous studies showed it is substantially stronger over most of BIS than in the southwestern portion along the northern shores of Long Island and near Montauk Point. They compared measured stratification to the theoretical h/U^3 index (water depth h over cube of tidal current U) developed by Simpson and Hunter (1974) for a one-dimensional balance between surface heating and turbulent mixing driven by tidal flow across seafloor roughness. Observed stratification was generally strongest in regions of high h/U^3 and vice-versa, in agreement with the theory, despite that it does not incorporate salinity stratification and horizontal advection which are both known to be important.

A comprehensive compilation of temperature observations in RIS is provided by Armstrong (1998), which depicts results of a 10-year campaign of monthly expendable bathythermograph sampling along a shore to shelf-break north-south oriented band of water centered on RIS and spanning most of its width. The 10-year mean seasonal cycle is characterized, much as described above but depicted in greater detail, and deviations from it in individual years are shown to reach up to several ^{o}C. Emphasis was on bottom temperatures, and the faster spring/summer warming and higher resulting temperatures at inshore sites was quantified.

Frontal boundaries, while generally not detectable by CTD surveys, are prominent in the 12 years of ~1 km resolution satellite SST observations analyzed by Ullman and Cornillon (1999; 2001). The fronts are dynamical features commonly exhibiting sharp gradients in both salinity and temperature, and typically separate fresher inshore water from saltier offshore water. As detected in SST, the seasons when they are most common are winter, then summer, then spring, and they are relatively uncommon during fall. Frontal probabilities are highest in the area south of Block Island and also high along a band that stretches roughly from there northward and eastward, east of Block Island, to west-central RIS. As discussed in the next section below, this distribution can be understood to mark the edge of the LIS outflow, which during low river flow may extend eastward only to mid-BIS but during high river flow can extend to central RIS. Satellite sea surface temperature (SST) observations were also analyzed by Fox et al. (2000), who examined vernal warming using 1997 data from areas of BIS, central RIS, and the portion of RIS that enters VS. They identified LIS outflow water by its cool temperature, and quantified its spatial extent and aspects of its pronounced weather-band temporal variability. They also noted that areas of BIS and VS tended to be cooler than central RIS, which they attributed to more efficient mixing of colder deep water to the surface.

CTD surveys were repeated several times in 1998-1999, mostly during the summer and winter months, at 5 stations near and north of the OSAMP domain boundary in the vicinity of the mouth of NB (Kincaid et al. 2003). The vertical structure and seasonal variations of temperature and salinity were consistent with those described above for northern RIS, and an east-west gradient, with salinity increasing eastward across the mouths of the West and East Passages, was noted. This was interpreted as evidence that the NB/MHB estuarine exchange circulation consists mostly of northward inflow of salty RIS waters through the eastern side of East Passage together with a southward outflow of fresher water through the western side of East Passage, and to a lesser extent the West Passage.

A number of analyses resulted from an intensive field program during 2000-2002 focused on investigating the dynamics of the frontal boundary of LIS outflow on the inner shelf south of Montauk Point and Block Island in the southwestern corner of the OSAMP region. Kirincich and Hebert (2005), based on vessel-based surveys using a CTD mounted on a towed undulator, described the vertical and across-shelf structure of the temperature, salinity, and density of the front in spring 2002. The front shoals in the offshore direction, consistent with thermal wind shear of the southward and westward moving outflow jet observed in concurrent velocity measurements. During their survey the front intersected the seafloor at about 30 m deep, where they noted the near-bottom tidal variability was substantial. O'Donnell and Houk (2009) presented results of two 48-hour CTD surveys of BIS, western RIS, and the southwestern SAMP inner shelf, collected under different wind conditions, demonstrating the substantial range of weather-band variability in the geographic extent and vertical structure of the LIS outflow. Moored CTD profiler sampling of vertical casts hourly for multi-week intervals showed evidence of a mid-depth pycnocline in fall, in contrast to stratification throughout the upper water column in spring (Codiga and Rear 2004). An analysis of historical archived CTD casts by Ullman and Codiga (2004) contrasted the timing and intensity of the seasonal cycle of stratification in areas inshore and offshore of the front, quantifying the across-front density difference and demonstrating that its temperature contribution opposes its salinity contribution in winter and spring, then reinforces it during summer and fall. They showed that the strengthening of the along-front current in summer was linked to the stronger density gradient through geostrophic dynamics. Levine et al. (2009) identified smaller-scale fronts in the vicinity of the gap between Montauk Point and Block Island, with sharp gradients in salinity and temperature on scales of 10s of m, and interpreted them as boundaries of tidally-driven headland eddies associated with swift tidal currents there. Significantly, they also reported the only direct measurements of small-scale turbulent kinetic energy dissipation rate within the OSAMP domain, demonstrating elevated levels of up to 10^{-5}-10^{-4} W/kg near these fronts and linking them to shear instabilities.

Finally, CTD casts were collected during a few days of April and September 2004 at a proposed dredge disposal site about 38 m deep in west-central RIS (SAIC 2005). Measured conditions fit well within the expected range based on previous studies, but vividly demonstrated that temperatures and salinities in the upper water column, and hence stratification, vary substantially on timescales of hours to days. Advection of inhomogeneous water properties by small-scale eddying motions, tidal currents, and wind-driven movements are clearly a strong influence on hydrographic fields on short timescales.

3.1.2 Satellite Sea Surface Temperature Observations

An analysis of sea surface temperature (SST) observations was performed with the aim of describing the seasonal and spatial variability of SST across the OSAMP region. Satellite-derived SST data provide a high-resolution (~1 km) view of surface ocean conditions multiple times per day. We used all available observations from the moderate resolution imaging spectroradiometer (MODIS) sensors aboard the NASA Terra and Aqua satellite platforms during the period 2002-2007. Level 2 SST data (in satellite coordinates) from the 11 μm channel and the corresponding data quality flag were obtained from NASA's Ocean Color website (http://oceancolor.gsfc.nasa.gov/). To facilitate subsequent statistical analyses, the satellite passes from this dataset were remapped into a standard equirectangular projection.

We present maps showing the mean and standard deviation of SST averaged over all seasons and years as well as these same statistics computed on a seasonal basis. For the purpose of this report, seasons are defined as follows: Winter: January-March; Spring: April-June; Summer: July-September; Autumn: October-December. Seasonal averages are calculated using data from all years during that particular season. To avoid contamination by clouds (which generally appear colder than the sea surface), the statistical measures of SST presented here were computed using only those data values passing the most stringent data quality tests (quality flag = 0). The mean and standard deviation estimates at a given pixel (location) are displayed only if at least 50 SST values passing this test are included in the average.

Figure 3 shows the mean SST field and its standard deviation averaged over all seasons and all years. Warmest temperatures (11-13 °C) occur in central RIS in a region that extends to the south into the open ocean and also in northeastern Buzzards Bay. BIS and the eastern margin of RIS are generally a degree or two colder, likely a result of stronger tidal mixing in these regions, which reduces summertime SST. The boundary between the cooler BIS and warmer RIS surface waters is located slightly to the east of Block Island and then extends southwestward in the area to the south of BIS. As noted above, this front, which is seen more clearly in the seasonal maps to be described below, is the surface temperature manifestation of the low salinity LIS outflow (Ullman and Codiga 2004). The SST standard deviation indicates the range of SST encountered during the averaging period. In this case, the variability is a combination of seasonal variability and year-to-year variability, with the latter presumably showing little spatial structure. Highest standard deviations (7-9 °C) occur in regions near the coasts and in the relatively shallow Buzzards Bay indicating the strong seasonal SST swings in these areas. BIS is characterized by

lower standard deviations (5-7 °C), consistent with a reduction in the amplitude of the seasonal cycle of SST due to enhanced vertical mixing, which tends to distribute seasonal heat gain in summer over a deeper water column, associated with stronger tidal currents.

Winter SST (Figure 4) in RIS and BIS ranges from 1 to 5 °C with highest temperatures in southern RIS over the western portion of Cox Ledge (Figure 2) and the deep channel to the west of the Ledge. Lowest temperatures occur in the relatively shallow waters on the periphery of the Sounds, where winter surface cooling distributed over a shallower water column results in lower surface temperatures than in deeper areas. It is notable that in the eastern part of RIS the strong temperature gradient region along the outer edge of the cold band (occurring at a temperature of about 3.5 °C) does not appear to follow the isobaths as it does in northwestern RIS and in BIS. This suggests that the heat balance in this region may be significantly influenced by the advection of cold water northwestward into RIS from Nantucket Shoals, where extremely low winter SST is observed (Ullman and Cornillon 1999). SST standard deviation in winter is generally low (less than 2.5 °C) with highest and lowest values in central RIS and western BIS respectively.

In spring (Figure 5), highest SST (10-11 °C) occurs in northern and central RIS, while BIS, the area around Block Island, and the nearshore regions in eastern RIS are relatively cooler (8-10 °C). A sharp gradient is apparent around the periphery of the cooler BIS waters. This SST front is coincident with a co-occurring front in surface salinity that delineates the region influenced by the low salinity surface outflow from LIS. Strong vertical mixing caused by intense tidal currents in eastern LIS and western BIS distributes the springtime surface heat flux over a large portion of the water column in the LIS outflow region. This results in a smaller increase in surface temperature during spring than in regions with weaker tidal currents (e.g. central RIS) where the effects of surface heating tend to be trapped in a shallow surface mixed layer. The presence of cool water in the shallow eastern parts of RIS is likely a result of this mechanism as well. SST standard deviations are largest in central RIS (4-5 °C) and lowest in BIS and along the eastern margin of RIS (3.5-4.5 °C). This reflects the fact that the latter regions exhibit a smaller springtime increase in SST from their winter values. It also likely results from the fact that inter-annual variation in surface heat flux produces larger temperature variations in areas where the surface flux is trapped in a thin surface layer (central RIS) rather than being mixed throughout the water column.

Summer SST patterns (Figure 6) are similar to those in spring. A strong contrast is evident between cool SST in BIS (less than 20 °C) and relatively warmer values in central RIS (greater than 20 °C) arising from the same mechanism discussed above. As in spring, surface waters in eastern RIS are relatively cool (less than 20 °C), and the boundary between these waters and the warmer central RIS waters is more pronounced than in spring. Summer SST standard deviations tend to be low (less than 2 °C) partly reflecting the fact that summer (like winter) is the period when seasonal SST changes are at a minimum due to the change in sign of the surface heat flux from net heating to net cooling.

In autumn (Figure 7), waters in the region cool from the summer peak, with mean SST during autumn between 10.5-13.5 °C. Central RIS remains about 1 °C warmer than BIS and the coastal areas in eastern RIS. Coastal areas in northern RIS near the mouth of NB, and around eastern Long Island, exhibit warmer temperatures (SST values of 13-14 °C) than those observed in deeper areas. It is not clear what causes this; further investigation is needed to determine if this is a real signal or an artifact of the averaging procedure performed. SST standard deviation during autumn tends to be lowest in central and southern RIS due to slower cooling of the deeper water column there.

3.1.3 Hydrographic Climatology: Temperature

In this subsection and the three that follow we describe the temperature, salinity, density, and density stratification across the OSAMP domain with emphasis on seasonal variations of large-scale geographic patterns and water column vertical structure. The analysis is based on a "hydrographic climatology" computed from a compilation of historical archived CTD casts from 1980 to 2007, including those of Hydrobase (e.g., Curry 2001) and many casts from the National Marine Fisheries Service (NMFS) Marine Resources Monitoring Assessment and Prediction (MARMAP) program (e.g., Mountain 2003) of the National Oceanographic and Atmospheric Administration (NOAA). Casts from January through March, April through June, July through September, and October through December are treated as the winter, spring, summer and fall seasons respectively. During each of the four seasons there are about 150-300 casts, collectively over the 27-year period, distributed non-uniformly across the OSAMP domain (Figure 8, upper). Taken as a whole these casts are adequate to characterize the seasonal cycle but too sparse in time and space to yield meaningful information regarding inter-annual variability, which will therefore not be considered. Furthermore, it should be noted that in BIS there are no casts except

in the southernmost and easternmost areas, where the seasonal distribution of casts is highly non-uniform. In the following descriptions, BIS conditions are therefore the least certain.

Values were assigned by objective analysis (Hendry and He 1996) to a grid (not shown) having an unstructured horizontal mesh with node spacing from about 3 to 8 km across the OSAMP domain, and 22 evenly spaced fractional-depth levels relative to a suitably smoothed bathymetry (in Figure 8 the bathymetry in the lower panel is the smoothed version; compare to the upper panel). Surfaces were then computed at constant-depth levels with 10 m vertical spacing, and at the seafloor. The resulting fields presented here cannot capture sharp horizontal or vertical gradients, such as the frontal boundaries and detailed pycnocline characteristics described above. However, they provide valuable insight because unlike nearly all previous studies they illuminate large-scale gradients spanning nearly the entire OSAMP domain. As importantly, for large expanses of central and eastern RIS this climatology represents the best available characterization of vertical structure, for example density stratification, and its seasonal cycle.

For each of the four water properties (temperature, salinity, density, and stratification), seven figures are presented that collectively convey seasonal changes, geographic patterns, and vertical structure. The first three figures are maps showing the seasonal progression at several depths. They are followed by the seasonal cycle of vertical structure, presented in two figures along a series of east-west oriented vertical sections, and in two figures along a series of north-south oriented vertical sections (Figure 8, lower, is a map showing the section locations).

The dominant characteristic of temperatures (Figures 9 to 15) consists of the seasonal shifts from minima of about 3-6 ^{o}C in winter to maxima of about 9-21 ^{o}C in summer. In winter, temperature gradients overall are modest. The coldest temperatures are in the northeastern portion of the domain. Relative to the offshore OSAMP region, inshore areas are cooler by about 1.5-2.0 ^{o}C with the gradient strengthening toward the west. The likely causes for this are more effective cooling of shallower waters by loss of heat through the air-sea interface, and cold temperatures of river runoff. The winter temperature pattern is also characterized by warming with depth, from surface to seafloor, by typically about 0.5-1 ^{o}C. This feature is evidence that cooling by loss of heat to the atmosphere lags at depth relative to near the surface. It intensifies toward the south and central west, where increased water depths and vertical salinity gradients allow such temperature differences to be more persistent. The destabilizing influence of temperature on density stratification is overcome by salinity increases with depth (described in

the next subsection). The warm deep temperatures are characteristic of shelf waters to the south of the OSAMP region.

Spring warming brings higher mean temperatures as well as a larger range, about 6 to 12 ^{o}C. The warmest values are found in the upper water column, where geographic variations are modest and consist mainly of increases by about 1 ^{o}C from east to west across the domain. Throughout the domain the temperatures decrease sharply with depth, with surface to seafloor differences of about 4-6 ^{o}C and the sharpest vertical gradients concentrated in the upper water column. Near the seafloor, the geographic pattern includes increases by up to 4 ^{o}C in shallower areas relative to deeper areas, opposite the winter pattern, a signature of more efficient penetration of vernal warming with depth where water is shallower. Spring temperatures are generally uniform across the domain geographically and decrease primarily with distance from the surface, a pattern consistent with the relatively homogenous distribution of solar heating that drives warming.

Summer mean temperatures span about 9-21 ^{o}C, with sharp decreases in depth similar to those in spring except that surface to bottom differences increase to 6-10 ^{o}C or more. At the surface and 10 m deep there is a slight increase in temperature in the offshore direction but throughout the water column below the gradient is reversed and the seafloor temperature pattern, much like that in spring, is characterized by values several degrees higher in shallow inshore areas. Coldest temperatures occur at depth offshore, particularly to the south and west of the domain where surface warming penetrates less deep as a result of stratification due to salinity (discussed below).

The fall mean temperatures are relatively uniform in the range from about 12-13.5 ^{o}C. The main geographic pattern is a weak gradient from cold to warm in the offshore direction, which can be interpreted in terms of the influence of surface cooling penetrating fastest in shallower areas. The warmest water occurs at about mid-depth in the southern portion of the domain, where upper water-column temperatures increase with depth, as in winter (as described above). The mid-depth temperature maximum can be understood as a remnant of the summer waters that were coldest at depth with near-surface layers now cooled by surface heat loss.

3.1.4 Hydrographic Climatology: Salinity

Seasonal-mean salinity values (Figures 16 to 22) range from about 29.75 to 33.50 practical salinity scale (PSS) units. The seasonal cycle is dominated by overall freshening of about 0.5-1.0

PSS during spring and summer, which is concentrated in the west and to a lesser extent in the north. The primary geographic patterns in salinity are an upper water column east-west gradient toward values up to 1 PSS lower in the west, and slightly weaker increases in the offshore direction deeper in the water column. This reflects the fact that the main process influencing salinities is river runoff, with the Connecticut River in LIS the main source of fresh water reaching the OSAMP domain, as discussed in the Introduction. Compared to that of temperature, the seasonal progression of salinity is far less pronounced; geographic variations of seasonal-mean values for a single season are generally comparable to changes between seasons.

Salinities increase in the offshore direction nearly everywhere throughout the OSAMP domain, and always increase with depth. The surface to bottom difference ranges from about 0.5 to 2 PSS, peaks in spring and remains strong in summer. It is largest in the western half of the domain, in particular in BIS and to the south and west of Block Island, where the persistent influence of the relatively fresh LIS outflow is felt. As will be described below, tidal currents are stronger in BIS than in RIS, so the more persistent salinity stratification in BIS relative to RIS is an indication of the extent to which the freshening influence of LIS outflow reduces tidally driven turbulent mixing there.

3.1.5 Hydrographic Climatology: Density

The density anomaly sigma-t (σ_t) (Figures 23 to 29) ranges from about 21.75 to 26.00 kg m^{-3}, with geographic, vertical, and seasonal changes that reflect the underlying temperature and salinity patterns, each of which make important contributions. Overall seasonal variations in sigma-t are modest, intermediate between that of temperature and salinity when compared to geographic variations in each. The least dense water occurs in BIS, and to a lesser extent other inshore areas, near the surface during spring and summer. The densest water occurs in RIS and offshore, at the bottom during fall and winter. Hence the upper water column geographic pattern is dominantly an east-west gradient, with eastward decrease across the domain toward BIS that peaks at about 1 kg m^{-3} during spring, while at depth it consists of increases in the offshore direction that peak at about 1.5 kg m^{-3} during summer. For most of the year, variations in salinity make the primary contribution to variations in density, with temperature becoming comparably important during summer. The season with the most uniform density is winter, under the homogenizing influence of wind-driven mixing, when the increase in temperature with depth has a destabilizing influence that counteracts the stabilizing increase of salinity with depth. Similarly, during winter the influence on density of the onshore-offshore gradient in temperature

counteracts that of salinity, weakening the lateral gradient of density, as shown by Ullman and Codiga (2004). In contrast, the vertical and onshore-offshore gradients in density peak when contributions from temperature and salinity are in the same sense during summer, and to a lesser extent spring. Vertical variations in sigma-t are hence distinctly seasonal, reaching peak surface to seafloor differences of about 3 kg m^{-3} in summer, intermediate values of about 1-1.5 kg m^{-3} in spring, and about 0.5 kg m^{-3} or less in winter and fall.

3.1.6 Hydrographic Climatology: Stratification

Density stratification (Figures 30 to 36) is quantified using the buoyancy frequency squared, $N^2 = -(g/\rho_o)d(\sigma_t)/dz$ where g is gravitational acceleration, ρ_o is a constant reference density, and z is the vertical coordinate positive upward. The vertical differences are calculated over 10 m distances and are thus likely lower limits for stratification at smaller vertical scales. In units of 10^{-4} s^{-2}, peak values range from 2-3 in winter and fall, to 5-6 in spring, to 10-12 in summer.

Geographic variations undergo a distinct seasonal cycle. In winter stratification is strongest in BIS, where wind and tidal mixing influences are counteracted most effectively by the freshening influence of LIS outflow, as described above. In spring, stratification is enhanced throughout eastern BIS and portions of western RIS as well as the southwestern offshore portion of the OSAMP domain, in association with LIS outflow which has a broader influence due to peak river runoff. In summer and fall, the influence of surface warming causes stratification more broadly across the OSAMP domain but peak values remain in the west, particularly south of Block Island.

The strongest stratification occurs at middle depths within the water column, corresponding to a pycnocline, which is consistent with the freshening influence of estuarine waters being homogenized across the upper water column by wind mixing. During fall the pycnocline is about 30-40 m deep south of Block Island where it is strongest, and during other seasons it is generally about 10-20 m deep.

3.2 Currents

3.2.1 Literature Review

The earliest efforts to analyze current observations from waters within the OSAMP domain focused mainly on tidal motions in BIS (LeLacheur and Sammons 1932), and at one station at the mouth of VS (Haight 1938). BIS tidal currents were shown to be mostly rectilinear and east-

west oriented by LeLacheur and Sammons, who deduced amplitudes of about 50 cm/s in eastern BIS that increase to about 75 cm/s or more in western BIS. They also noted "ebb dominance", which can now be recognized as the presence of a residual (persistent, non-tidal) flow westward out of LIS, was prevalent throughout southern BIS including the area just north of Block Island, with "flood dominance" in northern BIS and near Point Judith. Finally, they documented a distinct phase lead of the tidal current reversal near the seafloor, by up to about an hour earlier, compared to near the surface. Haight (1938) showed that in far eastern RIS, tidal currents rotate clockwise in time with speeds of about 10-25 cm/s.

That the tidal motions are shaped strongly by near resonance of the semidiurnal components with LIS was recognized by Riley. However, for some three decades after the 1930s compilations, progress understanding the non-tidal flow was mainly limited to qualitative inferences based on water properties due to the lack of direct current measurements in BIS and RIS. Early views of surface salinity distributions (discussed above) were interpreted (e.g., Riley 1952) as indicative of a residual drift that originates in LIS and moves through BIS eastward and then southward through the gap between Montauk Point and Block Island. By differencing flood and ebb tidal currents, Riley (1952) also concluded near-surface residual drift in BIS was southeastward and estimated its strength to be in the range of 2 to 7 cm/s. It wasn't until the mid 1960s that additional current observations were collected (Williams 1969; Meguire 1971; Long 1978), which showed a more detailed view of vertical structure of currents in BIS, and were used to estimate volume transport there.

In the 1960s and 1970s an improved view of the direction of non-tidal circulation patterns also emerged from a series of field campaigns using surface floats and seabed drifters. Seabed drifters were weakly negatively buoyant, with weighted plastic stems to help maintain suspension above the bottom. The drifters were released offshore, marked with offers of 50¢ rewards to those who return them along with the date and place where they were retrieved along the coastline, and statistics were compiled of the recovery sites and the number recovered relative to the number released. Interpretation of the results of such studies can be problematic due to the ambiguity between unrecovered drifters that were carried offshore and those which happened not to be recovered for other reasons. A seabed drifter study by Bumpus (1965) spanning the broader New England shelf, including a few releases in and near RIS and BIS, concluded that near-seafloor flow was onshore over the inner half of the shelf including all of the OSAMP domain.

Cook (1966) presented results of a study using both surface and seabed drifters that were deployed at an array of stations spanning most of RIS during a short series of cruises in each of the four seasons. Pronounced variability of the results in response to weather-band shifts in the winds prior to and during the cruises reinforced awareness of the strong wind influence on the circulation. The range of current speeds was crudely estimated to be 2 to 16 cm/s at the surface and about 0.1 to 3.5 cm/s near the bottom. Surface flow directions were variable but generally northward during the spring and summer sampling, commonly eastward between Point Judith and Block Island during most seasons, and interpreted to be southward during the winter and fall (largely based on the low drifter return rate). The most persistent attributes of near-bottom flow included motion westward in western RIS, westward through the gap between Point Judith and Block Island, and northward in central and northern RIS. These features were noted to be consistent with the influence of the surrounding estuaries, particularly LIS and NB. In later years, similar drifter methods were applied by Hollman and Sandberg (1972) along a north-south transect in east-central BIS and by Collins (1974) and Snooks and Jacobsen (1979) along north-south oriented transects from the southern RI coast to Block Island. At these BIS sites the surface flow directions were most commonly eastward and southward, with high variability that was attributed to wind forcing, while deep flow was quite persistently westward toward LIS.

The interpretation by Cook (1966) of drifter results, as well as the small number of other studies available from surrounding waters, included an argument that a cyclonic (counterclockwise) surface flow gyre occupies RIS during typical spring and summer conditions, but is broken up by river runoff events and by winds in fall and winter. The gyre consisted of flow entering RIS primarily from Nantucket Shoals but also from BIS, NB, and BB, moving around the periphery of RIS cyclonically, while exiting RIS mainly from its southwest corner but also towards VS. Along the southern boundary of RIS the gyre included eastward flow. Currents were also depicted exiting BIS southward through the gap between Montauk Point and Block Island. Despite the lack of support in modern measurements for the eastward current that closes the gyre in southern RIS, many aspects of this early conceptualization of the spring and summer residual circulation remain pertinent today, as will be seen below.

Moored current meter deployments that enabled current strengths and directions to be quantified on short timescales, unlike drifter studies, became more common starting in the late 1960s. Shonting (1969) reported on a 13-day summer 1967 deployment of four moorings in a 1 km square in central RIS, each with current sensors recording each 20 minutes at two depths

shallower than and deeper than the strong seasonal pycnocline at about 8-12 m deep. Measured speeds ranged from about 15-40 cm/s and 5-20 cm/s at the shallower and deeper depths respectively, reflecting the isolation by the pycnocline of the deep water from wind-forced variability of the surface layer. Surface residual drift was about 10-12 cm/s westward in the upper layer, and about 2 cm/s at depth with a northward component. Semidiurnal currents with amplitudes of up to several cm/s were apparent, as well as intermittent near-inertial (period 18.3 hours) rotary motions with amplitudes of up to 5-6 cm/s.

In the early 1970s moored current meters were deployed within a few m of the bottom near a 35 m deep dredge disposal site in eastern central RIS (Saila et al. 1972; Pratt et al. 1975; Griscom 1977). The range of current speeds was 0 to 5 cm/s more than half the time, with semidiurnal tidal currents of a few cm/s, and occasional increases associated with storms reaching about 20 cm/s. Long-term mean flow was mostly eastward, which was interpreted as movement towards VS, and noted to be in agreement with the Cook schematic described above.

Year-long moored current meter deployments were part of the mid-1970s fieldwork in northern and eastern BIS (Raytheon 1975; Snooks and Jacobsen 1979). Current speeds were mostly in the range of 20-45 cm/s, with an east-west oriented semidiurnal tidal component of magnitude 20-30 cm/s, and marked wind-driven variability that was enhanced modestly during winter and fall compared to spring and summer. Nearest the northern coast, flow was oriented mostly east-west parallel to the shore, with frequent reversals; long-term means were about 5 - 10 cm/s with variable directions near the surface but a westward component at nearly all sites and all seasons at depth. Drogued drifter deployments at this site (Raytheon 1975) lasting about a tidal cycle also confirmed the importance of tidal motions in the overall flow. Moving southward approaching Block Island the tidal, wind-driven and mean flow magnitudes were similar with increasingly larger ranges of directions occurring, though the east-west orientation was still most prominent, and both shallow and deep mean flow became increasingly eastward-directed. A related experiment (Krabach and Snooks 1977) measured currents and dye concentrations within about 5 km of the northern shore of BIS in order to estimate flushing times.

The next relevant current measurement program was nearly two decades later, when Geyer and Signell (1990) used new acoustic Doppler current profiler (ADCP) technology in a vessel-based survey to examine flow in VS at the eastern boundary of the OSAMP domain. They quantified the tidal current strengths at 50 to 70 cm/s, in association with swift water exchanges through VS. They also identified a non-tidal residual flow structure that included persistent

eddies several km in size, with flow up to 25 cm/s, on either side of a headland. Some 10 years later Kincaid et al. (2003; 2008) carried out a similar series of vessel-based ADCP surveys, and deployments of a bottom-mounted ADCP, near the mouth of NB at the northern boundary of the OSAMP domain. Based on the surveys, non-tidal currents were stronger at the East Passage opening to NB than at the West Passage opening, and there were pronounced horizontal and vertical gradients in the speed and direction of both tidal and non-tidal flow. Residual flow moved northward in to NB in the eastern side of East Passage but southward on its western side. A westward current in northern RIS, in proximity to the northern boundary of the OSAMP domain, was also identified in summer, with speeds of 5 to 15 cm/s; it was not present in winter observations. The moored instrument showed 10-15 cm/s weather-band variability related to wind and river runoff events, with surface and deep flow decoupled from each other most strongly during summer in a manner consistent with the findings of Shonting (1969).

Significant advances in understanding of several aspects of OSAMP domain currents were made during the early 2000s in association with intensive observational campaigns focused on the frontal boundary in hydrographic properties south of Block Island. An array of bottom-mounted ADCPs was deployed there for numerous season-length intervals; vessel-based ADCP and towed undulating CTD surveys were carried out; and a high-frequency (HF) radar system (described below, with most recent analysis; see section 3.2.2) was installed and began continuous operations that remain active. The HF radar measures surface currents hourly with ~2 km resolution over nearly all of BIS, an area extending about 20 km south of Montauk Point and Block Island, and a small portion of western RIS. In addition, surface drifters released in BIS (Ullman et al. 2006) gave a detailed view of east-west tidal motions in northern BIS and rapid southward flow out the gap between Montauk Point and Block Island.

Seasonal-mean patterns in surface flow were examined using the HF radar by Ullman and Codiga (2004) and Mau et al. (2007b). Southern and western BIS surface currents are dominated year-round by LIS outflow moving at about 15-30 cm/s towards and through the opening between Montauk Point and Block Island. Northern and eastern BIS surface currents are weaker and more variable. South of Montauk Point the LIS outflow continues, now directed southwestward. During summer, a 25 – 30 cm/s southwestward surface jet originating east of Block Island with mainly geostrophic dynamics joins the LIS outflow south of Block Island, where together they feed a westward coastal current along the southern shore of Long Island. During winter, flow south of Block Island shifts in direction to be nearly directly offshore, and

the jet east of Block Island is weak or absent. Together with the summer-only westward flow in northern RIS noted by Kincaid et al. (2003), the summer jet is consistent with the Cook (1966) schematic for counterclockwise flow in northern and western RIS during spring/summer.

Codiga (2005) used moored ADCP records to investigate the vertical structure of the seasonal-mean flow south of Montauk Point and Block Island, identifying a sharp frontal boundary in velocity that extends upward and offshore from the seafloor at about 25-40 m deep. Flow shallower than and inshore of the front is southwestward and strongest in spring, while motion deeper than and offshore of the front is weak in spring but in winter reaches 5-10 cm/s northeastward, opposite the shallow flow. Currents measured by vessel-based surveys during spring 2002 (Kirincich and Hebert 2005) had vertical-offshore structure consistent with this picture and were shown to be in geostrophic balance with the concurrently measured density field. Substantial temporal changes were observed to occur in response to weather band variations in wind and river inputs; a number of specific patterns in surface currents were identified by Mau et al. (2007b) using the HF radar data, and subtidal principal axes ellipses at both near-surface and near-bottom depths based on the moored ADCP array are about 15-25 cm/s (Mau et al. 2008).

Tidal currents are dominated by the M_2 constituent and have pronounced spatial structure across BIS and the area south of Montauk Point and Block Island, as demonstrated by Ullman and Codiga (2004) and Mau et al. (2007a) using HF radar and by Codiga and Rear (2004) using moored ADCP records. Tidal current ellipses are elongated toward LIS, owing to its near-resonance at semidiurnal frequencies, with major axes of about 80 cm/s, 30 cm/s, and 100 cm/s in western, northeastern, and southern BIS respectively. Decay of tidal currents offshore southward from Block Island is swift, from 55 to 20 cm/s across a 10 km moored array (Codiga and Rear 2004). As the seafloor is approached, in agreement with theory for frictional effects, tidal ellipses become smaller and more rectilinear, with an enhanced counterclockwise in time rotary component. South of Block Island, substantial reduction in the size of tidal current ellipses in the upper water column during spring was attributed by Codiga and Rear (2004) to interaction with the background lateral shear of the strong LIS outflow.

On timescales shorter than tidal, vessel-based ADCP current measurements with high vertical resolution at frontal locations by Levine et al. (2009) revealed very strong local shears, indicating shear instability is active and supports enhanced turbulence in these locations. Several-hour long bottom-mounted ADCP records with 1-minute resolution (SAIC 2005) revealed fluctuations of

up to several cm/s on timescales of 5-20 minutes, with substantial nonuniformity in depth, superposed on the ambient 10-12 cm/s tidal current.

3.2.2 Analysis of HF Radar Surface Current Observations

Observations of surface currents from shore-based HF radar were obtained from the University of Rhode Island's standard-range CODAR system. This system provides maps of surface currents, at hourly intervals with spatial resolution of approximately 2 km, over most of BIS and the inner shelf south of BIS. The system is comprised of three radar sites, located at Southeast Lighthouse on Block Island, Misquamicut State Beach on Rhode Island's south coast, and Montauk Point Lighthouse on the eastern tip of Long Island. Each site provides maps of the radial component (the component towards or away from the site) of the surface current field, and the measurements from 2 or more sites, in regions of overlapping coverage, are combined to provide estimates of the surface current vector field. Further details on the operation of this system can be found in Ullman and Codiga (2004). The radial combination step was performed using the least-squares methodology of Lipa and Barrick (1983) with an averaging radius of 2 km. The least squares estimation of the vector velocity components also provides scaled estimates of the uncertainty in the velocity components (e_x, e_y). These were used to form a mapping error, $e_{map} = \sqrt{e_x^2 + e_y^2}$, which is related to the Geometric Dilution of Precision (Gurgel 1994). Current vectors with mapping error greater than 1.25 were deemed highly uncertain and excluded from the analysis.

For the analysis presented here, surface current data from June 2000 through September 2008 were used. Over this time interval, there were a number of relatively short periods during which data were not available because of equipment problems at one or more of the radar sites. However, for this report, where we present long-term or seasonal averages, this was not considered to be a problem and is ignored. Variability in the effective range of an individual CODAR site arises due to changes in the local surface wave field and the level of external radio frequency noise, which results in corresponding variability in the region covered by the vector current map. We limit the subsequent analysis to those areas in the coverage region where valid current vectors (passing the mapping error criterion) are available at least 50% of the time.

In order to focus on the non-tidal surface currents, the tidal component of the current field was removed by application of a low-pass filter (4^{th} order Butterworth filter with cutoff period of 36 hours) to the multi-year time series at each CODAR gridpoint. The resulting timeseries are

composed of a mean component plus variability at timescales ranging from several days to seasonal and interannual periods. Figure 37 displays the overall mean surface current field as well as a measure of the variability at all subtidal frequencies, while Figures 38 to 41 show the same quantities averaged by season. The ellipses centered on the mean vector tips in the figures represent 1 standard deviation of variability. This means that 66% of the time, the tip of the non-tidal velocity vector will lie within the ellipse. If the ellipse encloses the vector origin (the diamonds), this indicates that the variability is large enough such that the non-tidal current flows in a direction opposite to the mean at a significant number of observation times.

The overall mean current vectors (Figure 37) show generally southeastward flow in BIS consistent with the mean surface outflow from LIS. Between Montauk and Block Island, surface currents veer southward and over the inner shelf currents are southwestward. This southwestward flow appears to originate to the east of Block Island, where the flow is southward. The overall pattern thus appears to be the merging of the LIS estuarine outflow, which exits BIS between Montauk and Block Island, with a southwestward current on the inner shelf. Subtidal variability, which in the case of the overall mean contains seasonal variability, is generally large relative to the mean over most of BIS and in the southeast part of the coverage region over the inner shelf. Western BIS and the inner shelf just south of the Montauk-Block Island line are the only places where the mean flow is large compared to the variability.

The seasonal cycle of the non-tidal surface currents is shown in Figures 38 to 41 which present averages over the winter (Jan.-Mar.), spring (Apr.-Jun.), summer (Jul.-Sep.), and autumn (Oct.-Dec.) periods of the entire 2000-2008 time series respectively. During all seasons, the general pattern of LIS outflow through BIS, exiting southward between Montauk and Block Island is present. This outflow is strongest in spring and summer and weakest in winter. The southwestward inner shelf flow is strong in spring and summer and weak during autumn and winter. During winter, and to a lesser extent in autumn, the flow over the inner shelf has a significant offshore (southeastward) component that is driven by strong westward winds in winter (Ullman and Codiga 2004). Subtidal variability is stronger over the inner shelf than within BIS and the variability increases in autumn and winter in response to increased wind variability during those seasons. The subtidal ellipses are generally elongated in the east-west direction, which is roughly the alongshelf direction along this portion of the coast.

A harmonic tidal analysis, using the T_TIDE MATLAB package (Pawlowicz et al. 2002), was performed on CODAR-derived surface currents over the entire 2005 year, a period when

data return was excellent. The five most energetic constituents are the principal lunar M_2, the larger lunar elliptic N_2, the principal solar S_2, the luni-solar diurnal K_1, and the principal lunar diurnal O_1. The M_2 (Figure 42) is by far the most important (note the different scales for the ellipses in Figures 42 to 46) with maximum amplitude of approximately 1 m/s. Tidal ellipses are highly elongated with the major axis generally oriented north-south on the inner shelf, rotating to be roughly east-west within BIS. Amplitudes increase from the inner shelf to BIS consistent with amplification associated with tidal resonance of Long Island Sound at the semi-diurnal period (see, e.g., Codiga and Rear 2004). Some increase in amplitude is also seen in the area between Montauk Point and Block Island, presumably caused by the presence of a relatively shallow sill there. M_2 tidal currents generally rotate clockwise in time (the few counterclockwise-rotation ellipses in Figure 42 are very elongated, indicating nearly rectilinear motion). The other semidiurnal tidal constituents, N_2 (Figure 43) and S_2 (Figure 44) have amplitudes of less than 20 cm/s throughout the coverage region and approximately rectilinear currents. As with M_2, a similar increase in amplitude moving from the inner shelf towards BIS is observed for these constituents. The K_1 (Figure 45) is the most energetic of the diurnal tidal constituents with maximum amplitude of approximately 10 cm/s, while O_1 amplitudes are generally less than 5 cm/s (Figure 46). Little amplification towards BIS and LIS is observed for the diurnal constituents, consistent with the fact that LIS is far from resonance at diurnal frequencies. Currents at the diurnal frequencies generally are clockwise rotating.

4 Characterization Based on Hydrodynamic Simulation

As is abundantly clear from the previous section there are large areas of the OSAMP domain, particularly in central and eastern RIS, in which very few if any observations have ever been collected. This is particularly true with respect to the circulation, to processes that occur at frequencies higher than tidal, and to mixing and dispersion. Hydrodynamic model simulations can therefore play an important role, not only in providing a view of what water properties and circulation characteristics may be in the most poorly sampled areas, but also in enhancing temporal and spatial resolution of processes in locales where there may be adequate measurements. This section begins with a literature review focused on hydrodynamic modeling studies that have addressed portions of the OSAMP domain. Next, the configuration and forcing functions of a representative model simulation are described in detail. Finally, the hydrographic and circulation fields of the model output are presented and discussed.

4.1 Literature Review

Modern methods of hydrodynamic modeling developed in the late 1970s and focused initially on tidal elevations and tidal currents (e.g., URI 1979). Spaulding and Gordon (1982) reviewed all earlier modeling and observational studies, then presented results of a barotropic simulation of tidal flow that incorporated realistic coastline and bathymetry spanning the OSAMP domain and surrounding estuaries. Horizontal resolution was 1.8 km and an offshore area of the shelf was included to improve handling of the open boundary condition. The amplification of the semidiurnal component towards and within LIS due to its near-resonance was captured, and good agreement was found with sea level observations. Tidal currents were noted to be mostly rectilinear in LIS, BIS, BB, and VS while more rotary in RIS. Although modeling techniques advanced substantially in the years that followed, and were applied to nearby systems (e.g. Signell (1987) in BB, Spaulding et al. (1996) in NB, Signell et al. (2000) in LIS), it was more than two decades later when the next modeling simulations were published that included analysis focused on a sizable portion of the OSAMP area.

An investigation of LIS outflow dynamics was carried out by Edwards et al. (2004a; 2004b) using the MIT general circulation model MITgcm (Marshall et al. 1997), a finite-volume c-grid Navier-Stokes solver, in hydrostatic mode with a length-scale turbulence closure scheme and a linear equation of state. The model was configured to include eastern LIS, BIS, RIS, and the surrounding shelf areas with horizontal resolution ranging from 0.5 km near BIS to 2-3 km along the open boundary; z-level grid spacing was 2 to 5 m in the vertical. Realistic tidal forcing was applied along the open boundary and estuarine buoyancy inputs were incorporated through relaxation toward climatological temperature and salinity observations. In Edwards et al. (2004a), wind forcing was omitted and the focus was on understanding dynamics of the front south of Block Island during the springtime 2000 period. A front having characteristics in agreement with available measurements occurred in the model at the location where it is observed, and a diagnosis of its dynamics demonstrated that tidal mixing in BIS, advection by the LIS outflow and inner shelf currents, and a tidally-driven residual flow headland eddy each played important roles. The h/U^3 theoretical boundary of tidally-mixed waters (Simpson and Hunter 1974) was shown to run approximately north-south through eastern central BIS then eastward to Block Island, and from there along an arc leading to the south shore of Montauk Point and extending southward by up to about 10 km. In Edwards et al. (2004b) the focus was on capturing the subtidal weather-band variability in currents that are prominent in observations.

Wind forcing and, more importantly, a barotropic inverse method using local moored ADCP records, were applied and shown to improve the model skill due to their representation of offshore processes otherwise not captured by the tide-only open boundary condition forcing.

Eastern RIS, though not addressed in any detail by Edwards et al., was within the area of interest in model simulations by He and Wilkin (2006) and Wilkin (2006) using the Regional Ocean Modeling System ROMS (e.g., Shchepetkin and McWilliams 2005). ROMS is a free-surface, finite difference, hydrostatic c-grid primitive equation solver with a terrain-following vertical coordinate, and the turbulence closure of Mellor and Yamada (1982) level 2.5 (MY2.5) was applied. Their domain was centered on Nantucket shoals and extended to eastern RIS, Cape Cod, and mid-shelf, with 1 km horizontal resolution. Data assimilation methods were applied by He and Wilkin (2006) and the focus was limited to barotropic tidal dynamics, which were shown to be shaped by interactions with the complicated coastlines and bathymetry of the area and consist of a complex response that has significant propagating and standing wave components. In eastern RIS, the dominant M_2 constituent had northwest-southeast oriented rotary ellipses with major and minor axes of up to 15-25 cm/s; magnitudes were similar in BB but amplified to 50 cm/s or more in VS. The theoretical h/U^3 tidal mixing front boundary was shown to lie east of the OSAMP domain boundaries. Tidally-induced residual circulation of about 5 cm/s flowed northwestward in to the eastern half of RIS from south of Martha's Vineyard. In Wilkin (2006), fine vertical resolution was included and realistic atmospheric, tidal, and open boundary forcing was applied in order to investigate the heat budget during summer 2002. Different dynamical balances controlled the heat budget in Nantucket Sound, Nantucket Shoals, and the area south of Martha's Vineyard. The eastern RIS area is most similar to the latter, where surface waters warm steadily through July and August because advection and tidally-driven mixing are relatively weak.

Mau et al. (2007a; 2008) investigated the circulation and hydrography of BIS and the LIS outflow using the Princeton Ocean Model (POM: e.g., Blumberg and Mellor 1987) configured to include LIS, the OSAMP domain, and portions of the surrounding shelf. POM is a c-grid primitive equation model with terrain-following vertical coordinate and it was run using MY2.5 turbulence closure with 1-2 km horizontal resolution and 16 equally-spaced vertical layers, for a year-long period. In Mau et al. (2007a) the focus was tidal currents and detailed comparisons of model output with HF radar and moored ADCP observations showed the model captured aspects of the horizontal and vertical structure of tidal ellipses (described above) well. In contrast, Mau

et al. (2008) examined dynamics of LIS outflow in year-long model simulations with realistic tidal forcing, observed winds applied uniformly over the domain, relaxation to a seasonal hydrographic climatology, and an open boundary condition that incorporated the ambient coastal current. Comparisons to a number of observational datasets were very favorable, with one main exception being a more pronounced Montauk Point headland eddy than seen in the HF radar measurements. From a series of runs suppressing individual processes, it was concluded that the surface plume strength is limited by tidal and wind mixing and enhanced by the presence of the ambient coastal current.

Finally, Cowles et al. (2008) investigated the low-frequency circulation and hydrography of the entire Gulf of Maine and New England shelf region using data-assimilative simulations with the Finite Volume Coastal Ocean Model (FVCOM). FVCOM (described in the next section) was forced with spatially-resolved meteorological model output for winds and air-sea fluxes, realistic tides, and freshwater inflows from major rivers, and used the MY2.5 turbulence closure. Across the OSAMP domain the horizontal resolution was about 8-10 km, substantially lower than in the simulations described above. Dynamics of the OSAMP region were not investigated in detail, since most of the analysis was centered on demonstrating that model skill was high with respect to a comprehensive set of observations from a 70 m deep mid-shelf site south of Martha's Vineyard. A discrepancy between model and observations was mid-shelf near-surface salinities that were not as fresh in the model as observed during May 1997. It was concluded that the LIS outflow plume in the model did not extend as far offshore as observed due to advection by a westward model current near that location which was stronger than the actual flow.

4.2 A Representative Simulation: FVCOM During 2006

In keeping with the scope of this report, output from a model simulation was sought in order to facilitate an investigation of hydrographic and circulation attributes across the OSAMP domain, with emphasis on geographic, vertical, and seasonal variations. The simulation needed to be representative of current modeling practices, including assimilation of observations (see previous section); have adequate horizontal and vertical resolution across the entire OSAMP domain; incorporate realistic bathymetry and coastline; be driven by realistic meteorological, river runoff, tidal, and open boundary forcing; have duration of at least a full year; and be available to us for purposes of this analysis. The model output selected is a simulation of the year 2006 using FVCOM (Chen et al. 2006) for a similar Gulf of Maine and southern New England shelf regional domain and model configuration as that of Cowles et al. (2008), but with a higher

grid resolution (about 0.25 – 2.5 km) across the OSAMP domain. Different models have differing strengths and weaknesses with respect to various analysis objectives; use of this model output is not intended as endorsement of it as the best-performing, rather it was selected because it met the requirements listed above in the most complete way.

FVCOM is a prognostic, unstructured-grid, finite-volume, free-surface, 3-D primitive equation model consisting of momentum, continuity, temperature, salinity and density equations with parameterization of turbulence closure. The grid used ("Gulf of Maine generation two") extends from Nova Scotia to New Jersey and offshore past the shelf break. The horizontal grid is unstructured triangular cells with increased resolution near the coastline and the shelf break, and the vertical coordinate is terrain-following with 30 layers. The numerical solver uses a second-order accurate discrete flux calculation in the integral form of the governing equations. Wind stress and air-sea flux forcing were from the fifth-generation mesoscale meteorological model (MM5, Grell et al. 1994). The MY2.5 turbulence closure scheme and quadratic bottom friction were applied. The largest 7 rivers, including the Connecticut River, were forced (in contrast to the 29 rivers in Cowles et al. (2008)) using United States Geological Survey data uncorrected for ungauged areas. Along the open boundary, tidal elevations were forced and temperature and salinity were nudged toward hydrographic climatology observations. Inner shelf sea level setup near the northern limits of the domain, far from the OSAMP area, was handled following Pringle (2006). Sea surface temperatures were nudged to post-processed satellite SST.

The model bathymetry in the OSAMP area (smoothed relative to upper frame of Figure 8), the horizontal model grid, and the vertical sections along which model fields are plotted (the same as for the hydrographic climatology in sections 3.1.3 to 3.1.6 above) are shown in Figure 47. Simulation fields were analyzed at the free surface, constant-depth levels spaced 5 m apart, and a seafloor layer. Tidal elevation and current constituents were computed using the t-tide package (Pawlowicz et al. 2002) using the entire simulation year. Subtidal currents were computed using a low pass 5^{th} order Butterworth filter with 30-hour cutoff. Seasonal-averaged quantities were computed using the same seasonal intervals as used in prior sections (Jan.-Mar, Apr.-Jun., Jul.-Sep., and Nov.-Dec. for winter, spring, summer, and fall respectively). Model outputs, referred to as "the simulation" from here forward, are described in detail in the next section.

The simulation period is the year 2006 only, so the fields presented are not representative of long-term average conditions, nor can the analysis address inter-annual variability. This should

be borne in mind when comparisons are made to measurements taken in years other than 2006, and to multi-year mean fields such as the hydrographic climatology presented above. The year 2006 had an anomalously wet late spring period and a summer with relatively weak winds. In surrounding estuaries such as NB, this led to stronger than average stratification during the spring and summer periods, and similar conditions could be expected to have occurred in the OSAMP domain. On the other hand, influences of estuarine freshwater delivery on the model hydrography and circulation in the OSAMP area may be underestimated because the simulation was forced by only the 7 largest rivers, among many more that exist across the Nova Scotia to New Jersey domain, and river flows were uncorrected for ungauged area. Despite the potential difficulties of interpretation that these aspects of the analysis may cause, the insight gained through the model analysis is a constructive complement to the spatially and temporally sparse observational analyses presented earlier.

4.3 Simulation Seasonal Means and Subtidal Variability

4.3.1 Hydrography: Seasonal Means and Standard Deviations

The spatial structures and seasonal cycles of temperature (Figures 48 to 54), salinity (Figures 55 to 61), density anomaly (Figures 62 to 68), and stratification (Figures 69 to 74) in the simulation share most of the gross features of satellite SST (described in section 3.1.2) and the hydrographic climatology from archived CTD casts (described in sections 3.1.3 to 3.1.6). The simulation differs from the hydrographic climatology in its finer spatial detail due to its higher horizontal and vertical resolution, and in its span of the entire OSAMP domain and surrounding areas, including, importantly, all of BIS. In the following discussion, the emphasis is on differences from, and extensions relative to, the results from earlier analyses of satellite SST and the hydrographic climatology.

Simulation surface temperatures agree well with the range of values and geographic patterns in the multi-year mean satellite SST observations on scales of 10s of km. On smaller scales there are differences, notably within a several km of the shoreline, where the satellite data shows more substantial spring/summer cooling in areas such as the western end of VS. Given that the simulation assimilates satellite SST, this is most likely due to real differences between 2006 SST and the multiyear mean of the climatology, but it may reflect an inaccurate balance in the simulation between vertical mixing and arrival of estuarine water.

With few exceptions the simulation temperatures agree with the seasonal evolution in the range of values, the geographic patterns, and the sense of the inshore-offshore gradients of the hydrographic climatology. The primary difference is that the simulation does not have warmer temperatures at depth during the winter, as in the climatology. The reason for this is not clear but potential explanations include: the model portrays 2006 conditions well but warm water did not occur at depth that year; warm water at depth occurred in the simulation but persisted for a short enough duration that it is not apparent in the season-length means; or that in the simulation the balance between vertical mixing and fall/winter surface cooling does not result in the needed surface water temperature reduction.

The fine temporal resolution of the simulation supports calculation of subtidal standard deviations, as were computed for satellite SST but not for the hydrographic climatology due to its sparse underlying sampling. Standard deviations (shown for surface and seafloor depths) are based on 30-hour low-pass timeseries and thus are an indication of both weather-band variability and the trend of the seasonal cycle that occurs during a given season (most pronounced for spring and fall). Comparison between simulation surface temperature standard deviation (lower, Figure 48) and that of satellite observations (section 3.1.2) shows substantial differences in geographic patterns and magnitudes. As noted above, this is probably due to real differences between 2006 conditions and the multi-year climatology. At the seafloor, simulation temperature standard deviations (lower, Figure 50) are smallest during winter, when they decrease across the OSAMP domain towards the north and east where the coldest temperatures occur. Temperature standard deviations are largest in spring and fall, when they peak in western BIS and BB, due to seasonal warming/cooling, and decrease towards the central south OSAMP area. In summer, there is a region of western RIS, oriented roughly north-south, where maximum seafloor temperature standard deviations occur. Given the weak overall warming/cooling during this season, a likely cause for it is weather-band variability. The summer region of high seafloor temperature standard deviation occurs near where a strong southward summer current flows (e.g., section 3.2.1, and upper frame of Figure 6) and may be the signature of weather-band meandering of the current and an associated hydrographic front that intersects the seafloor. There summer seafloor salinity standard deviation (Figure 57, lower) is also enhanced in this region, which is consistent with this interpretation since such fronts are typically characterized by both salinity and temperature gradients.

Simulation BIS temperatures are warmer in summer and colder in winter, compared to central RIS. Temperature gradients across BIS are not as extreme as in RIS; in the horizontal this may be because its shallow sills mean that deeper shelf water affect it more weakly, while in the vertical it is likely due at least in part to the enhanced influence of tidal mixing in BIS associated with shallower water depths and stronger tidal currents.

While the general sense and magnitude of horizontal gradients in simulation salinities (Figures 55 to 61) agree with those of the hydrographic climatology, there are more substantial differences between them, particularly as regards salinity magnitudes, than for temperatures. The most prominent example is that in the simulation the freshest waters (about 29.6 PSS) are seen in western BIS in fall, and to a lesser extent summer; in the climatology they occur in spring and summer, though also at the most western locales (eastern BIS for the climatology). Simulation vertical salinity gradients are substantially weaker than in the hydrographic climatology. It is possible these differences reflect real differences between 2006 conditions and the multi-year climatology; this would be consistent with the fact that many observations suggest the seasonal cycle in salinity is not strongly more pronounced than inter-annual variability. Alternatively, the budget for fresh water in the simulation may be inaccurate, due to the way river forcing has been implemented (mentioned in the previous section), given that 2006 had more spring river runoff than a typical year. Simulation salinity standard deviations (lower frames, Figures 55 and 57) are most pronounced near the surface, as expected given the strong influence buoyant estuarine outflow have on them; during spring and summer they are strongest and peak in offshore areas, during winter they peak in western BIS, and during fall they are weakest. At the seafloor the pattern of standard deviations is similar to that at the surface in winter, but weaker in spring and summer, and there is pronounced peak during fall in the offshore area south of Block Island, and including the area west of Block Island where seafloor temperature standard deviations also peak as discussed earlier in this section.

The simulation density anomaly field (sigma-t; Figures 62 to 68) reflects the combined contributions of temperatures and salinities just described, and differs from the hydrographic climatology in corresponding ways. As in the climatology, the overall seasonal cycle in simulated densities reflects mainly the influence of temperature. However, salinity makes an important contribution to density stratification in all seasons, while that of temperature is becomes important mainly in spring and summer. As expected given its higher vertical resolution, in the simulation the stratification (Figures 69 to 74; note different scale for each

season) tends to be concentrated in a pycnocline that spans a narrower range of depths than in the climatology. Simulation buoyancy frequency squared is lowest in winter, when there is a weak pycnocline only in deeper RIS and the offshore area, centered at about 30 m deep and strengthening offshore. In fall the pattern is similar to winter but with higher buoyancy frequencies, and also a thin strongly stratified layer very near the surface in the northern half of BIS occurs. In spring and summer a sharp pycnocline occurs in central RIS and the offshore areas, at about 10 m deep or less, and strengthens considerably in the offshore direction. Relative to the hydrographic climatology, the simulation stratification does not occur as uniformly across the OSAMP region; this is probably due to the limited ability of the spatially coarse climatology to capture geographic variations. In the simulation, BIS remains unstratified or very weakly stratified in all seasons; the stratification seen in the portions of BIS included in the climatology clearly differs, but is based on very few data so may be more representative of the individual years they were collected than it is of long-term average conditions.

4.3.2 Sea Level: Seasonal Means and Standard Deviations

Results of this subsection are based on analysis of the non-tidal low-passed filtered simulation sea level. The seasonal-mean sea level takes maximum overall values in spring, and minima in fall (Figure 75, upper). The main spatial features consist of a peak offshore gradient of up to several cm across the OSAMP domain, due to high values in inshore areas, during spring and summer, but a weaker oppositely-directed gradient in winter and fall. The spring/summer offshore gradient is associated with the strongest alongshore southwestward currents in the offshore area, as discussed by Ullman and Codiga (2004) in interpreting sea level observations. They concluded that the steric effect of freshwater outflow is likely responsible for peak values in inshore areas during spring, and the inshore set-down during winter is consistent with the influence of upwelling-favorable winds and weakening of the alongshore flow. The simulation sea level in the vicinity of Montauk Point is persistly low year-round, which could be associated with tidally-driven headland eddy dynamics there, as discussed by Edwards et al. (2004a) and Mau et al. (2008); the latter analysis concluded a headland eddy was more pronounced in their model than in HF radar observations, which may also be true for this simulation. The standard deviation of simulation sea level (Figure 75, lower) is minimal in summer, modest in spring, and strongest in fall and winter with values increasing across the domain from about 5-6 cm towards their peaks of about 10-12 cm in BIS. This is consistent with the seasonality of wind fluctuations and probably represents wind-driven variability in the circulation. Tidal sea level variations are

generally substantially larger than these seasonal and subtidal fluctuations, and are discussed in detail in section 4.4.1.

4.3.3 Currents: Seasonal Means and Subtidal Principal Component Ellipses

Seasonal means, and principal axes components of subtidal flow, were calculated (Figures 76 to 87) from simulation horizontal currents as for HF radar currents (section 3.2.2), using the non-tidal low-passed model output for each season at several depths. The ellipses thus primarily reflect weather-band variability. The results are presented as vectors (seasonal-means) and ellipses (subtidal principal axes) on maps (Figures 76 to 79), east-west vertical sections (Figures 80 to 83), and north-south vertical sections (Figures 84 to 87). In all figures, including the vertical sections, the vectors and ellipses appear in plan view showing eastward and northward flow upward and rightward on the page, respectively; no vertical velocities are shown. Only Eulerian means are considered and no particle-tracking nor Lagrangian-mean analysis in included. In this section, the seasonal-mean vectors (red arrows in figures) are described first, followed by the subtidal ellipses.

In southern and central BIS, including the area just north of Block Island, changes in flow from season to season are modest. Seasonal-mean currents near the surface range from about 5-15 cm/s, with a persistently eastward component and peak values during the summer. This can be identified as the outward component of the LIS estuarine exchange flow, which Codiga and Aurin (2007) observed to peak during summer in eastern LIS. With increasing depth the eastward flow weakens in magnitude, and becomes directed more northward in the east near Block Island. In northern BIS, currents are generally weaker (about 1-5 cm/s) and have a westward component except in winter when flow is mostly southeast as driven by strong southeastward winds; an exception is the very shallow, northwest-most location, adjacent to shore in BIS, where flow is strongly westward. These westward movements are likely part of the inward return component of the exchange with LIS. In the north-south oriented gap between Point Judith and Block Island, flow in the northern half is westward and weaker than the eastward flow just described in the southern half. The two-way nature of flow in this gap is likely influenced by the LIS estuarine exchange flow (see Table 1).

In the vicinity of the east-west oriented southern opening of BIS, there is eastward flow of about 10-15 cm/s that persists in all seasons along the shoal immediately south and east of Montauk Point. Together with southward and southwestward flow to the east and south of there, this is likely a portion of a tidally-driven headland eddy (discussed by Edwards et al. (2004a) and

Mau et al. (2008)). The southward/southwestward current over the canyon outside southern BIS strengthens sharply in spring and summer, reaching speeds of 20 cm/s or more, the strongest anywhere across the domain. It is a combination of LIS outflow and a southward current to the east of Block Island that also intensifies strongly in spring/summer, reaching up to 20 cm/s while typically 5 cm/s or less in fall and winter. The western RIS spring/summer intensified southward current in the simulation, identified as a jet by Ullman and Codiga (2004) in HF radar observations and described in section 3.2.2 above, flows westward along the southern edge of Block Island, and together with the eastward flow off Montauk causes a strongly convergent pattern on the inner shelf just outside the southern opening of BIS. Some of this water moves through the jet then northward along the western side of Block Island, particularly at depth, so that in all seasons the flow between Montauk Point and Block Island has both a southward and northward component, another signature likely associated with the LIS estuarine exchange flow. There is evidence that mean flow very near to Block Island circulates around all of its sides in the clockwise sense.

There are pronounced season-to-season changes in the offshore portion of the OSAMP domain. In winter and fall this offshore region, as well as most of RIS, are characterized by weak mean flow, a few cm/s, in the south and east direction offshore in the upper water column, and onshore north and east at depth. This is consistent with an upwelling circulation driven by the strong winds in those seasons, which are southeastward and hence have an offshore component as well as a component in the upwelling alongshore direction. In spring and summer this flow pattern changes, in the offshore areas, to a stronger (about 10 cm/s) east-southeastward directed current along the southern boundary of RIS. This current is strongest at the surface in spring and just beneath the surface in summer, and weakens modestly with depth but extends throughout the water column with only minor changes in orientation. This current likely originates on Nantucket Shoals and only a fraction of it enters RIS, most instead moving from south of Martha's Vineyard directly along the southern boundary of RIS to the area south of Block Island.

Within RIS, where seasonal mean currents are generally the weakest, the near-surface offshore winter flow becomes westward and northward in spring, apparently driven by the inflow from Nantucket Shoals. Summer mean flow is very weak, except for the far eastern and northern portions of RIS where a narrow current of up to 5-10 cm/s moves counterclockwise around its edges and ultimately feeds the southward jet in western RIS. This system of flow is similar to the "cyclonic eddy" described by Cook (1966), except that in the simulation it does not close on

itself because flow at the southern edge of RIS is westward not eastward. It seems likely that the counterclockwise flow along the western, northern, and eastern edges of RIS is associated with the hydrographic boundary between stratified and unstratified waters, marked by the tidal mixing front. In fall and winter the stratification in RIS is diminished, hence the hydrographic front weakened, as is the current along it.

A prominent attribute of simulation subtidal currents (blue ellipses in figures) is that, over most of the OSAMP domain and during much of the year, they have semi-major and semi-minor axes of about 5-15 cm/s, and are thus stronger than the seasonal mean flow. This is evidenced by vectors for which the head and tail both lie within the ellipse. It is most pronounced near the surface, the most directly responsive to wind forcing. This feature underscores the strong relationship between the currents at a given time, which are commonly oriented toward a substantially different direction than they were a few days earlier, and the strength and direction of the wind over the past several days. Subtidal ellipses larger than seasonal-mean flow vectors are seen in all four seasons over all of central RIS and most of eastern RIS, as well as in the central and eastern offshore region in winter and fall. Areas where seasonal-mean current vectors are larger than subtidal ellipses, indicative that changes in direction of flow are much less common, include the system of stronger currents just described, and BIS, which is not as exposed to wind influences and hence generally has slightly weaker weather-band variability.

Subtidal ellipses are larger in winter and fall than in spring and summer, which is consistent with fluctuations that are predominantly wind-driven, given that the strongest wind stress variability occurs in fall and winter. In the open areas outside BIS that are less constrained by bathymetry and coastline geometry, the increased ellipse size in winter and fall is mostly in the east-west component; nearly round spring/summer ellipses become elongated in the east-west direction during winter and spring. This is indicative that a major component of variability is upwelling/downwelling circulation oriented along the larger-scale east-souteastward/west-northwestward regional coastline orientation.

Subtidal ellipses diminish with depth in all seasons, to half of their surface amplitudes or less at the seafloor. In winter and fall, the decay in depth is quite uniform over the water column. In summer and spring, in locations where stratification is strong such as in central RIS, the ellipse amplitudes diminish sharply just deeper than the pycnocline, and are weak everywhere deeper, relative to the 10-20 m deep surface layer. This characteristic of the simulation is in very good agreement with the early observations of Shonting (1969).

4.4 Simulation Tidal Processes

4.4.1 Tidal heights

The most energetic constituents in harmonic fits to simulation sea level are M_2, N_2, S_2, K_1, and O_1, the same five included in the above HF radar currents analysis (section 3.2.2). The amplitude and Greenwich phase lag of each constituent is presented (Figures 88 to 92). The tidal response in the area is complicated, as discussed by He and Wilkin (2006) for eastern RIS, by reflection and refraction by the complex coastline and bathymetry, in addition to the influence of resonances in nearby semi-enclosed water bodies.

Collectively, the resultant of the five constituents leads to tidal height amplitudes of about 1 m, with pronounced spring-neap variability, across much of the OSAMP domain. The M_2 constituent (Figure 88) amplitude is in the range of 35-65 cm across the OSAMP domain, while the amplitudes of N_2 (Figure 89) and S_2 (Figure 90) are in the range of about 8-13 cm each. These three semidiurnal constituents have very similar spatial patterns in amplitude and Greenwich phase lag. Amplitudes are maximal in northern RIS and towards BB and decrease from there offshore and towards BIS, where they take their minima in central southwestern BIS near Montauk Point. Modest Greenwich phase lag variations of about 30-40^o occur across the domain, with maxima in western BIS, decreases eastward across BIS from there, and relatively uniform values across the rest of the domain. The nearly quarter-wave resonance response of LIS to semidiurnal frequencies plays a large role in these patterns, since eastern LIS has characteristics of a node.

The two diurnal constituents K_1 (Figure 91) and O_1 (Figure 92) each have amplitudes in the range of about 5-7 cm, and similar spatial patterns of amplitude and Greenwich phase lag to each other. Amplitudes are maximal in western BIS and decay across BIS eastward. For K_1, amplitudes decrease relatively uniformly toward BB, and for O_1 they are relatively uniform across the rest of the domain. Greenwich phase lags only vary by about 15^o, with peak values near Montauk Point and decreases across the domain toward minima along the eastern and northern edges of RIS. Unlike the semidiurnal constituents, these diurnal constituents are not near the resonance frequency of LIS, which therefore influences their spatial patterns much less strongly.

4.4.2 Tidal currents

In harmonic analysis of simulation currents, in addition to the above five constituents the currents of the main quarter-diurnal non-linear M_4 and the smaller solar elliptic L_2 are energetic. While the M_4 and L_2 components of sea level variability were not significant, their currents were stronger than the diurnal constituents over much of the region, so are included in this analysis. It is likely their generation is through nonlinear interactions. HF radar in BIS and surroundings, as well as moored ADCP records on the inner shelf south of BIS, do not show a level of M_4 and L_2 energy as high as in the model output. Additional measurements are needed from areas further east, including RIS, to assess whether this aspect of the simulation agrees with observations there.

The relative importance of tidal currents to the total (tidal and non-tidal) flow field can be quantified as the ratio (expressed as a percentage, Figure 93) between the variances of the tidal currents and the total currents. This percentage is very high (> 90%) throughout BIS, except in a small area adjacent the western shore of Block Island, as well as areas extending about 5-10 km outside of BIS southward on the inner shelf and eastward in western RIS. It is also very high (>80%) within 5-10 km of the mouths of NB, BB, and VS. These areas are associated with amplification due to coastline constrictions and/or resonant responses of adjacent water bodies. In contrast, the percentage is lower (40-60%), in northern RIS very near to Sakonnet passage, in the open-water area extending from southeast of Block Island toward south-central RIS, and over the western offshore area. This results from relatively weak tidal currents or stronger weather-band variability (discussed above). Over most of central eastern RIS and the offshore area to its south, tidal current variance is about 60-80% of total current variance.

Spatial structure of tidal flow for each constituent is revealed by maps of tidal current ellipses, with instantaneous flow vectors, at the surface and seafloor (Figures 94 to 100). For the most energetic M_2 constituent (Figure 94), the ellipses are presented with a scale such that their size corresponds to the distance a passive particle would be advected during one tidal period by that constituent alone, in order to emphasize the tidal advection length and how it varies across the domain. Surface M_2 ellipses are elongated towards LIS throughout BIS and the areas southeast and northeast of Block Island; generally rotate clockwise in time; and reach maximum semi-major axes of up to 80-90 cm/s in southern BIS then decay over 10-20 km southward to about 10-20 cm/s. These features are consistent with the HF radar observations described above. In offshore areas and most of RIS, simulation ellipses also rotate clockwise in time and are more

round; semi-major axes over much of this area are 5-10 cm/s and increase gradually eastward to more than 50 cm/s within a few km of BB and VS. Similar amplification is not seen at the mouth of NB, where, in the area east of Point Judith, currents rotate counterclockwise in time. The M_2 ellipses at the seafloor are about half as large as those at the surface but share most of their general characteristics, with the exception of an amplified counterclockwise-in-time component; over most of the domain, this results in more narrow ellipses that still rotate clockwise in time, while in contrast across much of BIS and an expanded area east of Point Judith they become counterclockwise in time. The amplification of the counterclockwise component as the seafloor is approached is a fundamental feature of frictional tidal boundary layers (e.g., Soulsby 1990) and has been observed on the inner shelf south of BIS (Codiga and Rear 2004); an alternative explanation could be superposition of incident and reflected/refracted waves causes by interaction with the complex coastal boundaries, although it is not obvious how this would lead to enhancement of counterclockwise-in-time rotation near the seafloor. For the N_2 (Figure 95) and S_2 (Figure 96) constituents, ellipse amplitudes are lower (see scale in figures; amplification factor relative to advection is also noted in captions), but all the ellipse characteristics just described for M_2 are very similar.

The diurnal constituents K_1 and O_1 (Figures 97 and 98) have very similar amplitudes and geographic patterns to each other. They are much weaker than the semi-diurnal constituents (note different scales in figures) and much more uniform spatially across the region, with relatively round ellipses and rotation in time clockwise. Moderate amplification occurs in eastern RIS, and in BIS where there is a tendency for deep ellipses to rotate counterclockwise in time.

The M_4 constituent is relatively uniform across the domain, with nearly round ellipses and rotation counterclockwise in time. Amplification occurs in the mouth of VS, and in BIS where ellipses are amplified and rotate clockwise in time. Variations with depth are modest.

For the L2 constituent over areas outside of BIS, ellipses are elongated northeast-southwest and rotate clockwise in time at the surface but counterclockwise in time at the seafloor. In BIS amplitudes are amplified and rotation is clockwise in time at both the surface and seafloor.

Additional information about the vertical variation of tidal current amplitudes within the water column is seen in vertical section plots of the RMS semi-major and semi-minor axes of the tidal current ellipses along the transects in Figure 47. The pattern for semi-diurnal constituents is represented by that of M_2 (Figure 101 upper; Figure 102 left) and consists of modest decreases uniformly from surface to seafloor across most of the domain, but sharper decay in the vertical

within BIS where enhanced frictional influences due to bed-driven turbulence are expected due to the amplified currents there. In contrast, the pattern for diurnal constituents, represented by K_1 (Figure 101 lower; Figure 102 right), consists of moderate vertical gradients that are more uniform over the domain, since amplification in BIS and eastern RIS is so much more modest. For M_4 and L_2 the vertical amplitude variations (Figures 103 and 104) over most the domain are relatively weak, with sharp vertical decay occurring only in small areas of BIS, and to a lesser extent eastern RIS, where amplification is significant.

5 Summary

A stylized schematic depiction of prominent seasonal-mean hydrographic and circulation features of the OSAMP domain and immediate surroundings has been constructed (Figure 105) in order to concisely summarize the main aspects of geographic variations, vertical structure, and the seasonal cycle. This section gives a detailed explanation of the schematic, which was prepared based on all aspects of the above analysis including the literature review, observations, and hydrodynamic model output. It is important to note that the schematic does not include wind-driven or tidal currents, which are both typically stronger than the seasonal-mean currents that appear in it. However, most of the important features of wind-driven and tidal current variations are seen in Figure 80 and Figure 94 respectively; thus a reasonably complete view of the characteristics of OSAMP domain hydrography and circulation can be ascertained using three key graphics (Figures 80, 94, and 105).

The schematic (Figure 105) includes gray bathymetric contours at 10 m intervals (starting from 20 m) and depicts hydrographic properties at five representative sites (BIS, south of Block Island, central RIS, south of RIS, and northeastern RIS) using a set of three colored bars for temperature, salinity, and density anomaly (see legend, upper right frame). The height of the colored bars represents the water depth at each site. Each colored bar includes shallow and deep portions, divided by the pycnocline, which varies in depth from site to site and season to season as shown. The scales for temperature, salinity, and density anomaly are presented in the color legends in the lower right frame. Density stratification is depicted using the difference $\Delta\sigma_t$ between deep and shallow density anomaly (sigma-t) values, and shown in a bar plot immediately above each set of three color bars; in the bar plot, the left-most and middle bars (white) are $\Delta\sigma_t$ due to temperature and salinity respectively, and the right-most (black) bar is the total $\Delta\sigma_t$.

The key features of the hydrographic fields, as described in detail in prior sections, are apparent in the schematic:

- Temperature changes from season to season that far exceed geographic variations during a given season: the dominant influences are the combined effects of air-sea heat exchange and solar radiative forcing, which have modest spatial variations
- Geographic variations in salinity during a given season that have magnitude comparable to that of the seasonal cycle; inshore areas are generally fresher, by an extent determined through mixing between estuarine waters and saltier shelf waters
- BIS salinities generally freshest relative to other areas, owing to the dominance of volume transports to and from OSAMP waters by LIS exchange flow which carries outflow from the Connecticut River, the largest river in the region
- Temperatures that are slightly cooler in shallow inshore areas in winter, and warmer in summer, reflecting interplay there between enhanced tidal mixing and stronger influence of temperature extremes associated with estuarine waters
- Minimal temperature differences between shallow and deep layers during winter and fall, owing to cooling of surface waters and enhanced wind mixing
- Shallow temperatures higher than deep temperatures by about 4-6 ^{o}C in spring and up to 11 ^{o}C in summer due to surface solar heating
- Salinity differences between shallow and deep layers of about 0.2 to 0.9 PSS year-round, maintained by arrival of freshened estuarine waters from surrounding water bodies
- Density stratification that is minimal in winter and fall, when temperature contributes little to stratification (or, in some areas, is destabilizing due to cooling of the shallow layer), and the weak pycnocline is about 30-40 m deep due to effective wind mixing at shallower depths
- Density stratification, in terms of $\Delta\sigma_t$, reaching about 1.5 kg m^{-3} in spring, when the temperature influence is comparable to that of salinity, and about 2.5 kg m^{-3} in summer when the temperature influence is more important than salinity; a sharp pycnocline about 10-20 m deep during these seasons

- Seasonal cycle of density stratification that is more pronounced in RIS than in BIS, with BIS more weakly stratified than RIS in summer as limited by tidal mixing, but more strongly stratified in winter due to LIS exchange flow
- An estuarine outflow front (sharp horizontal gradient) to the south of Block Island that bounds fresher inshore water from saltier offshore water, and lies farther from land in spring and summer, when it extends northward to the east of Block Island
- In summer and to a lesser extent spring, a tidal mixing front that divides the more homogenous inshore water column from more strongly stratified deeper water: along the northern and eastern boundaries of RIS, and along an arc between the southern sides of Montauk Point and Block Island

Seasonal-mean velocities of the shallow and deep layers are depicted using green and blue arrows respectively. Some key circulation features, which for clarity are only labeled in a single frame of the figure, are nonetheless present year-round:

- LIS exchange flow, in western BIS: eastward flow in the southern portion, most strongly in the shallow layer, and westward flow in the northern portion in both deep and shallow layers
- Eastern BIS exchange flow, in the gap between Point Judith and Block Island: eastward flow nearest Block Island and strongest in the shallow layer, with westward flow in both layers near Point Judith
- Southern BIS exchange flow, in the gap between Montauk Point and Block Island: southward flow in the shallow layer, strongest toward the west, and northward flow at depth in the eastern portion
- Weak westward and southward flow outside the mouth of NB
- LIS outflow, east and south of Montauk Point, that is directed southward then westward with increasing distance offshore, is bounded on its offshore edge by the outflow front, and is likely bounded on its inshore edge by a tidally-driven clockwise headland eddy
- A southward current in western RIS along the eastern side of Block Island
- A coastal current westward along the southern Long Island shore to the south and west of Montauk Point

Seasonal shifts in the seasonal-mean flow in and near BIS are modest compared to the rest of the domain, and consist of a strengthening in spring and summer of the exchange circulations, LIS outflow, southward flow east of Block Island. The latter three currents are most closely associated with a horizontal gradient in density, from less dense to more dense in the offshore direction, with a dominantly geostrophic dynamical balance such that the current is stronger when the gradient is sharper. The gradient sharpens in summer because, while the salinity distribution maintains the density gradient year-round due to the continual freshening influence of estuaries on inshore areas, inshore-offshore temperature differences act to weaken the density gradient in the winter and strengthen it in summer.

Across RIS and the offshore portion of the OSAMP domain, there are substantial changes in the direction and strength of seasonal-mean currents, as follows:

- In winter and fall, flow shows only weak geographic variations and is consistent with a wind-driven upwelling circulation: shallow flow is weakly offshore toward the southeast, while deep flow is slightly slower in essentially in the opposite direction
- In spring the inshore edge of the southern New England shelf flow, a strong current in both shallow and deep layers, flows along the offshore OSAMP area directed just south of westward; in RIS, flow is weak and generally westward in both layers
- In summer the southern New England shelf flow is slightly weaker than in spring and bifurcates at the eastern end of the domain, with a significant component moving northward as the RIS current, a narrow flow likely linked to the horizontal density gradient associated with the tidal mixing front and moving counterclockwise around the strongly stratified interior of RIS in both shallow and deep layers
- In spring and summer the southward-flowing western RIS portion of the RIS current strengthens considerably and occupies both shallow and deep layers; south of Block Island it merges with the southern New England shelf flow and the LIS outflow, all of which ultimately feed in to the coastal current along the southern shore of Long Island

6 Knowledge Gaps

It is apparent that there are numerous important gaps in knowledge of physical oceanography of the OSAMP waters. First and foremost is probably the lack of measurements, using modern instrumentation, of even baseline conditions over most of central and eastern RIS. However, even in the better-sampled areas where enough measurements are available to piece together the

seasonal patterns that have been described above, there is a pronounced need for more observations with dense spatial coverage in the horizontal and vertical and finer temporal sampling. This applies to both hydrographic and circulation fields. The need arises due to the sampling demands of the highly variable conditions, which result from complex interactions of wind, tidal, and buoyancy forcing on timescales as short as hours to days and as long as the seasonal cycle and inter-annual variability. For example, our ability to estimate transports of water and water properties between the OSAMP domain and surrounding areas, and transports passing through key constrictions such as the gaps from Block Island to Point Judith and Montauk Point, is severely constrained by the lack of measurements with sufficient coverage and resolution in the space and time. Two topic areas seem worthy of designation as having had the most inadequate attention to date. The first is turbulence characteristics and processes, including horizontal and vertical rates of mixing and dispersion. The second is the potential importance of processes occurring on timescales shorter than tidal, such as the nonlinear internal waves that are known to be energetic in other inshore shelf seas.

Acknowledgements

We thank Carlton Hunt (Battelle) for providing an excellent starting point for the literature reviews of observations; Charles Law (Oregon Health and Science University) and Kevin Ruddock (Nature Conservancy) for providing the objectively analyzed archived hydrographic measurements; and Changsheng Chen (UMass Dartmouth) for providing FVCOM model output.

References

Armstrong, R.S. 1998. Water Temperatures and Climatological Conditions South of New England, 1974-83. *NOAA Technical Report NMFS 134, U.S. Department of Commerce*.

Beardsley, R.C., W.C. Boicourt. 1981. On estuarine and continental shelf circulation in the Middle Atlantic Bight. In: Anonymous (Ed.), MIT Press, Cambridge, MA, USA, pp. 198-233.

Beardsley, R.C., R. Limeburner, C. Chen. 2007. Nantucket Sound Circulation - Observations, Analysis and Model Development. *Sea Grant Project Report Website*, http://www.whoi.edu/science/PO/Nobska_Mooring/index.html.

Blumberg, A.F., G.L. Mellor. 1987. A description of a three-dimensional coastal ocean circulation model. . *Three-Dimensional Coastal ocean Models, edited by N. Heaps. American Geophysical Union.*, 208 pp.

Bowman, M.J., W.E. Esaias. 1981. Fronts, stratification, and mixing in Long Island and Block Island Sounds. *J. Geophys. Res.* 86, 4260-4264.

Bumpus, D.F. 1965. Residual drift along the bottom on the continental shelf in the middle Atlantic bight area. *Limnology and Oceanography* 10(Supplement), R50-53.

Bumpus, D.F., R.E. Lynde, D.M. Shaw. 1973. Coastal and offshore environmental inventory - Cape Hatteras to Nantucket Shoals: Physical Oceanography. In: Anonymous (Ed.), Univ. Rhode Island., Kingston, RI (USA). pp. 1-72.

Butman, B., R.P. Signell, P. Shoukimas, R.C. Beardsley. 1988. Current observations in Buzzards Bay, Massachusetts, 1982-1986. *United States Geological Survey, Open File Report 88-5*, 211pp.

Chapman, D.C., R.C. Beardsley. 1989. On the origin of shelf water in the Middle Atlantic Bight. *J. Phys. Oceanogr.* 19(3), 384-391.

Chen, C., R.C. Beardsley, G. Cowles. 2006. An unstructured grid, finite-volume coastal ocean model (FVCOM) system. *Oceanography: Special Issue "Advance in Computational Oceanography"* 19(1), 78-89.

Codiga, D.L., L.V. Rear. 2004. Observed tidal currents outside Block Island Sound: Offshore decay and effects of estuarine outflow. *J. Geophys. Res.* 109, doi:10.1029/2003JC001804.

Codiga, D.L. 2005. Interplay of wind forcing and buoyant discharge off Montauk Point: seasonal changes to velocity structure and a coastal front. *J. Phys. Oceanogr.* 35, 1068-1085.

Codiga, D.L., D.A. Aurin. 2007. Residual circulation in eastern Long Island Sound: Observed transverse-vertical structure and exchange transport. *Continental Shelf Research* 27, 103-116.

Codiga, D.L. 2009. Circulation in Block Island Sound, Rhode Island Sound, and adjacent waters, with emphasis on subsurface flows. In: Schwartz, M.L., A. Desbonnet,B.A. Costa-Pierce (Eds.), Sound Connections: The Science of Rhode Island and Block Island Sounds. Proceedings of the 7th Annual Ronald C. Baird Sea Grant Science Symposium, Block Island, Rhode Island. [http://seagrantadm.gso.uri.edu/Baird_08/Abstracts/codiga.pdf].

Collins, B.P. 1974. Suspended material transport in lower Narragansett Bay and western Rhode Island Sound. *MS Dissertation, University of Rhode Island. Kingston, RI.*, 85pp.

Cook, G.S. 1966. Non-tidal circulation in Rhode Island Sound-- drift bottle and sea bed drifter experiments (1962-1963). *Technical Memorandum 369, Naval Underwater Weapons Research Engineering Station*, Newport, RI, 37pp.

Cowles, G., S. Lentz, C. Chen, Q. Xu, R.C. Beardsely. 2008. Comparison of observed and model-computed low frequency circulation and hydrography on the New England shelf. 113(C09015), doi:10.1029/2007JC004394.

Curry, R. 2001. HydroBase 2: A Database of Hydrographic Profiles and Tools for Climatological Analysis. *Woods Hole Oceanographic Institution, Draft Technical Reference*, ftp://flotsam.whoi.edu/HydroBase2/DOC/TechRef_draft.pdf.

Edwards, C.A., T.A. Fake, P.S. Bogden. 2004a. A numerical model investigation of spring-summer frontogenesis at the mouth of Block Island Sound. *J. Geophys. Res.* 109 C12021, doi:12010.11029/12003JC002132.

Edwards, C.E., T.A. Fake, D.L. Codiga, P.S. Bogden. 2004b. Combining ADCP records with a GCM using a linear depth-averaged inverse model: the effect of low frequency motions on fronts near Block Island Sound. *J. Geophys. Res.* 109(C12022), doi:10.1029/2003JC002133.

Fox, M.F., D.R. Kester, J.E. Andrews, A. Magnuson, C.G. Zoski. 2000. Seasonal warming of Narragansett Bay and Rhode Island Sound in 1997: Advanced very high resolution radiometer sea surface temperature and in situ measurements. *Journal of Geophysical Research* 105(C9).

Geyer, W.R., R.P. Signell. 1990. Measurements of Tidal Flow Around a Headland With a Shipboard Acoustic Doppler Current Profiler. *J. Geophys. Res.* 95, 3189-3197.

Grell, G.A., J. Dudhia, D.R. Stauffer. 1994. A description of the fifth generation Penn State/NCAR Mesoscale Model (MM5). *National Center for Atmospheric Research, Tech. Note 398+STR.*

Griscom, C.A. 1977. Near Bottom Currents and their potential for sediment resuspension as measured by an EM Current Meter. *In: A study and report on oceanographic conditions in the vicinity of Browns Ledge. RIS Report 2, Division of Marine Resources, University of Rhode Island, Kingston, RI.*

Gurgel, K.W. 1994. Shipborne measurement of surface current fields by HF radar. *L'Onde Electr.* 74, 54-59.

Haight, F.J. 1938. Currents in Narragansett bay, Buzzards bay, and Nantucket and Vineyard sounds. *U.S. Coast and Geodetic Survey, Washington DC*, 103pp.

Hardy, C.D. 1972. Hydrographic data report : Long Island Sound, 1970, Part II. . *Marine Sciences Research Center, State University of New York, Stony Brook, with support from Nassau-Suffolk Regional Planning Board*.

He, R., J.L. Wilkin. 2006. Barotropic tides on the southeast New England shelf: A view from a hybrid data assimilative modeling approach. *Journal of Geophysical Research* 111, C08002, doi:08010.01029/02005JC003254.

Hendry, R., I. He. 1996. Technical Report on Objective Analysis Project. *Prepared for Bedford Institute of Oceanography*, http://www.mar.dfo-mpo.gc.ca/science/ocean/coastal_hydrodynamics/Oax/download/techrep.

Hollman, R., G.R. Sandberg. 1972. The residual drift in eastern Long Island Sound and Block Island Sound; a preliminary report. N.p.

Hollman, R. 1974. An interdisciplinary study of the estuarine and coastal oceanography of Block Island Sound and adjacent New York coastal waters: ground truth, final report. *New York Ocean Science Laboratory, Montauk, NY,* Technical Report 27.

Ichiye, T. 1967. Tidal variation of hydrography of Block Island Sound observed in August 1965. *Lamont Geological Observatory, Palisades, NY.* Technical Report No CU-15-67, Office Of Naval Research Contract Nonr 266-48

Ingham, M.C. 1982. Summary of the physical oceanographic processes and features pertinent to pollution distribution in the coastal and offshore waters of the northeastern United States, Virginia to Maine. In, NOAA, Woods Hole, MA.; Woods Hole, MA, pp. 1-166.

Kincaid, C., R.A. Pockalny, L.M. Huzzey. 2003. Spatial and temporal variability in flow at the mouth of Narragansett Bay. *J. Geophys. Res.-Oceans* 108.

Kincaid, C., D.L. Bergondo, K. Rosenberger. 2008. The dynamics of water exchange between Narragansett Bay and Rhode Island Sound. In: Desbonnet, A.,B.A. Costa-Pierce (Eds.), Science for ecosystem-based management: Narragansett Bay in the 21st Century, Springer Series on Environmental Management, New York, pp. 301-324.

Kirincich, A., D. Hebert. 2005. The structure of the coastal density front at the outflow of Long Island Sound in spring 2002. *Continental Shelf Research* 25, 1097-1114.

Krabach, M.H., J.H. Snooks. 1977. Coastal zone flushing characteristics, NEP 1 & 2, Charlestown, RI. *Yankee Atomic Electric Company, Nuclear Services Division, Westborough, MA.*

LeLacheur, E.A., J.C. Sammons. 1932. Tides and currents in Long Island and Block Island sounds. *U.S. Coast and Geodetic Survey, Special Publication 174*, 181pp.

Lentz, S.J. 2008a. Observations and a model of the mean circulation over the Middle Atlantic Bight continental shelf. *J. Phys. Ocean.* 38, 1203-1221.

Lentz, S.J. 2008b. Seasonal variations in the circulation over the Middle Atlantic Bight continental shelf. *J. Phys. Ocean.* 38, 1486-1500.

Levine, E.R., L.R. Goodman, J. O'Donnell. 2009. Turbulence in coastal fronts near the mouths of Block Island and Long Island Sounds *Journal of Marine Systems* 78(3), 476-488.

Lipa, B.J., and D. E. Barrick. 1983. Least-squares methods for the extraction of surface currents from CODAR crossed-loop data: Application at ARSLOE. *IEEE J. Oceanic Eng.* 8, 226-253.

Long, E.E. 1978. Tide and tidal current observations from 1965 through 1967 in Long Island Sound, Block Island Sound, and tributaries. Dept. of Commerce, National Oceanic and Atmospheric Administration, National Ocean Survey, Rockville, Md.

Marshall, J.C., A. Adcroft, C. Hill, L. Perelman, C. Heisey. 1997. A finite-volume, incompressible navier stokes model for studies of the

ocean on parallel computers. *J. Geophys. Res.* 102, 5753– 5766.

Mau, J.-C., D.-P. Wang, D.S. Ullman, D.L. Codiga. 2007a. Comparison of observed (HF radar, ADCP) and model barotropic tidal currents in the New York Bight and Block Island Sound. *Est. Coast. Shelf. Sci.* 72, 129-137.

Mau, J.-C., D.-P. Wang, D.S. Ullman, D.L. Codiga. 2007b. Characterizing Long Island Sound outflows from HF radar using self-organizing maps. *Est. Coast. Shelf. Sci.* 74, 155-165.

Mau, J.-C., D.-P. Wang, D.S. Ullman, D.L. Codiga. 2008. Model of the Long Island Sound outflow: Comparison with year-long HF radar and Doppler current observations. *Cont. Shelf Res.* 28, 1791-1799.

Meguire, R.E. 1971. Tidal currents and water exchanges in western Block Island Sound. *M.S. Thesis, Long Island University,* 83pp.

Mellor, G.L., T. Yamada. 1982. Development of a turbulence closure model for geophysical fluid problems. *Rev. Geophys. Space Phys.* 20, 851-875.

Moody, J.A., B. Butman, R.C. Beardsley, W.S. Brown, P. Daifuku, J.D. Irish, D.A. Mayer, H.O. Mofjeld, B. Petrie, S. Ramp, P. Smith, W.R. Wright. 1984. Atlas of tidal elevation and current observations on the Northeast American continental shelf and slope. In, U. S. Geological Survey, Reston, VA, United States (USA), pp. 1-122.

Mountain, D.G. 2003. Variability in the properties of Shelf Water in the Middle Atlantic Bight, 1977-1999. *Journal of Geophysical Research-Oceans* 108, 3014-3014.

O'Donnell, J., A.E. Houk. 2009. The structure and variability of the hydrography of the Block Island Sound. In: Schwartz, M.L., A. Desbonnet,B.A. Costa-Pierce (Eds.), Sound Connections: The Science of Rhode Island and Block Island Sounds. Proceedings of the 7th Annual Ronald C. Baird Sea Grant Science Symposium, Block Island, Rhode Island. [http://seagrantadm.gso.uri.edu/Baird_08/Abstracts/codiga.pdf].

Pawlowicz, R., B. Beardsley, S. Lentz. 2002. Classical tidal harmonic analysis including error estimates in MATLAB using T-TIDE. *Computers & Geosciences* 28, 929-937.

Powers, C.F. 1953. Circulation in the Newport Bight - Block Island Sound - New York Bight Area. *Status Report No. 25, Contract N6, Office of Naval Research 264, Task 15 NR #083-033.* Cornell University.

Pratt, S.D., C.A. Griscom, R.A. Heavers. 1975. Survey of currents, water turbidity, and benthic biology in the vicinity of Browns Ledge, Rhode Island Sound. *Marine Experiment Station, Graduate School of Oceanography, University of Rhode Island. Kingston, RI.*, 114pp.

Pringle, J.M. 2006. Sources of variability in Gulf of Maine circulation, and the observations needed to model it *Deep-Sea Research-II* 53(23-24)

2457-2476.

Raytheon. 1975. Charlestown Hydrographic Study, April 1974 to April 1975. *Final Technical Report, Prepared for Yankee Atomic Electric Company, Westborough, Massachusetts.*

Riley, G.A. 1952. Hydrography of the Long Island and Block Island Sounds. *Bulletin of the Bingham Oceanographic Collection* 3, Article 3.

SAIC. 2005. Disposal Plume Tracking and Assessment at the Rhode Island Sound Disposal Site, Spring 2004. *US Army Corps of Engineers, New England District, Concord, MA.* DAMOS Contribution No. 166., 184pp.

Saila, S.B., S.D. Pratt, T.T. Polgar. 1972. Dredge spoil disposal in Rhode Island Sound *University of Rhode Island, Kingston, RI.*, 48pp.

Shchepetkin, A.F., J.C. McWilliams. 2005. The Regional Ocean Modeling System (ROMS): A split-explicit, free-surface, topography-following coordinates ocean model. *Ocean Modelling* 9(4), 347-404.

Shonting, D., D. Cook. 1970. On the seasonal distribution of temperature and salinity in Rhode Island Sound. *Limnol. & Oceanogr.* 15, 100-112.

Shonting, D.H., D. Cook, F.G. Wyatt. 1966. Seasonal distribution of oceanographic variables in Rhode Island Sound during 1963-1964, A data report. . *CONSEC No. 423, Naval Underwater Weapons Research Engineering Station, Newport, R.I.,* 121pp.

Shonting, D.H. 1969. Rhode Island Sound Square Kilometer Study 1967 - Flow Patterns and Kinetic Energy Distribution. *Journal of Geophysical Research* 74, 3386-&.

Signell, R., J. List, A. Farris. 2000. Bottom Currents and Sediment Transport in Long Island Sound: A Modeling Study. *Journal of Coastal Research* 16, 551-566.

Signell, R.P. 1987. Tide- and Wind-Forced Currents in Buzzards Bay, Massachusetts. *M.S. Thesis.* Massachusetts Institute of Technology, 86 pp.

Simpson, J.H., J.R. Hunter. 1974. Fronts in the Irish Sea. *Nature* 250, 404-406.

Snooks, J.H., J.P. Jacobson, W.P. Kramer. 1977. Summary of temperature and salinity observations in Block Island Sound during July 1975 through September 1976. *Prepared for New England Power Company / Yankee Atomic Electric Company, Westborough, Mass.*

Snooks, J.H., J.P. Jacobsen. 1979. Currents and Residual Drift in Block Island Sound during the Period February through December 1977. *Yankee Atomic Electric Company, Environmental Sciences Group. Westborough, MA.*

Soulsby, R.L. 1990. Tidal-current boundary layers. In: Le Mehaute, B., Hanes, D.M (Ed.), The Sea; Ocean Engineering Science Vol. 9A, Wiley-Interscience, New York, pp. 523-566.

Spaulding, M.L., R.B. Gordon. 1982. A nested numerical tidal model of the southern New England bight. *Ocean Engineering* 9(2), 107-126.

Spaulding, M.L., T. Opishinksi, S. Haynes. 1996. COASTMAP: an integrated monitoring and modeling system to support oil spill response. *Spill Science and Technology Bulletin* 3(3), 149-169.

Ullman, D.S., P.C. Cornillon. 1999. Satellite-derived sea surface temperature fronts on the continental shelf off the northeast US coast. *J. Geophys. Res.-Oceans* 104, 23459-23478.

Ullman, D.S., P.C. Cornillon. 2001. Continental shelf surface thermal fronts in winter off the northeast US coast. *Continental Shelf Research* 21, 1139-1156.

Ullman, D.S., D.L. Codiga. 2004. Seasonal variation of a coastal jet in the Long Island Sound outflow region based on HF radar and Doppler current observations. *J. Geophys. Res.* 109, doi:10.1029/2002JC001660.

Ullman, D.S., J. O'Donnell, J. Kohut, T.A. Fake, A. Allen. 2006. Trajectory prediction using HF radar surface currents: Monte Carlo simulations of prediction uncertainties. *Journal of Geophysical Research* 111 (C12005), doi:10.1029/2006JC003715.

URI. 1979. Model-predicted tidal current charts, Long Island Sound to Buzzards Bay. *Marine bulletin (University of Rhode Island)* Kingston, RI. No. 30, 27pp.

USACE. 2002. Final Report: Results of Literature Review and Data Gaps Assessment. US Army Corps of Engineers, Rhode Island Region Long Term Dredge Material Disposal Site Evaluation Project. Contract No. DACW33-01-D-0004, 222pp.

Wilkin, J. 2006. The summertime heat budget and circulation of southeast New England shelf waters. *J. Phys. Oceanogr.* 36, 1997-2011.

Williams, R.G. 1969. The physical oceanography of Block Island Sound. U. S. Navy Underwater Sound Laboratory, New London, Conn.

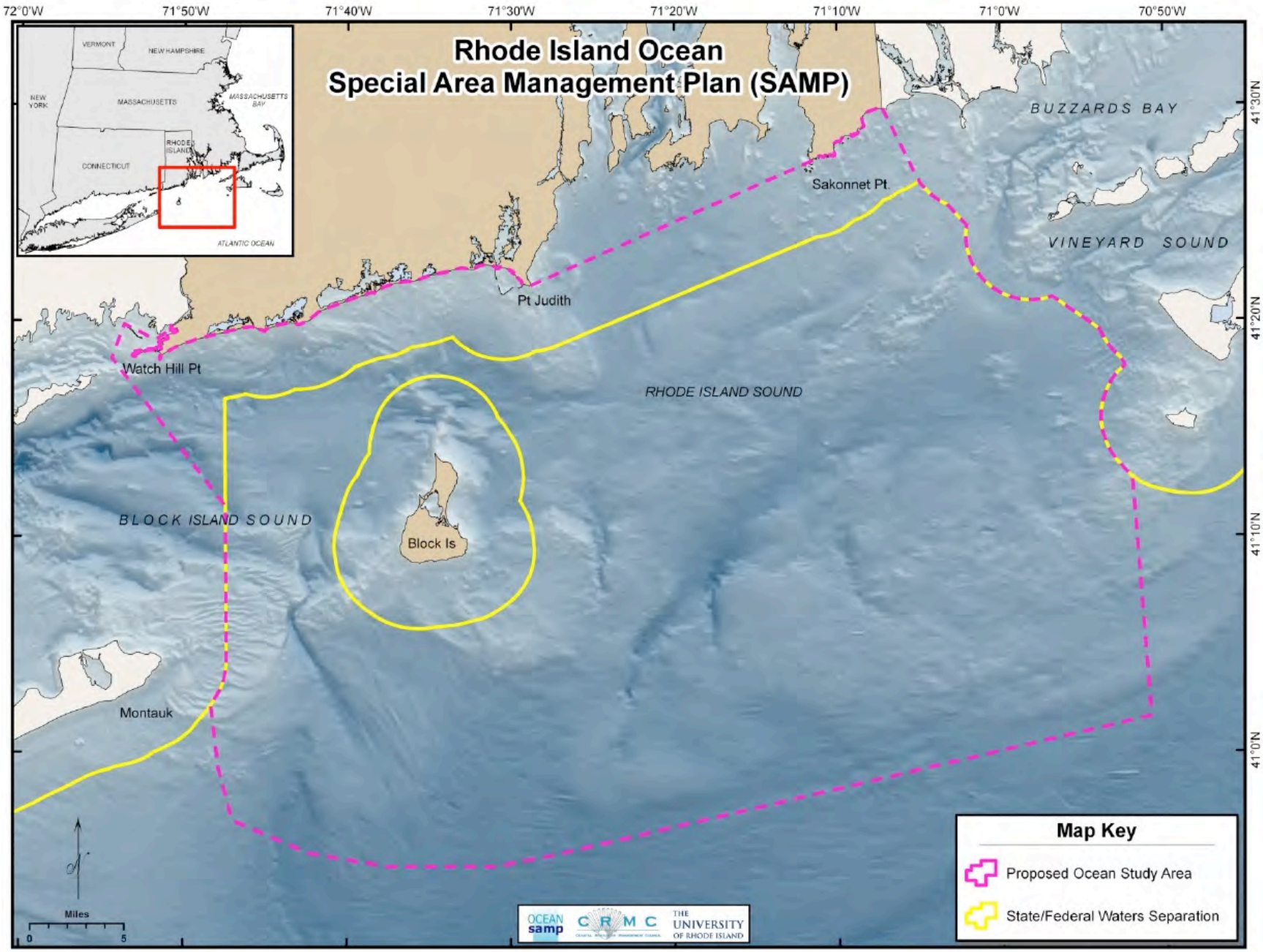

Figure 1. Map of OSAMP domain, boundary marked by dashed magenta line.

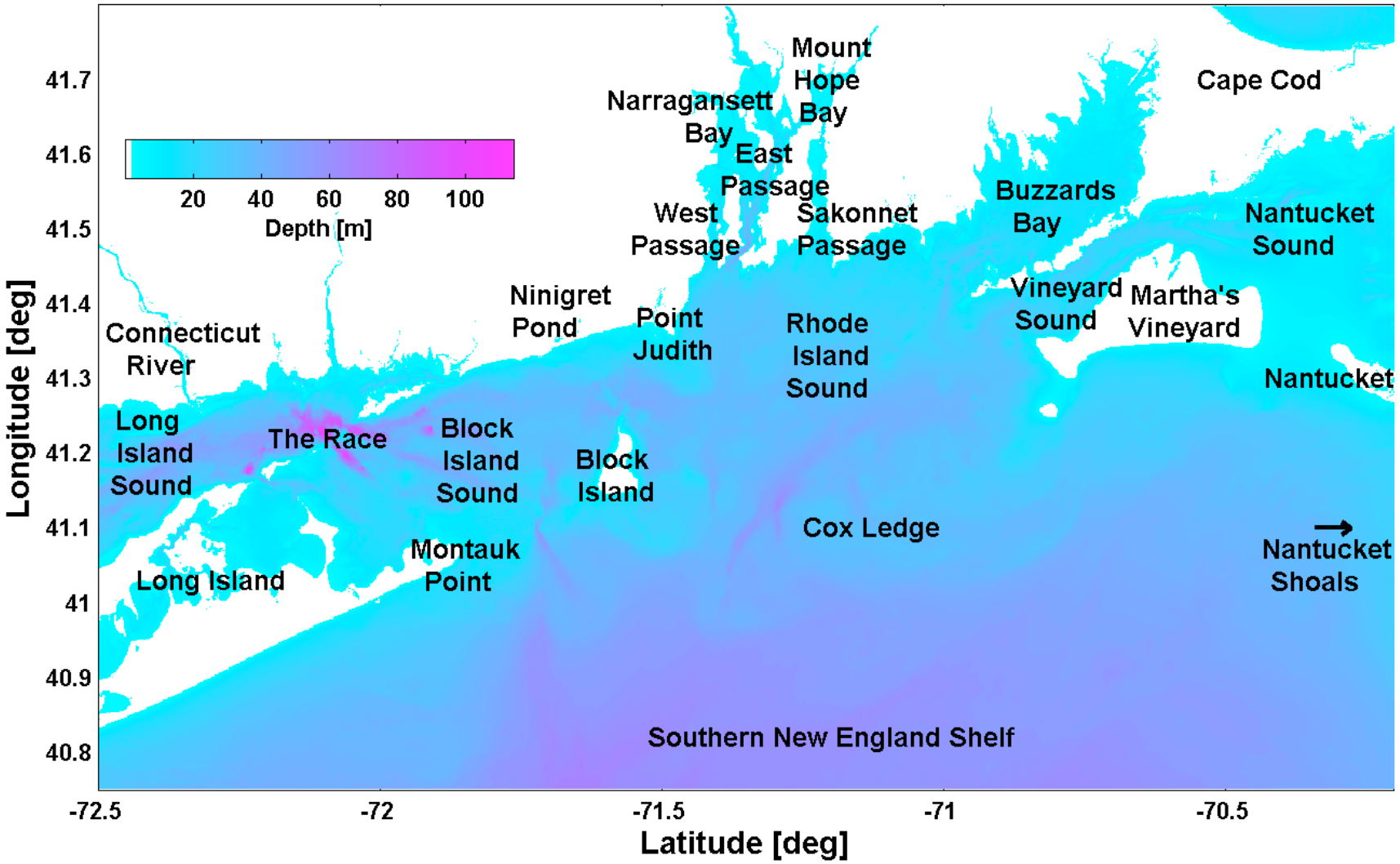

Figure 2. Bathymetry and geographic features of regional setting surrounding OSAMP domain..

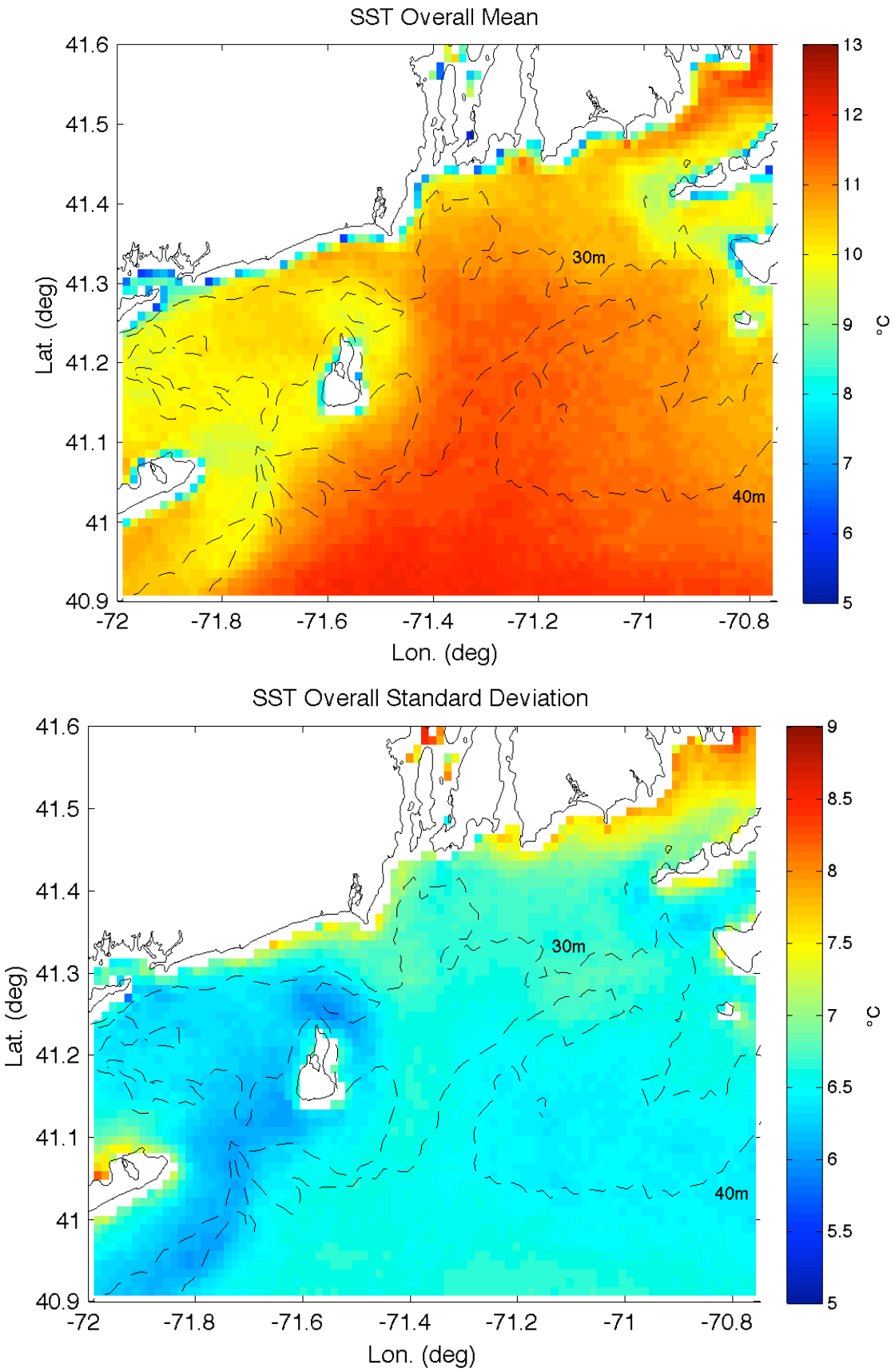

Figure 3. SST: All seasons 2002-2007. (upper) Mean. (lower) Standard deviation.

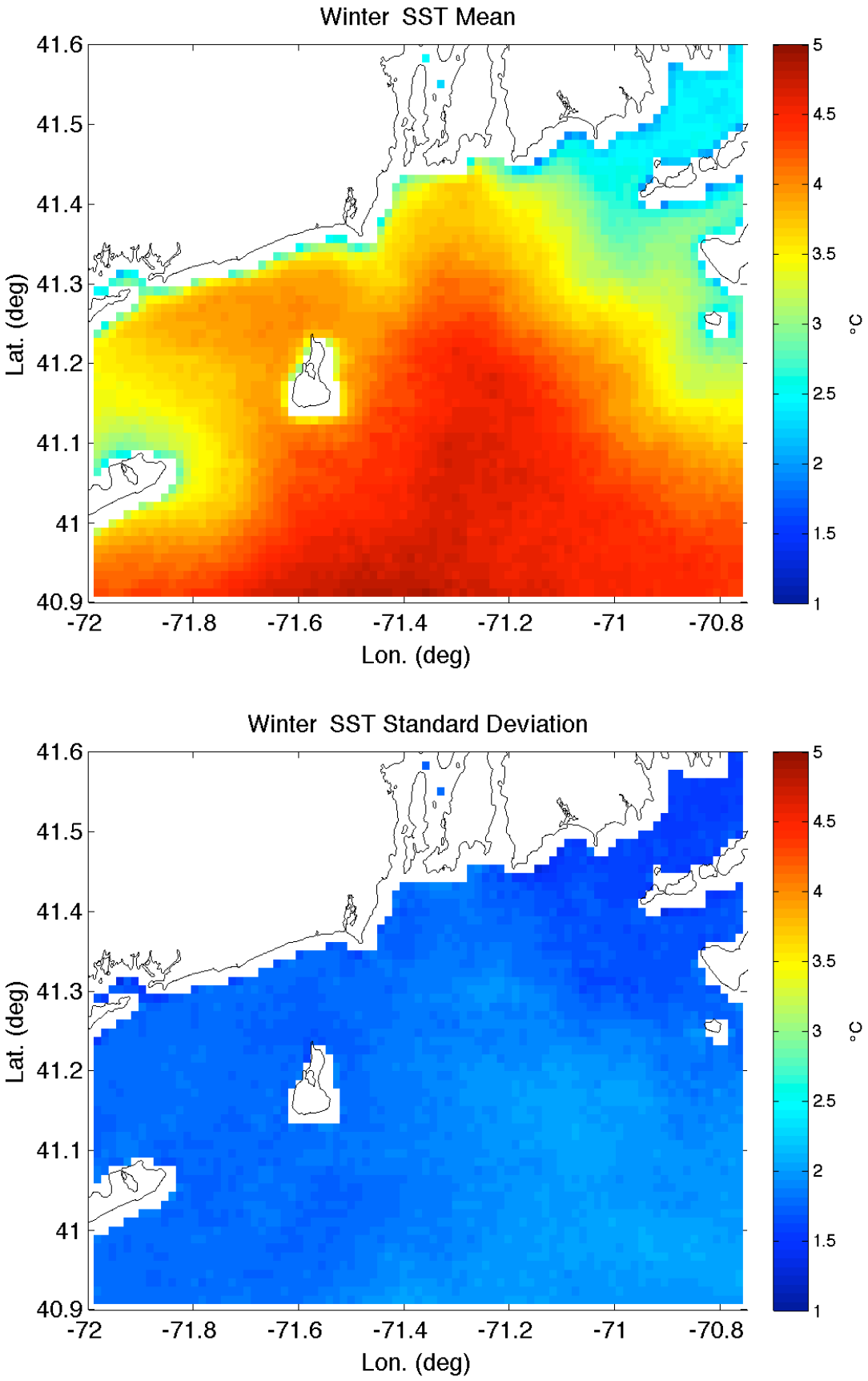

Figure 4. SST: Winter 2002-2007. (upper) Mean. (lower) Standard deviation.

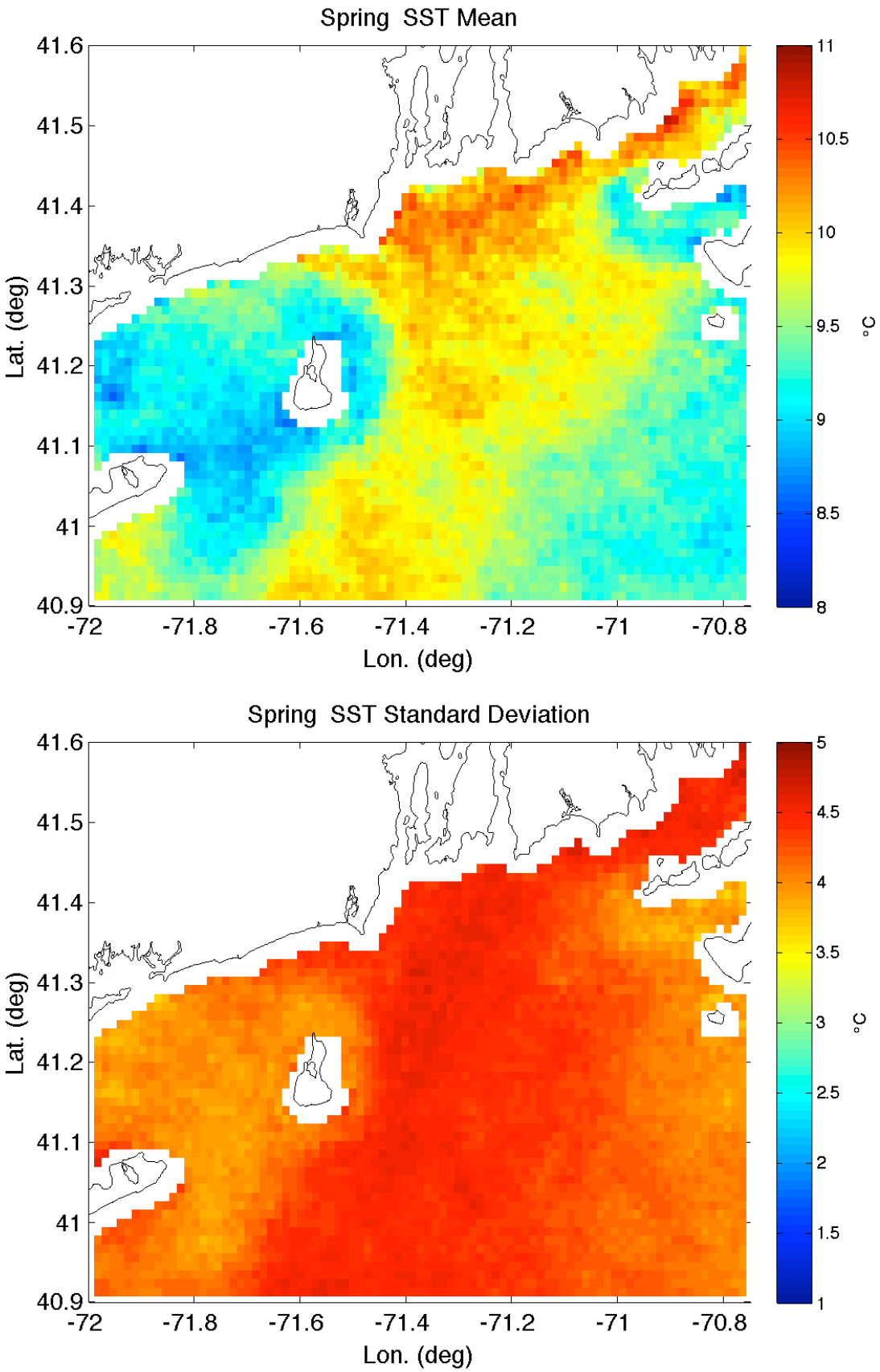

Figure 5. SST: Spring 2002-2007. (upper) Mean. (lower) Standard deviation.

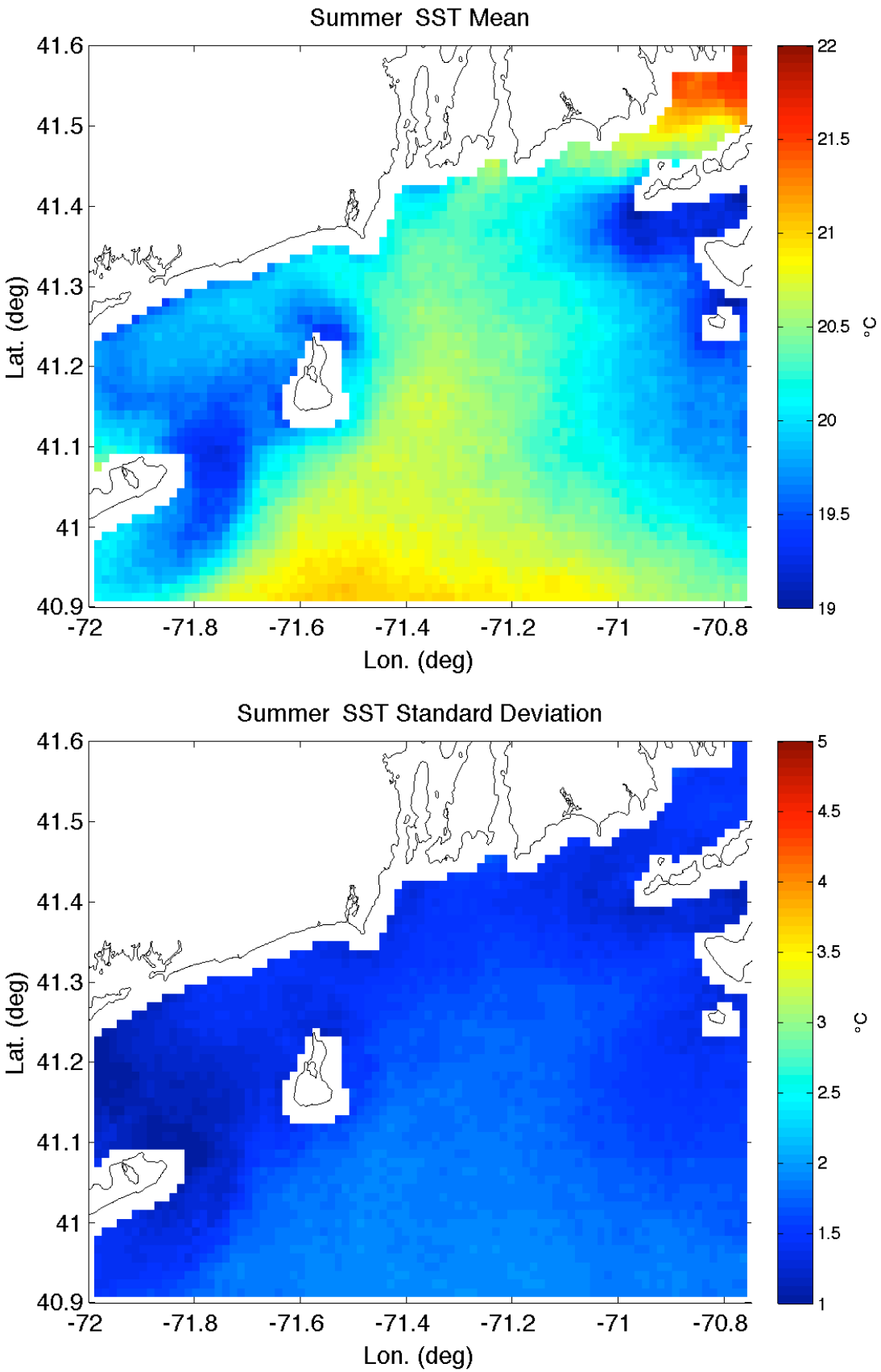

Figure 6. SST: Summer 2002-2007. (upper) Mean. (lower) Standard deviation.

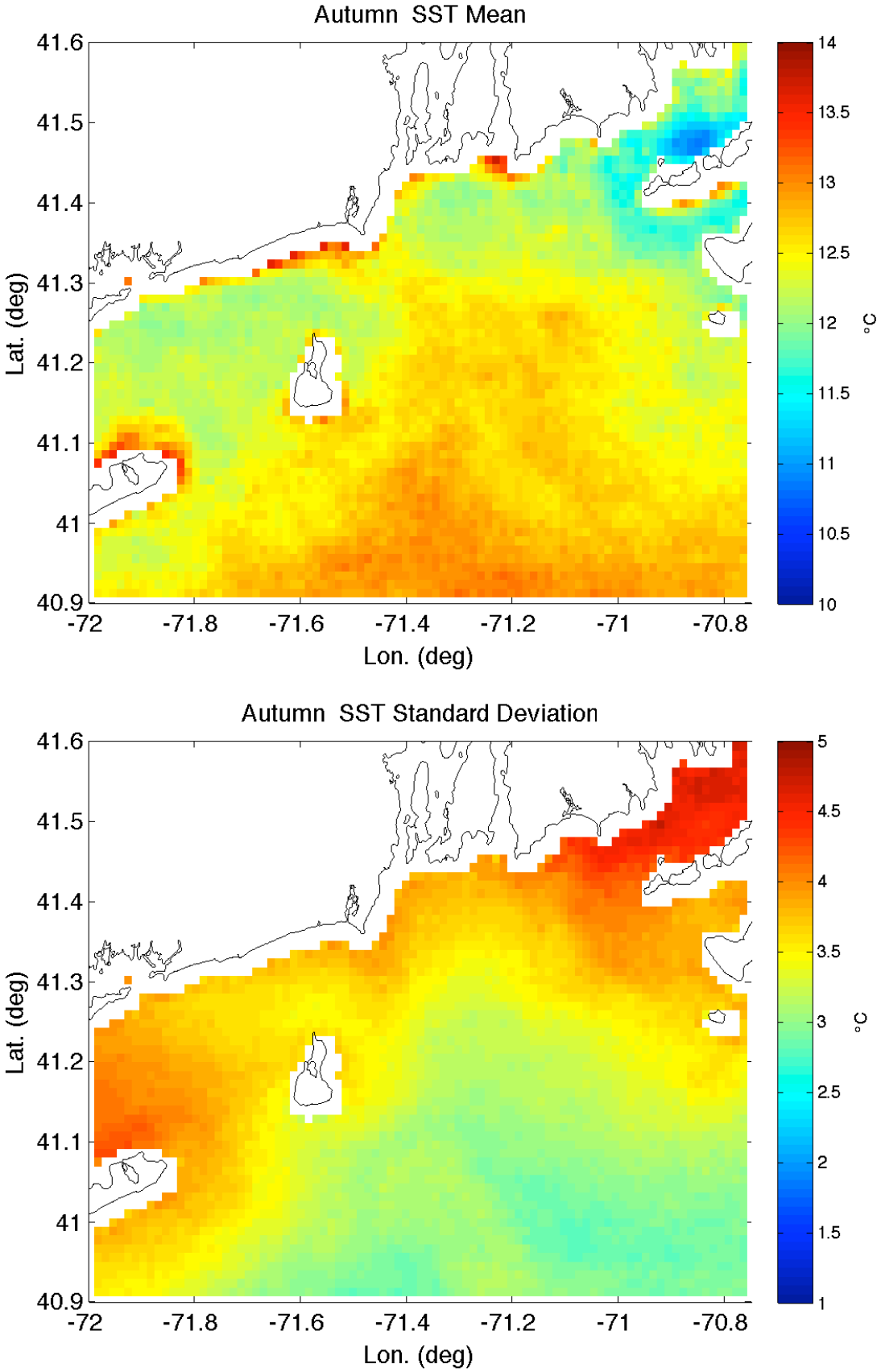

Figure 7. SST: Fall 2002-2007. (upper) Mean. (lower) Standard deviation.

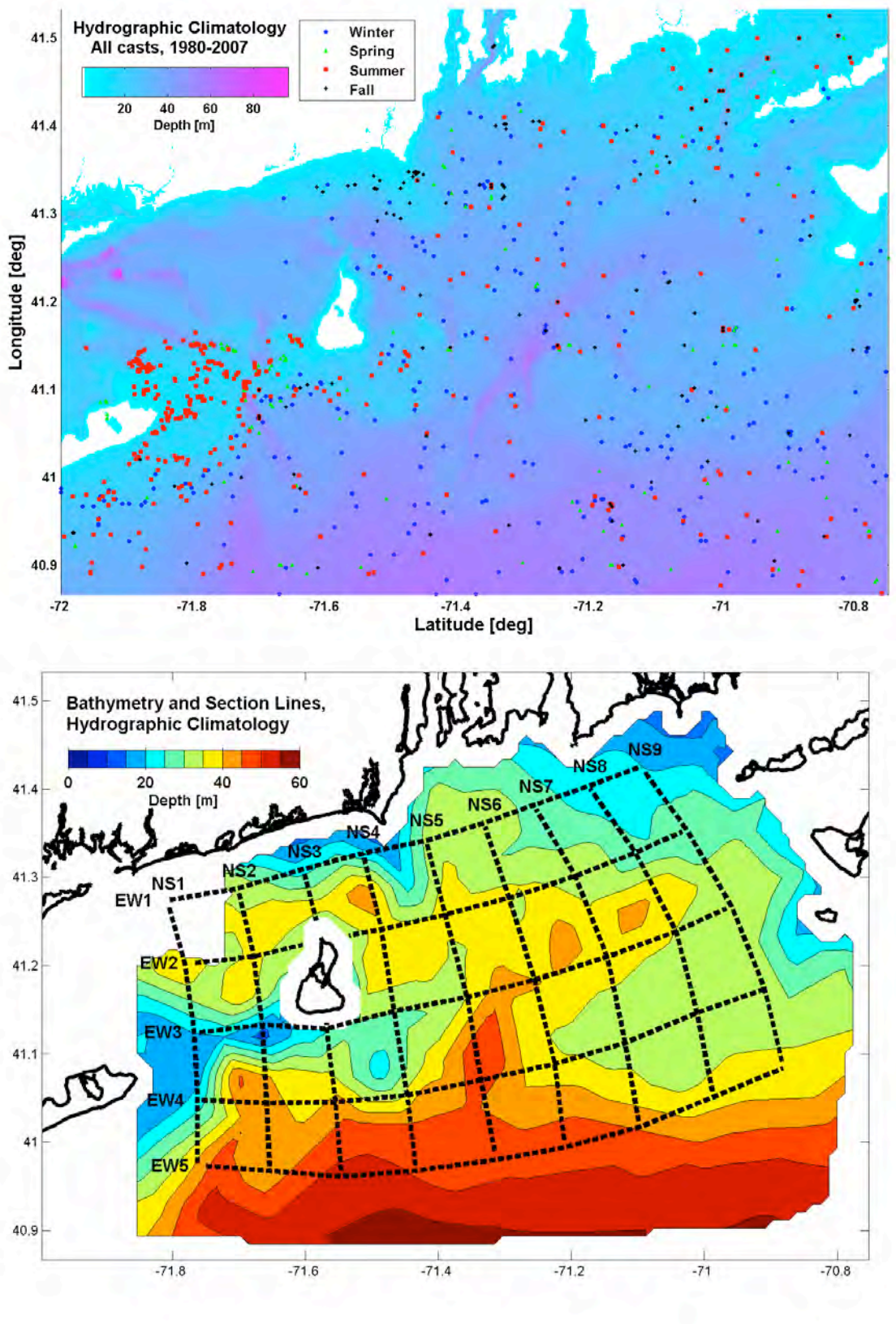

Figure 8. Hydrographic climatology. (upper) Cast locations. (lower) Section lines.

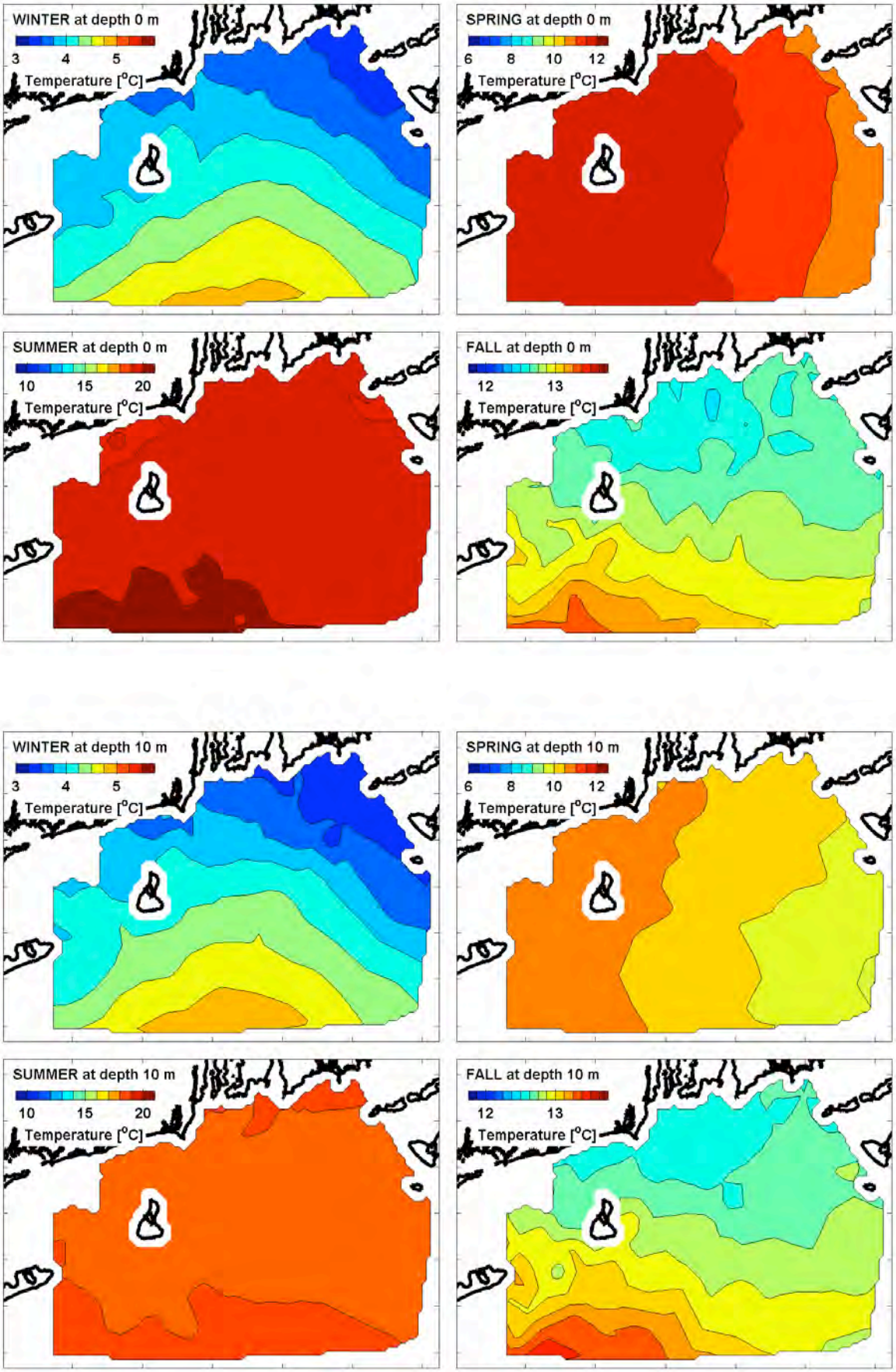

Figure 9. Hydrographic climatology. Temperature. (upper) Surface. (lower) Depth 10 m.

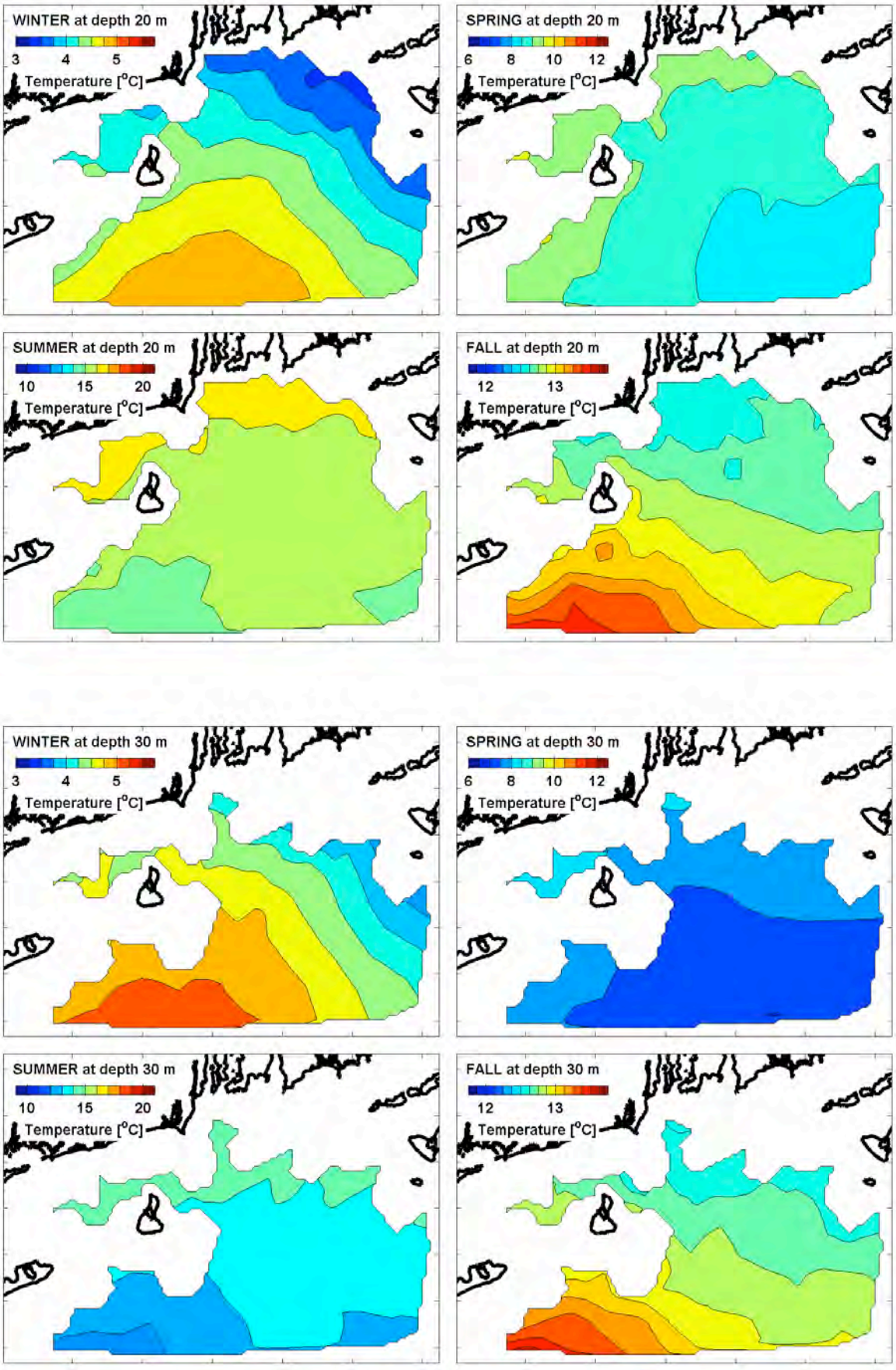

Figure 10. Hydrographic climatology. Temperature. (upper) Depth 20 m. (lower) Depth 30 m.

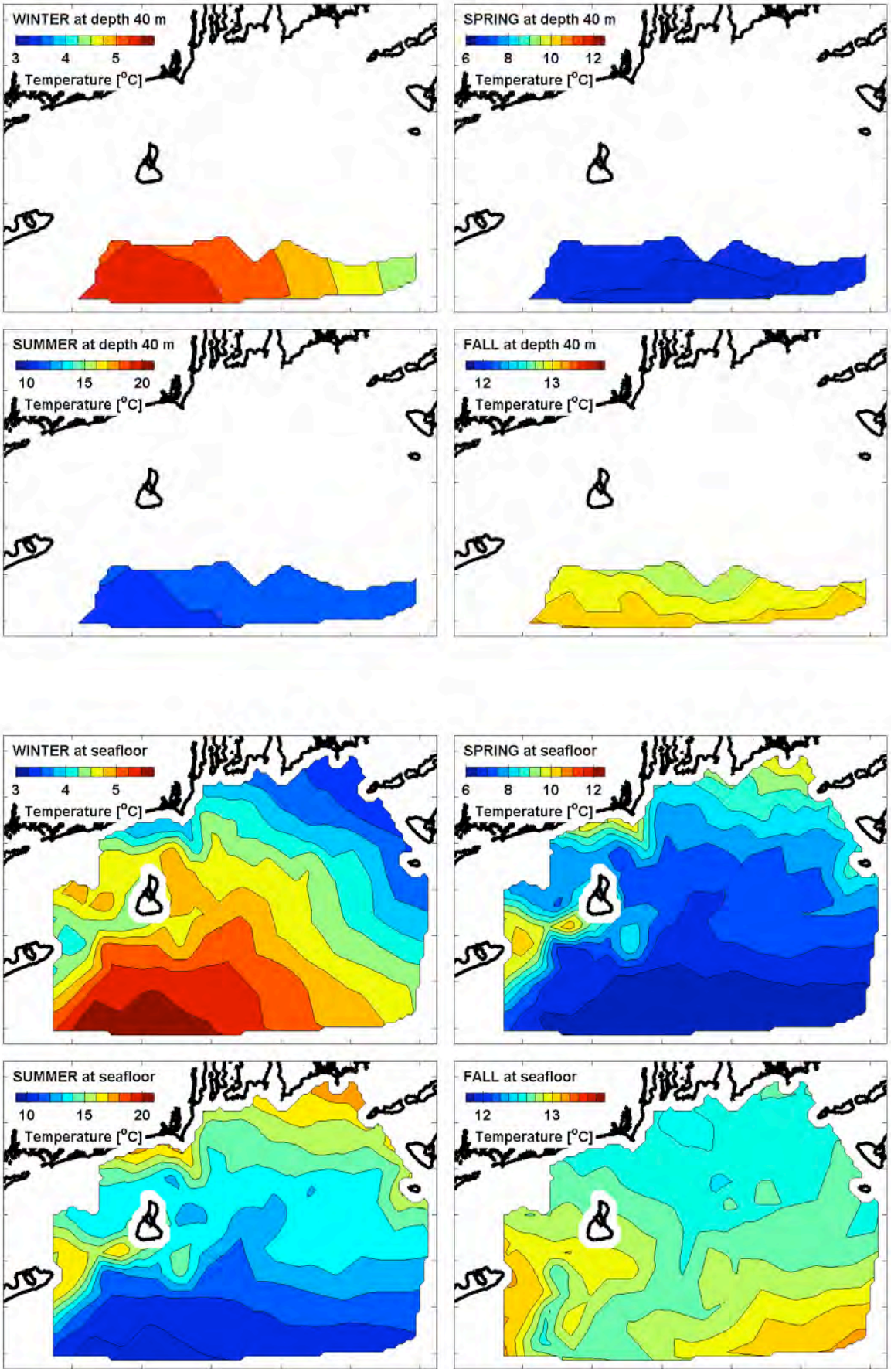

Figure 11. Hydrographic climatology. Temperature. (upper) Depth 40 m. (lower) Seafloor.

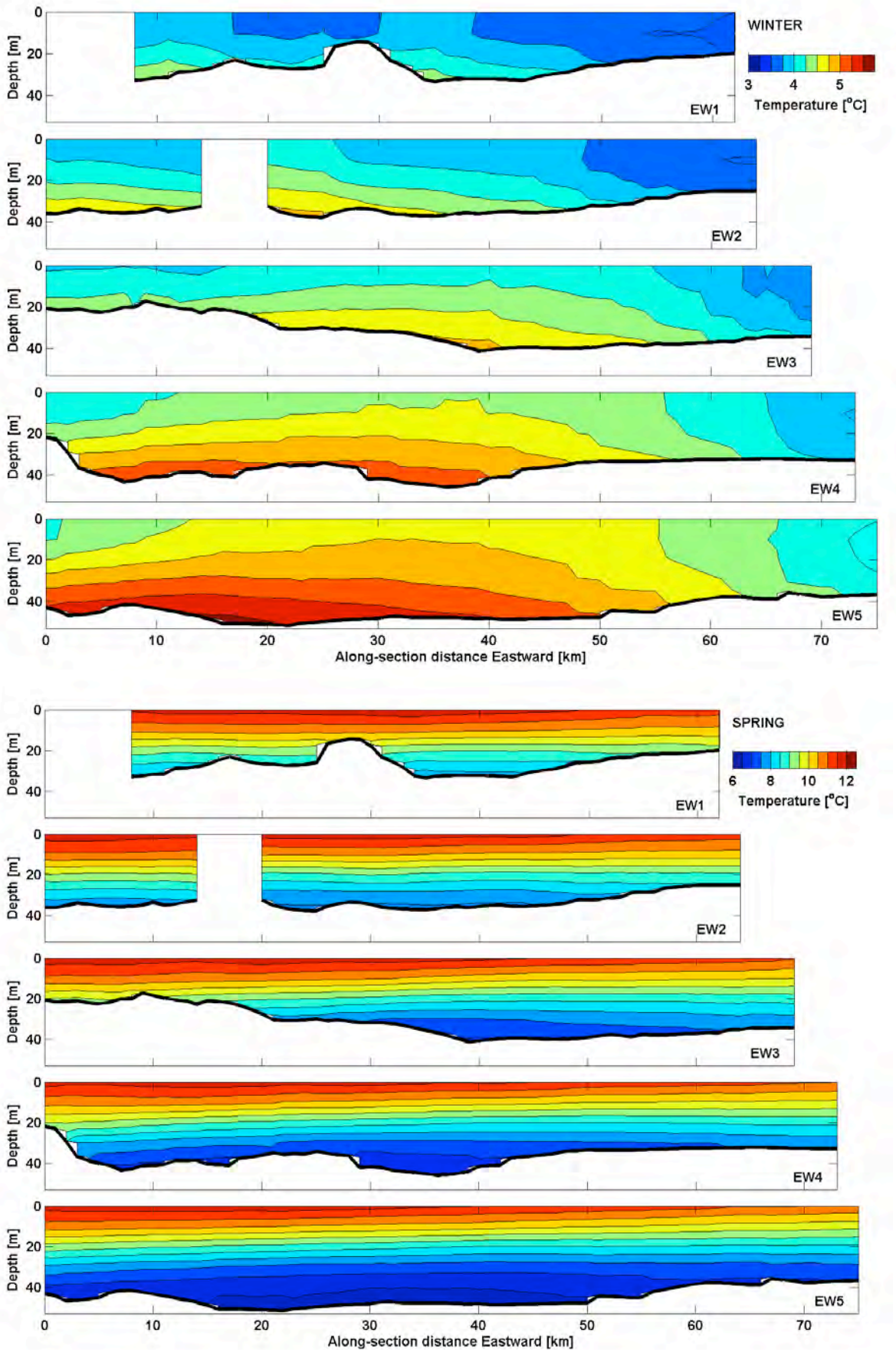

Figure 12. Hydrographic climatology. Temperature. EW. (upper) Winter. (lower) Spring.

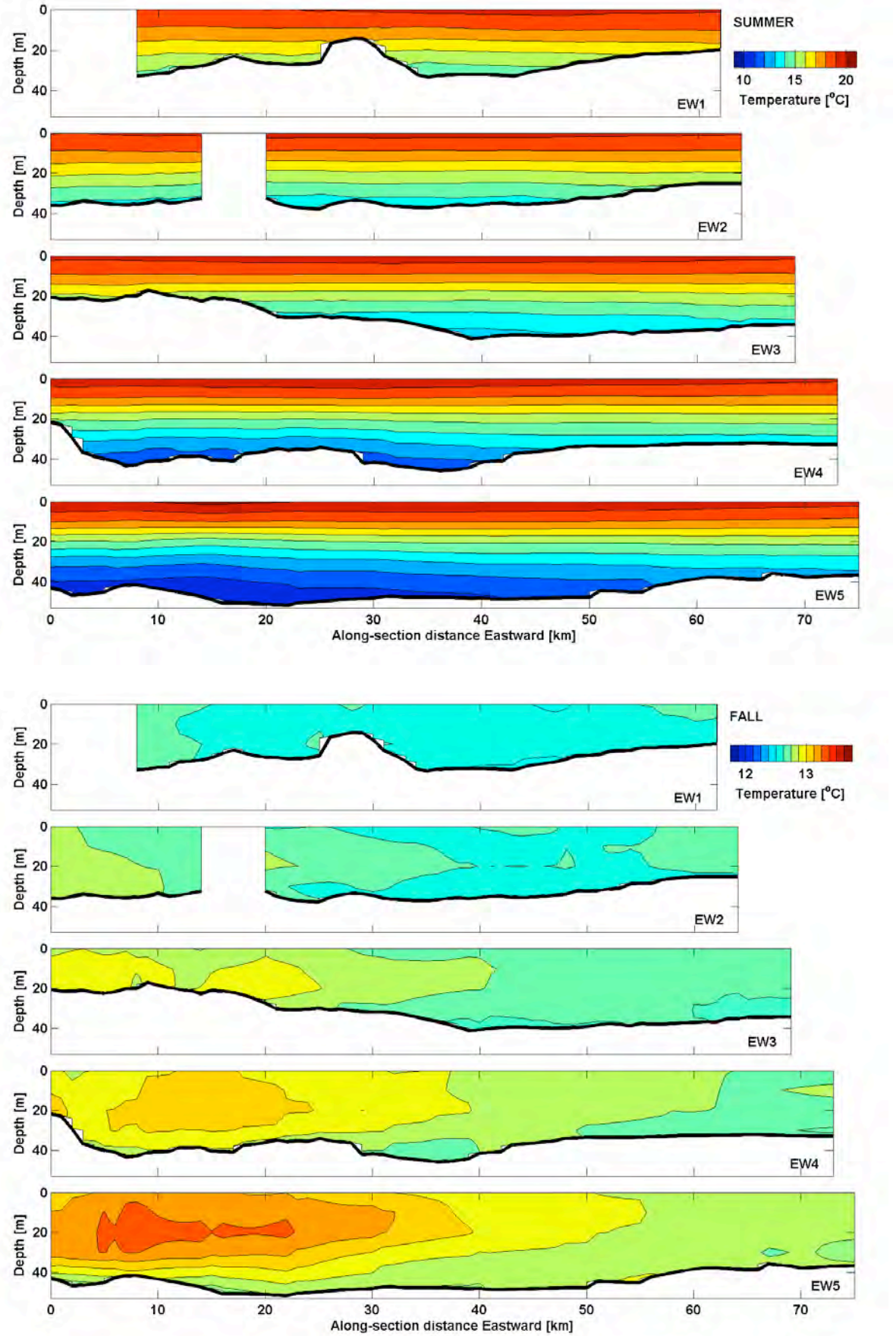

Figure 13. Hydrographic climatology. Temperature. EW. (upper) Summer. (lower) Fall.

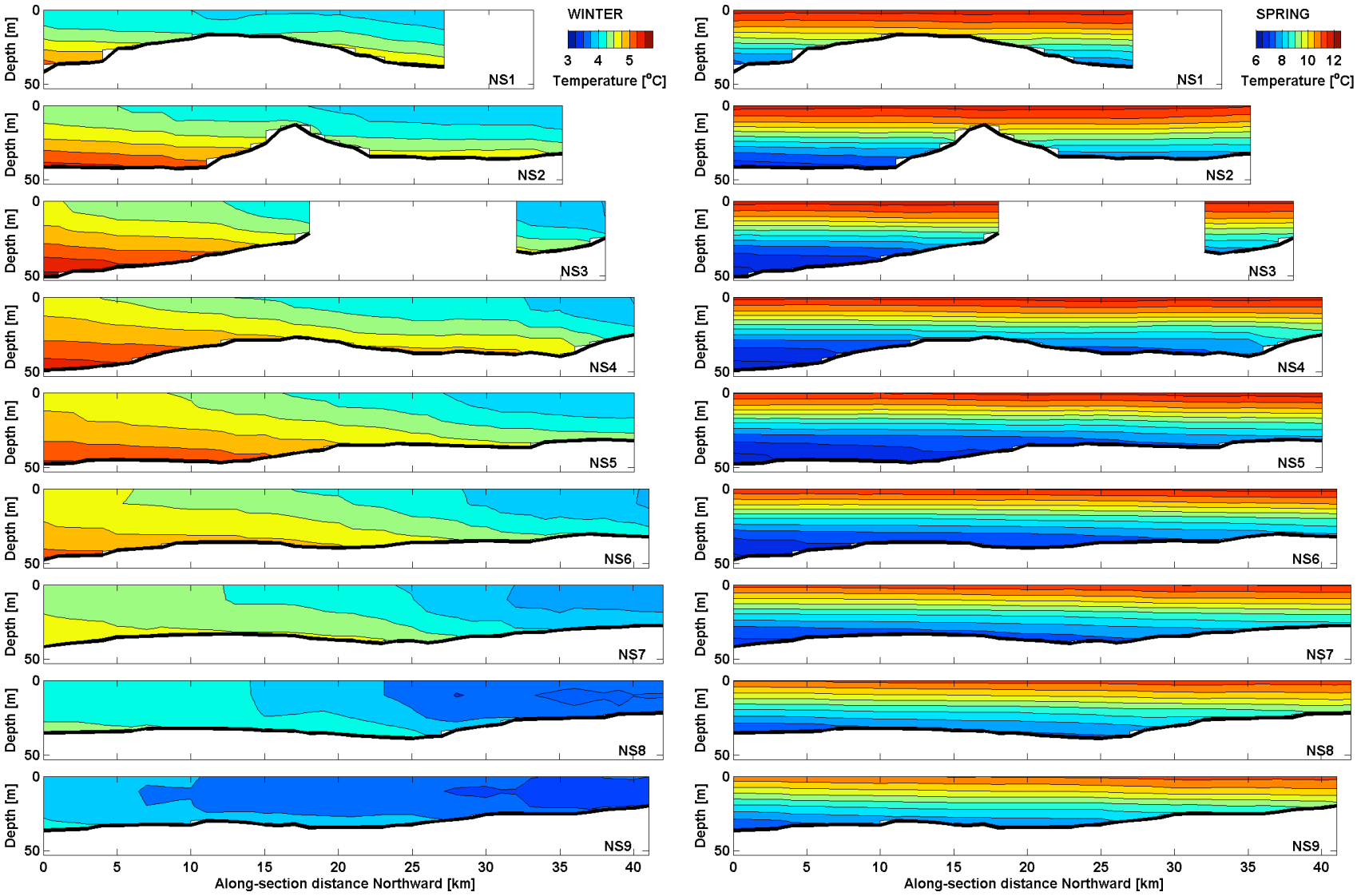

Figure 14. Hydrographic climatology. Temperature. NS. (left) Winter. (right) Spring.

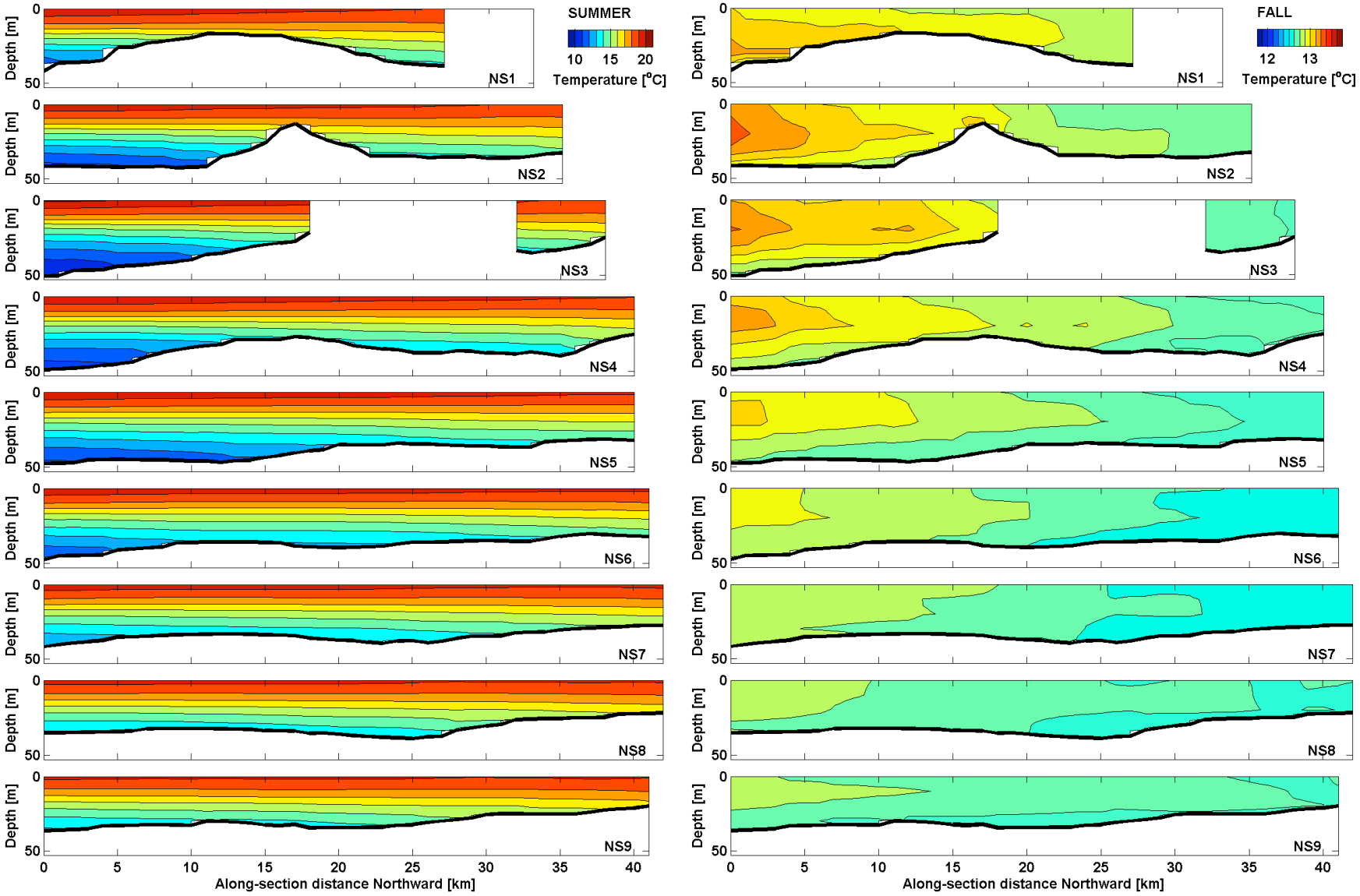

Figure 15. Hydrographic climatology. Temperature. NS. (left) Summer. (right) Fall.

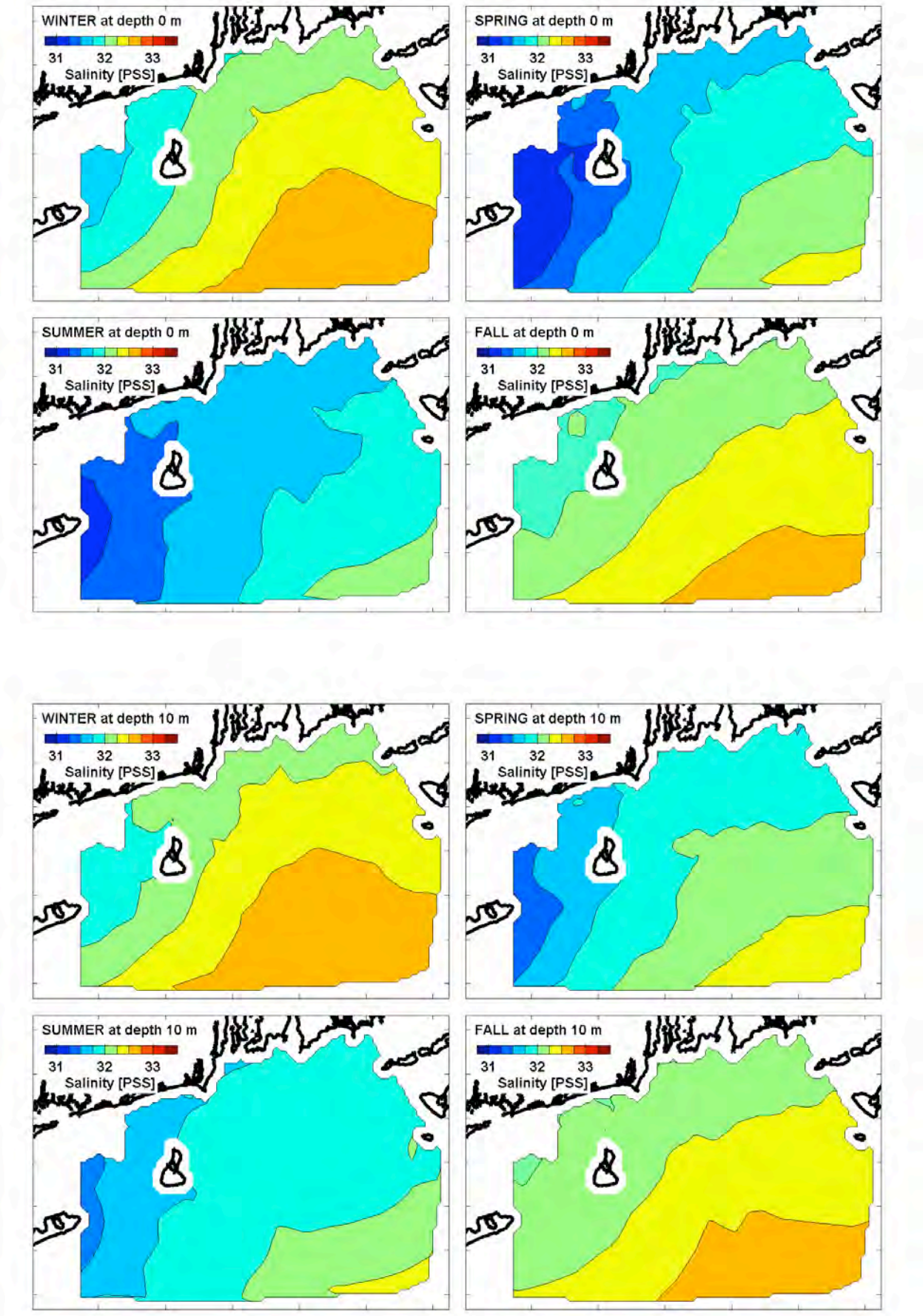

Figure 16. Hydrographic climatology. Salinity. (upper) Surface. (lower) Depth 10 m.

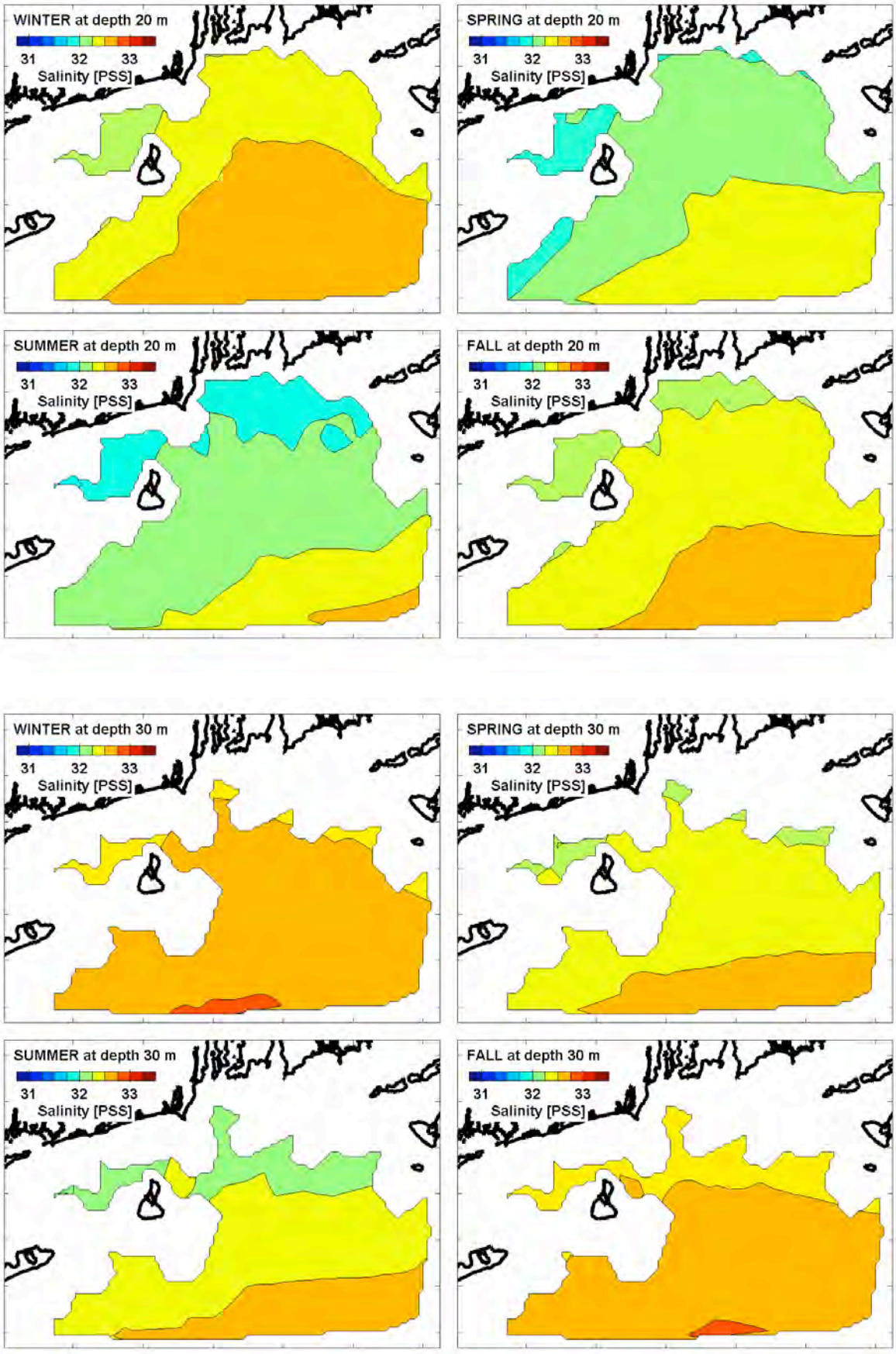

Figure 17. Hydrographic climatology. Salinity. (upper) Depth 20 m. (lower) Depth 30 m.

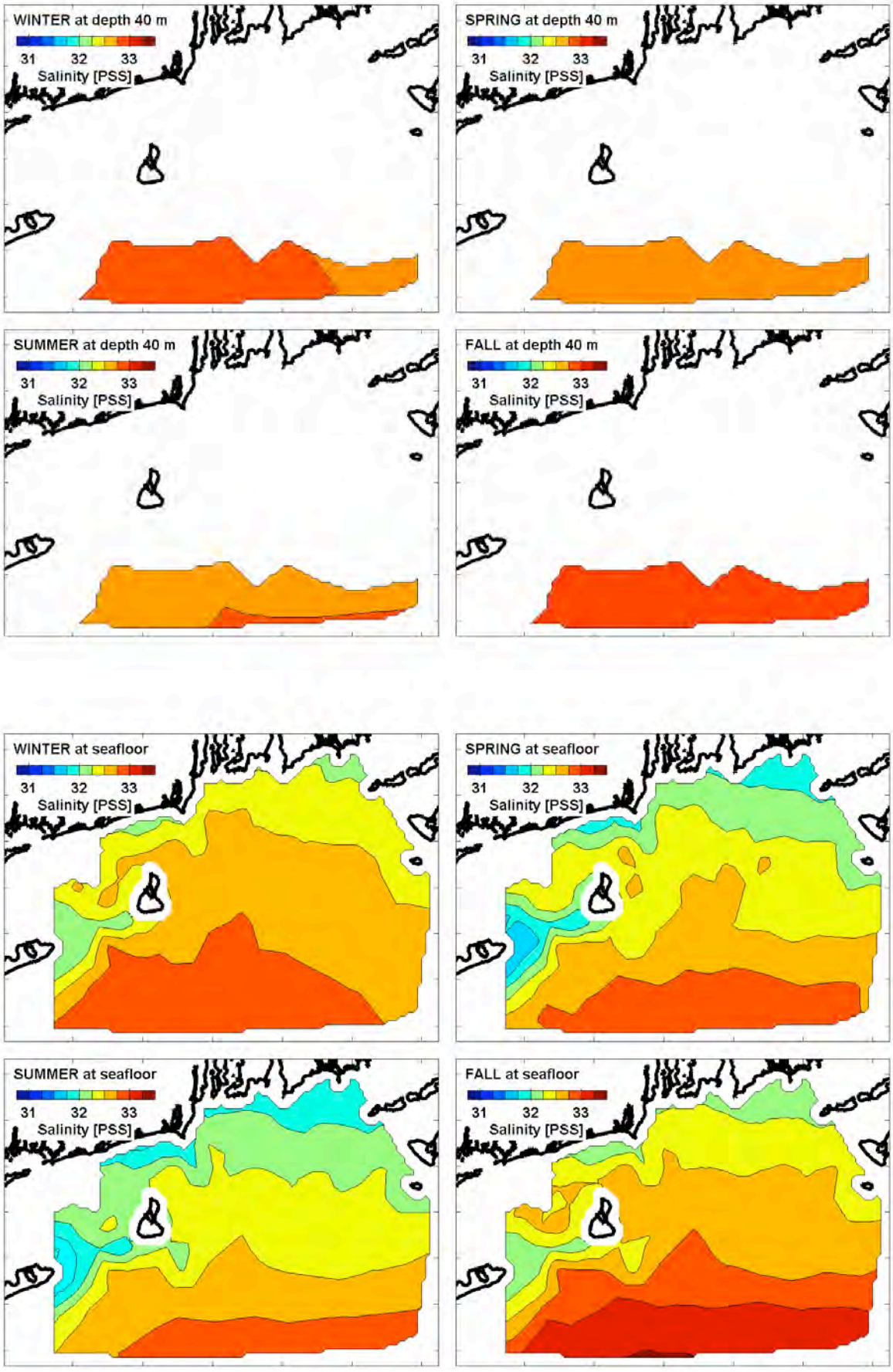

Figure 18. Hydrographic climatology. Salinity. (upper) Depth 40 m. (lower) Seafloor.

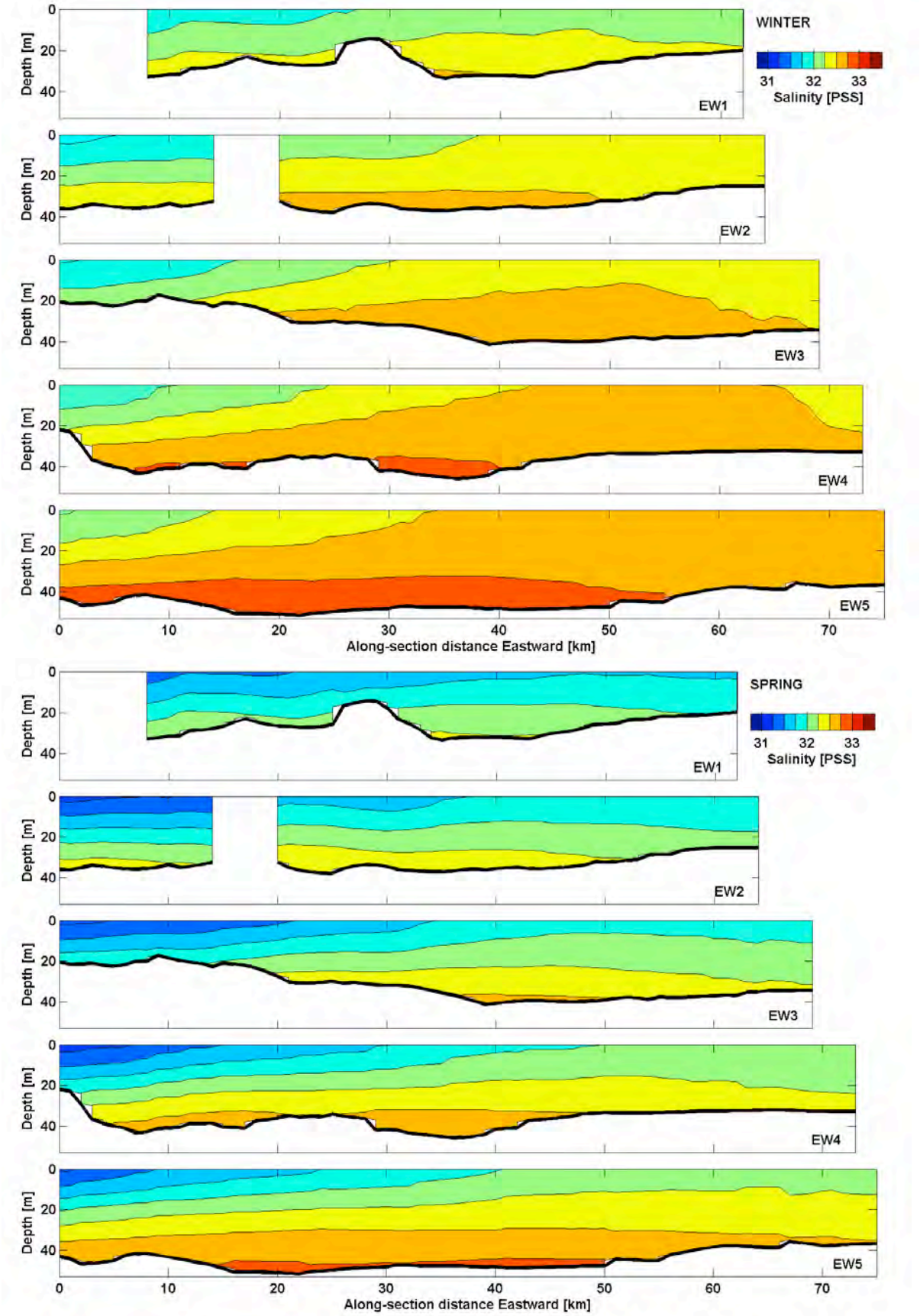

Figure 19. Hydrographic climatology. Salinity. EW. (upper) Winter. (lower) Spring.

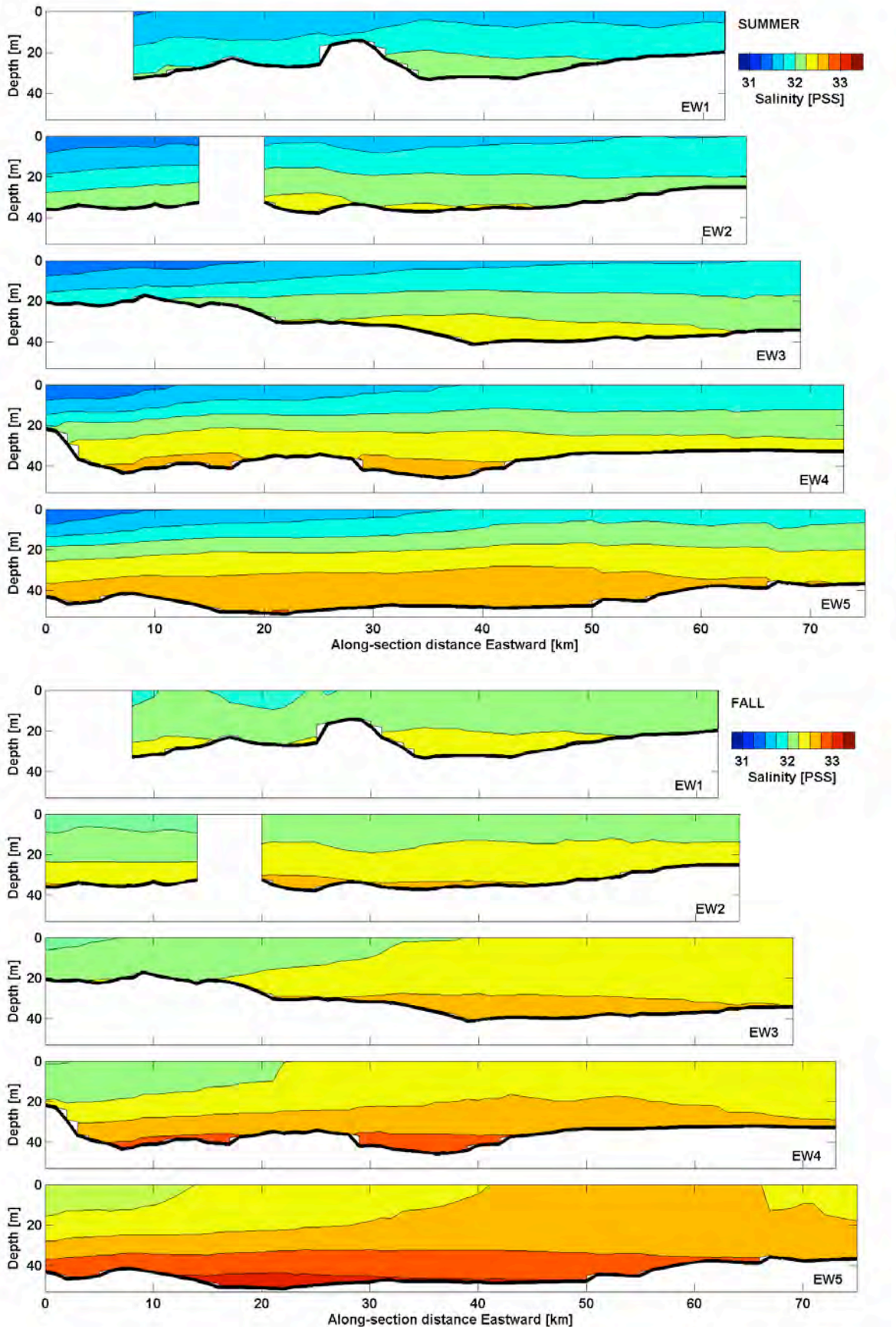

Figure 20. Hydrographic climatology. Salinity. EW. (upper) Summer. (lower) Fall.

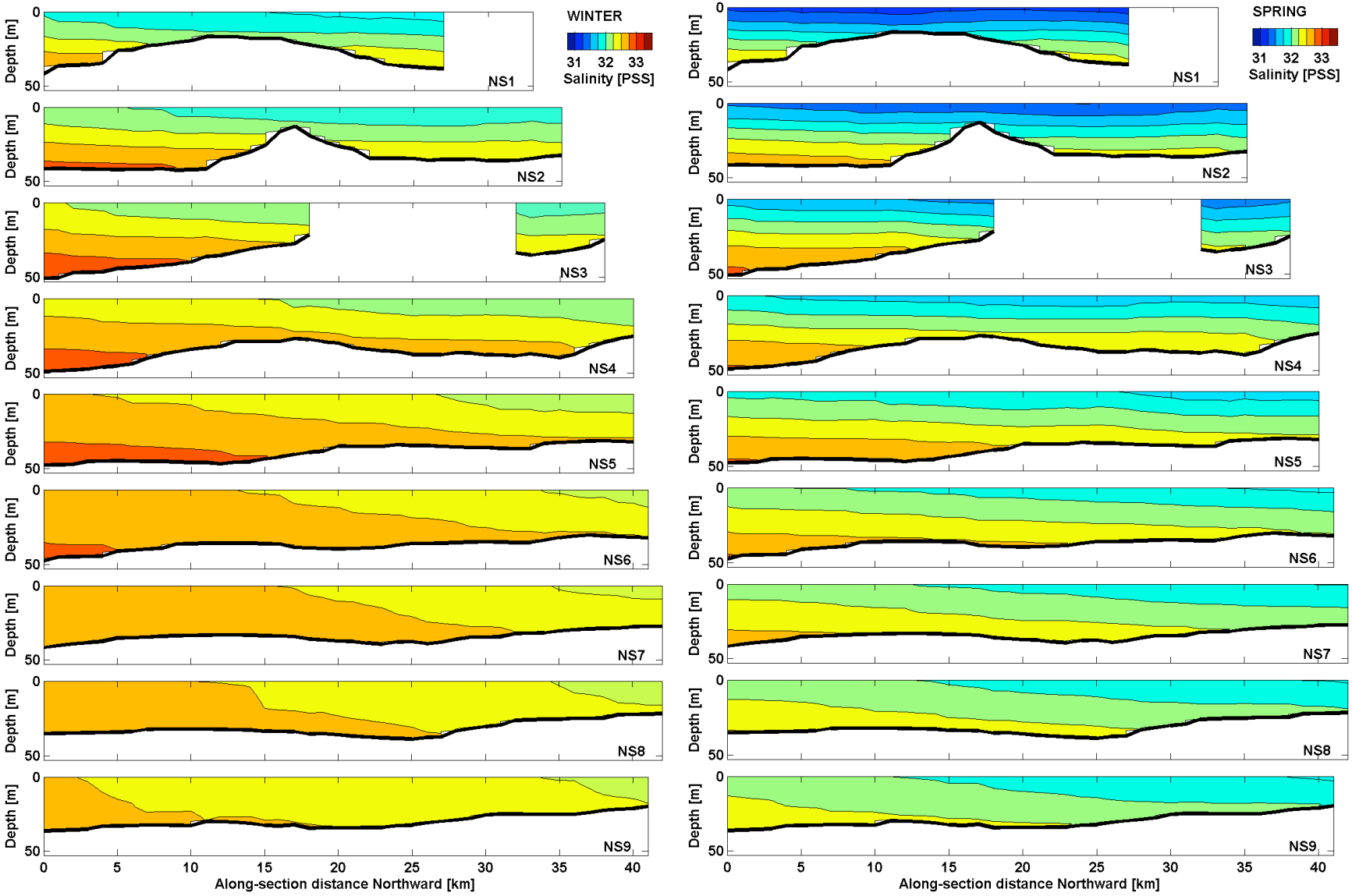

Figure 21. Hydrographic climatology. Salinity. NS. (left) Winter. (right) Spring.

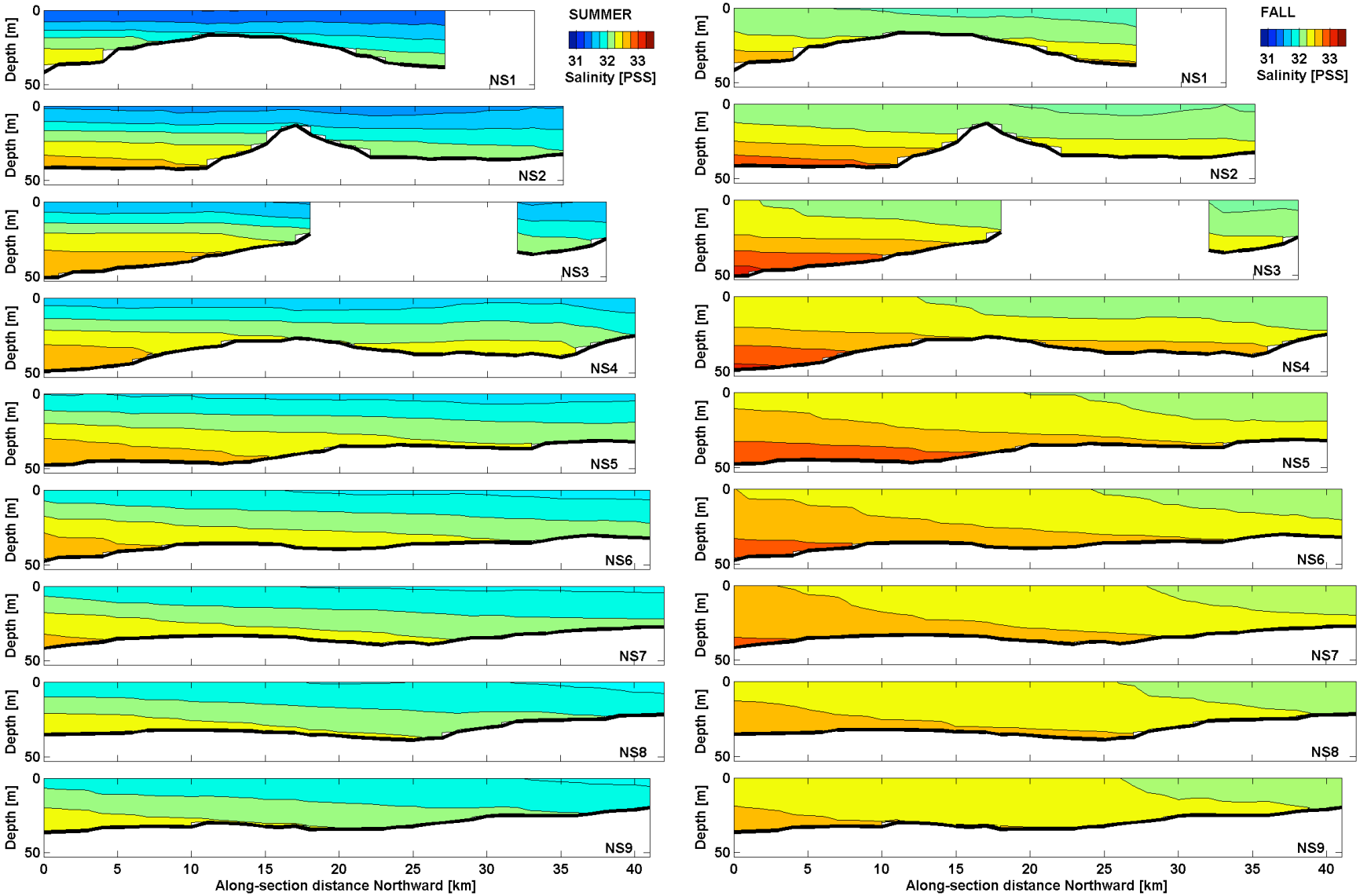

Figure 22. Hydrographic climatology. Salinity. NS. (left) Summer. (right) Fall.

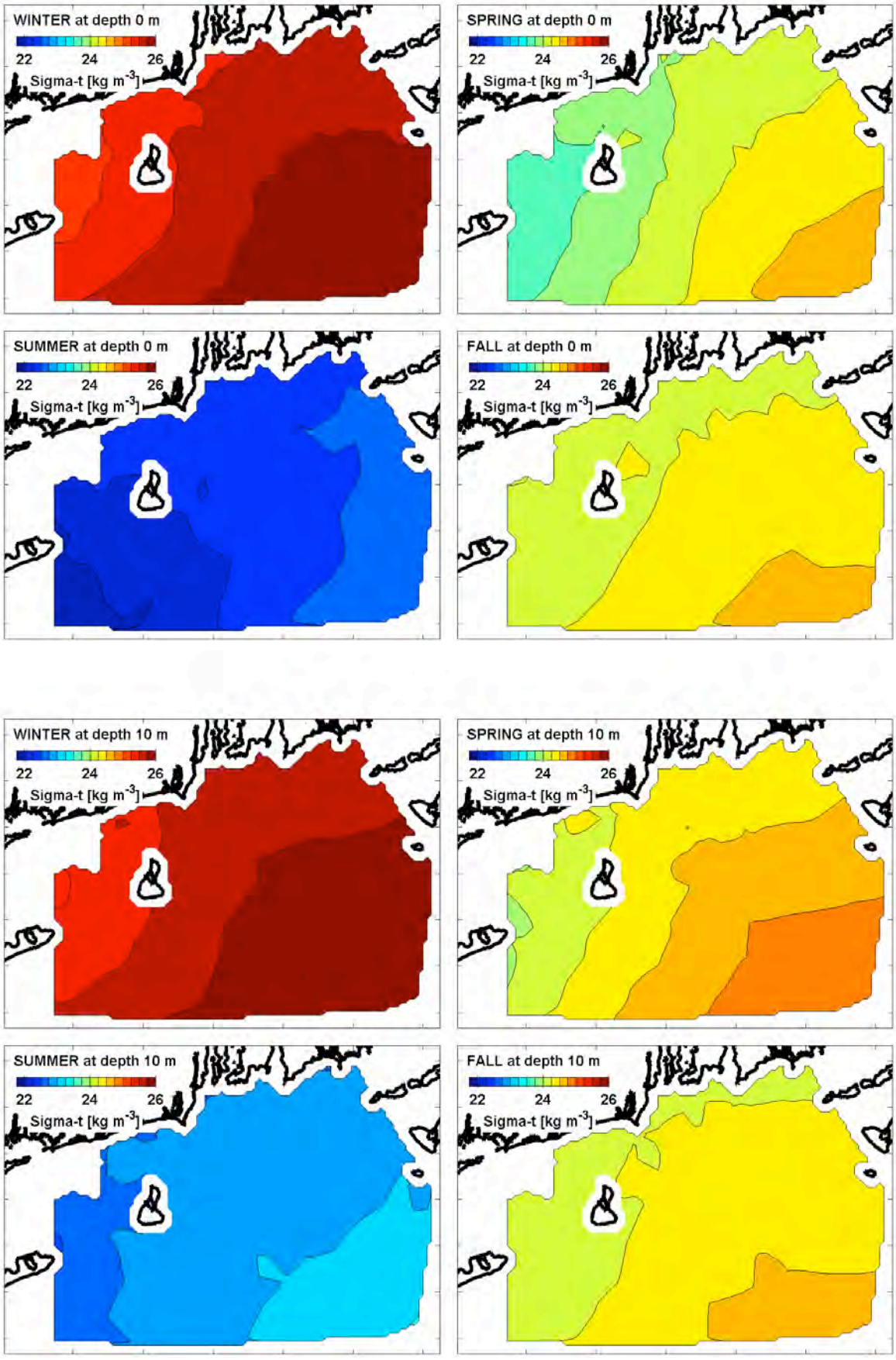

Figure 23. Hydrographic climatology. Density anomaly. (upper) Surface. (lower) Depth 10 m.

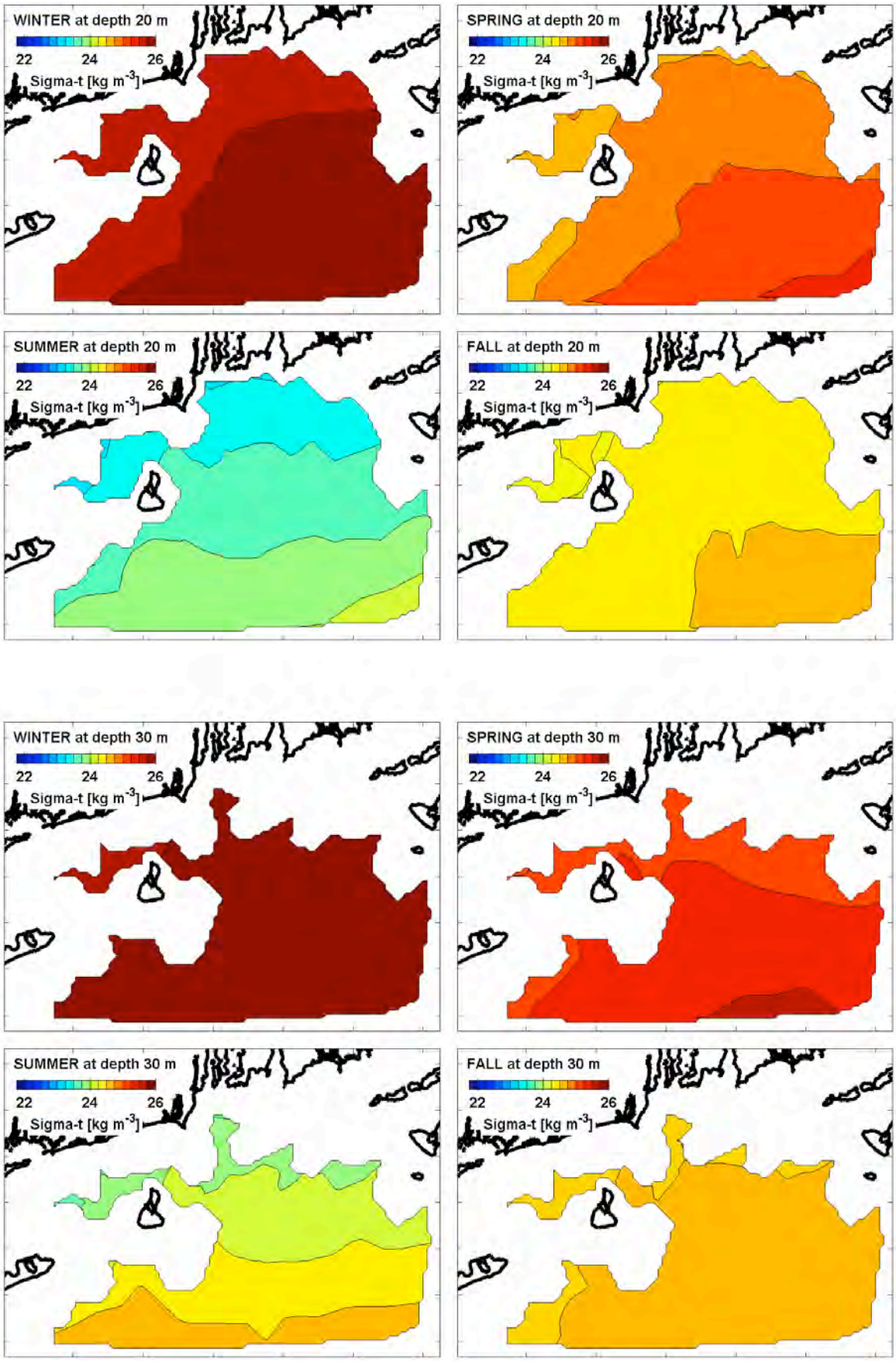

Figure 24. Hydrographic climatology. Density anomaly. (upper) Depth 20 m. (lower) Depth 30 m.

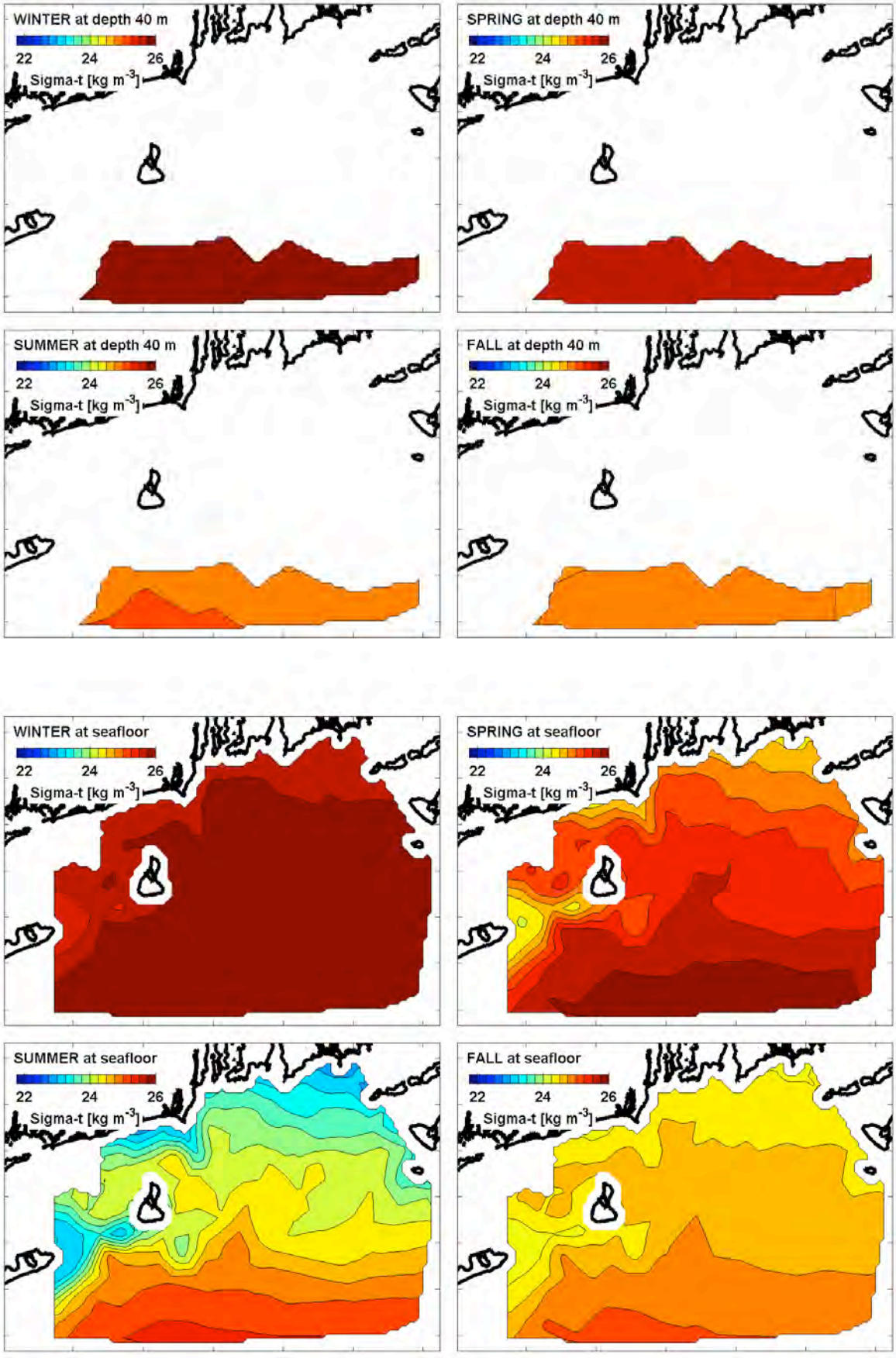

Figure 25. Hydrographic climatology. Density anomaly. (upper) Depth 40 m. (lower) Seafloor.

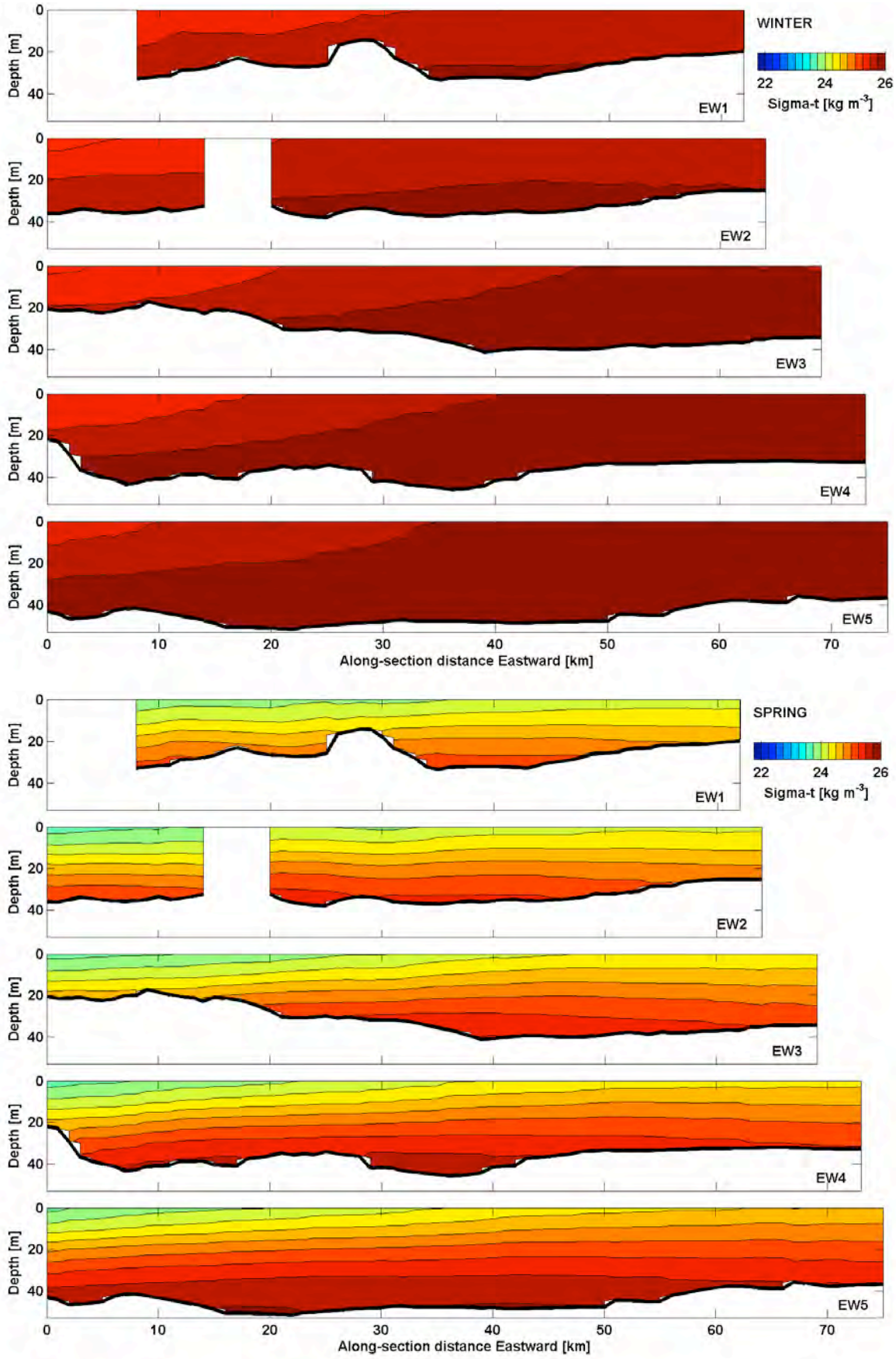

Figure 26. Hydrographic climatology. Density anomaly. EW. (upper) Winter. (lower) Spring.

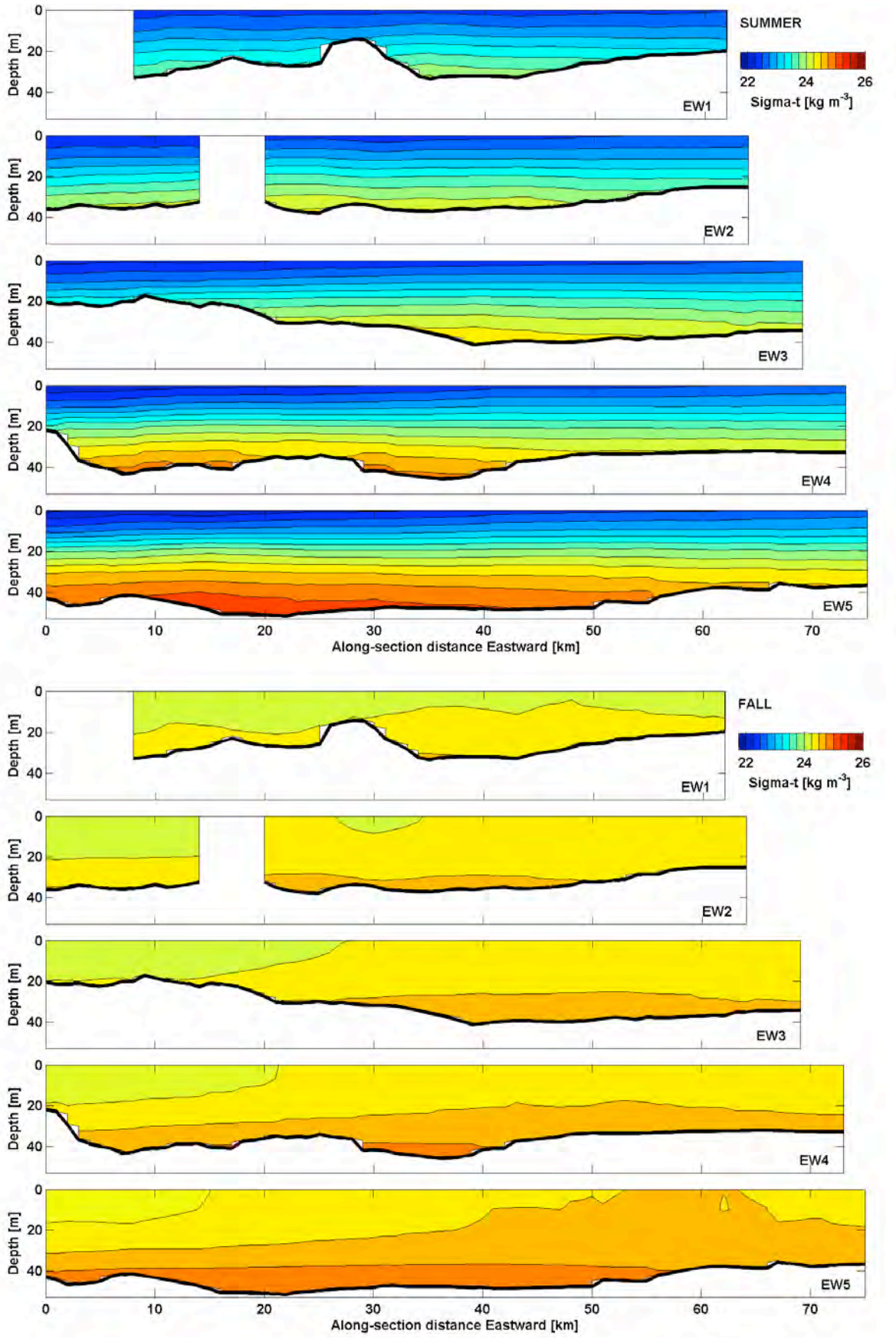

Figure 27. Hydrographic climatology. Density anomaly. EW. (upper) Summer. (lower) Fall.

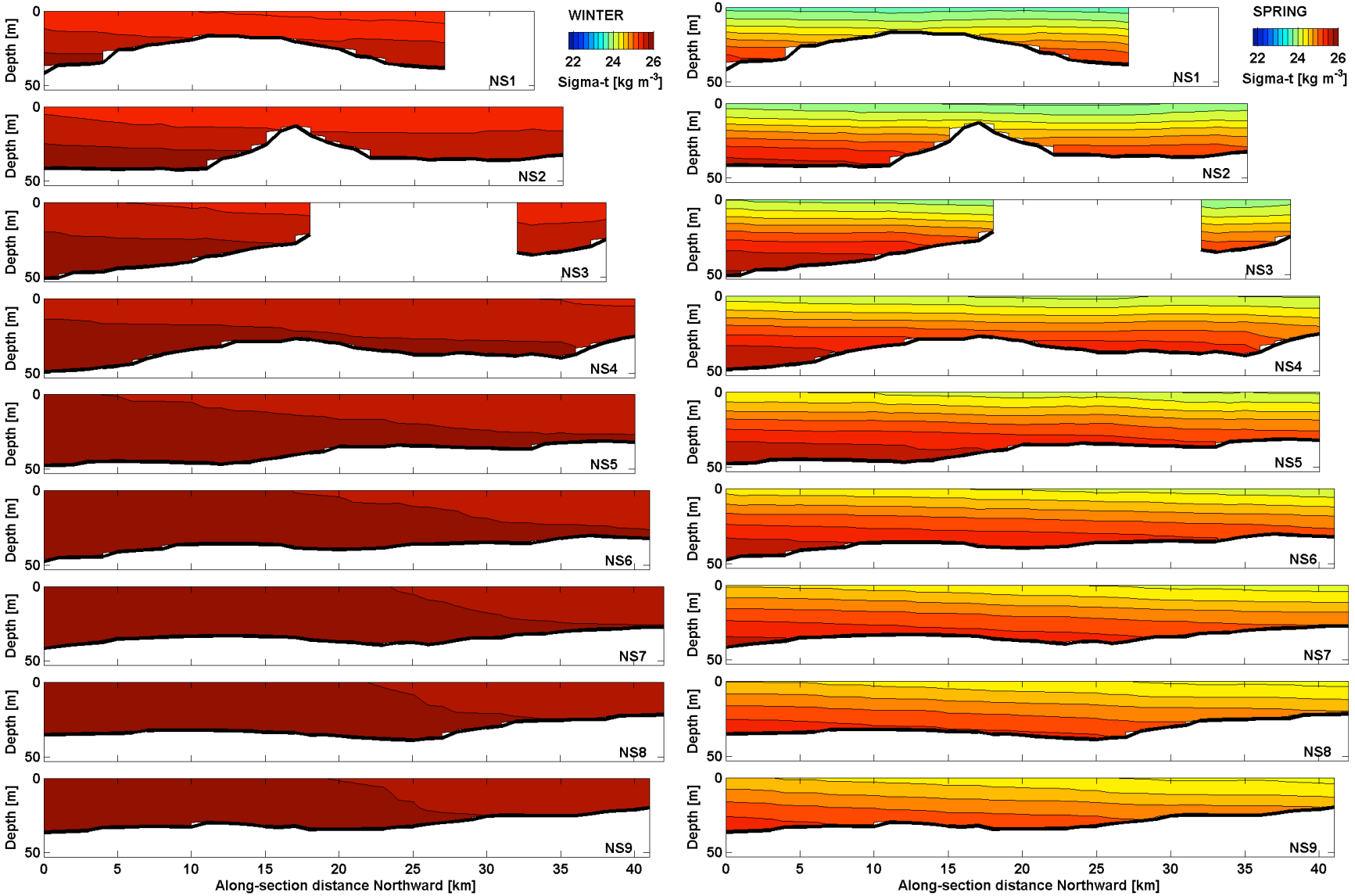

Figure 28. Hydrographic climatology. Density anomaly. NS. (left) Winter. (right) Spring.

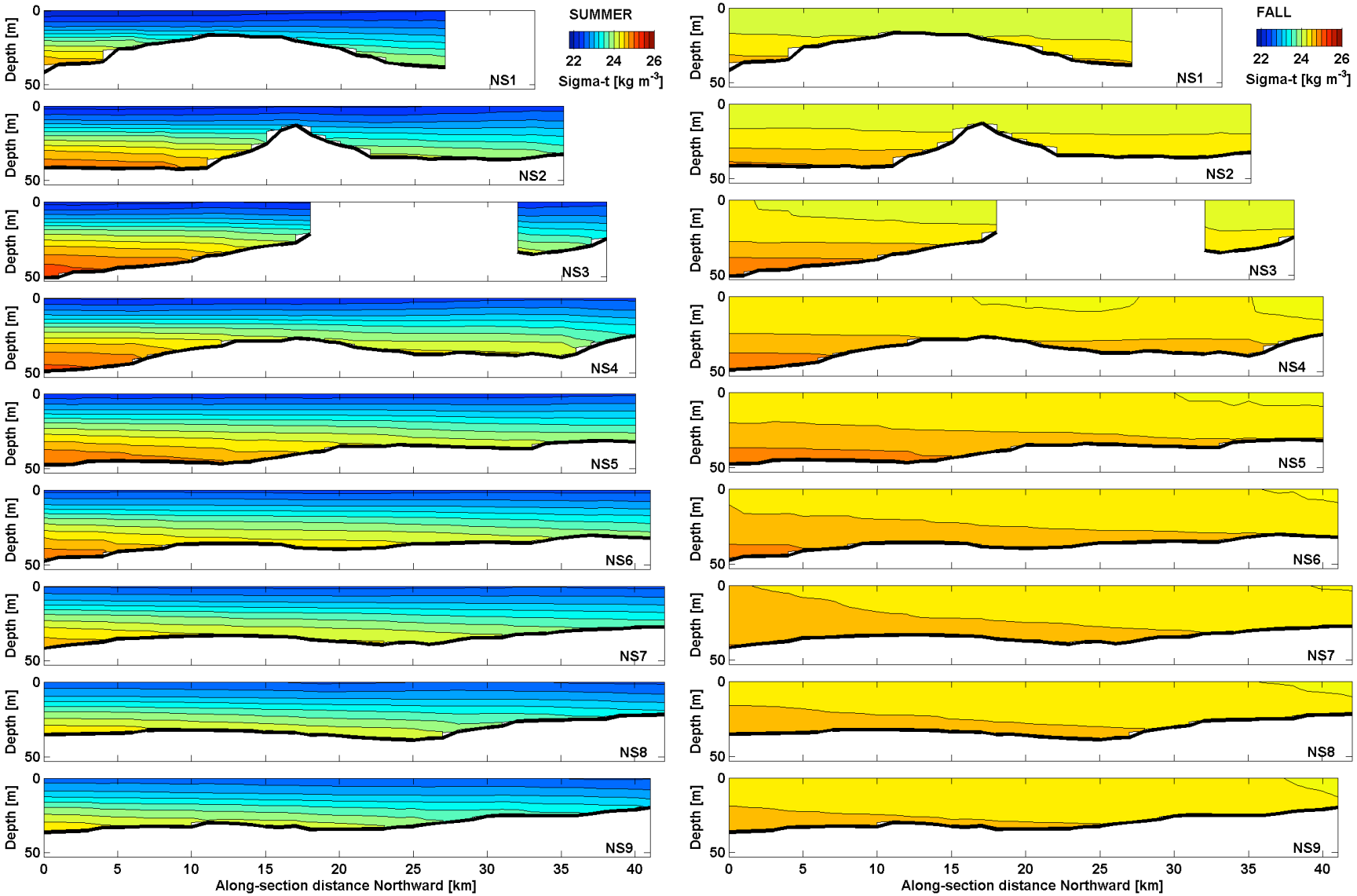

Figure 29. Hydrographic climatology. Density anomaly. NS. (left) Summer. (right) Fall.

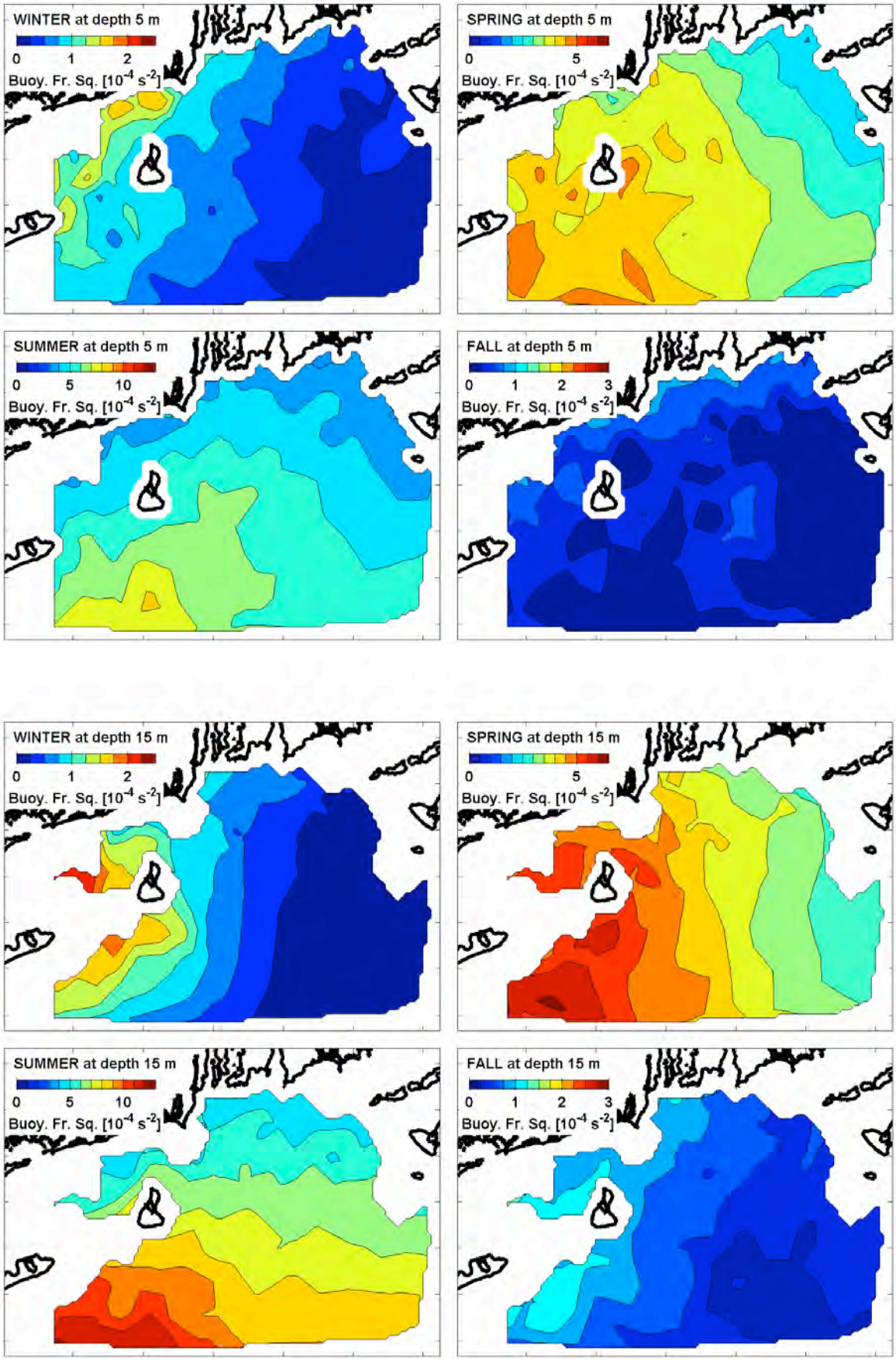

Figure 30. Hydrographic climatology. Stratification. (upper) Depth 5 m. (lower) Depth 15 m.

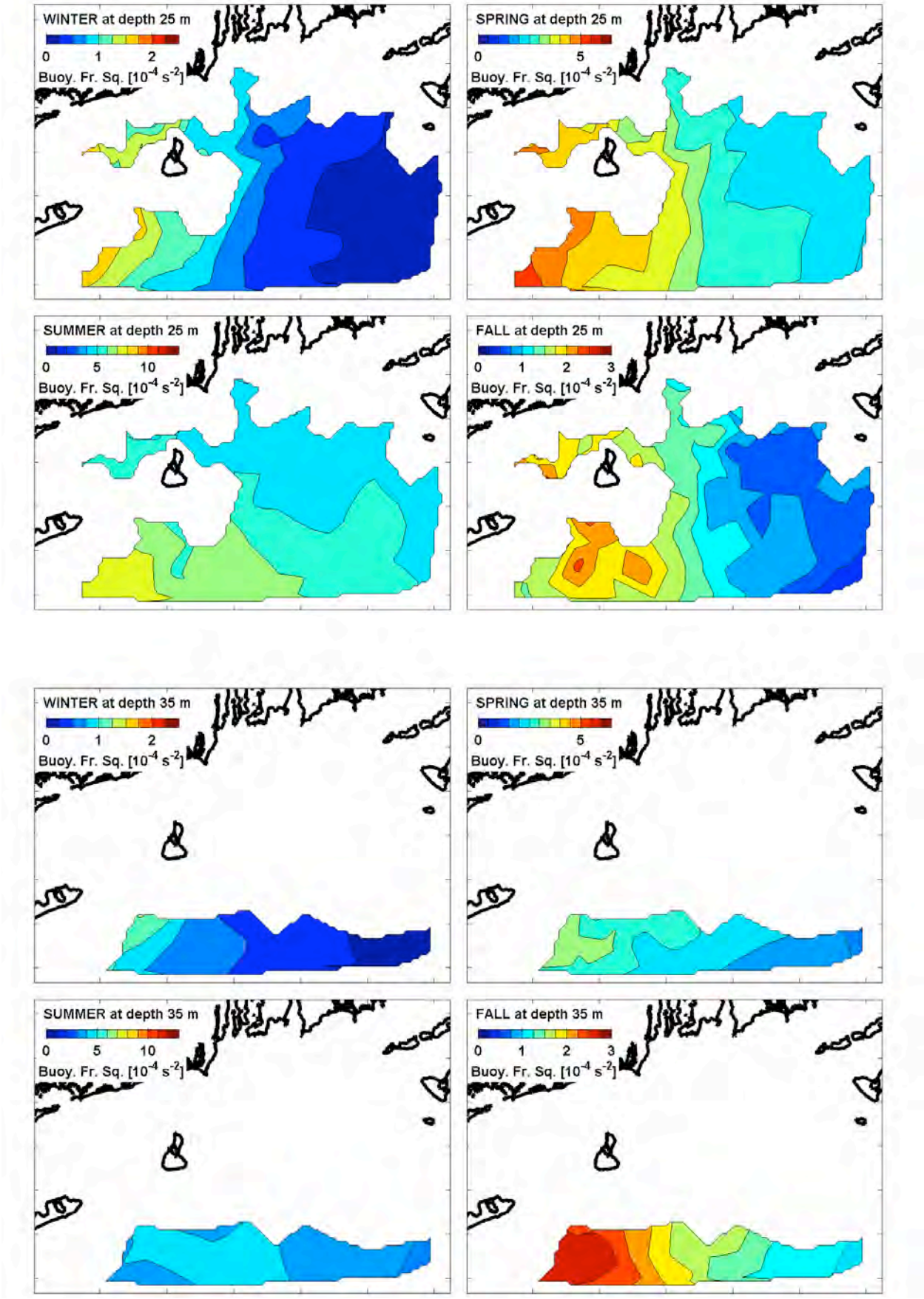

Figure 31. Hydrographic climatology. Stratification. (upper) Depth 25 m. (lower) Depth 35 m.

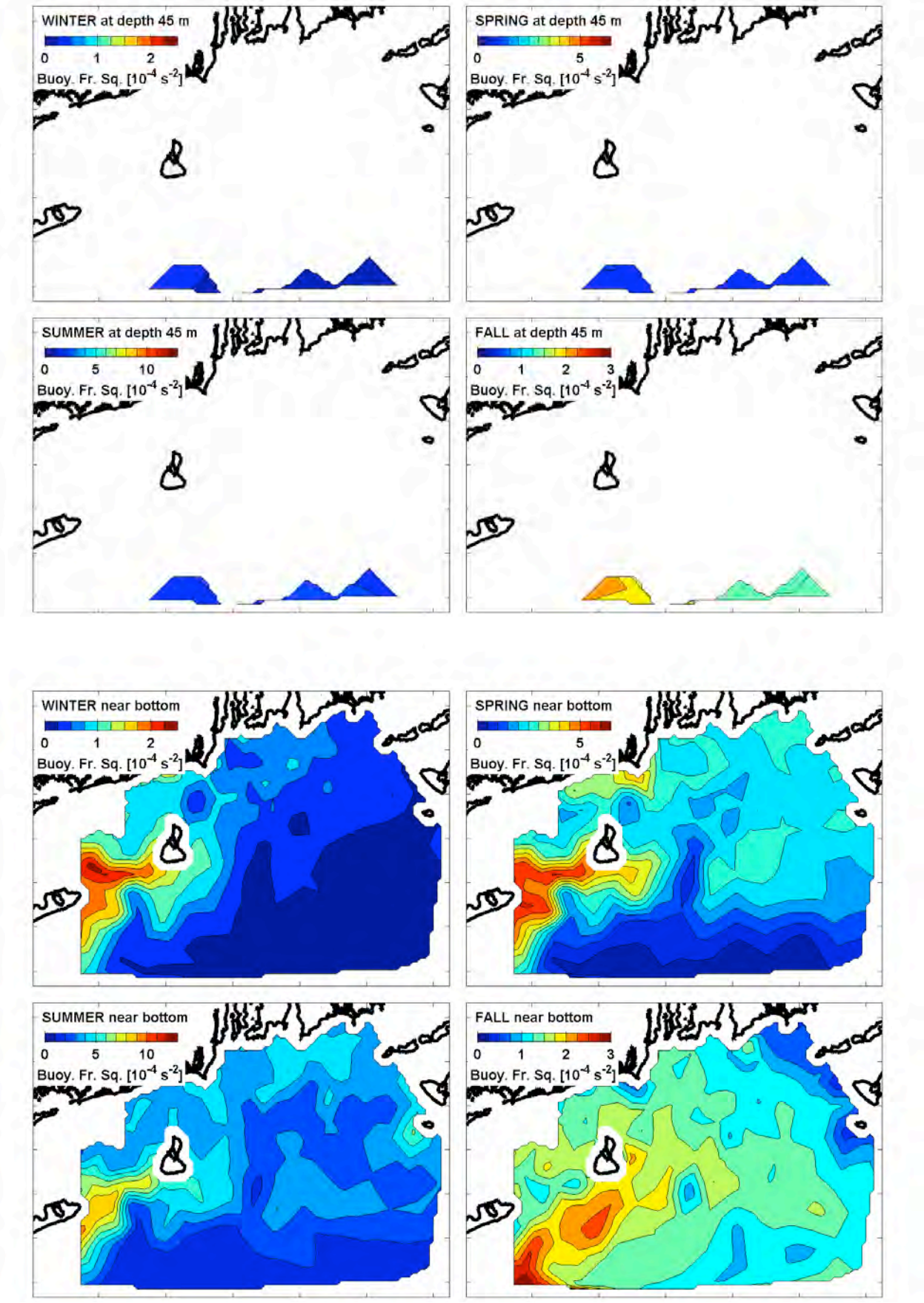

Figure 32. Hydrographic climatology. Stratification. (upper) Depth 45 m. (lower) Near seafloor.

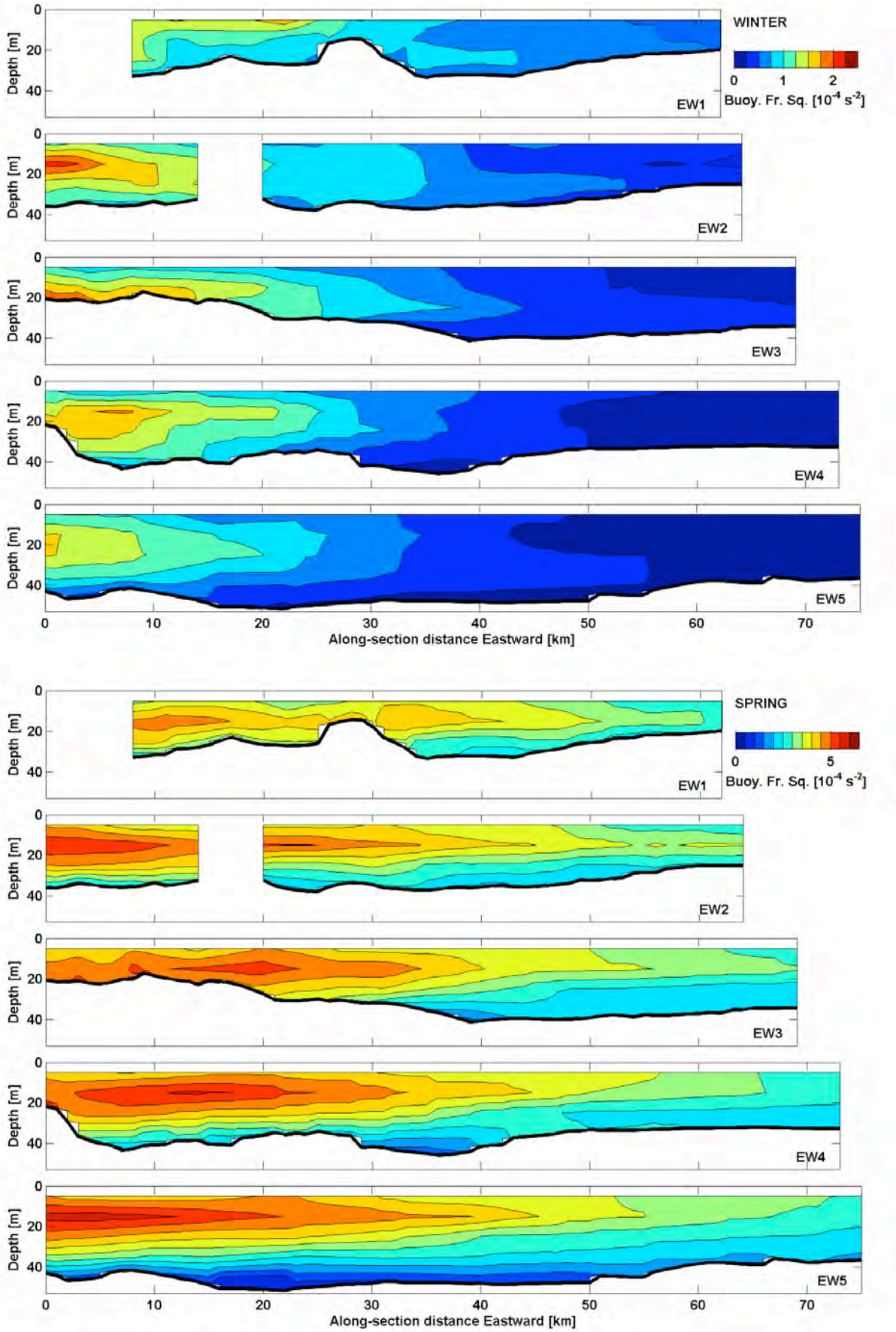

Figure 33. Hydrographic climatology. Stratification. EW. (upper) Winter. (lower) Spring.

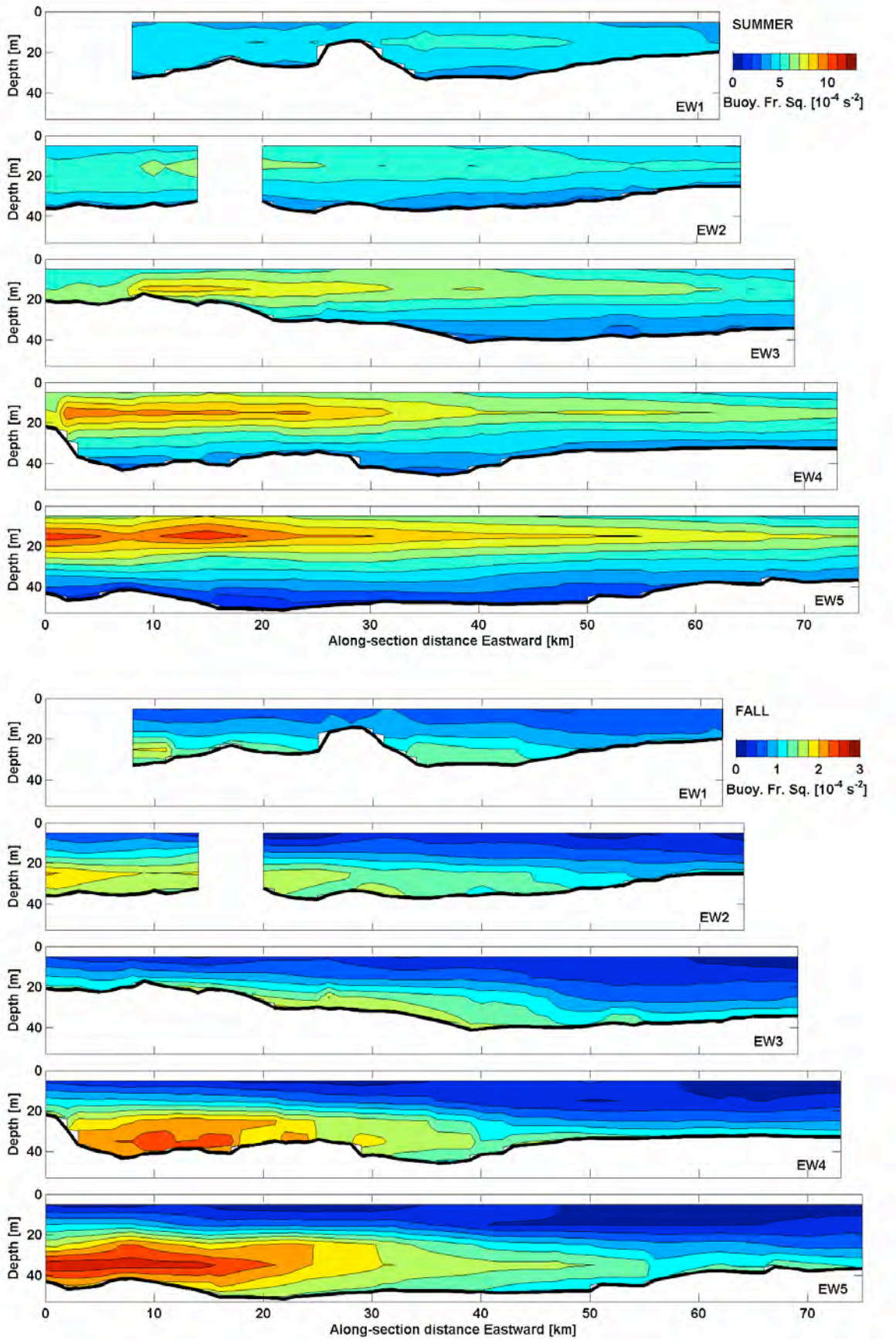

Figure 34. Hydrographic climatology. Stratification. EW. (upper) Summer. (lower) Fall.

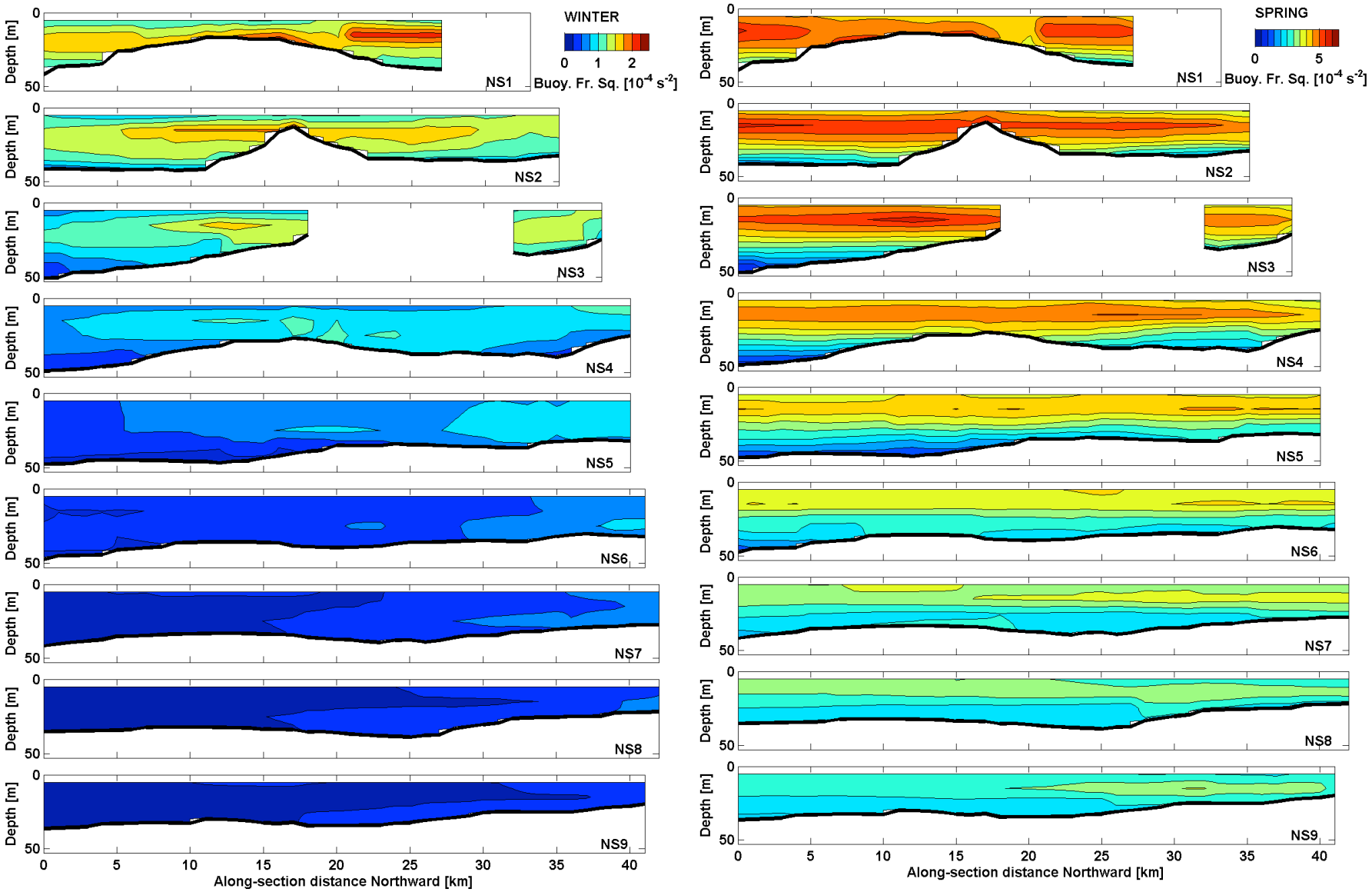

Figure 35. Hydrographic climatology. Stratification. NS. (left) Winter. (right) Spring.

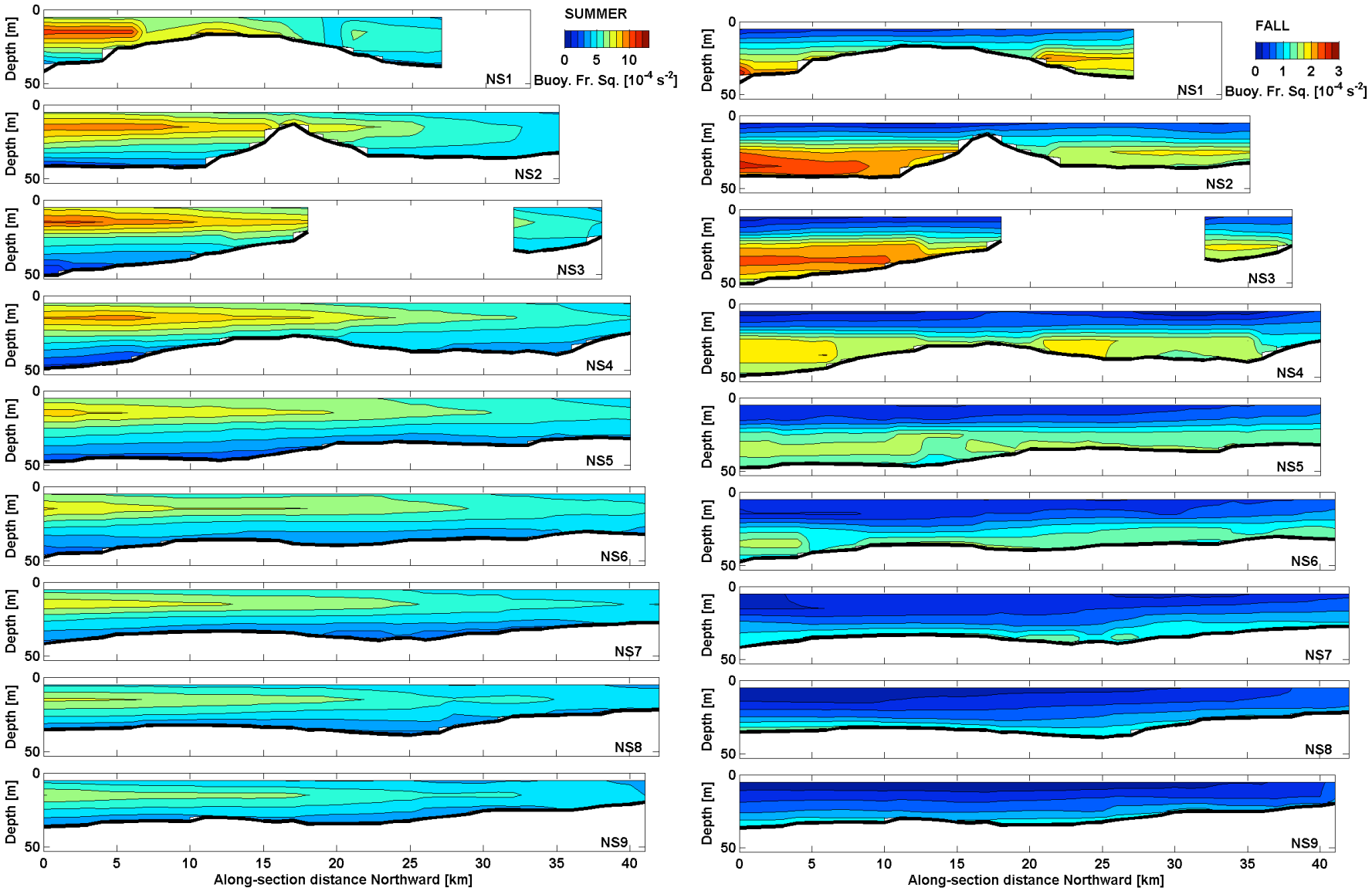

Figure 36. Hydrographic climatology. Stratification. NS. (left) Summer. (right) Fall.

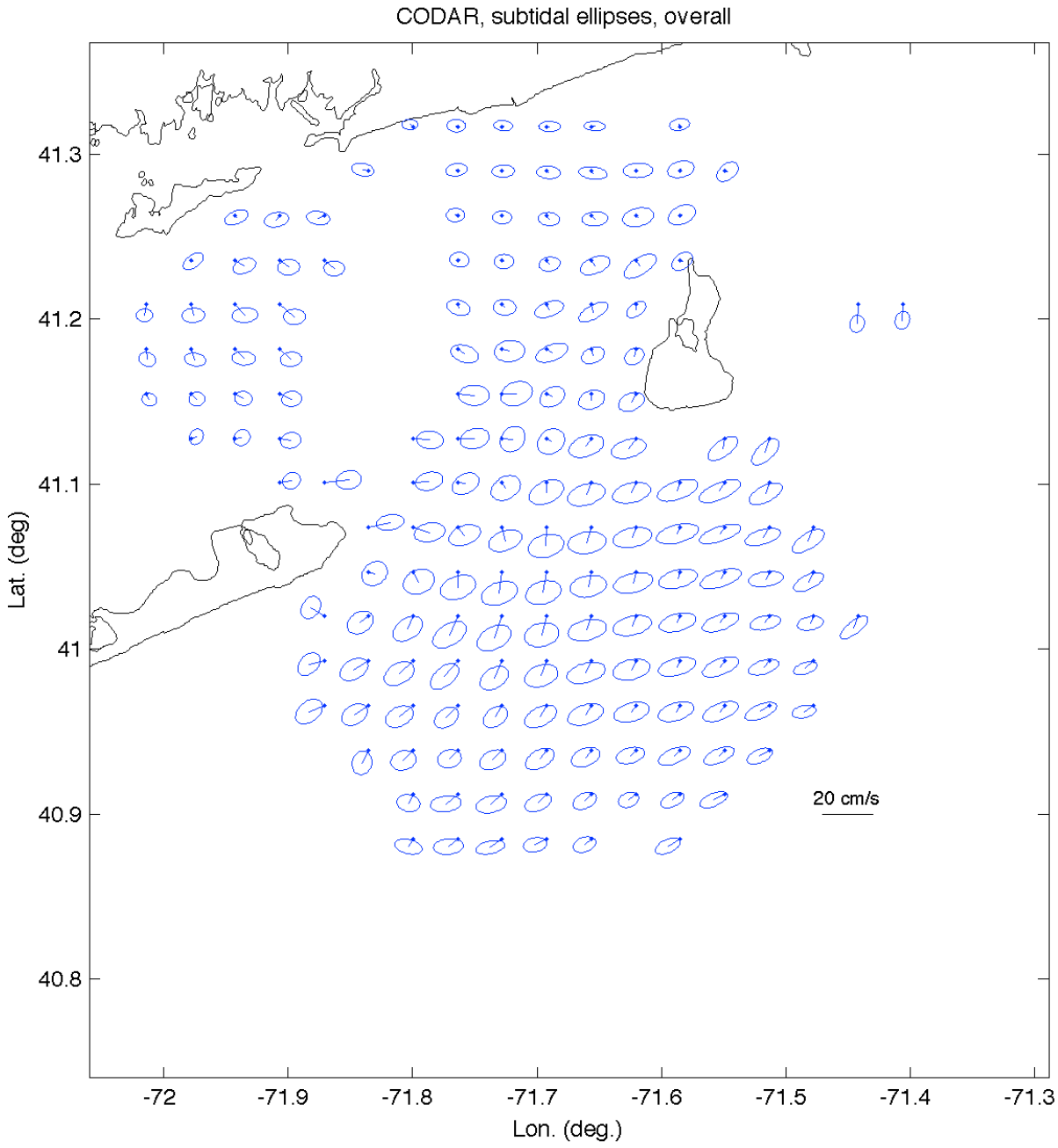

Figure 37. HF radar currents. All seasons mean flow and subtidal principal component ellipses.

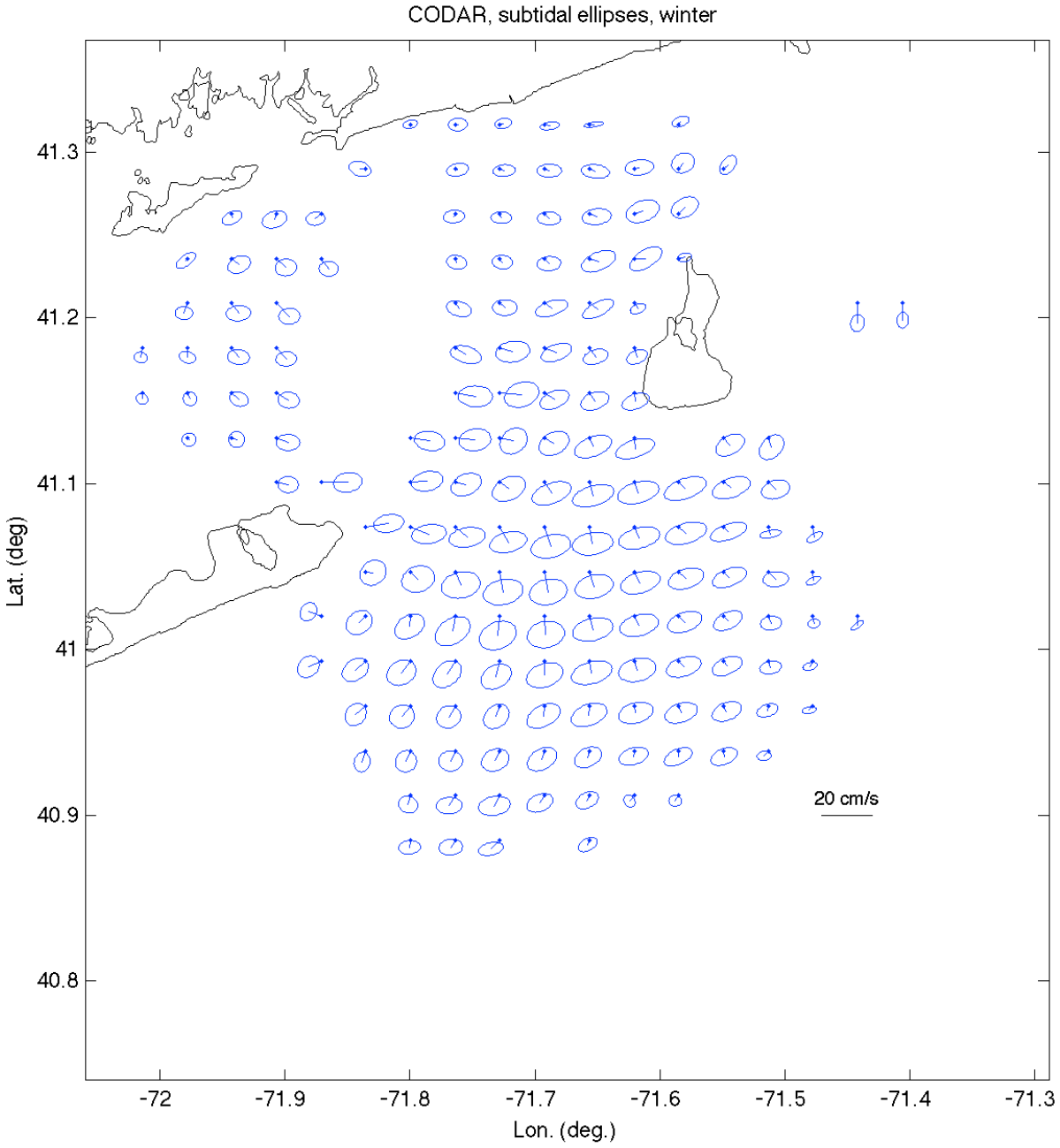

Figure 38. HF radar currents. Winter mean flow and subtidal principal axes ellipses.

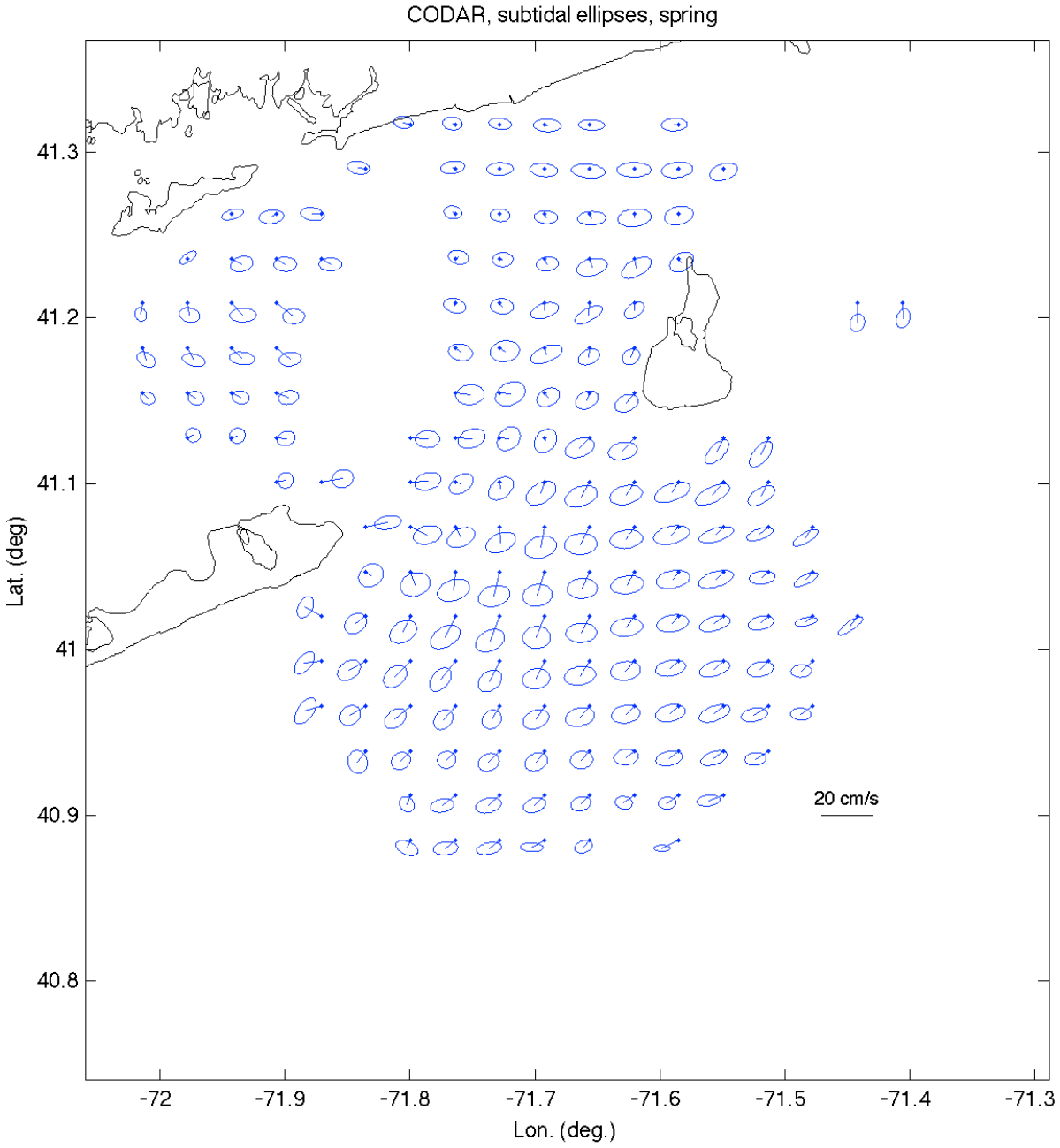

Figure 39. HF radar currents. Spring mean flow and subtidal principal axes ellipses.

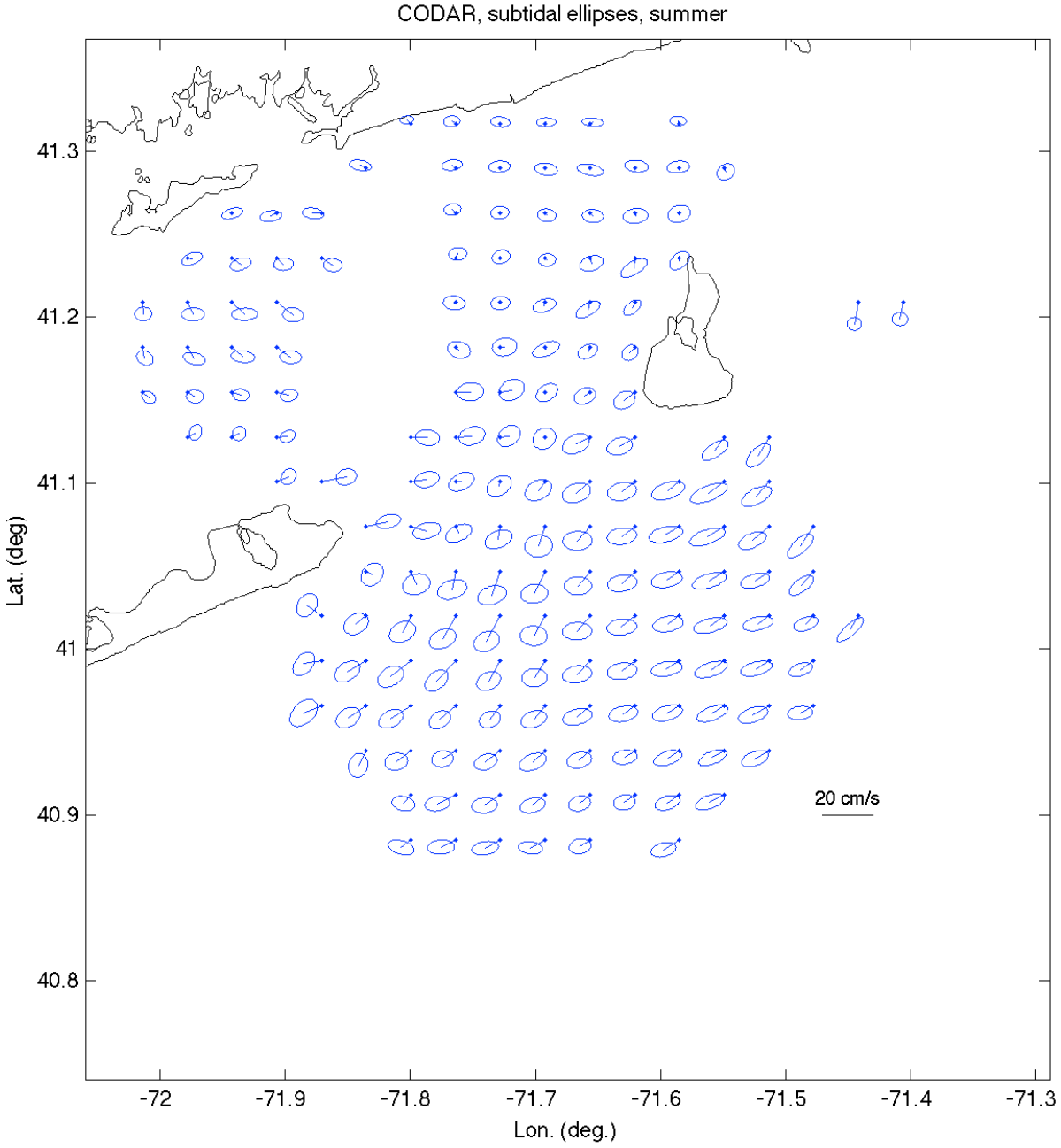

Figure 40. HF radar currents. Summer mean flow and subtidal principal axes ellipses.

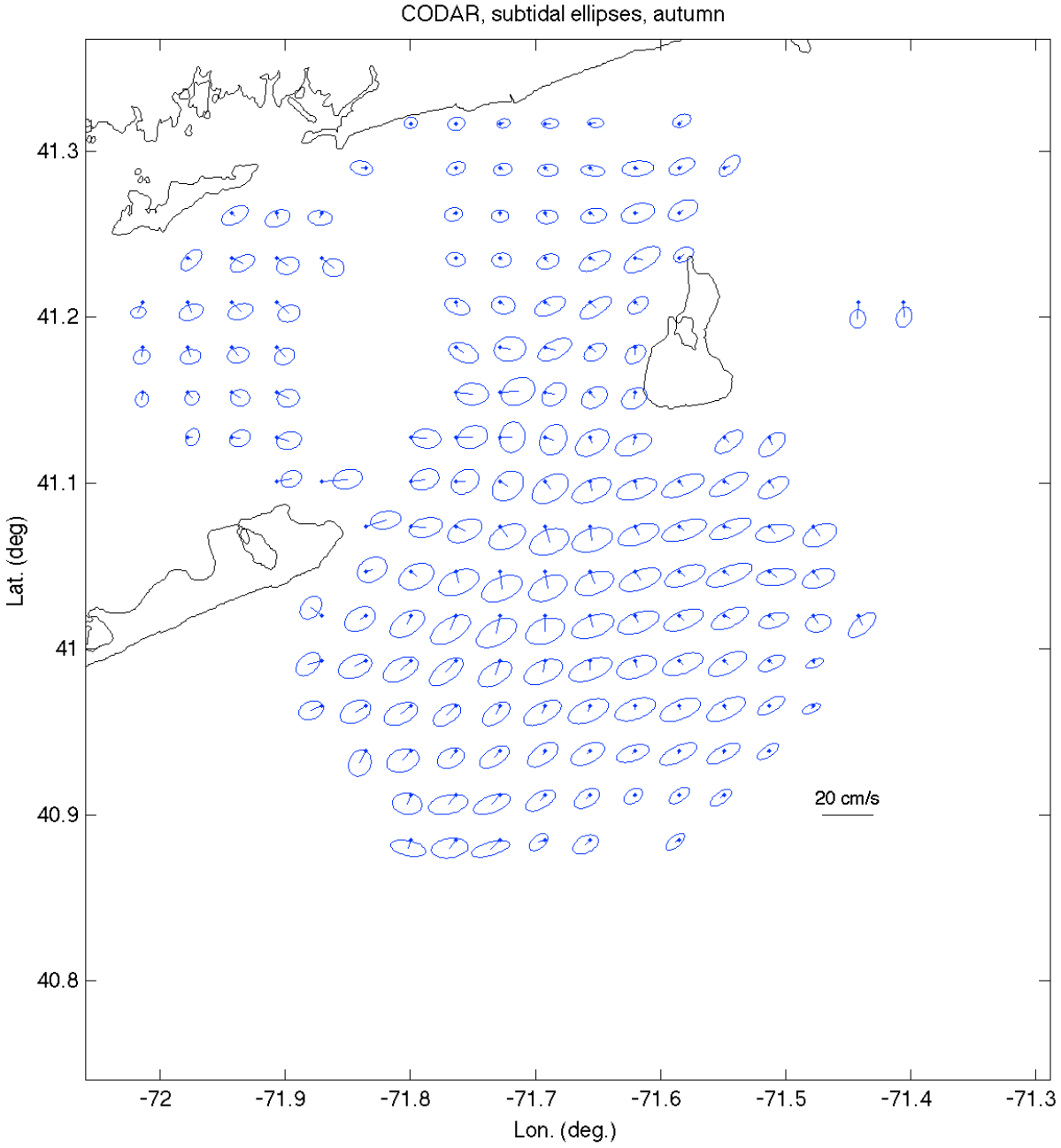

Figure 41. HF radar currents. Fall mean flow and subtidal principal axes ellipses.

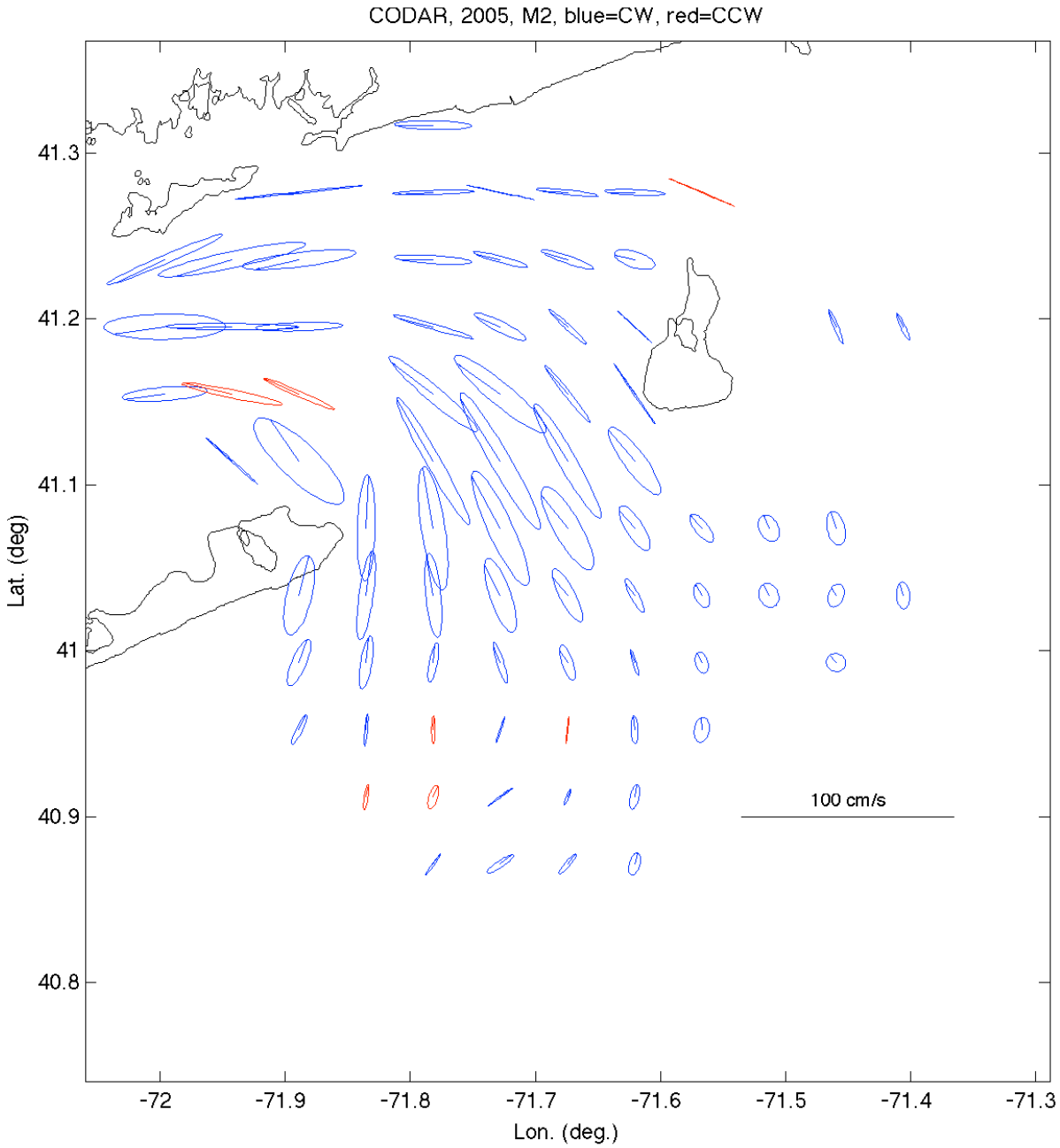

Figure 42. HF radar currents: M_2 tidal ellipses.

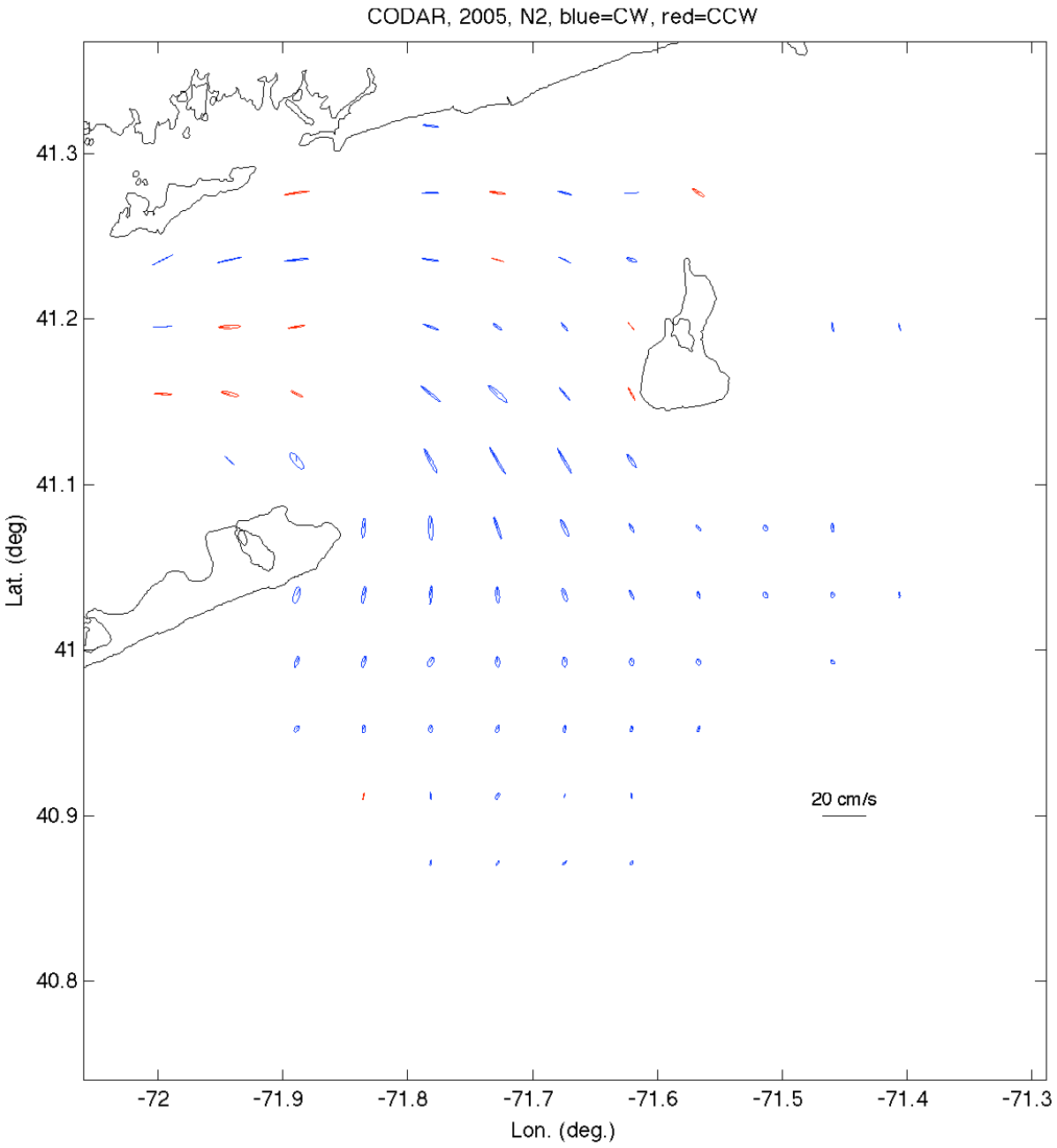

Figure 43. HF radar currents. N_2 tidal ellipses.

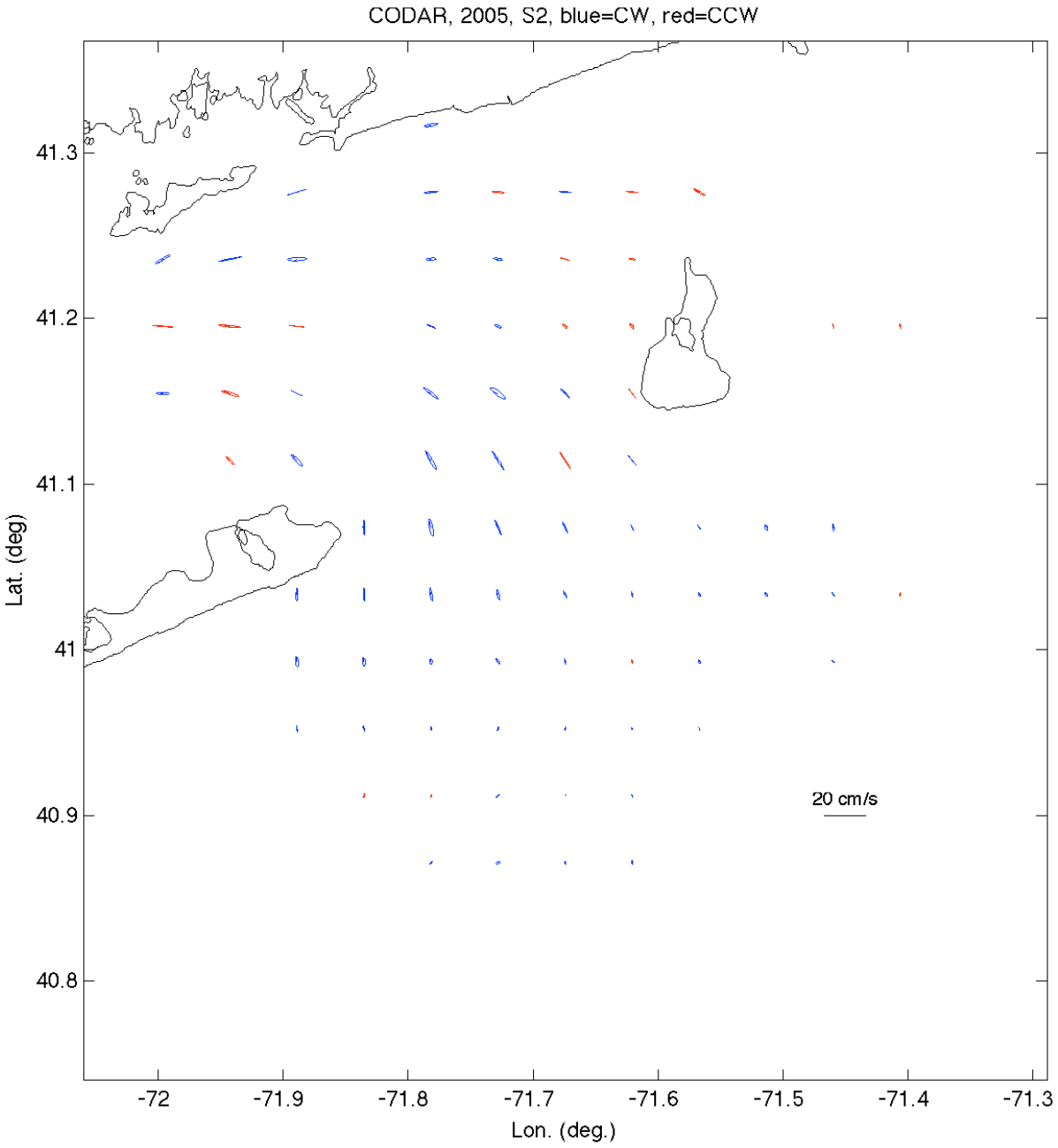

Figure 44. HF radar currents. S_2 tidal ellipses.

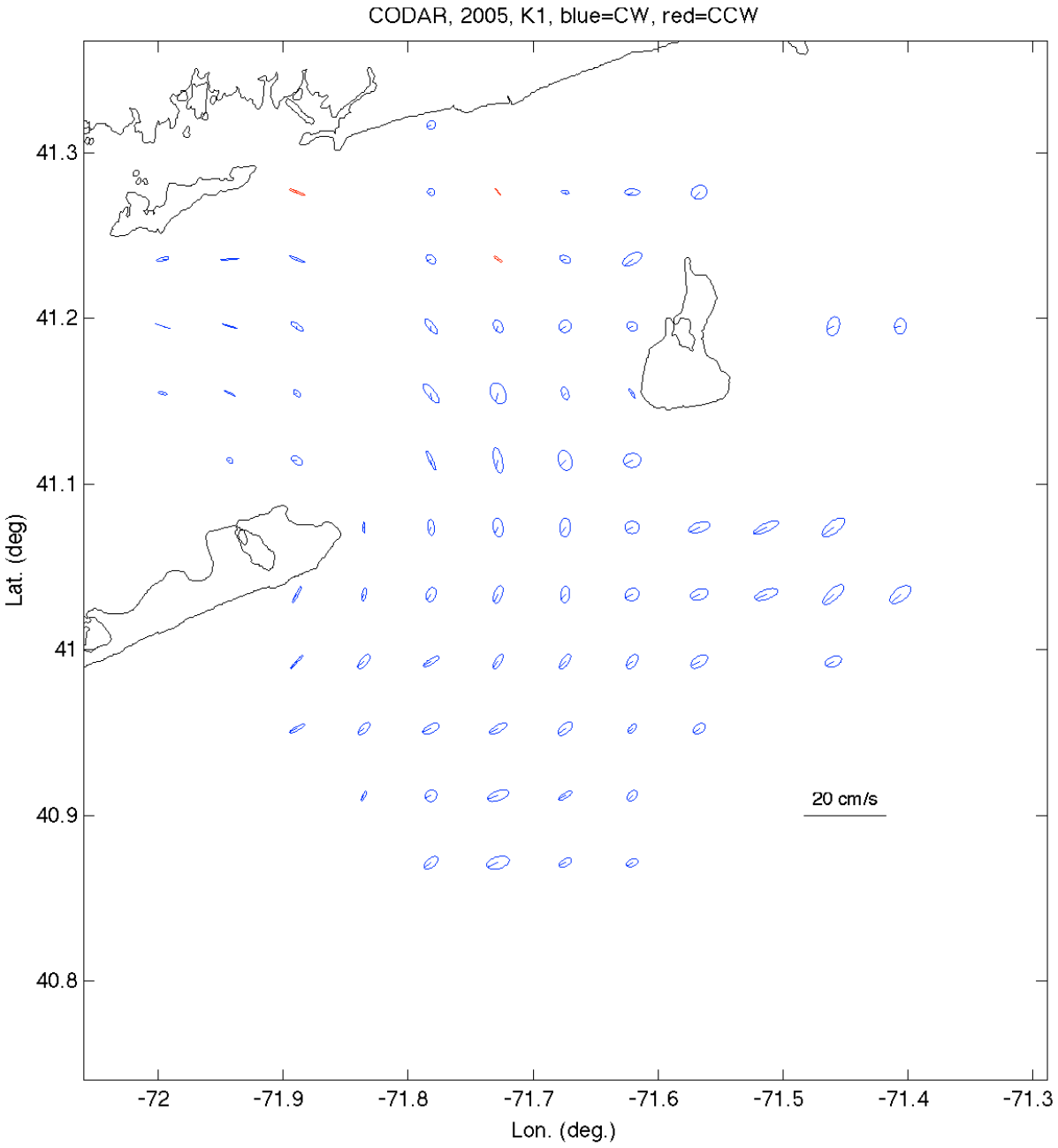

Figure 45. HF radar currents. K_1 tidal ellipses.

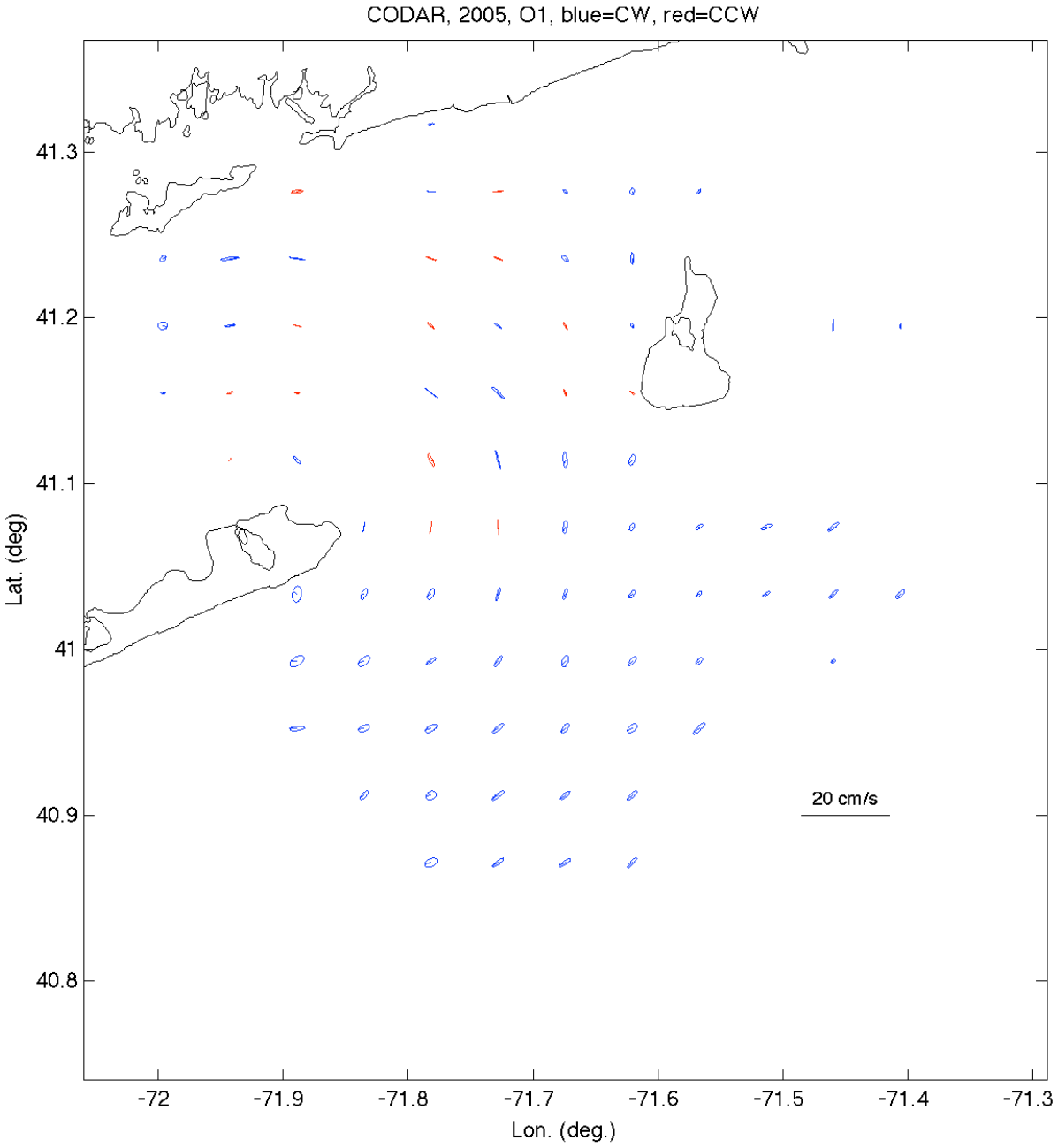

Figure 46. HF radar currents. O_1 tidal ellipses.

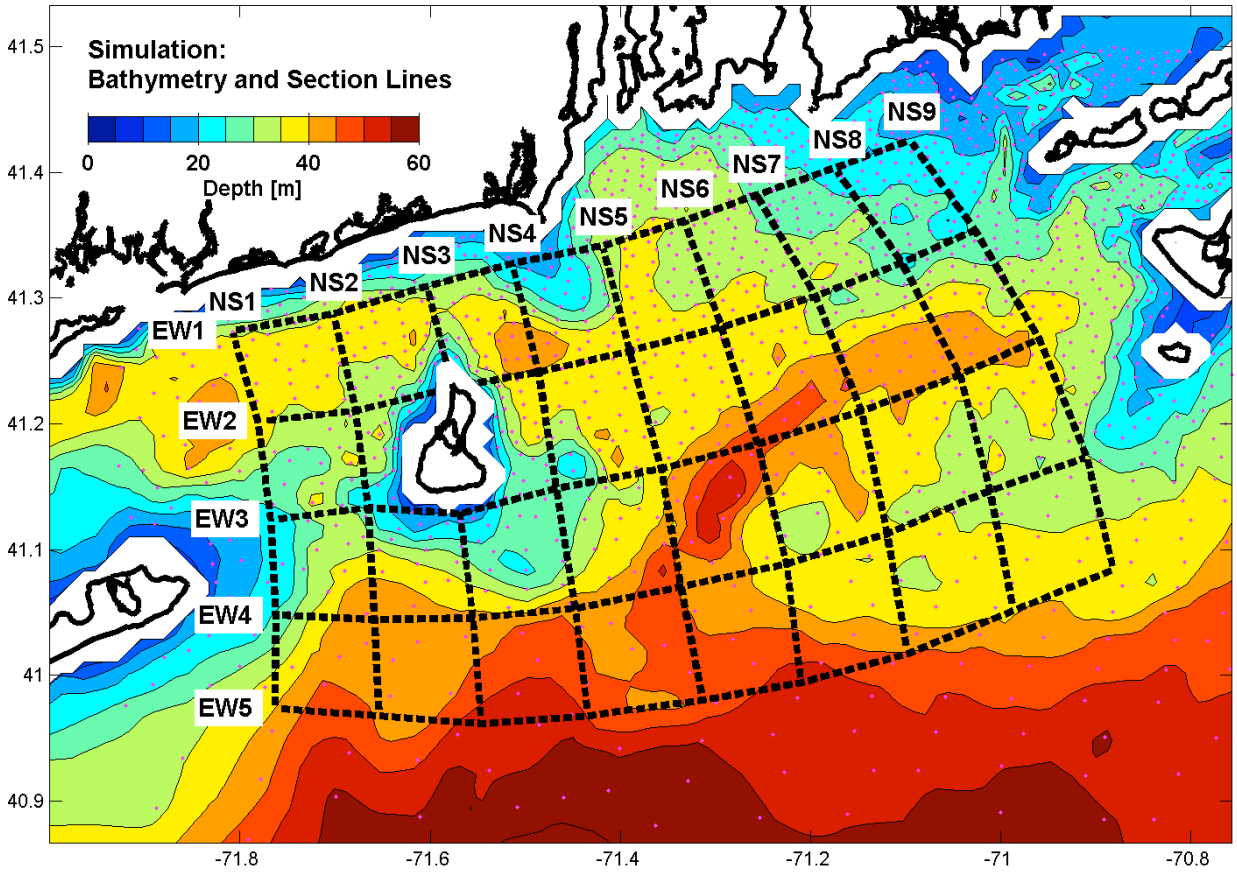

Figure 47. Simulation: Bathymetry, section lines, and grid nodes (sparsified by 3 for clarity).

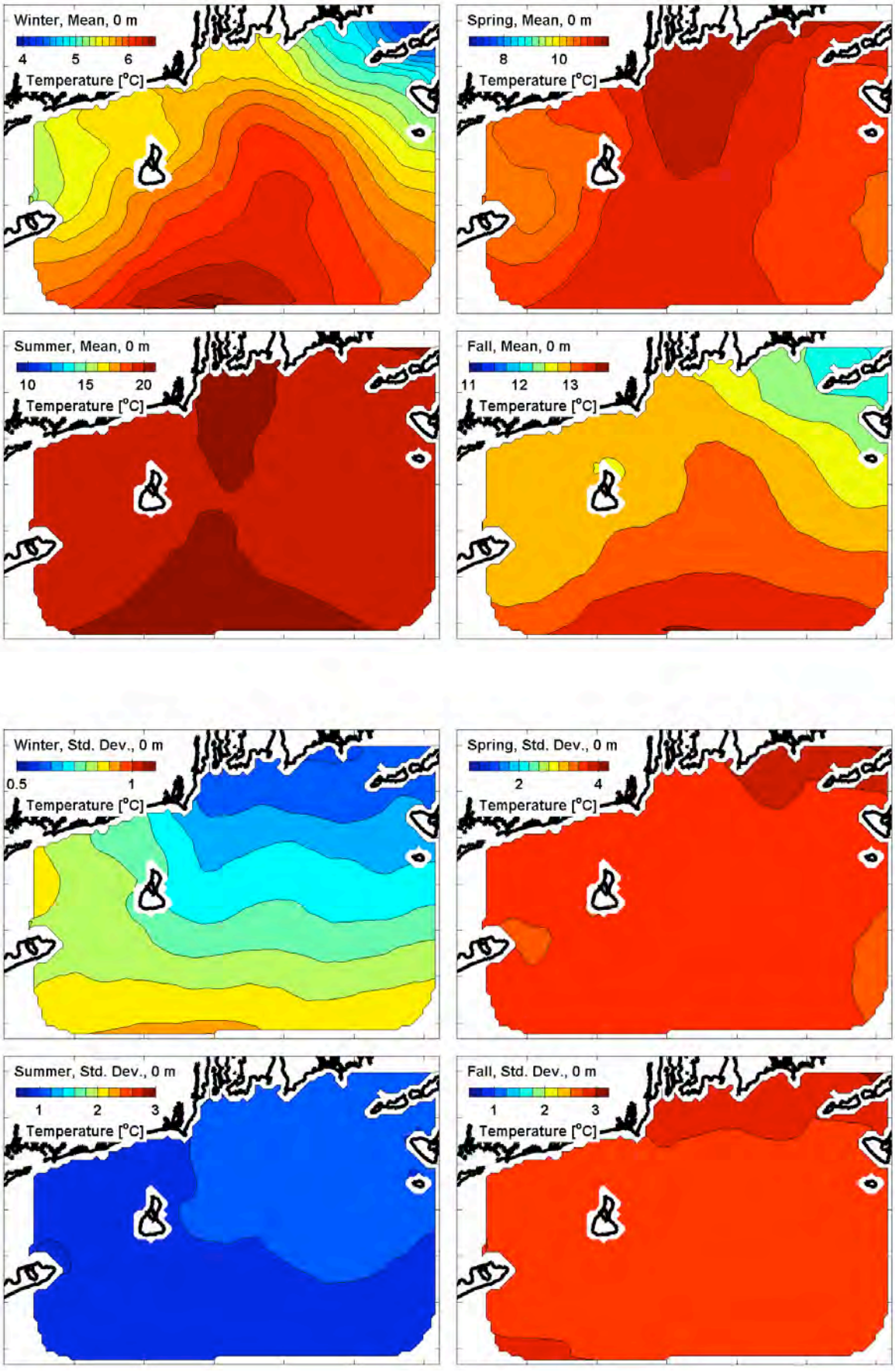

Figure 48. Simulation: Temperature, four seasons, surface. (upper) Mean. (lower) Std. dev.

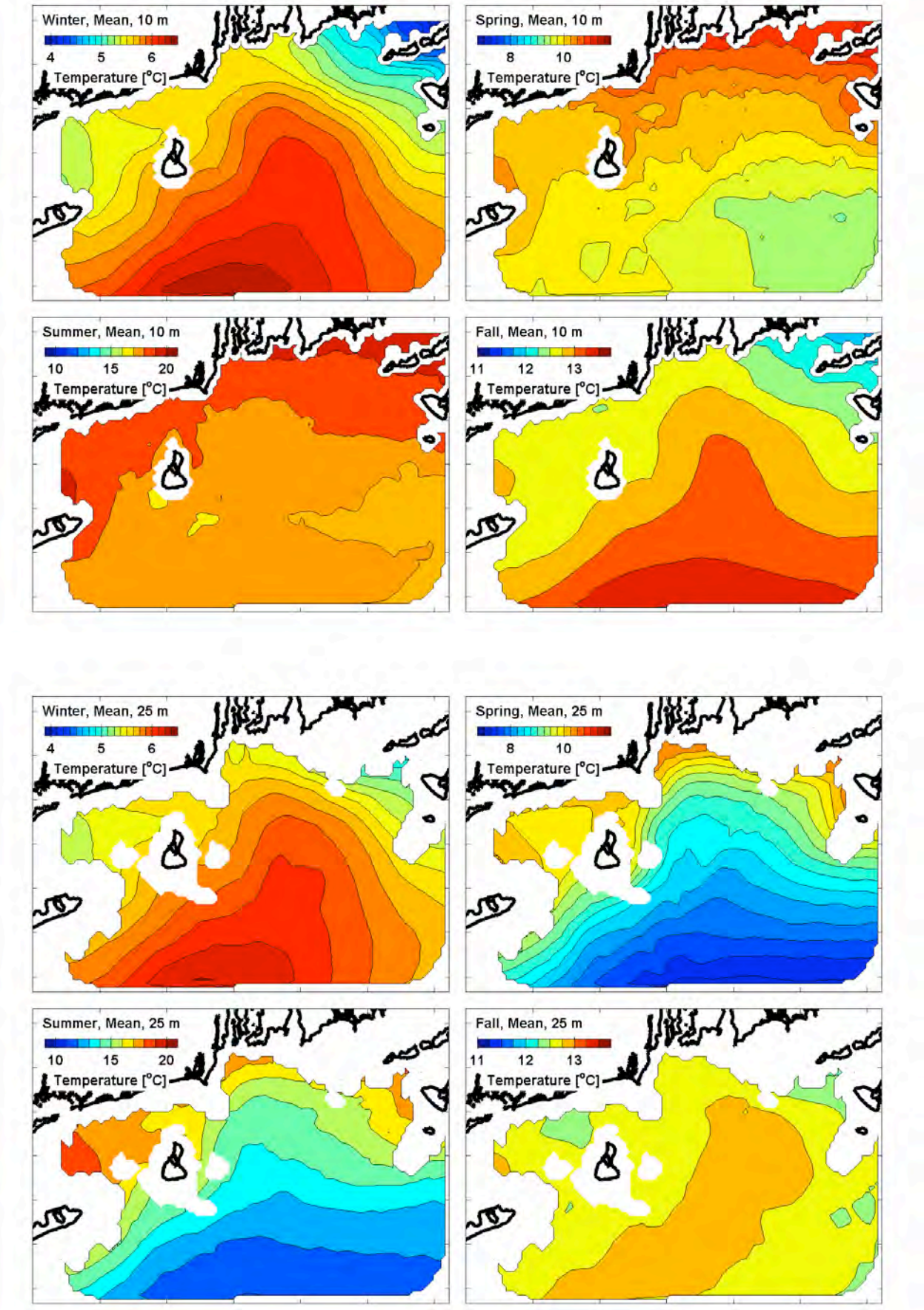

Figure 49. Simulation: Temperature, seasonal-mean. (upper) 10 m deep. (lower) 25 m deep.

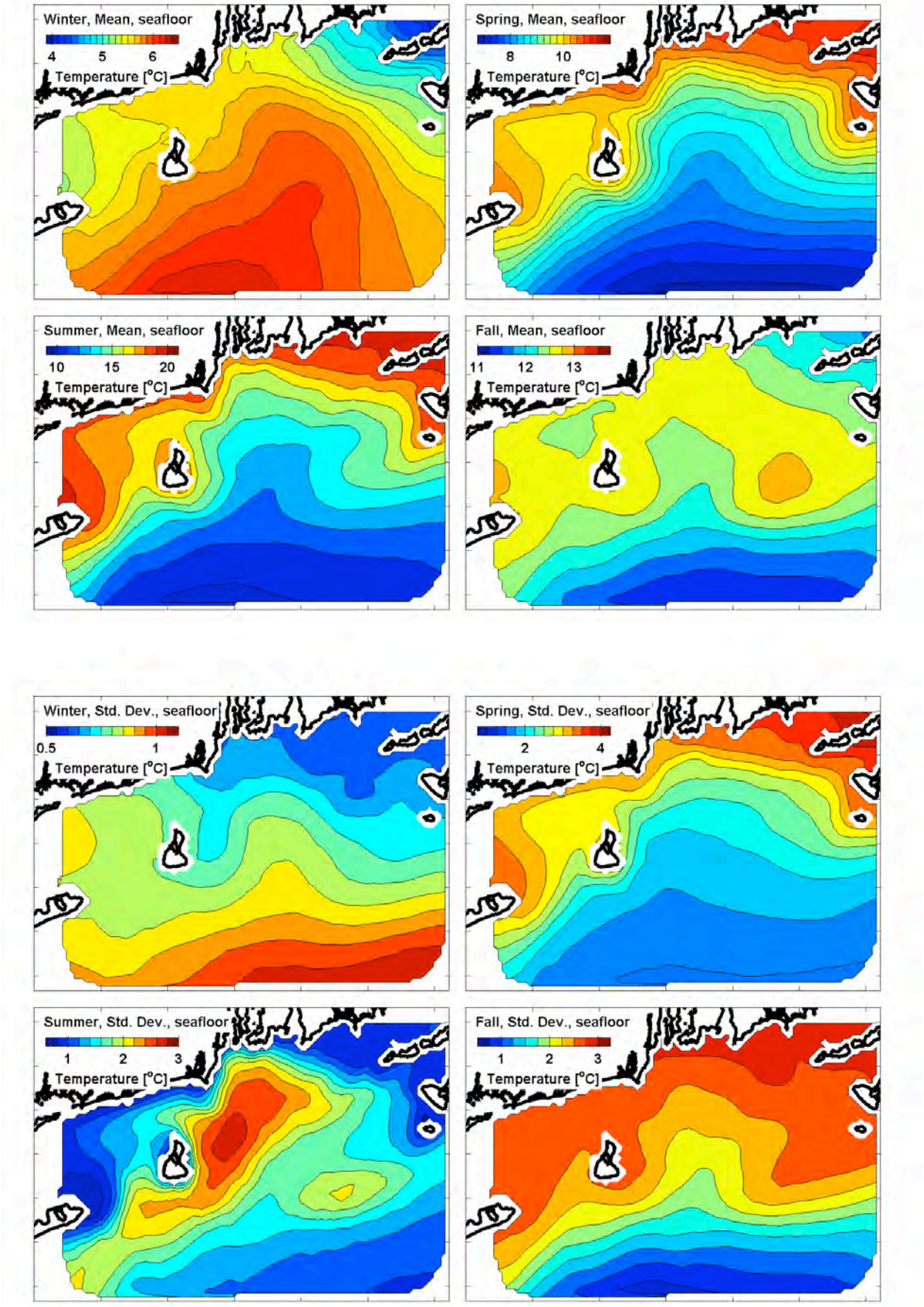

Figure 50. Simulation: Temperature, four seasons, seafloor. (upper) Mean. (lower) Std. dev.

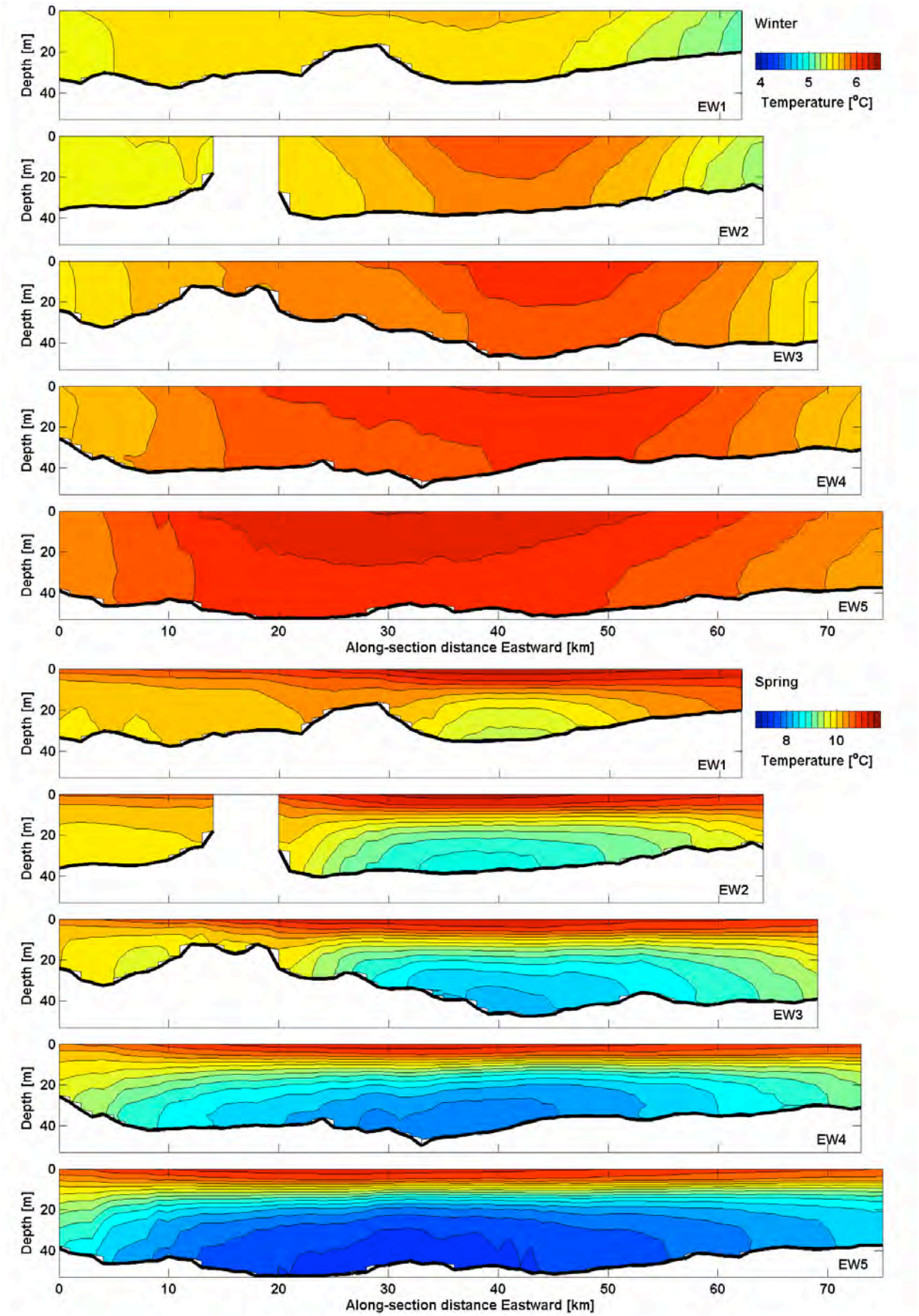

Figure 51. Simulation: Temperature, seasonal-mean, EW. (upper) Winter. (lower) Spring.

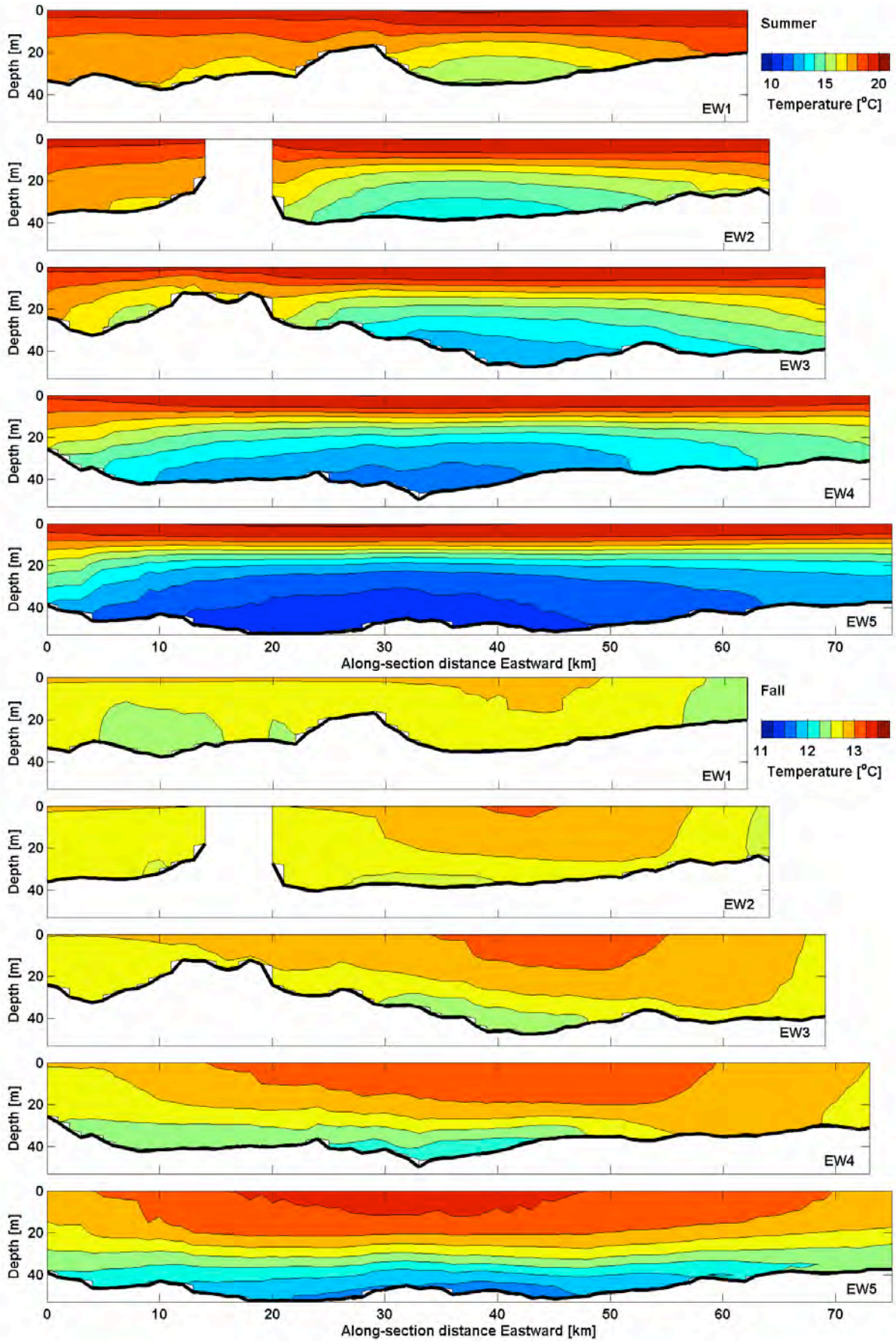

Figure 52. Simulation: Temperature, seasonal-mean, EW. (upper) Summer. (lower) Fall.

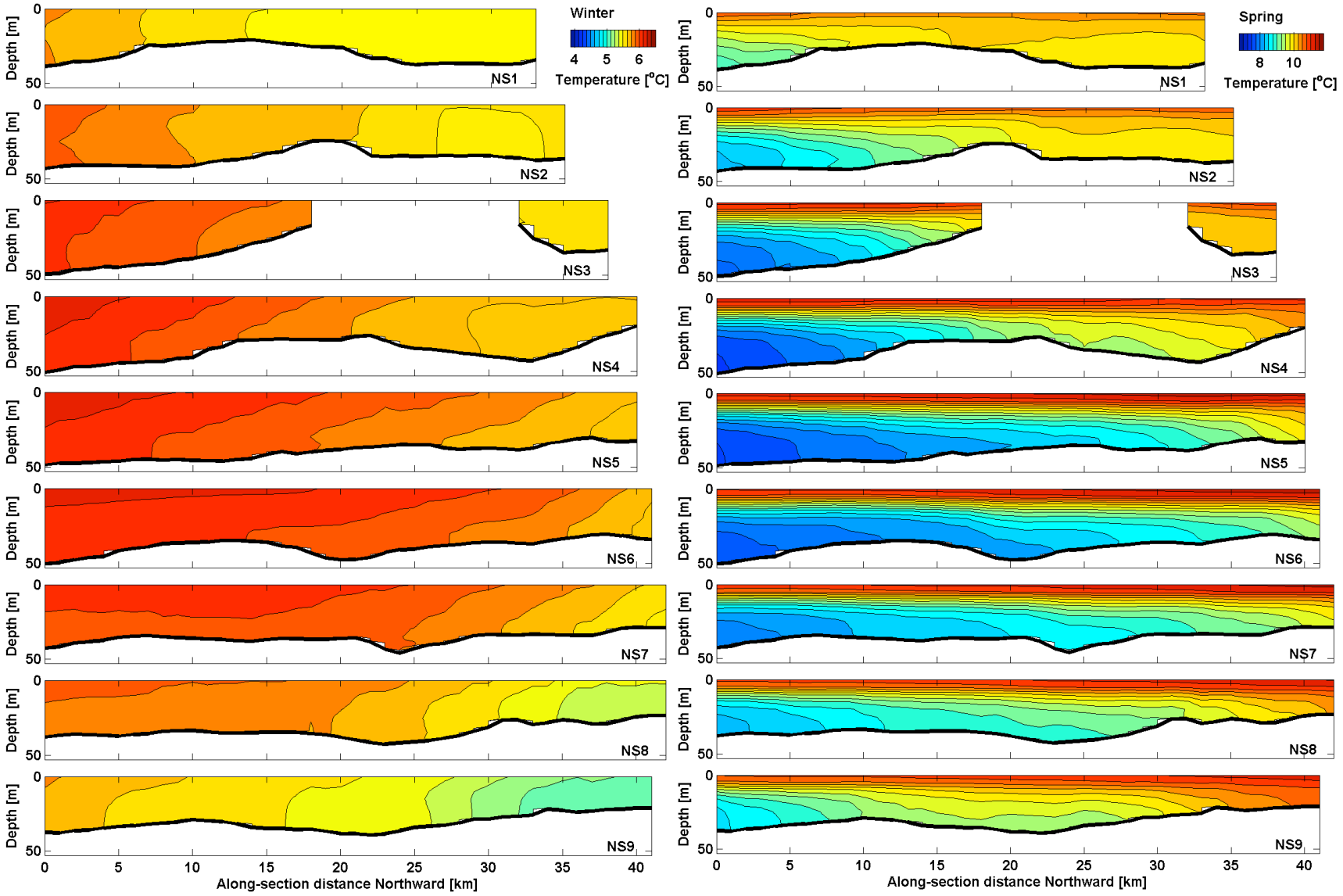

Figure 53. Simulation: Temperature, seasonal-mean, NS. (left) Winter. (right) Spring.

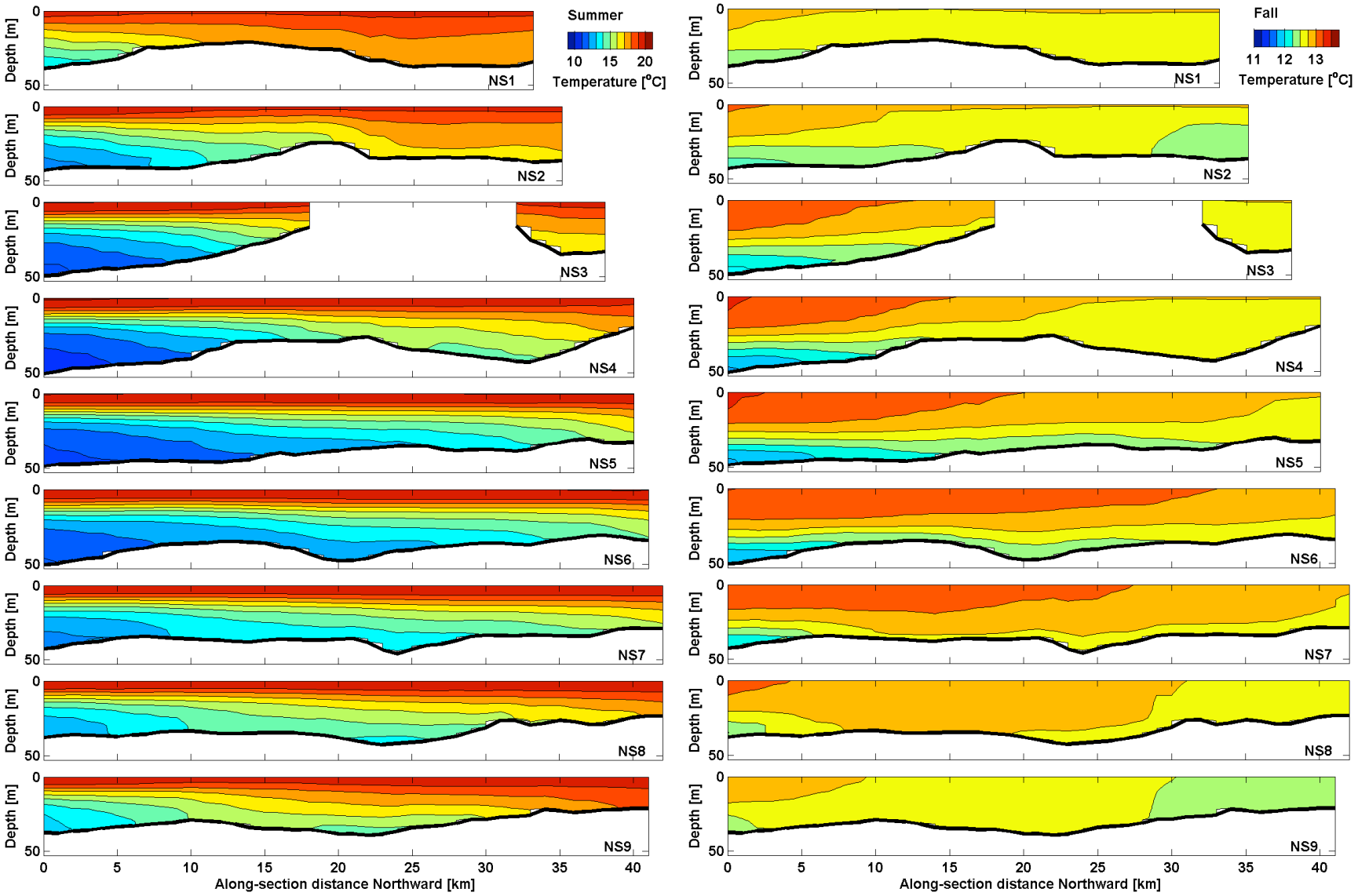

Figure 54. Simulation: Temperature, seasonal-mean, NS. (left) Summer. (right) Fall.

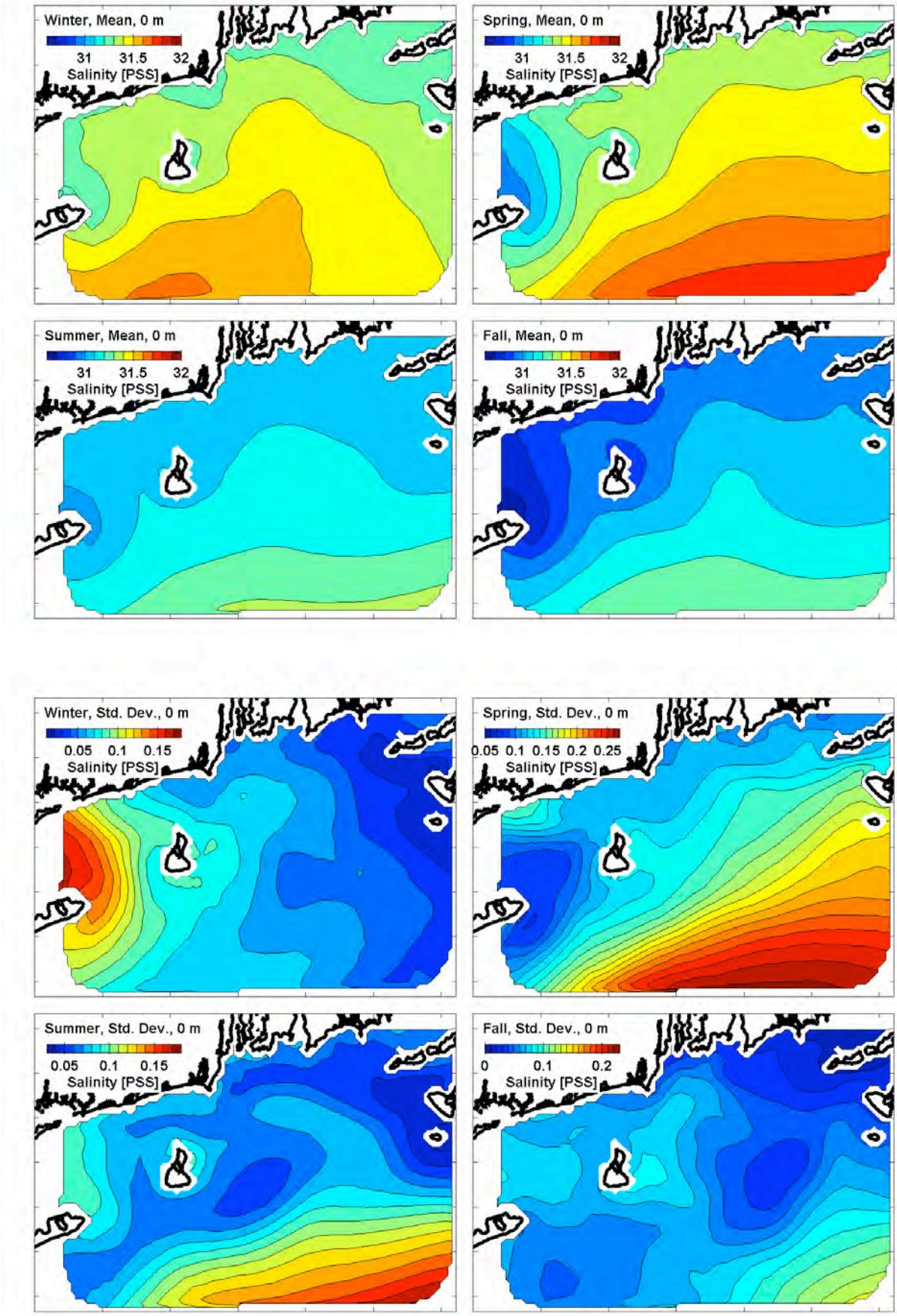

Figure 55. Simulation: Salinity, four seasons, surface. (upper) Mean. (lower) Std. dev.

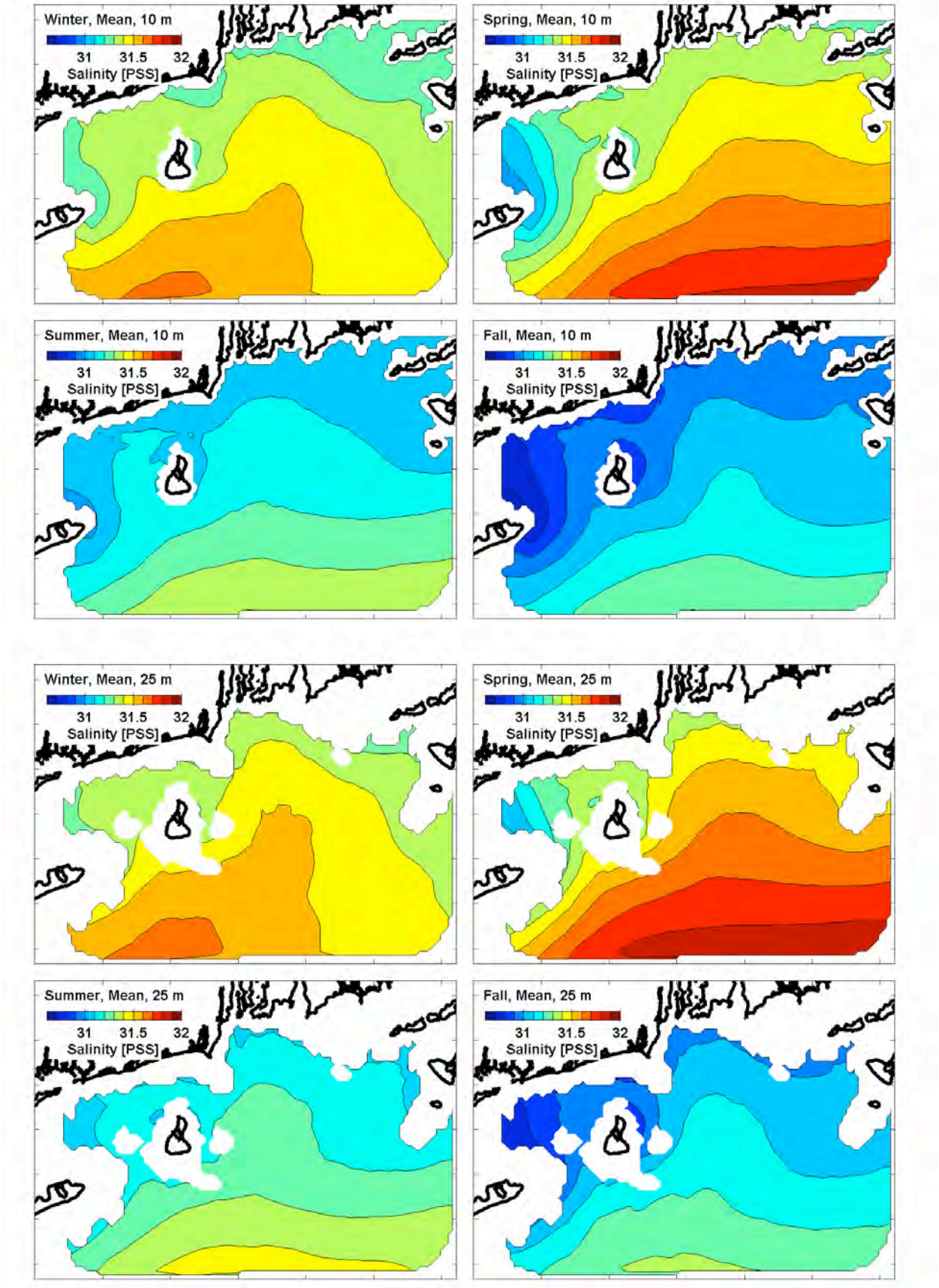

Figure 56. Simulation: Salinity, seasonal-mean. (upper) 10 m deep. (lower) 25 m deep.

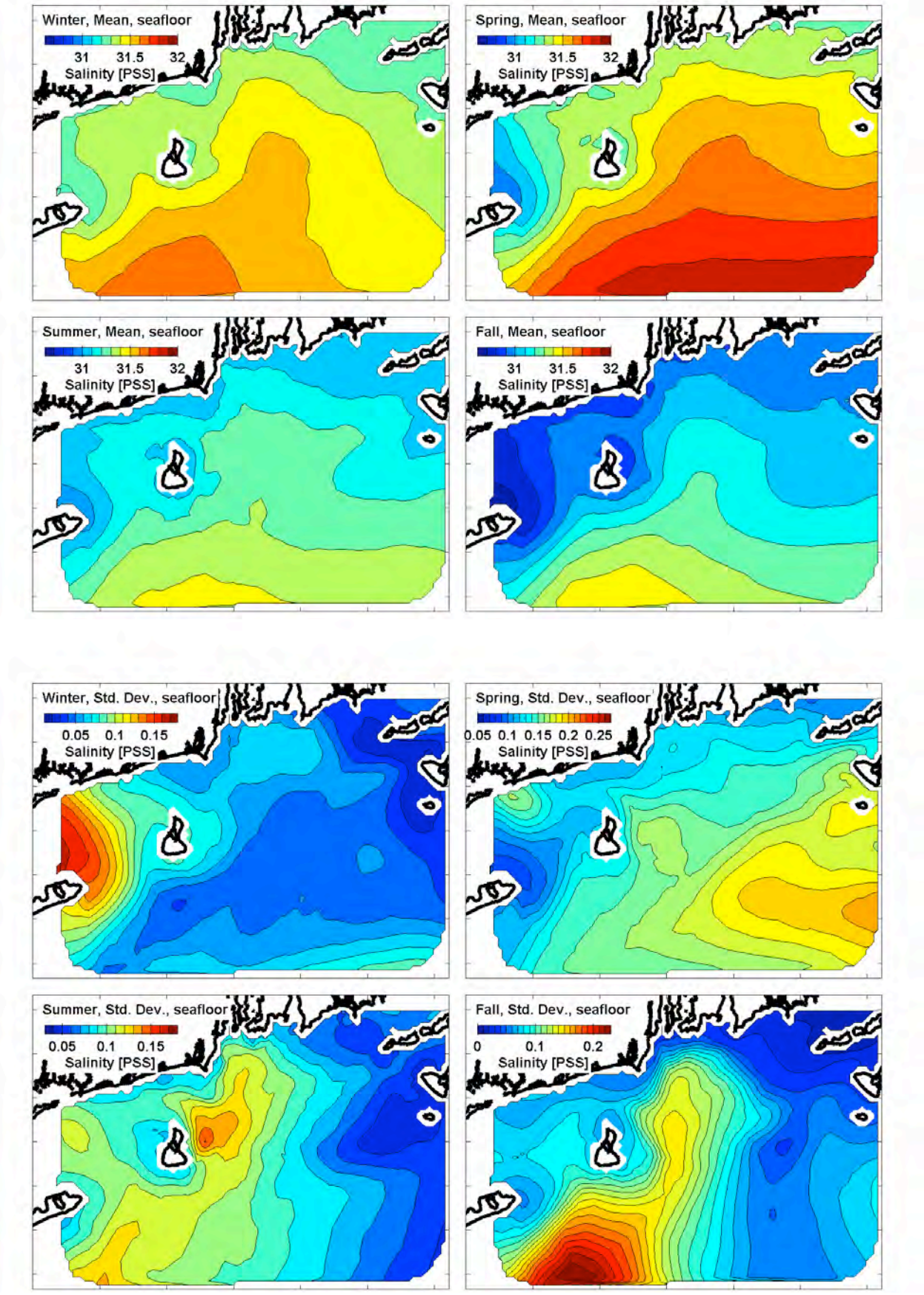

Figure 57. Simulation: Salinity, four seasons, seafloor. (upper) Mean. (lower) Std. dev.

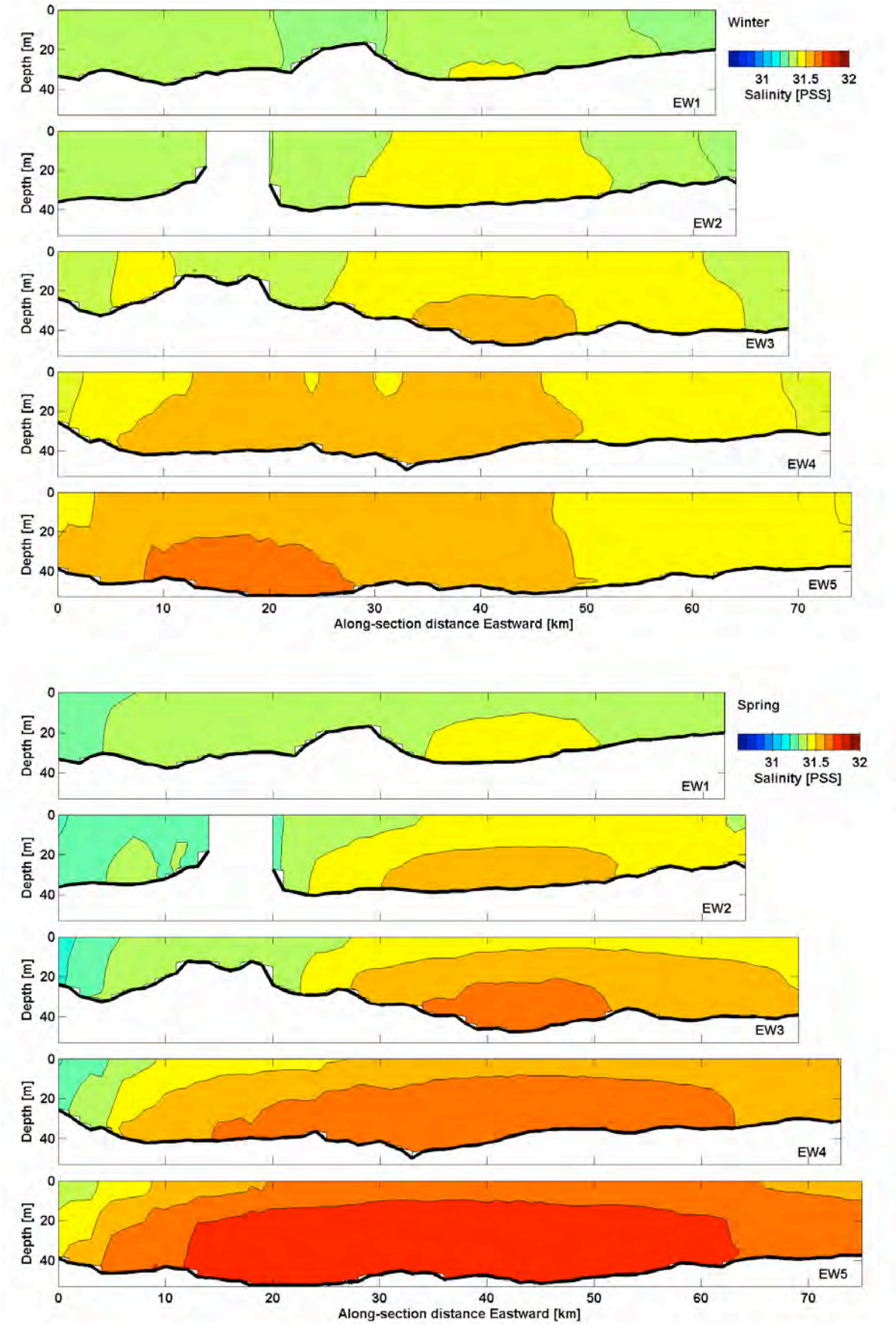

Figure 58. Simulation: Salinity, seasonal-mean, EW. (upper) Winter. (lower) Spring.

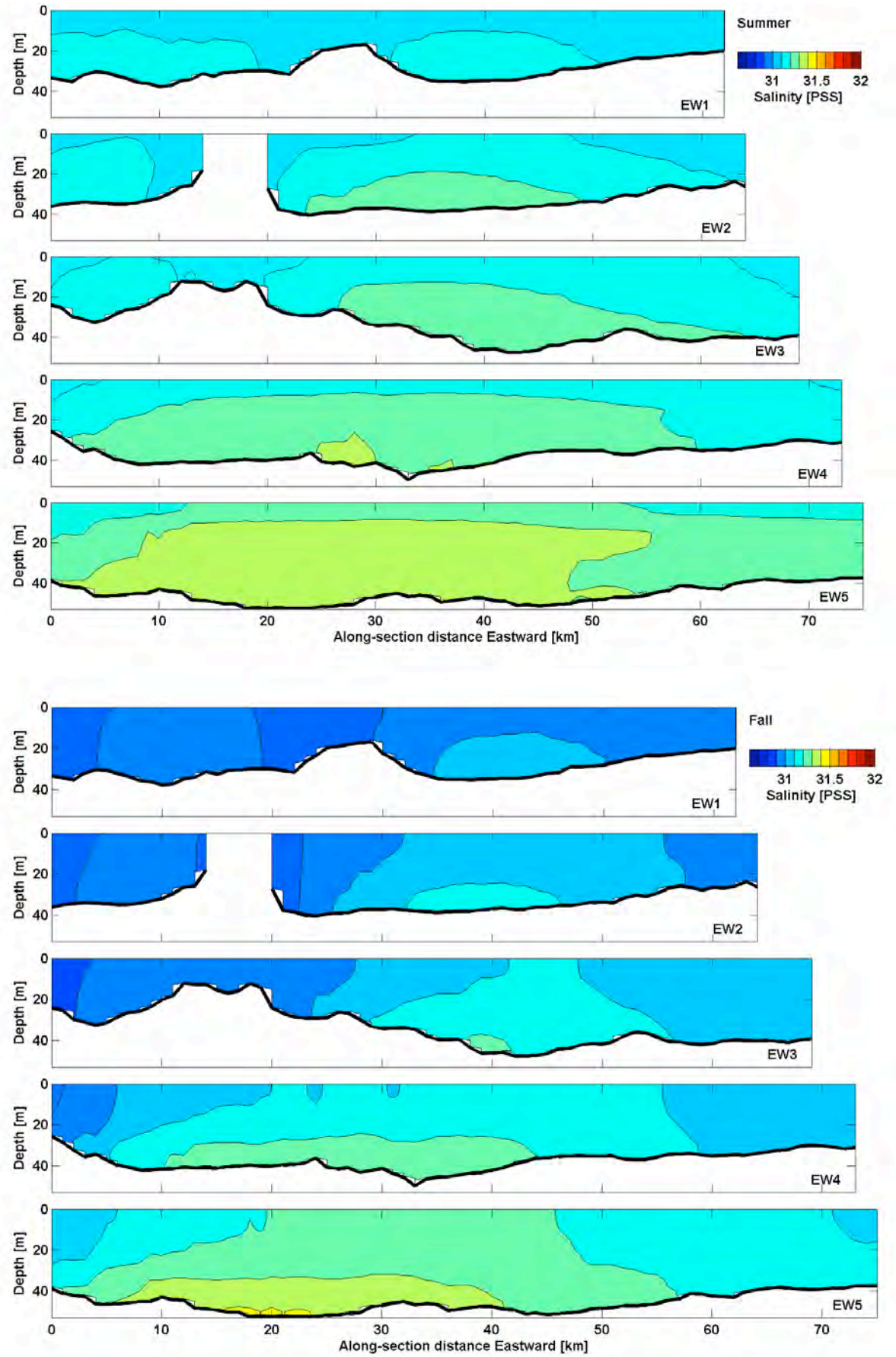

Figure 59. Simulation: Salinity, seasonal-mean, EW. (upper) Summer. (lower) Fall.

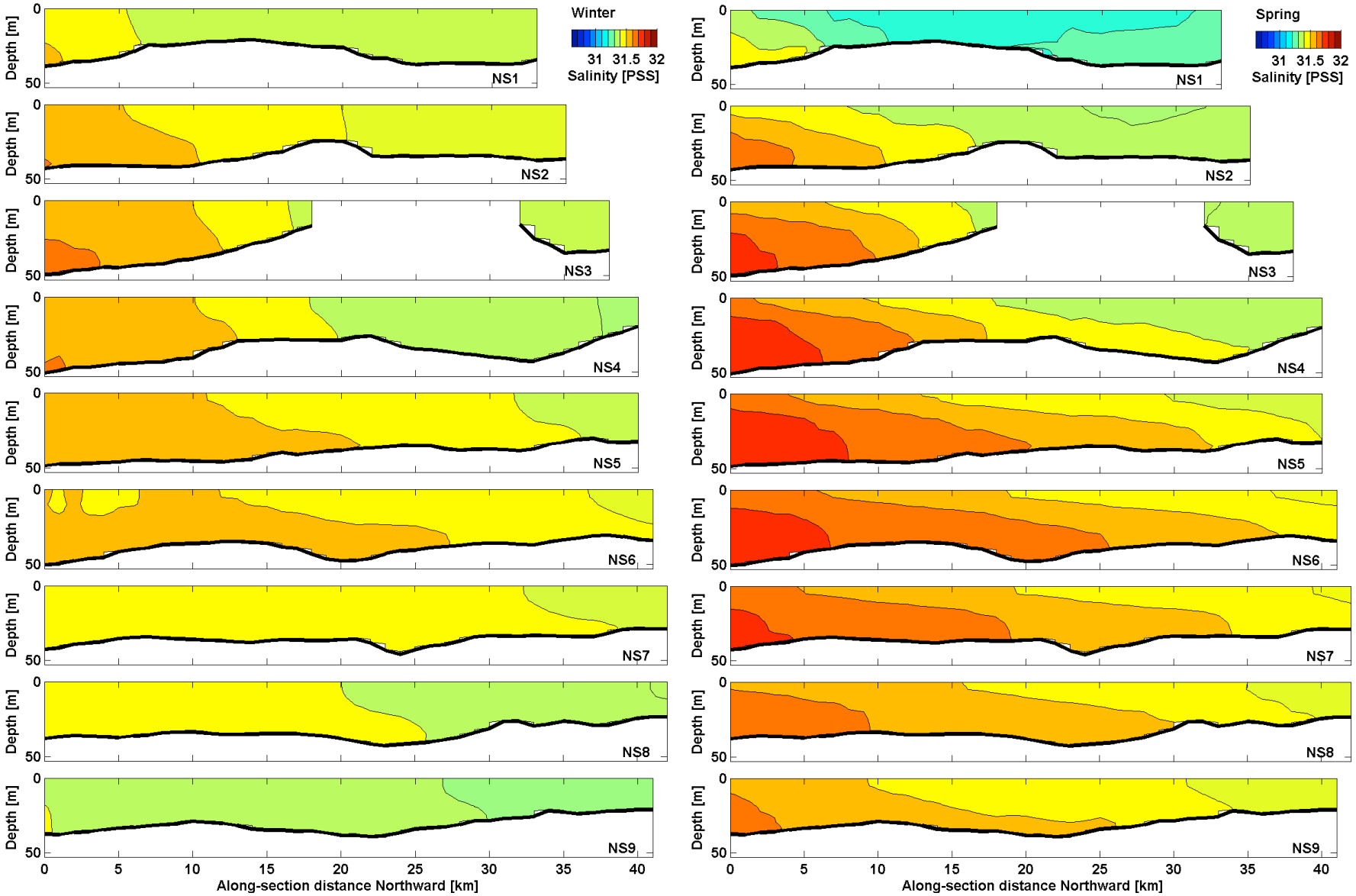

Figure 60. Simulation: Salinity, seasonal-mean, NS. (left) Winter. (right) Spring.

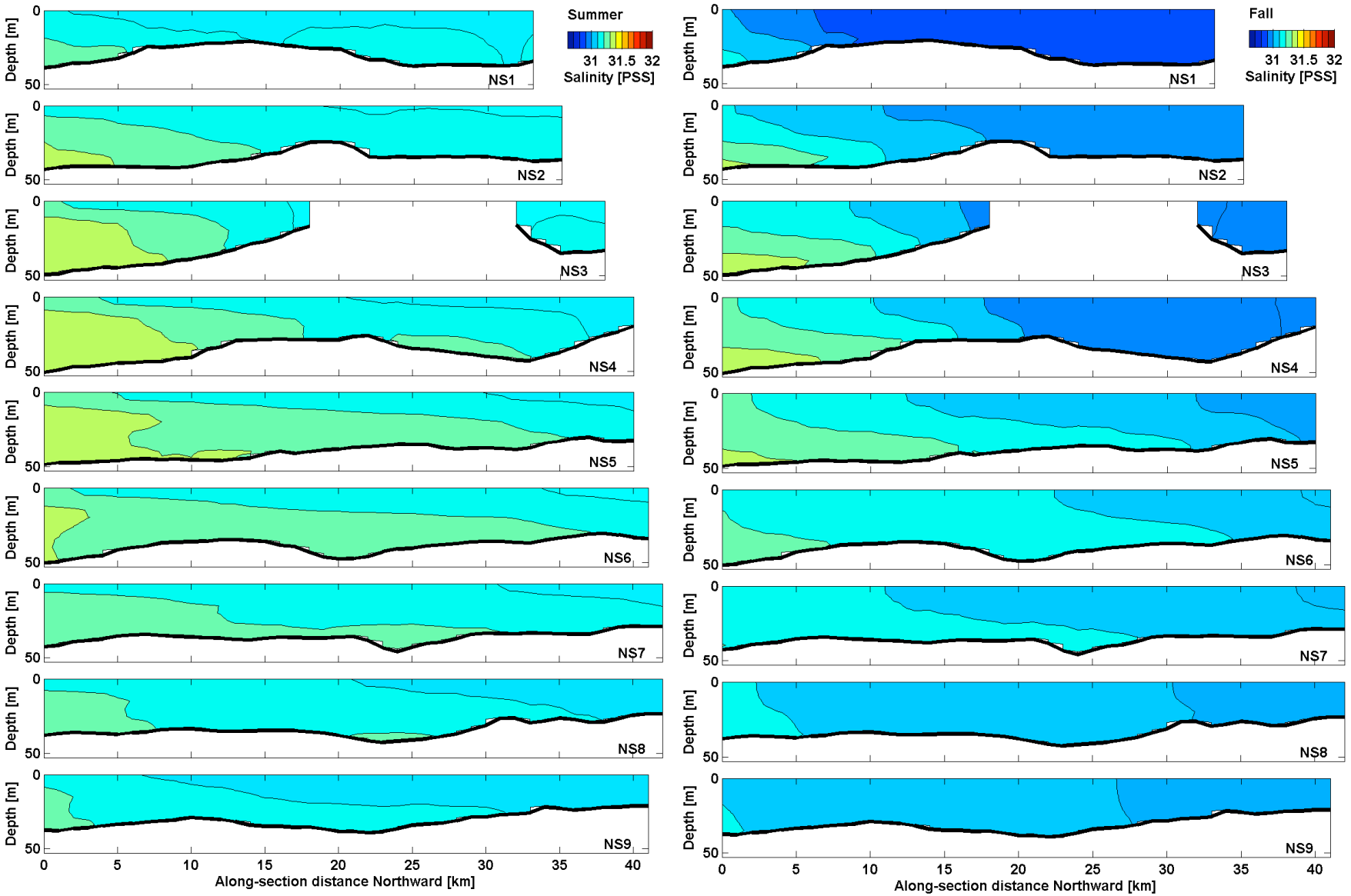

Figure 61. Simulation: Salinity, seasonal-mean, NS. (left) Summer. (right) Fall.

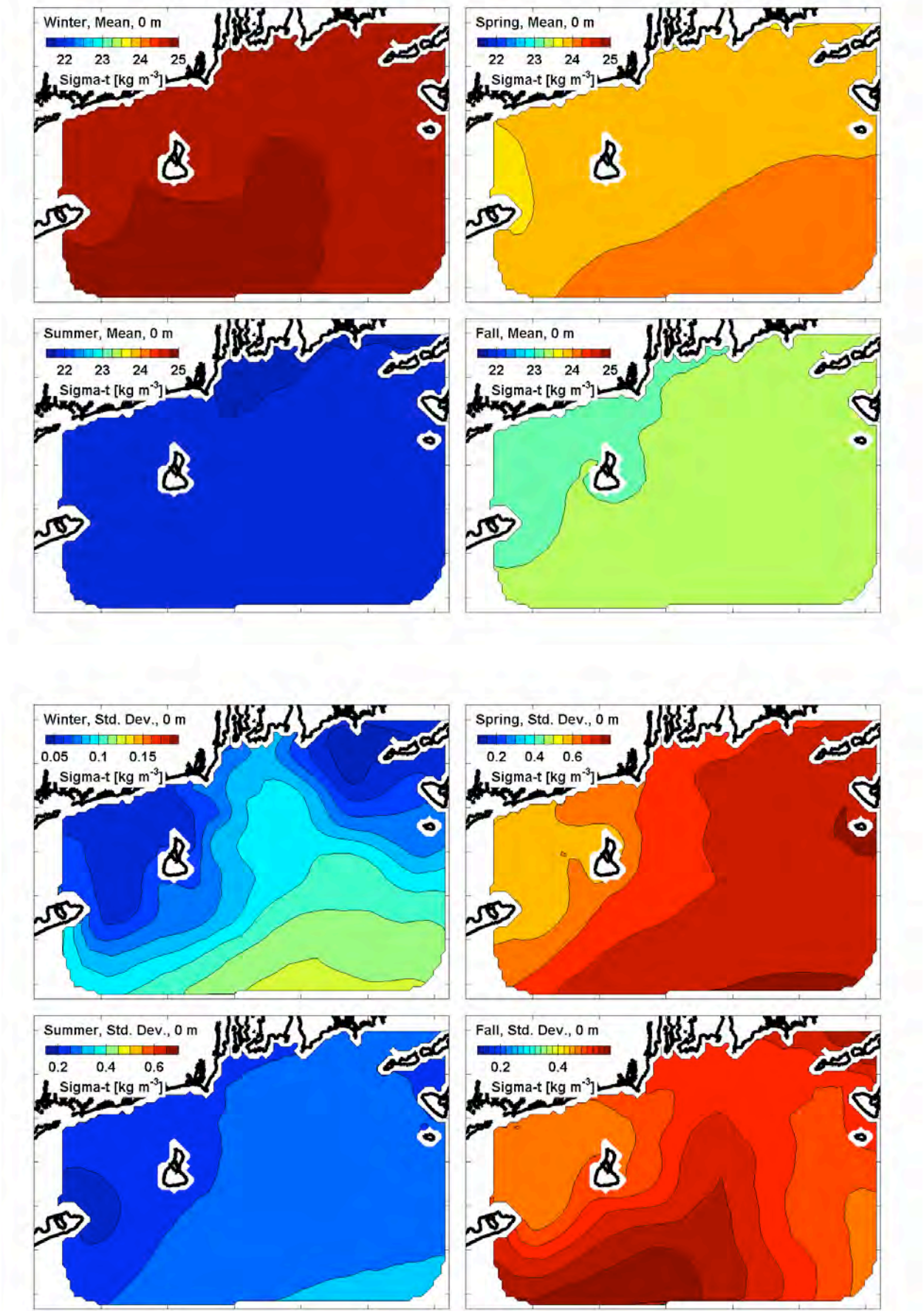

Figure 62. Simulation: Density anomaly, four seasons, surface. (upper) Mean. (lower) Std. dev.

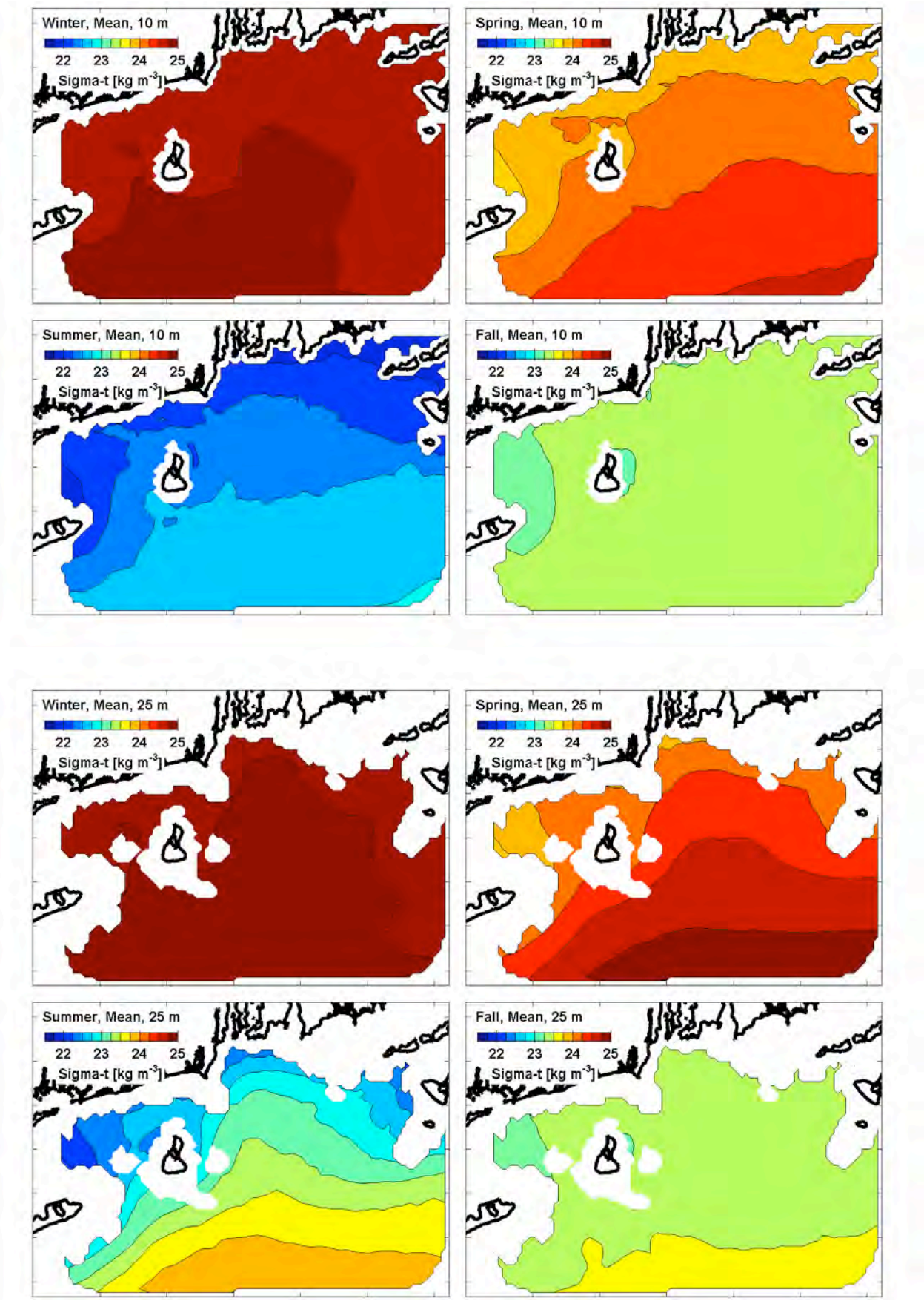

Figure 63. Simulation: Density anomaly, seasonal mean. (upper) 10 m deep. (lower) 25 m deep.

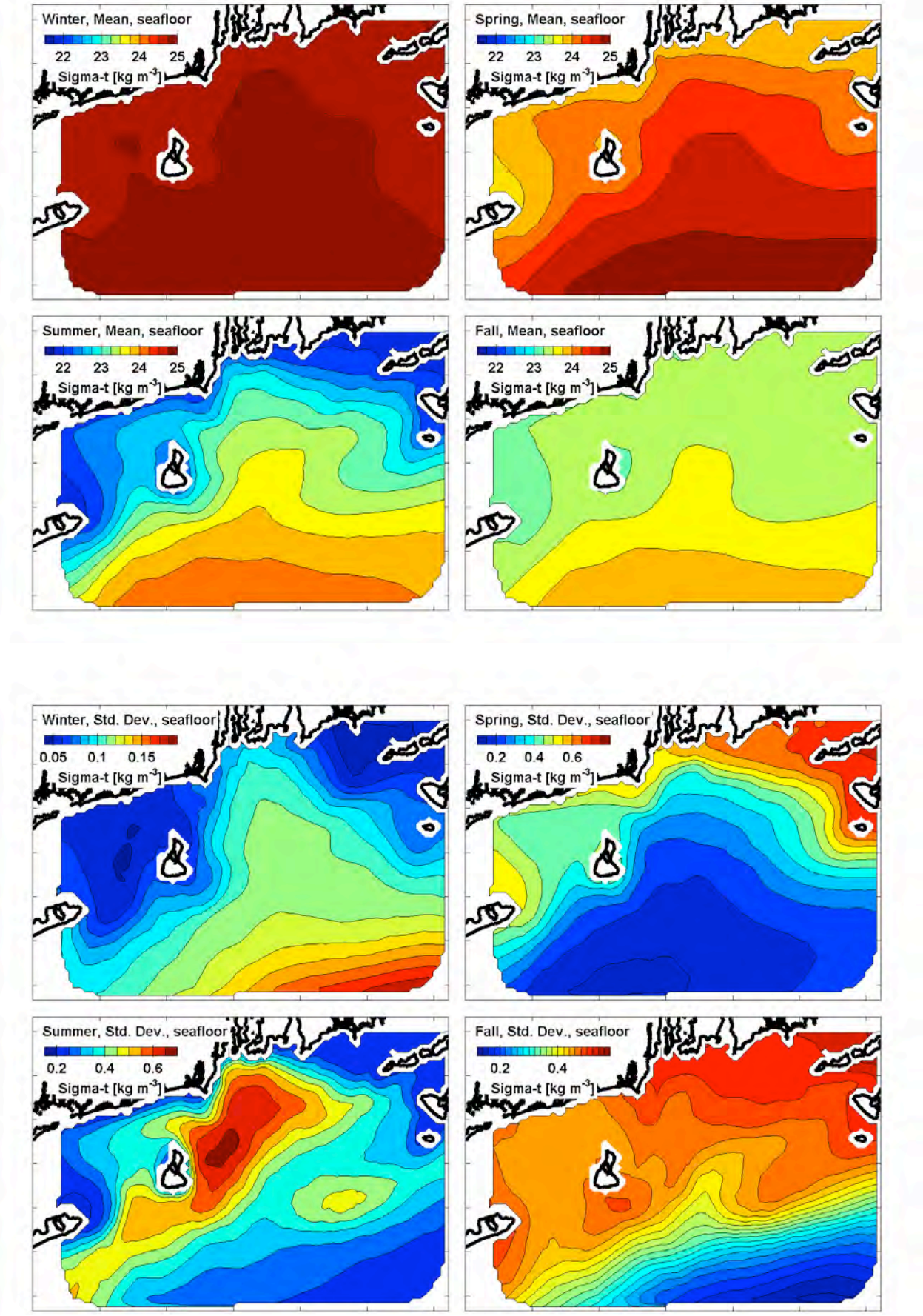

Figure 64. Simulation: Density anomaly, four seasons, seafloor. (upper) Mean. (lower) Std. dev.

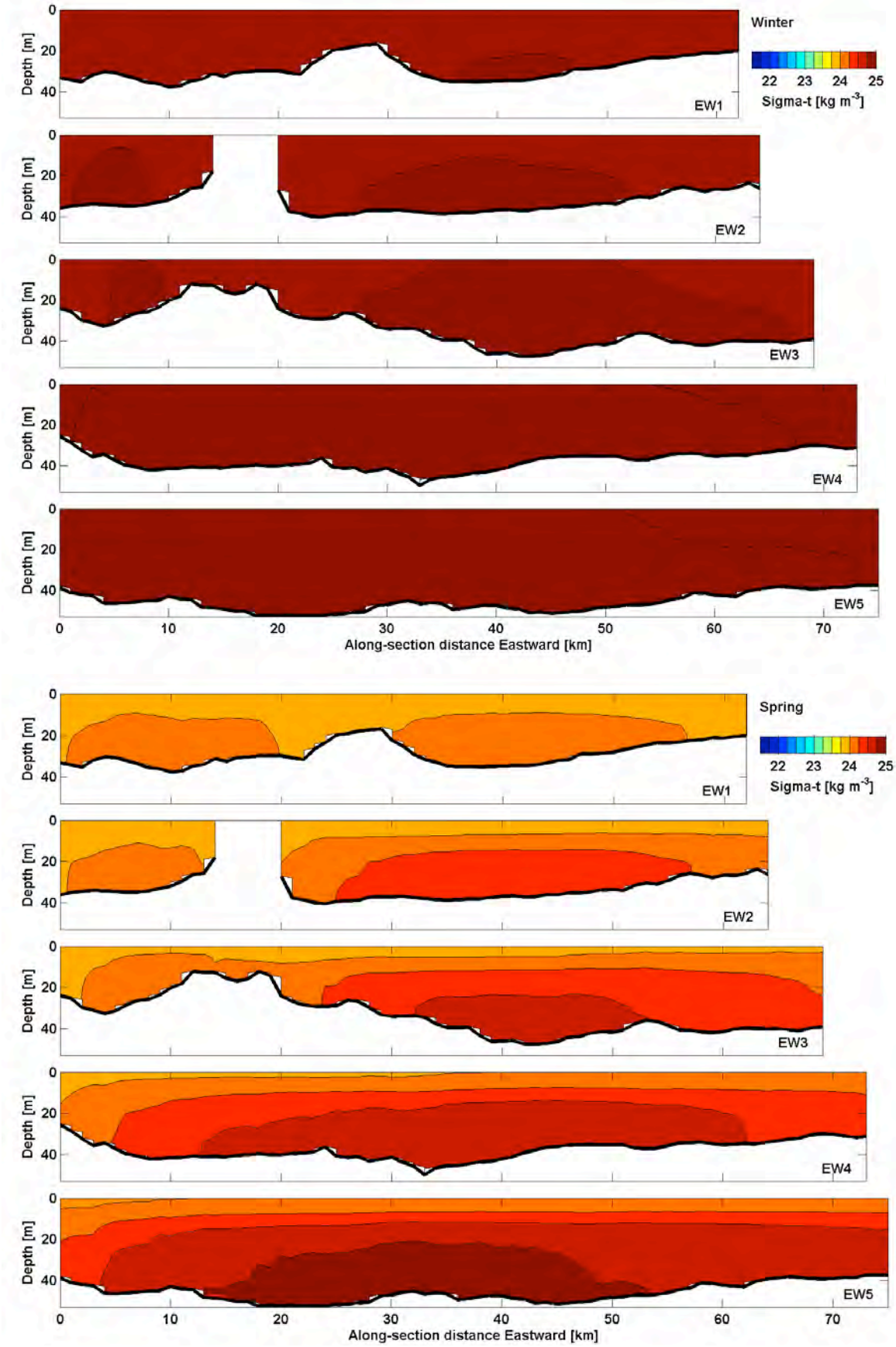

Figure 65. Simulation: Density anomaly, seasonal-mean, EW. (upper) Winter. (lower) Spring.

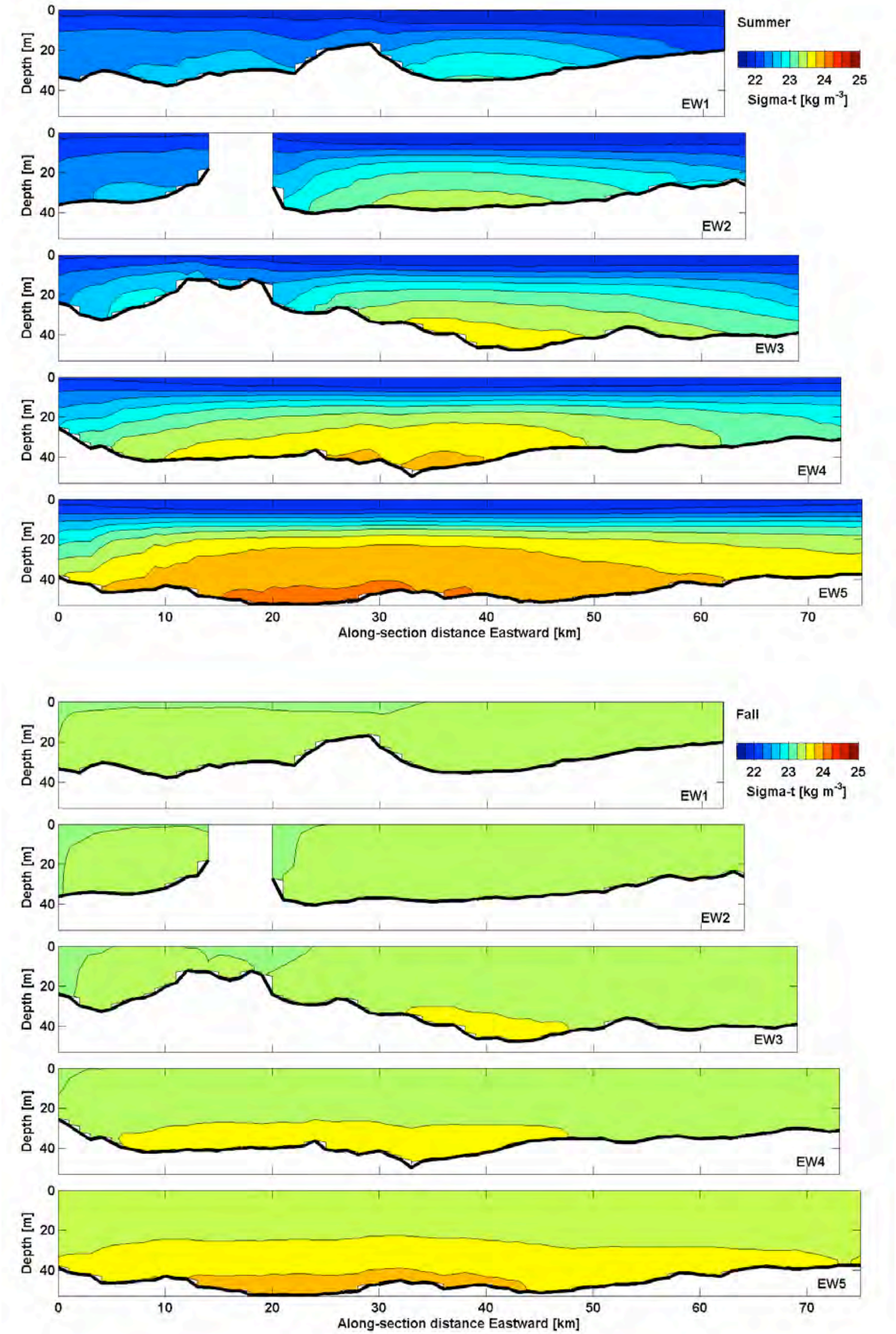

Figure 66. Simulation: Density anomaly, seasonal-mean, EW. (upper) Summer. (Lower) Fall.

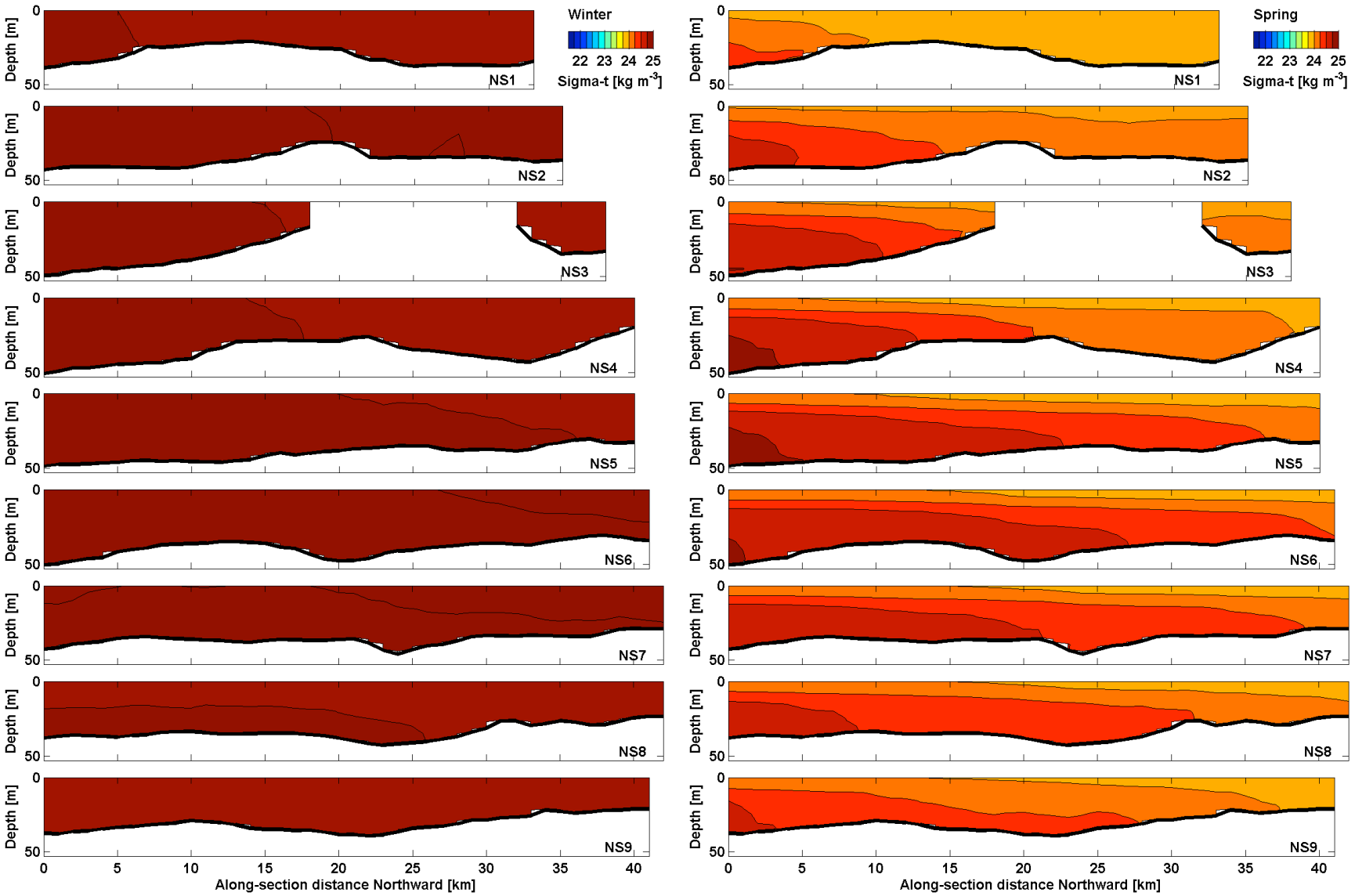

Figure 67. Simulation: Density anomaly, seasonal-mean, NS. (left) Winter. (right) Spring.

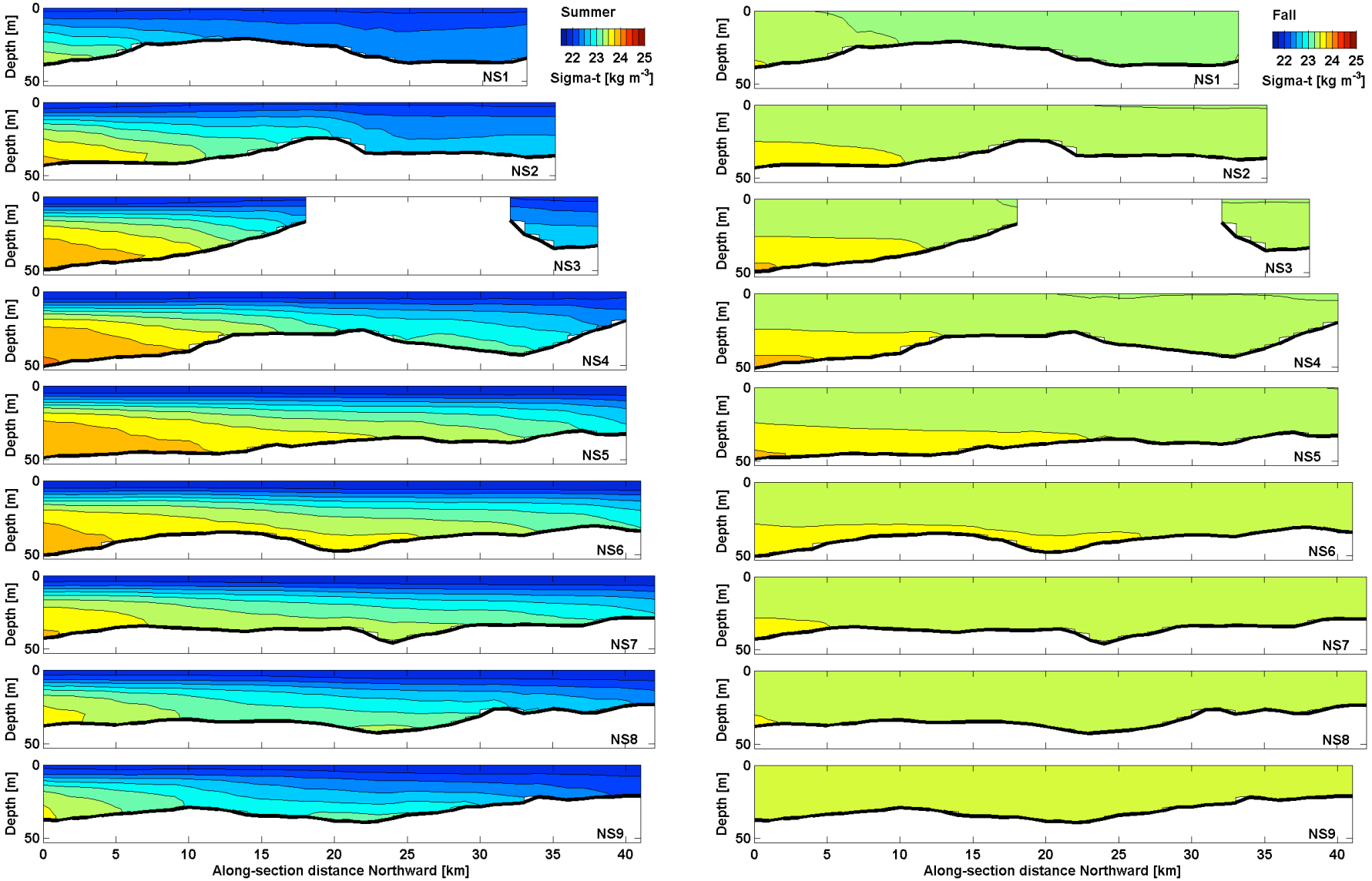

Figure 68. Simulation: Density anomaly, seasonal-mean, NS. (left) Summer. (right) Fall.

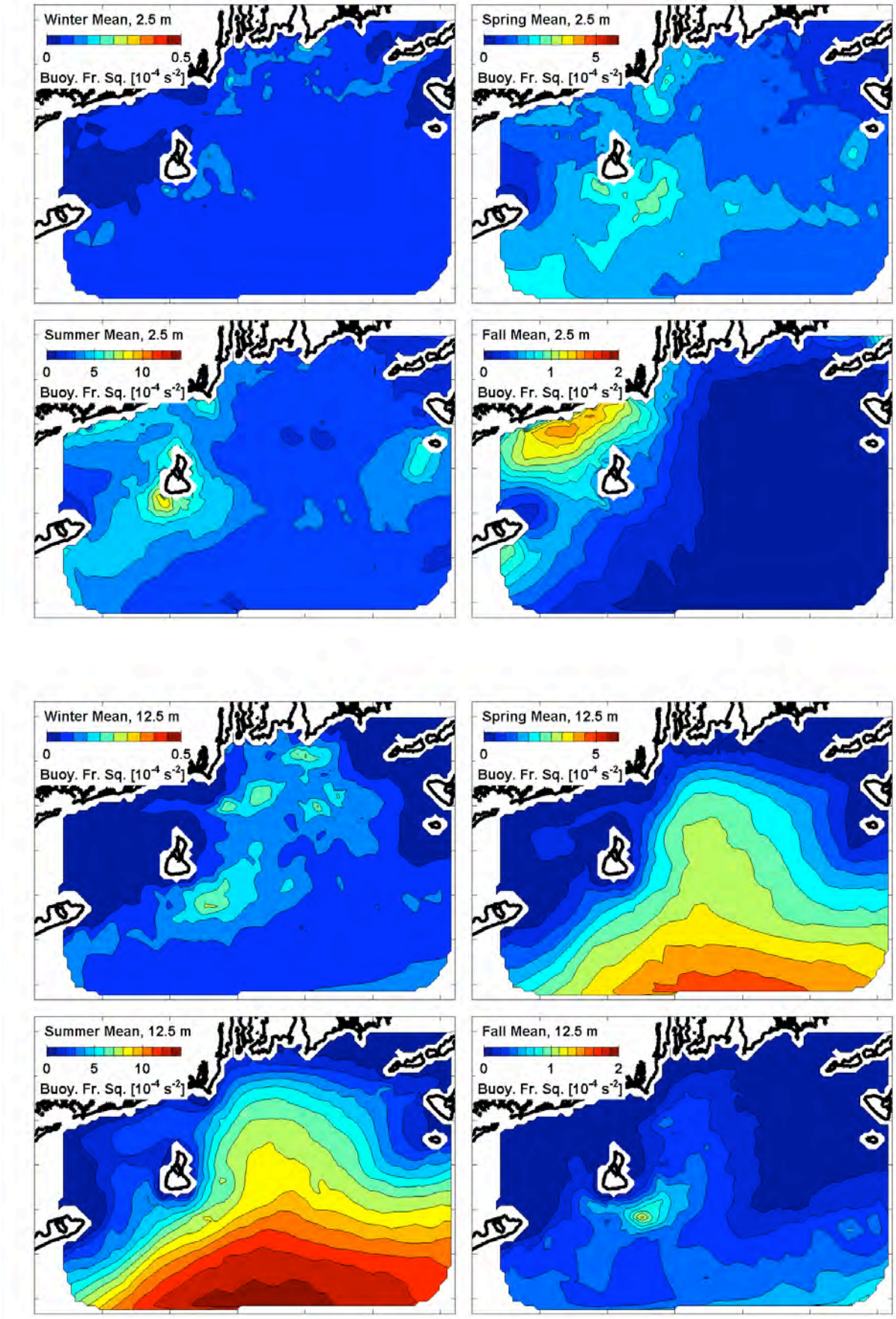

Figure 69. Simulation: Stratification, seasonal-mean. (upper) 2.5 m deep. (lower) 12.5 m deep.

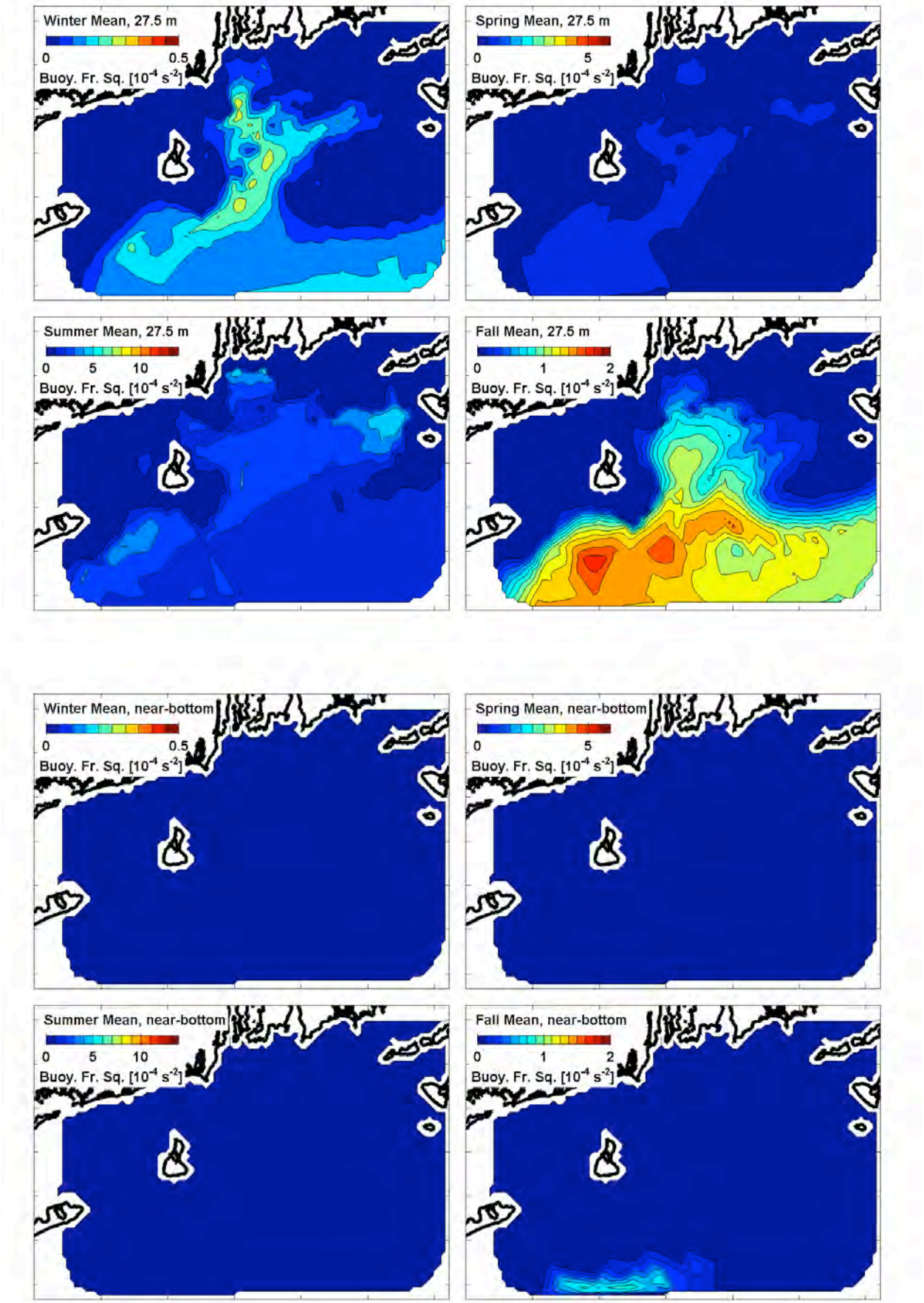

Figure 70. Simulation: Stratification, seasonal-mean. (upper) 27.5 m deep. (lower) near seafloor.

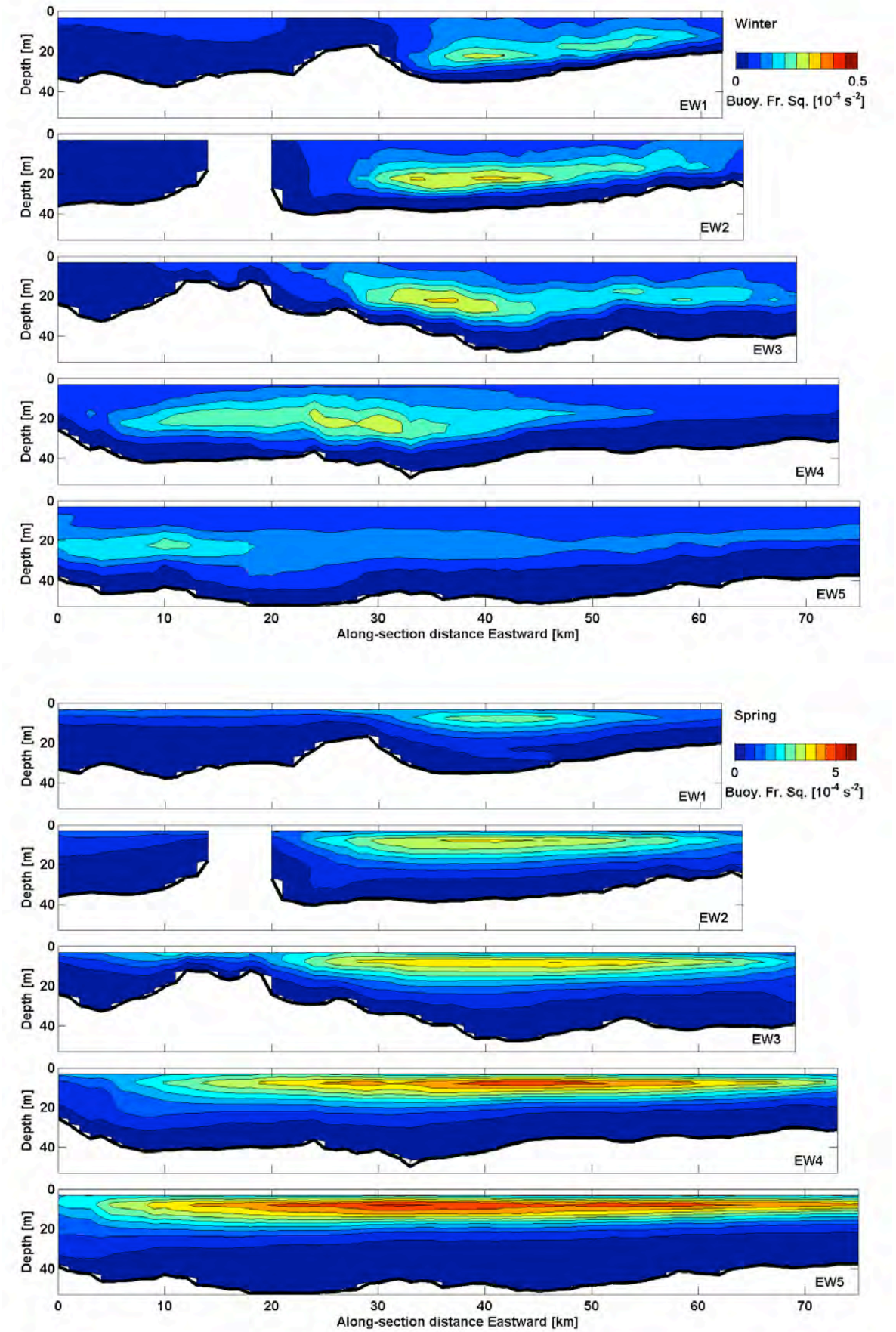

Figure 71. Simulation: Stratification, seasonal-mean, EW. (upper) Winter. (lower) Spring.

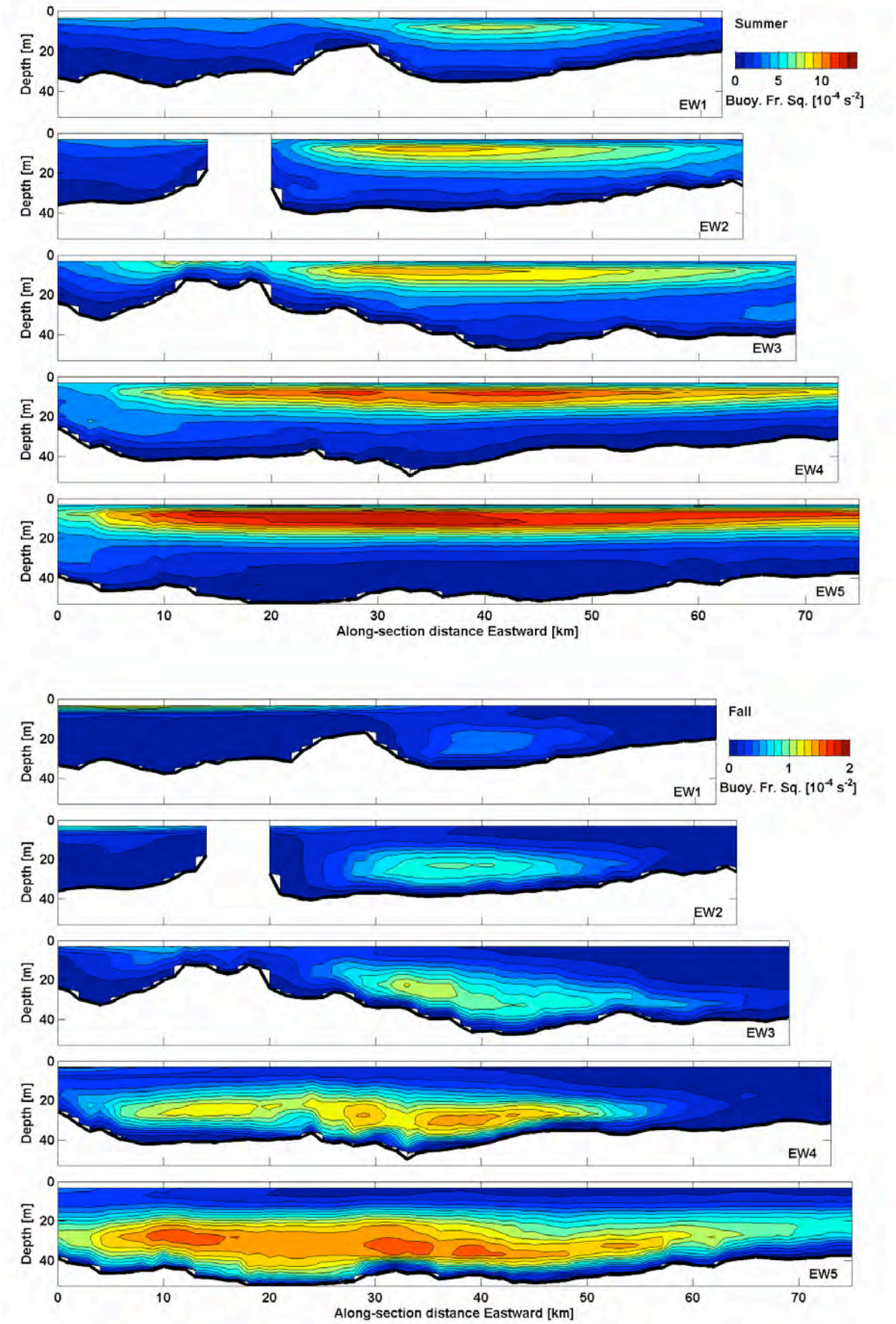

Figure 72. Simulation: Stratification, seasonal-mean, EW. (upper) Summer. (lower) Fall.

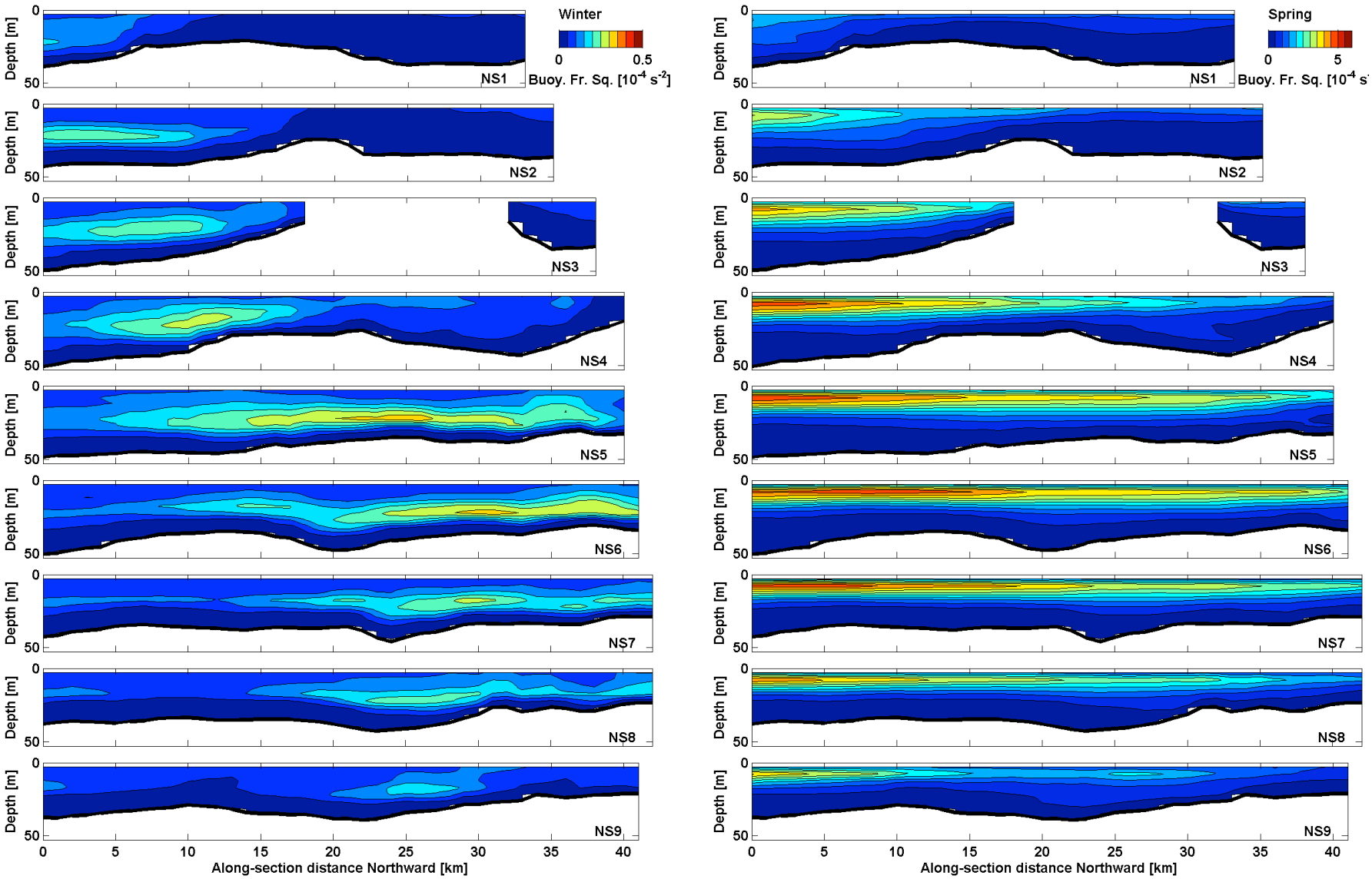

Figure 73. Simulation: Stratification, seasonal-mean, NS. (left) Winter. (right) Spring.

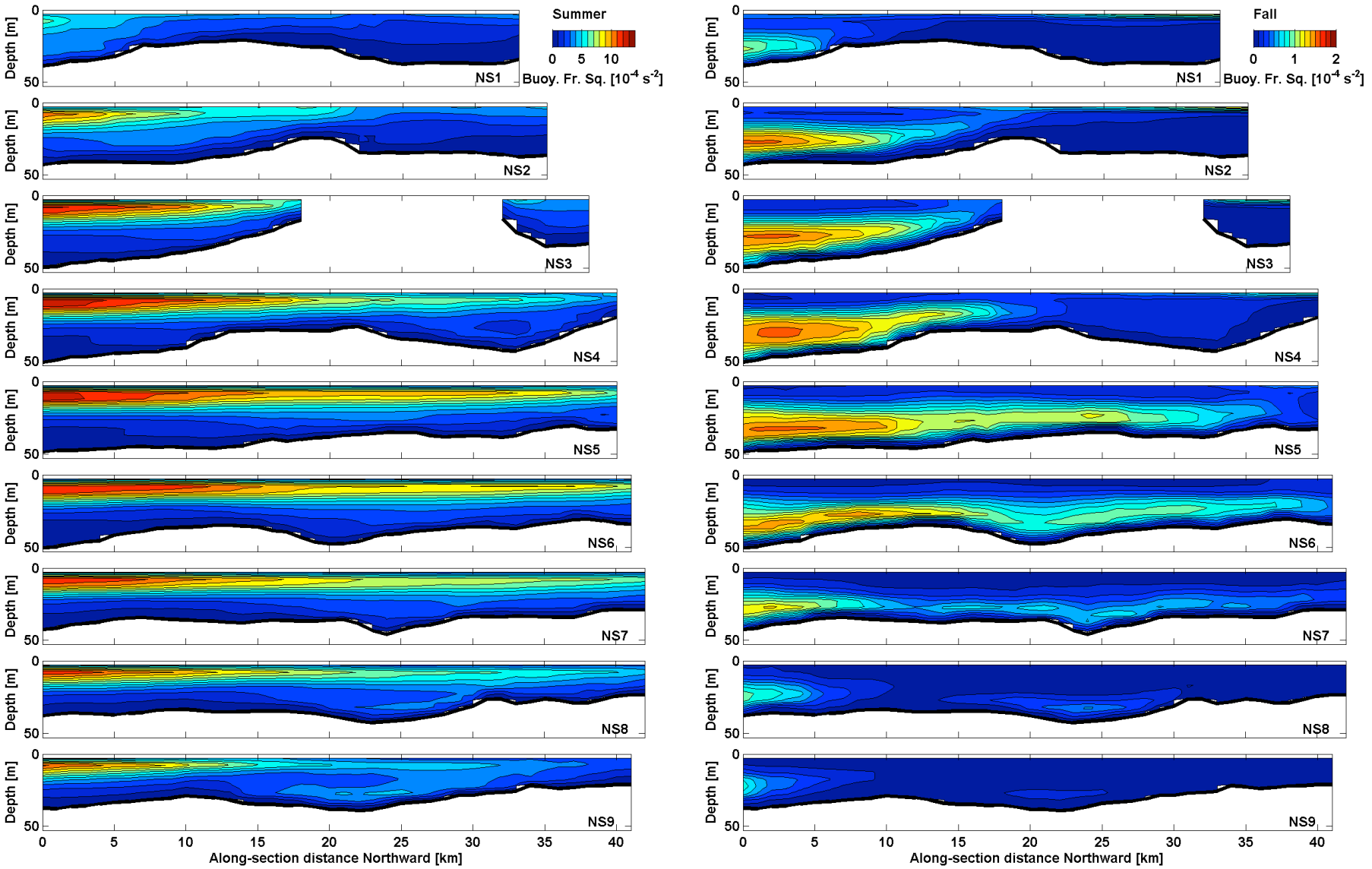

Figure 74. Simulation: Stratification, seasonal-mean, NS. (left) Summer. (right) Fall.

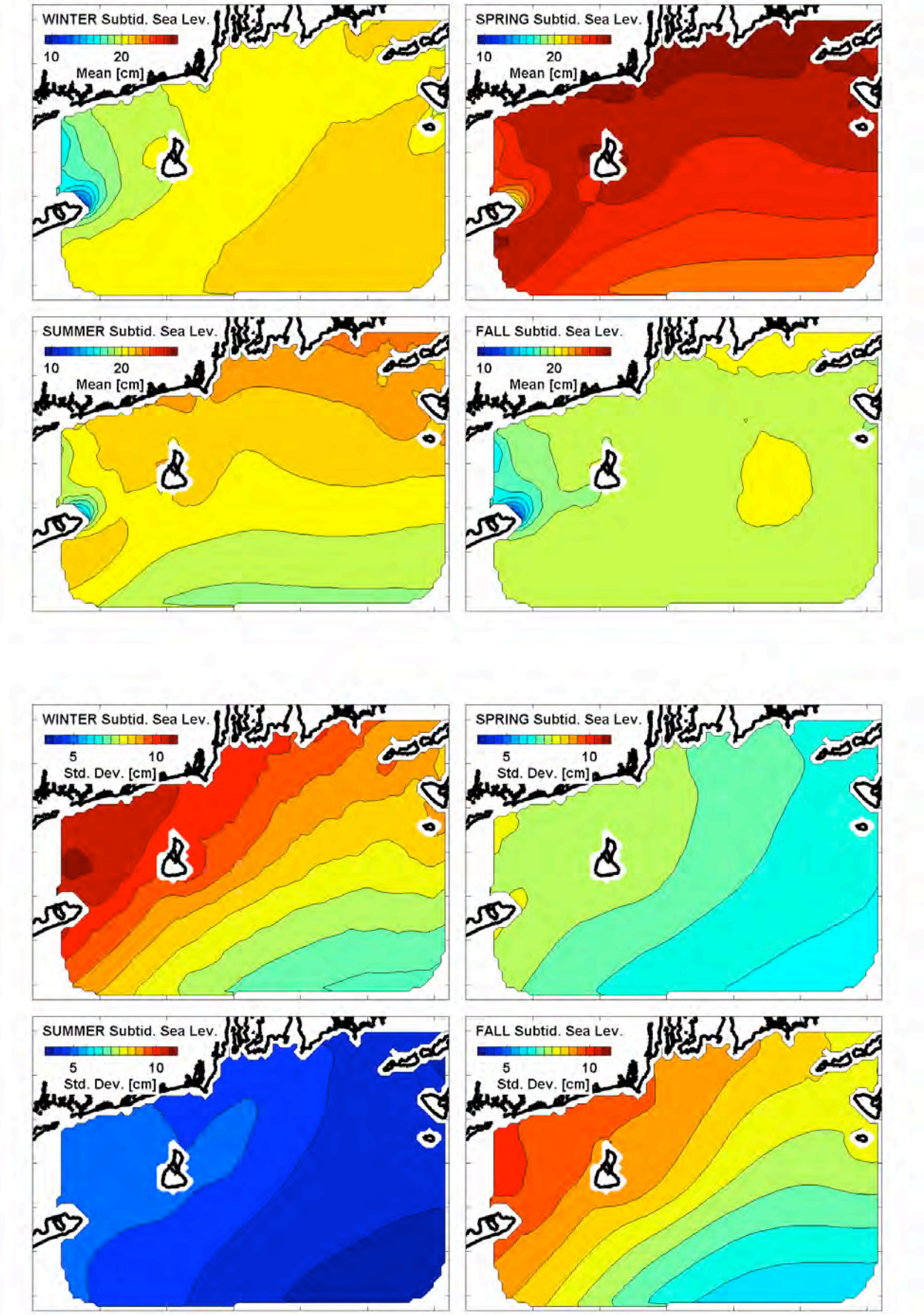

Figure 75. Simulation: Subtidal sea level, four seasons. (upper) Mean. (lower) Std. dev.

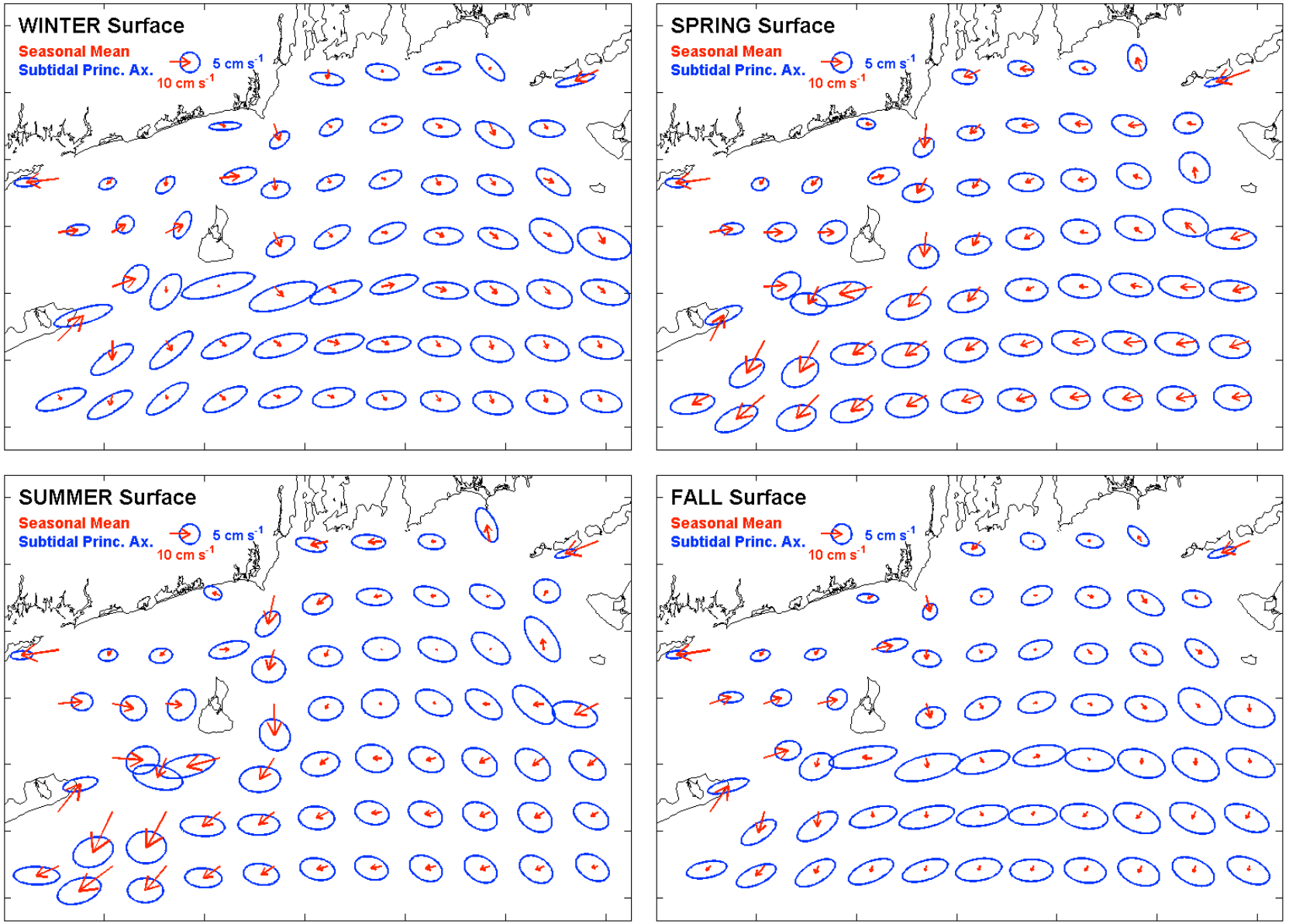

Figure 76. Simulation: Currents, seasonal-mean & subtidal ellipses. Surface.

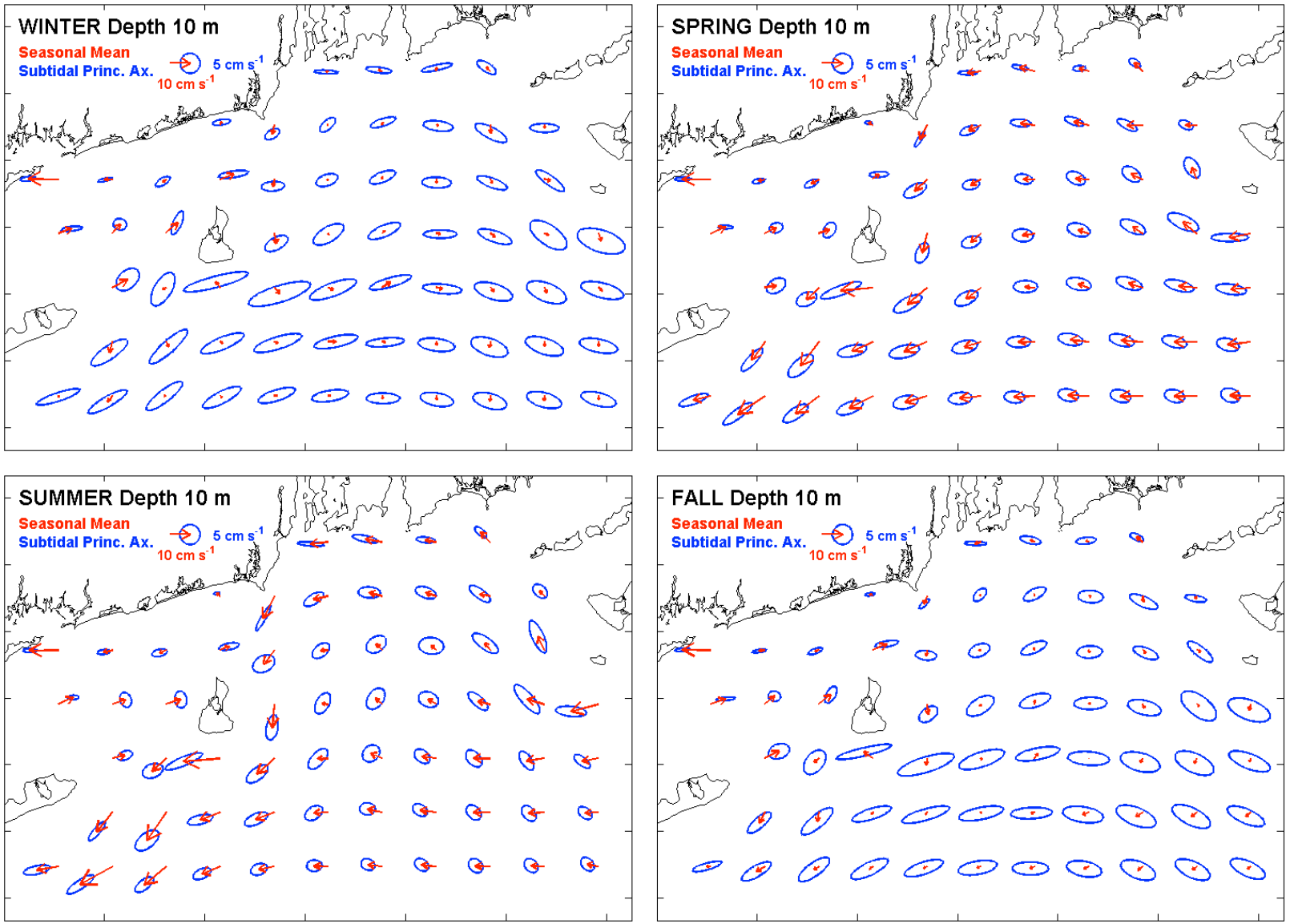

Figure 77. Simulation: Currents, seasonal-mean & subtidal ellipses. Depth 10 m.

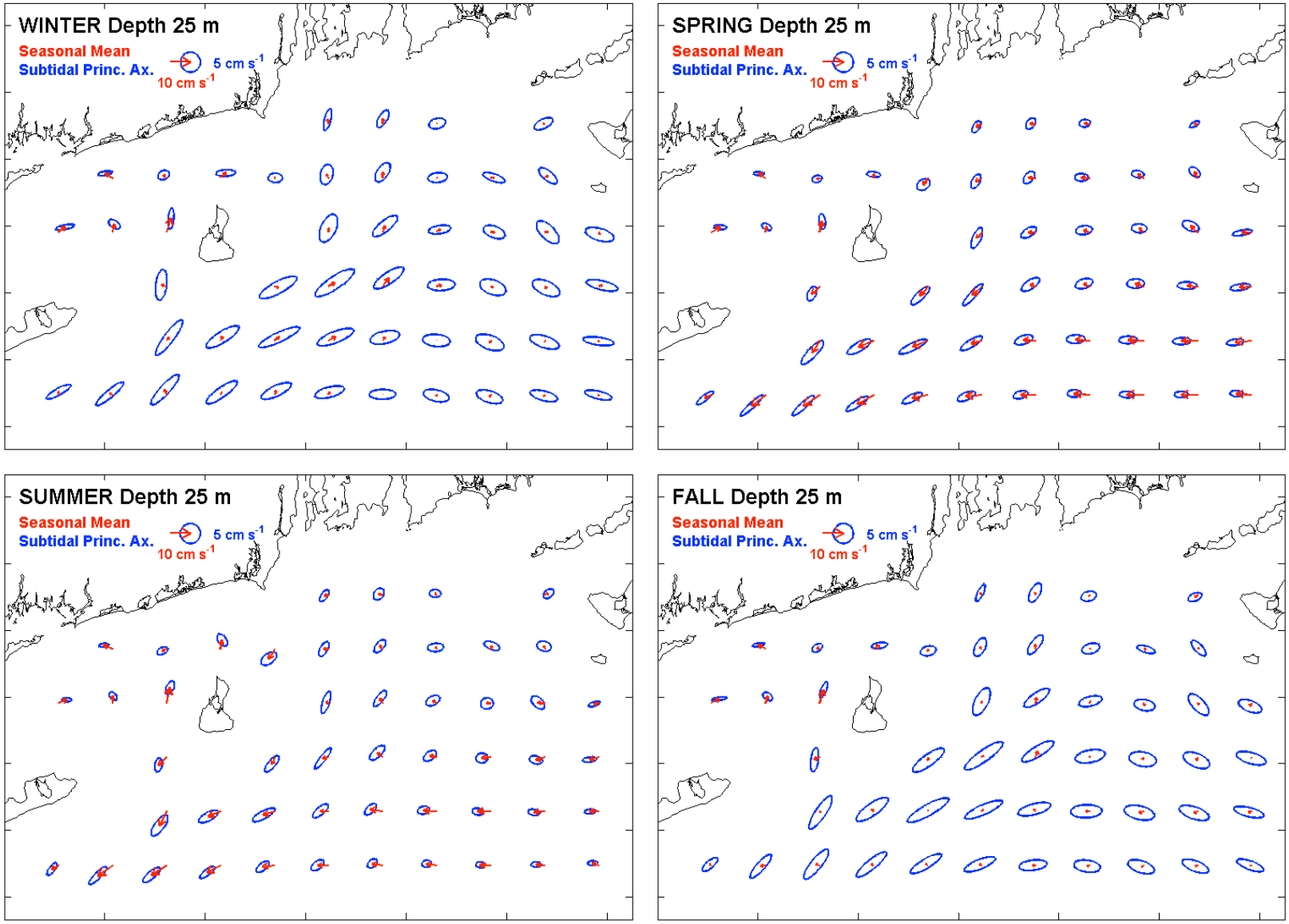

Figure 78. Simulation: Currents, seasonal-mean & subtidal ellipses. Depth 25 m.

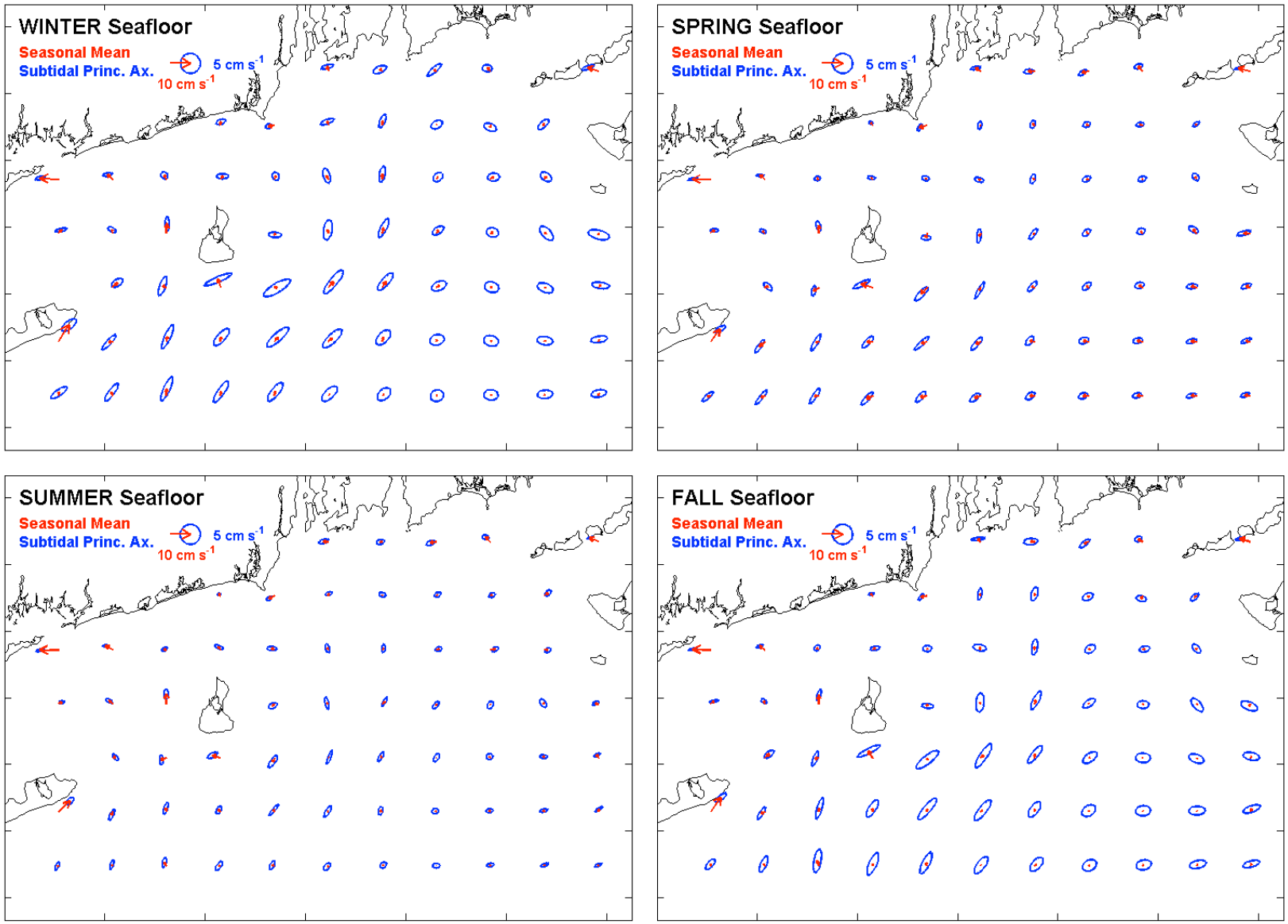

Figure 79. Simulation: Currents, seasonal-mean & subtidal ellipses. Seafloor.

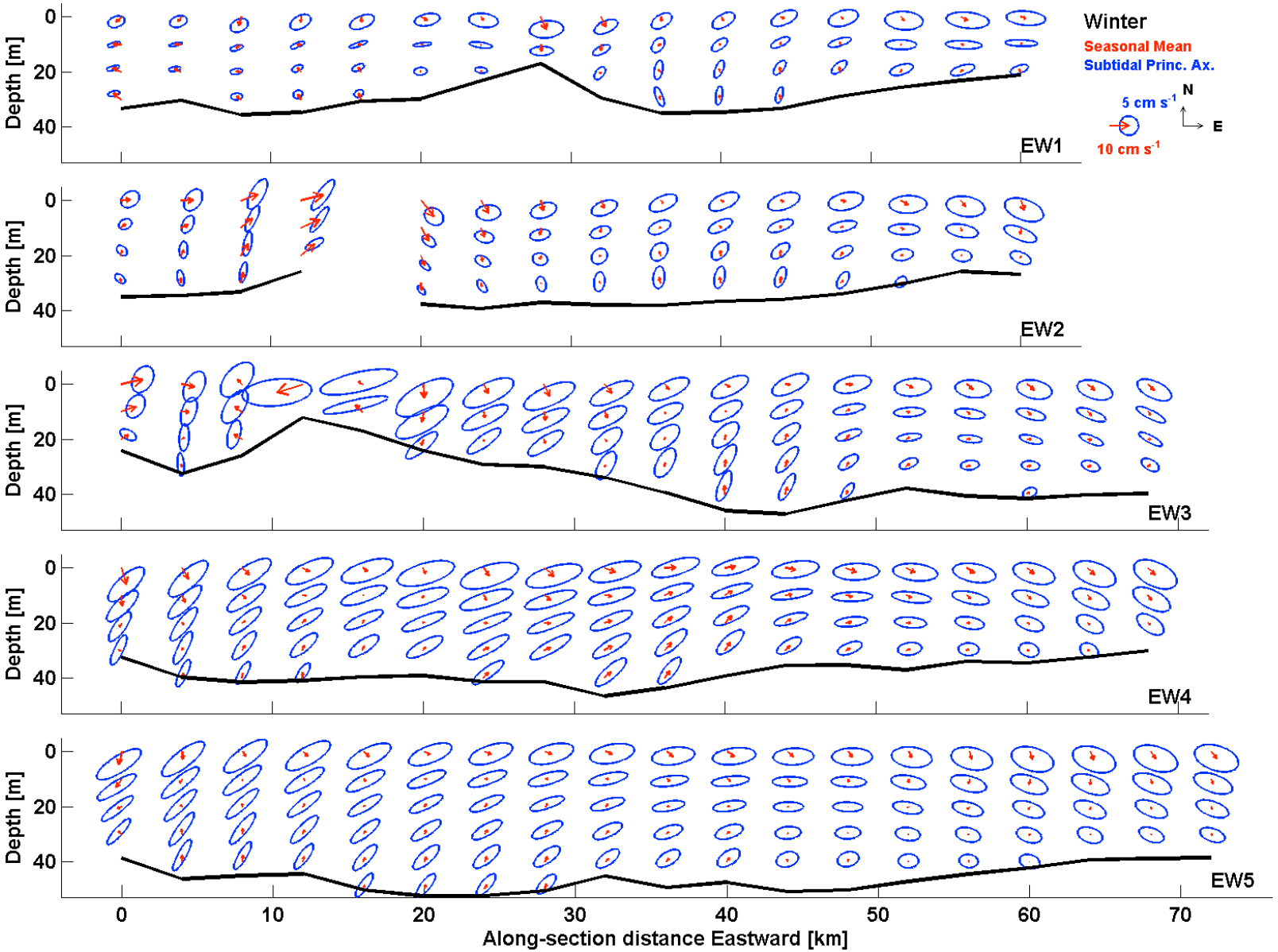

Figure 80. Simulation: Currents, plan view seas. mean & subtid. ellipses. EW sections, winter.

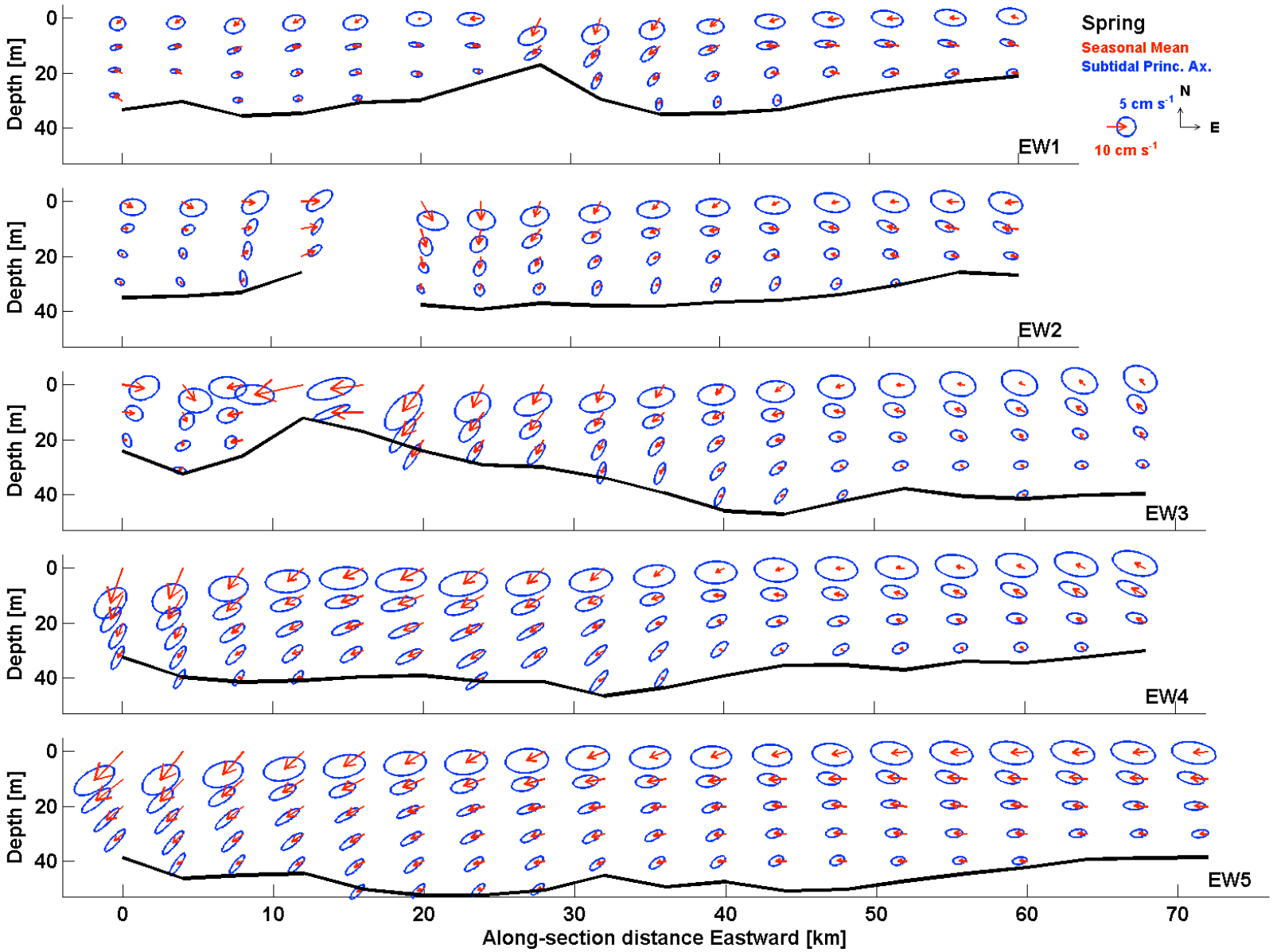

Figure 81. Simulation: Currents, plan view seas. mean & subtid. ellipses. EW sections, spring.

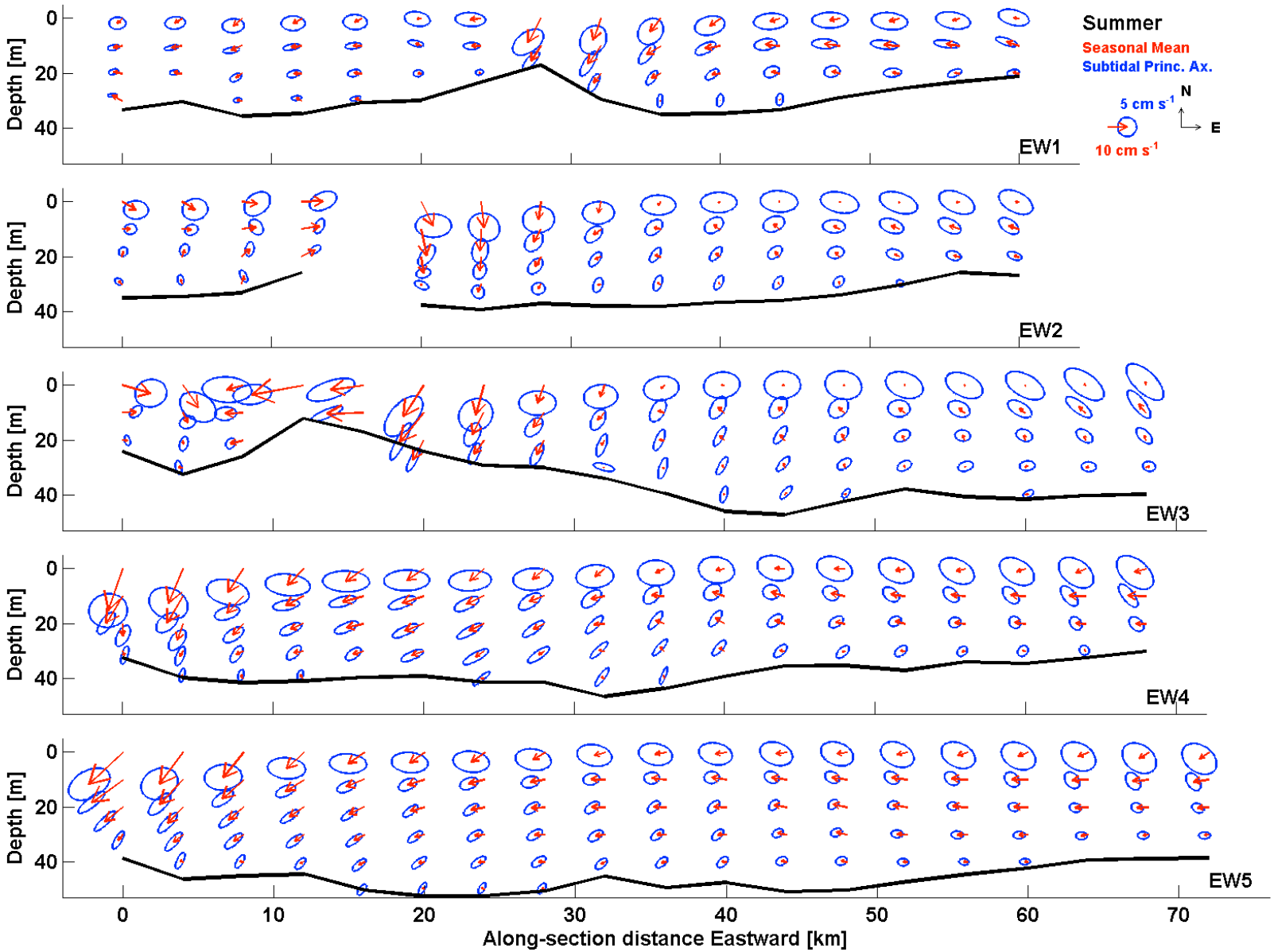

Figure 82. Simulation: Currents, plan view seas. mean & subtid. ellipses. EW sections, summer.

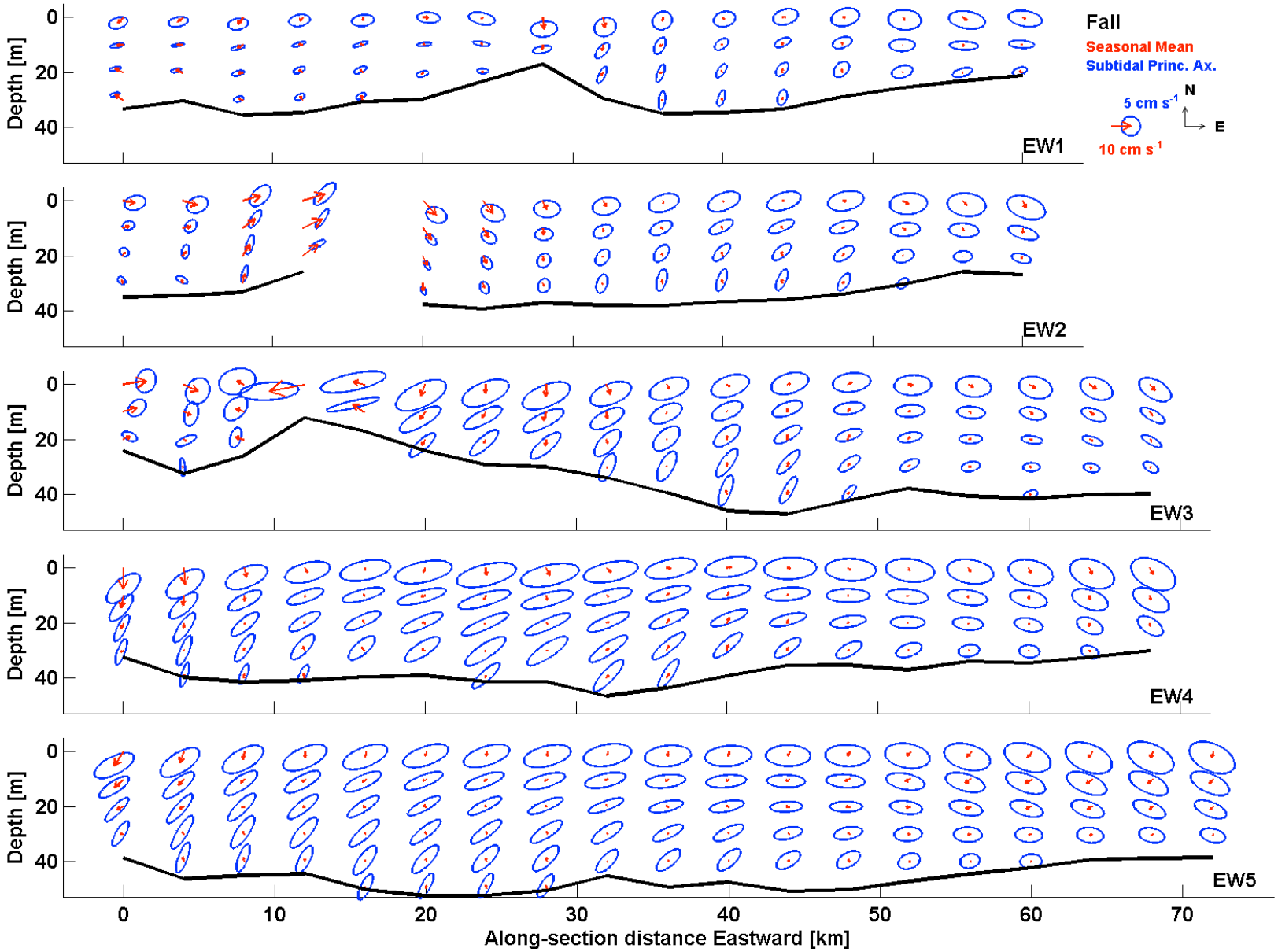

Figure 83. Simulation: Currents, plan view seas. mean & subtid. ellipses. EW sections, fall.

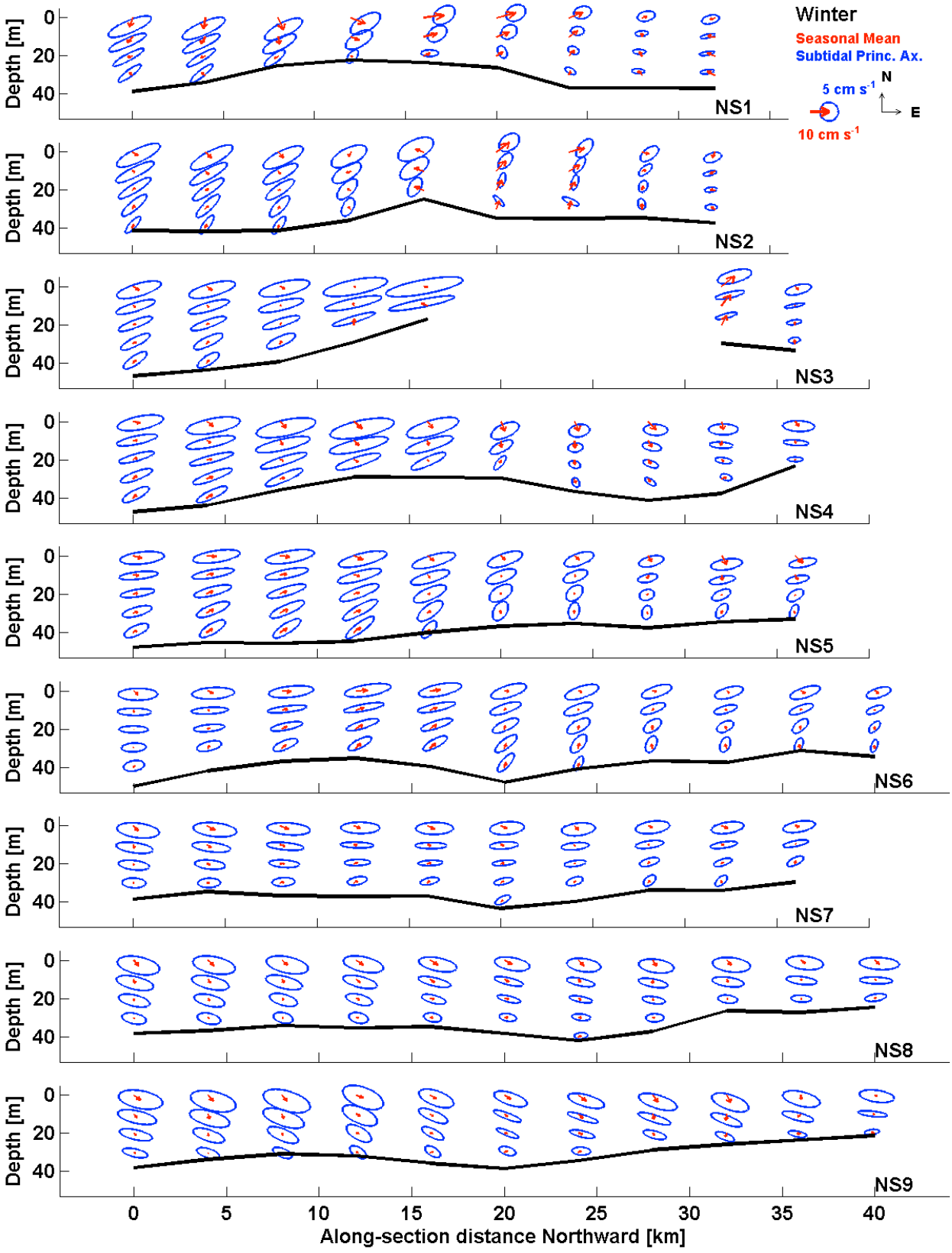

Figure 84. Simulation: Currents, plan view seas. mean & subtid. ellipses. NS sections, winter.

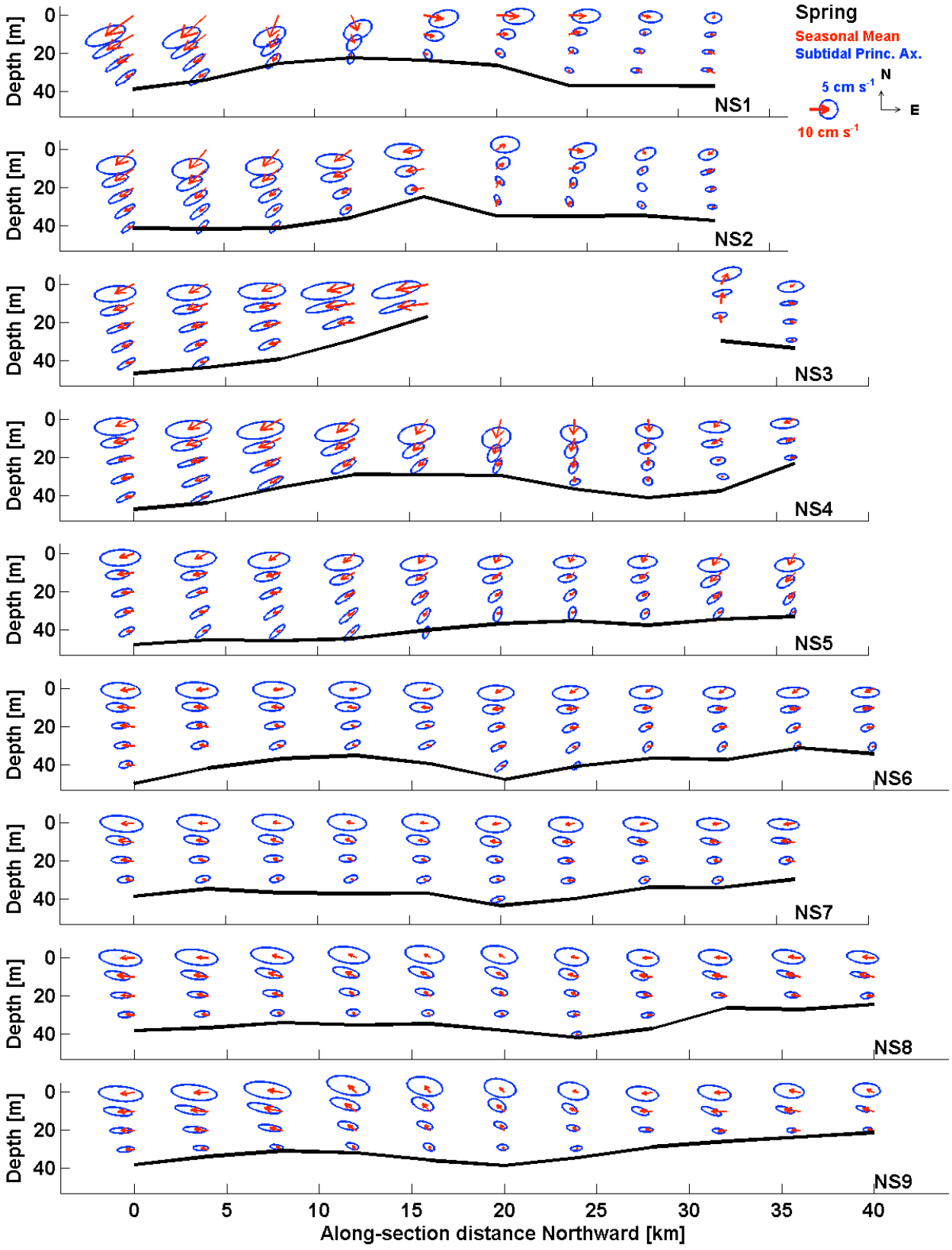

Figure 85. Simulation: Currents, plan view seas. mean & subtid. ellipses. NS sections, spring.

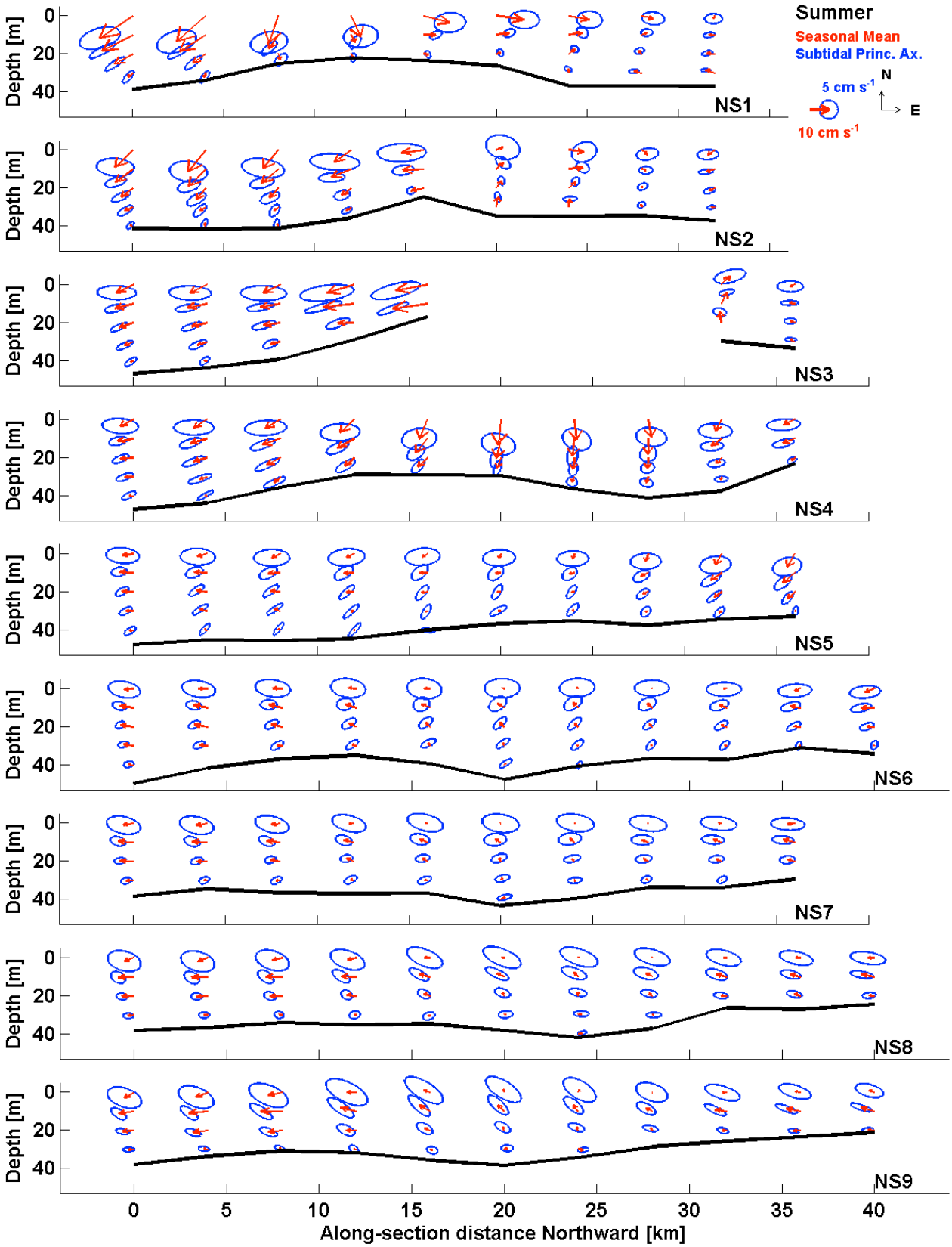

Figure 86. Simulation: Currents, plan view seas. mean & subtid. ellipses. NS sections, summer.

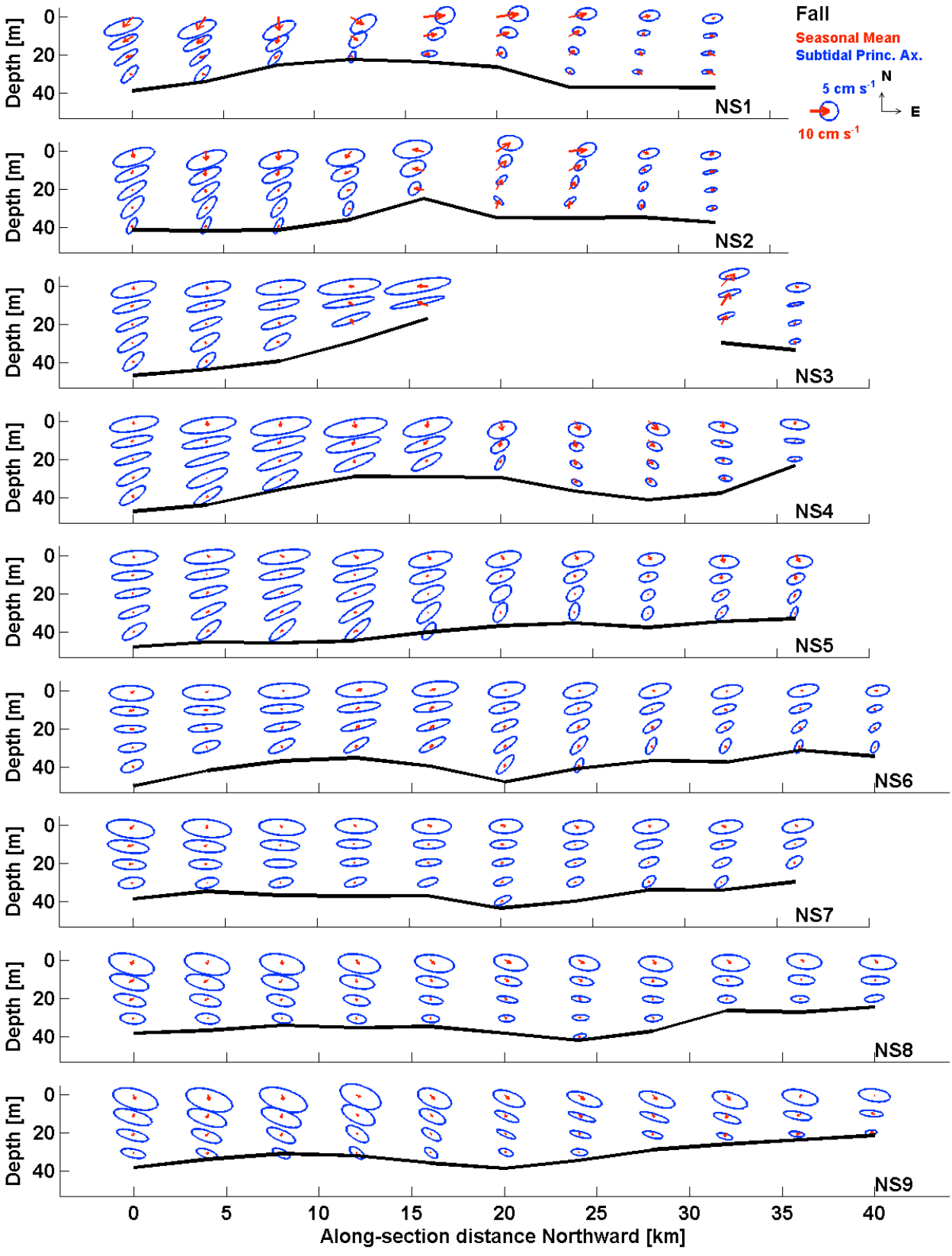

Figure 87. Simulation: Currents, plan view seas. mean & subtid. ellipses. NS sections, fall.

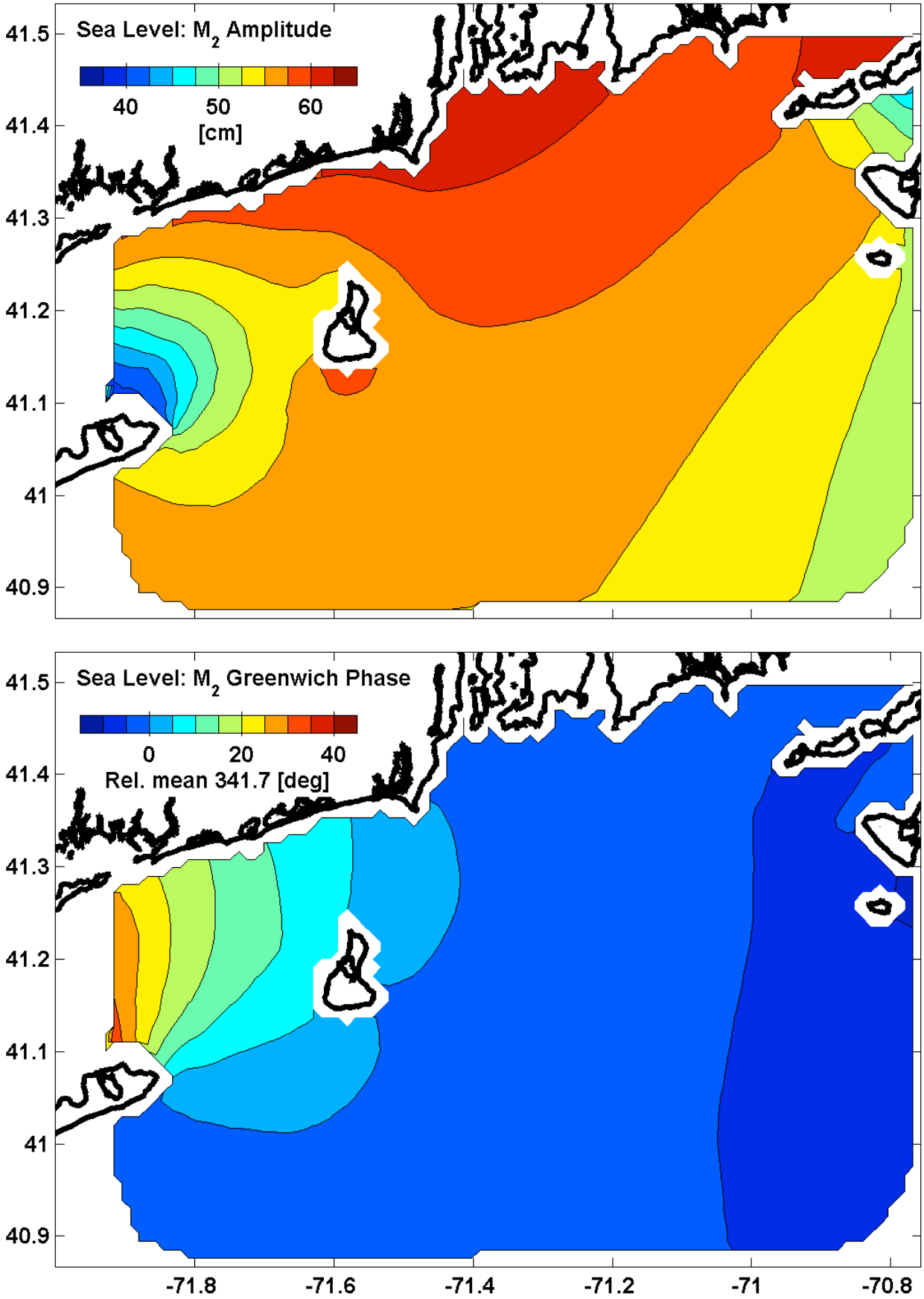

Figure 88. Simulation: Tidal height, M_2 constituent. (upper) Amplitude. (lower) Phase.

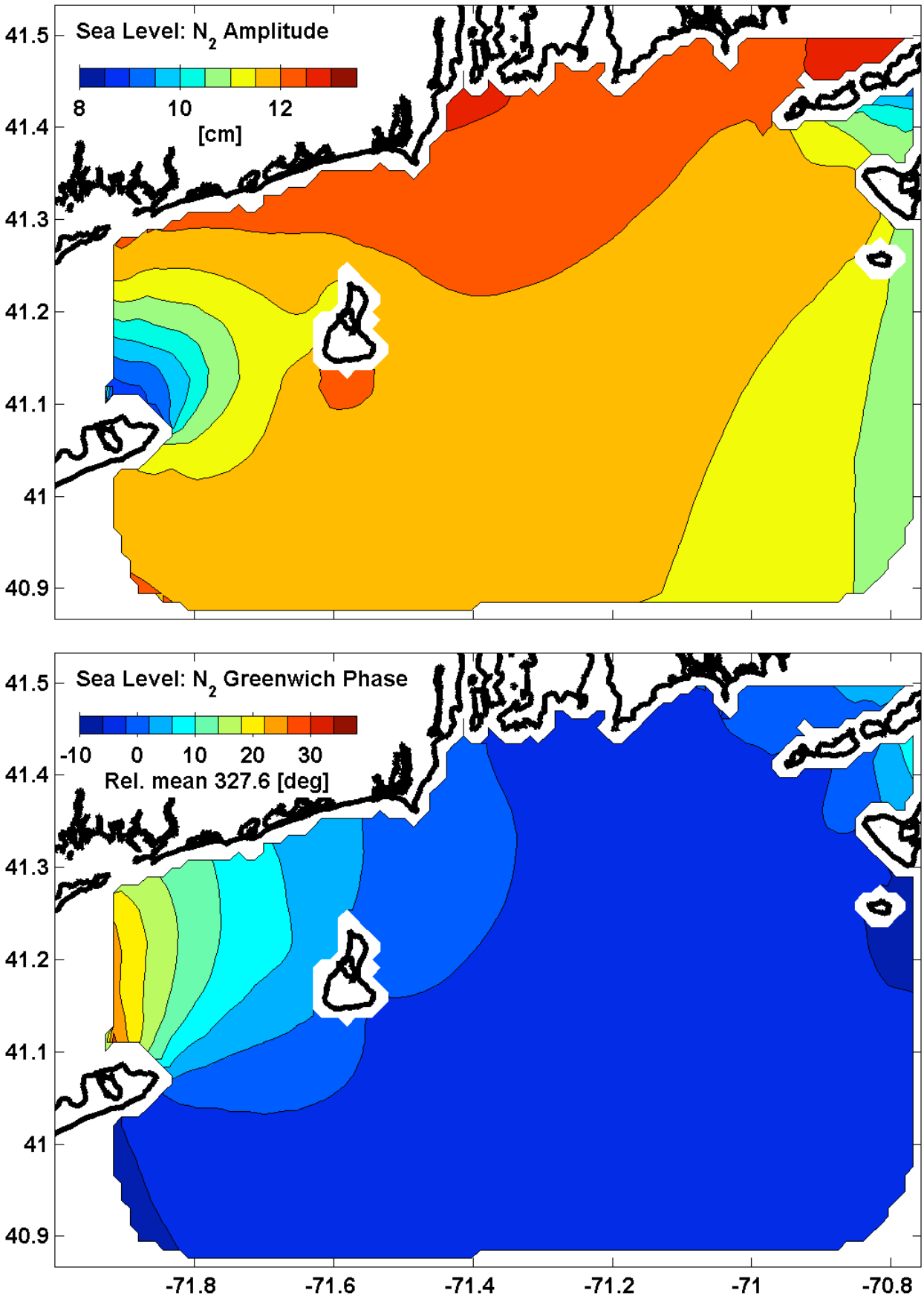

Figure 89. Simulation: Tidal height, N_2 constituent. (upper) Amplitude. (lower) Phase.

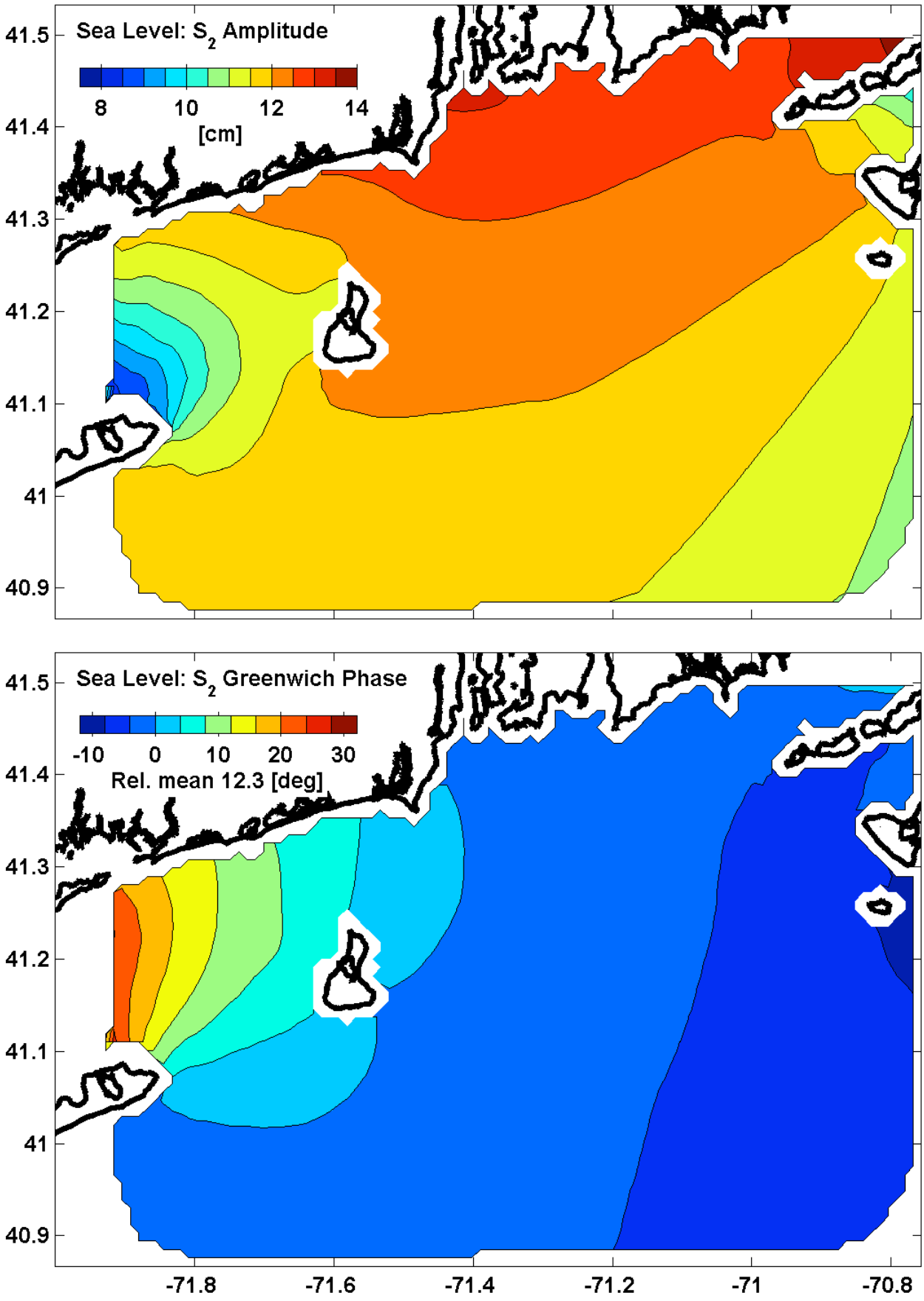

Figure 90. Simulation: Tidal height, S_2 constituent. (upper) Amplitude. (lower) Phase.

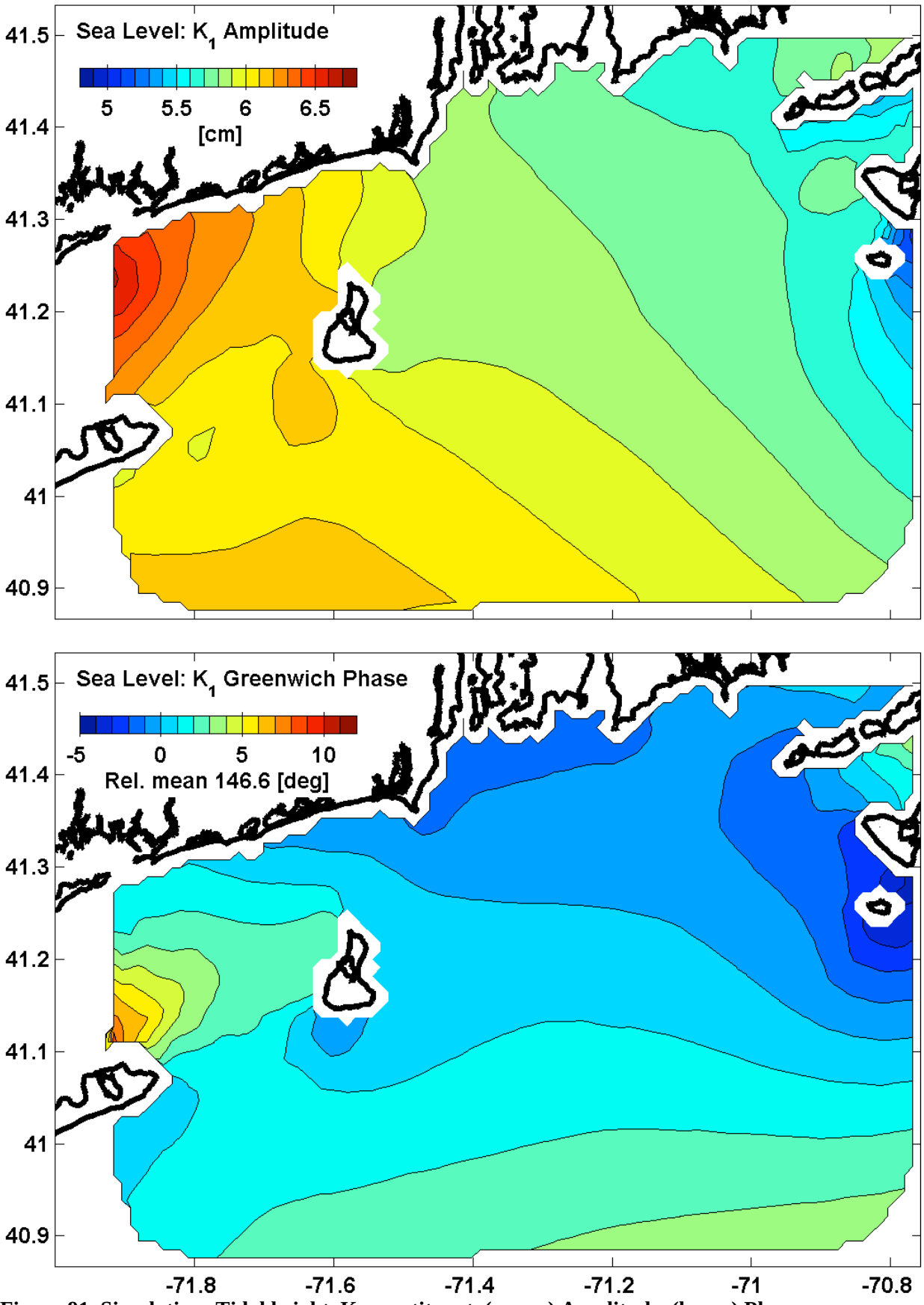

Figure 91. Simulation: Tidal height, K_1 constituent. (upper) Amplitude. (lower) Phase.

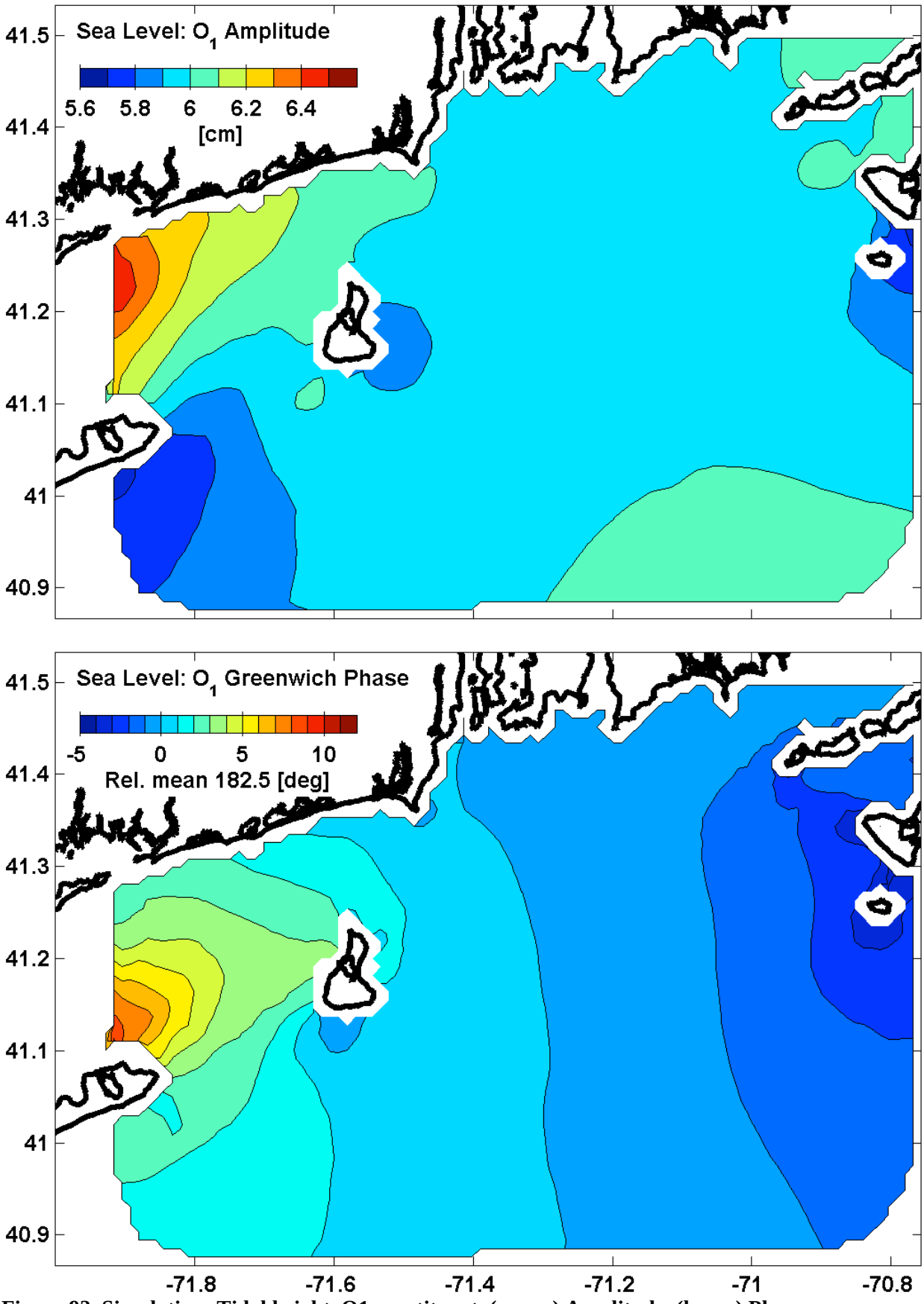

Figure 92. Simulation: Tidal height, O1 constituent. (upper) Amplitude. (lower) Phase.

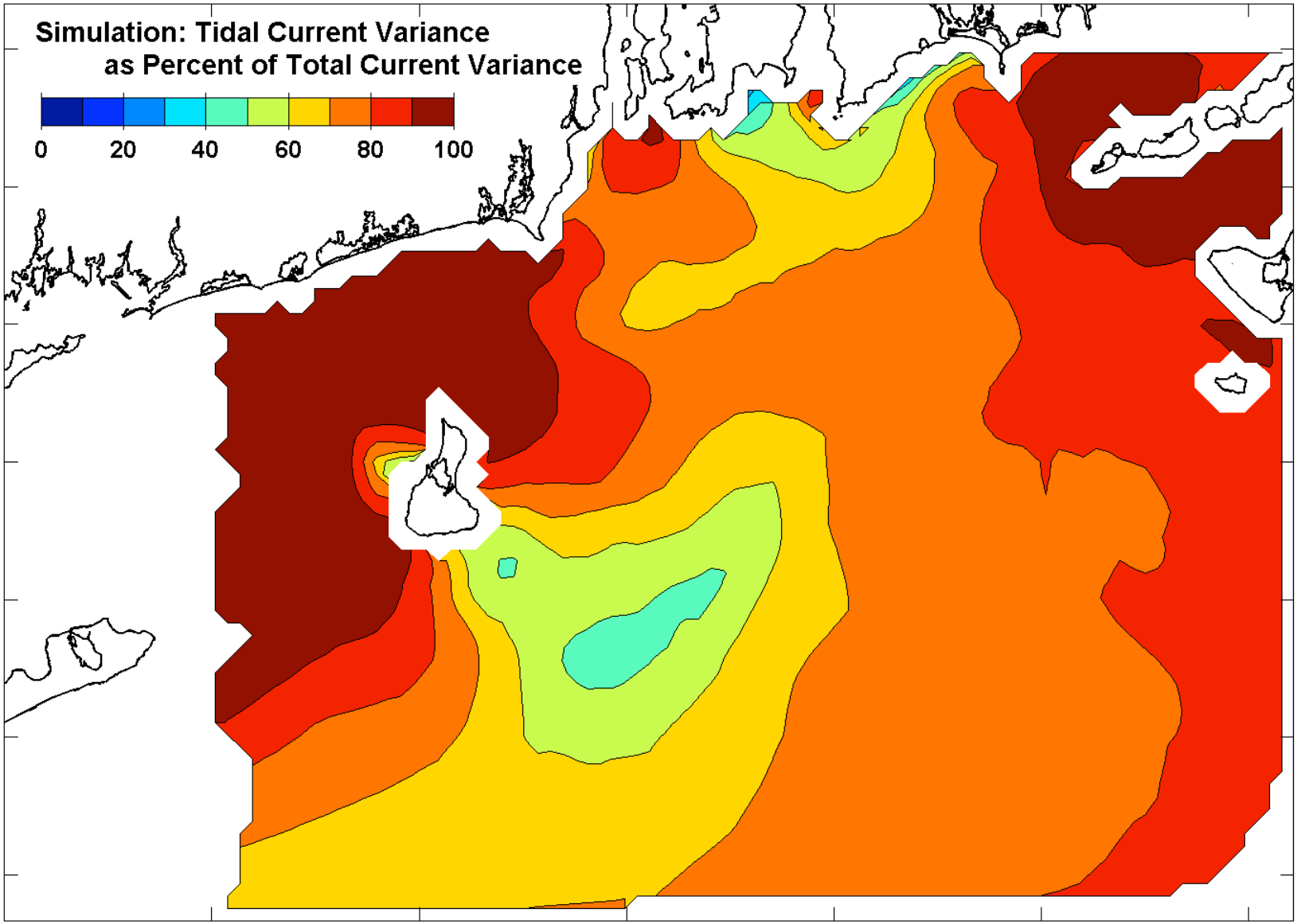

Figure 93. Simulation: Tidal current KE variance, pct. of summed tidal/non-tidal KE variances.

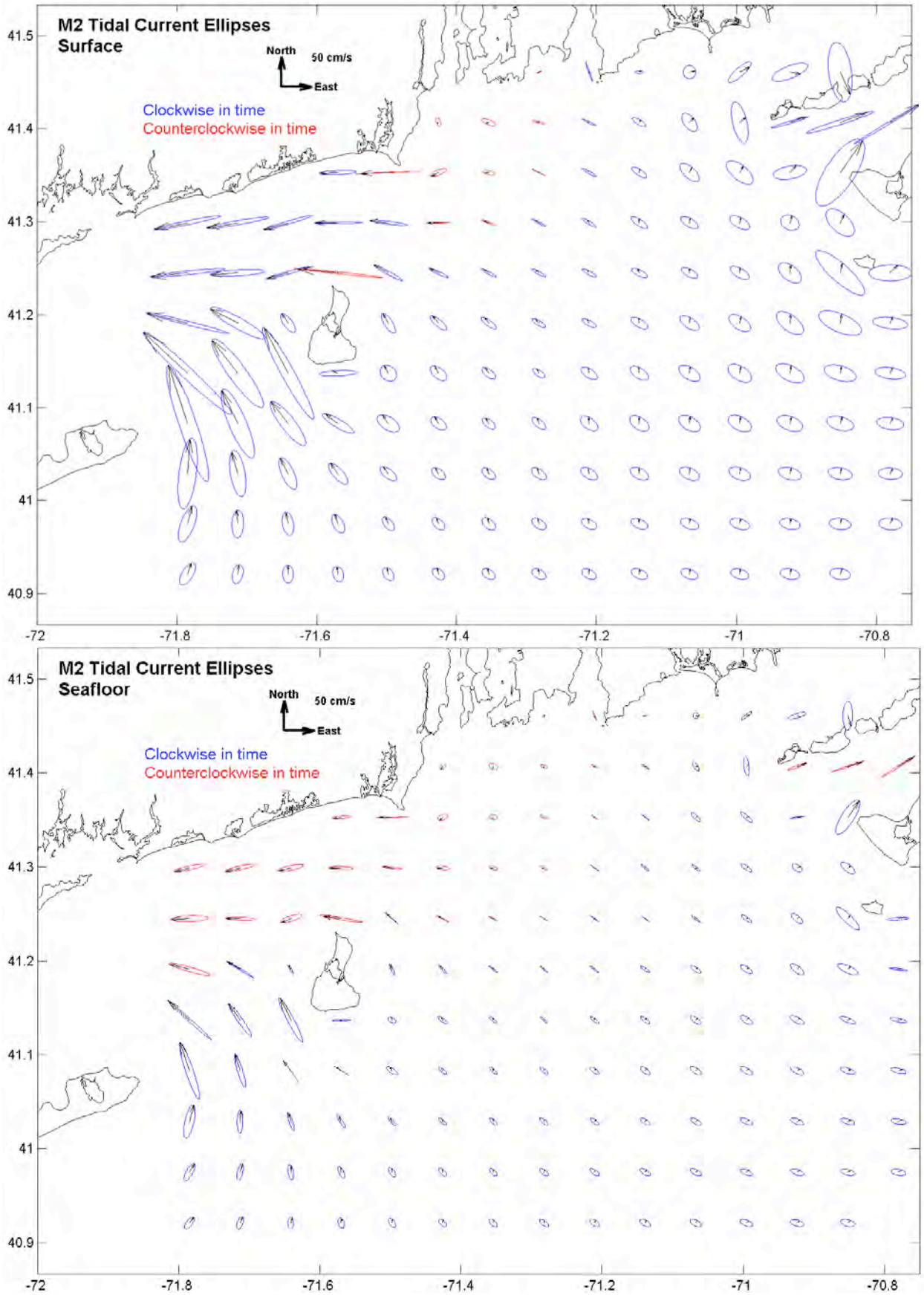

Figure 94. Simulation: Tidal currents, M_2, size 1X advection. (upper) Surface. (lower) Bottom.

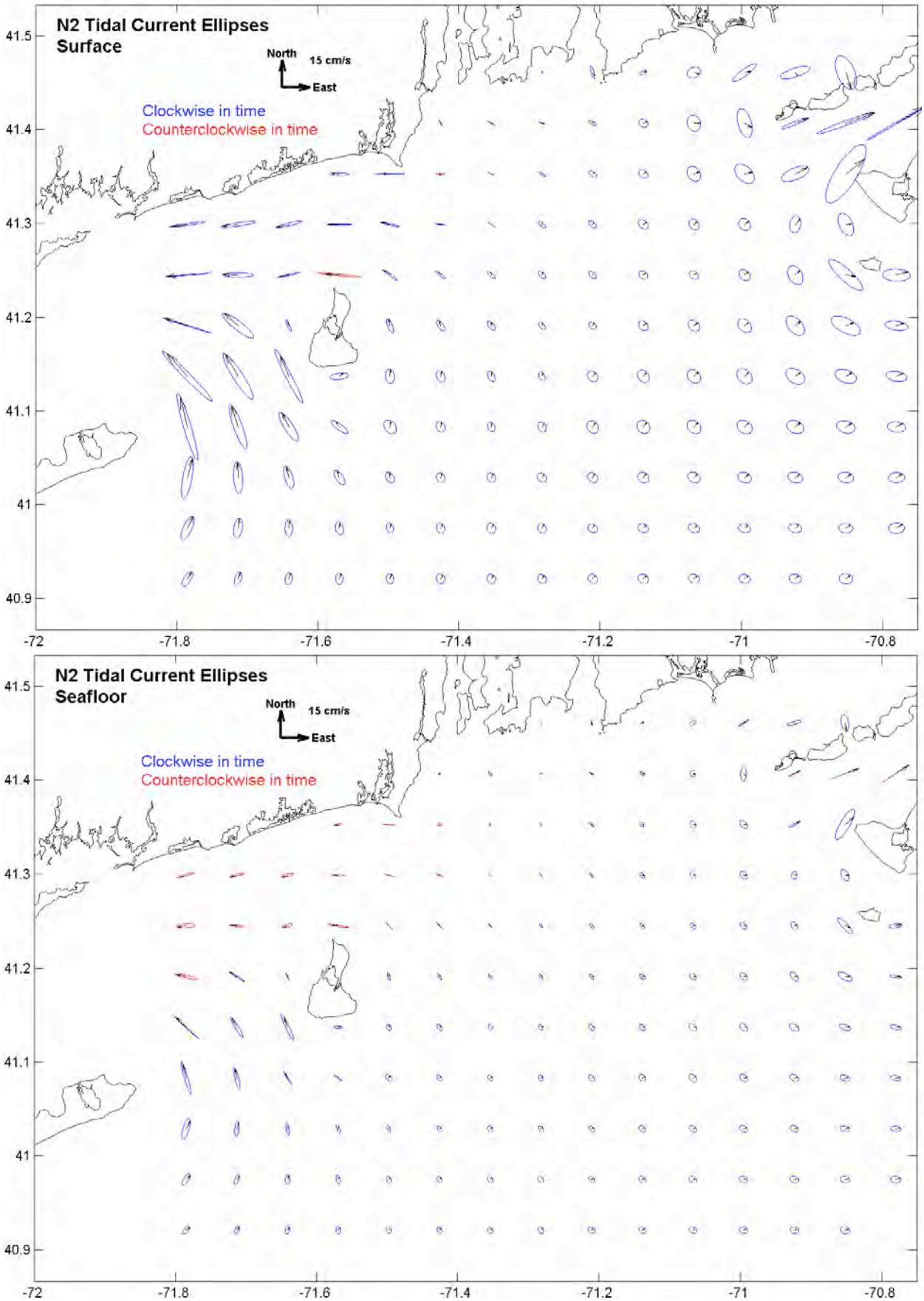

Figure 95. Simulation: Tidal currents, N_2, size 3X advection. (upper) Surface. (lower) Bottom.

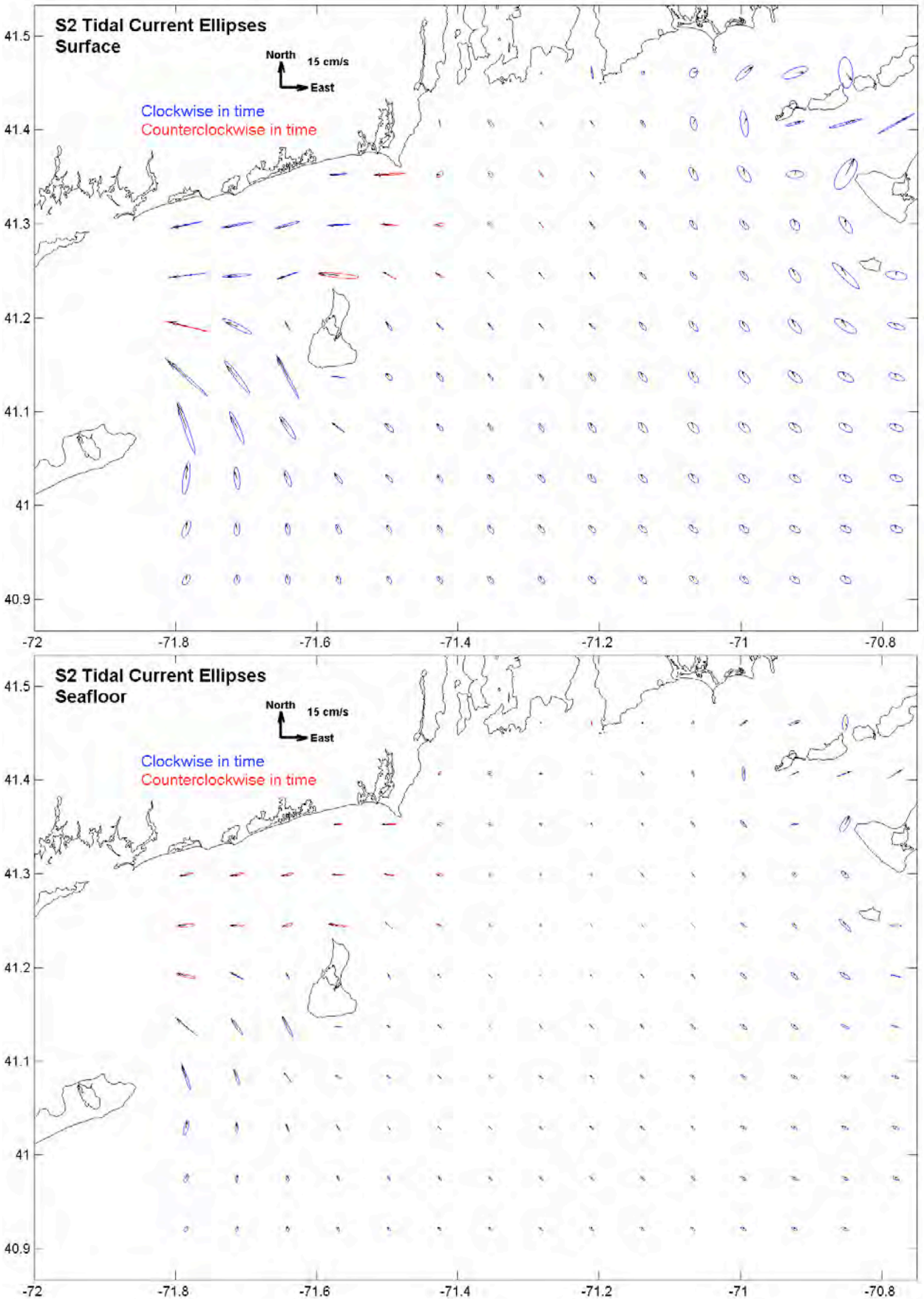

Figure 96. Simulation: Tidal currents, S_2, size 3X advection. (upper) Surface. (lower) Bottom.

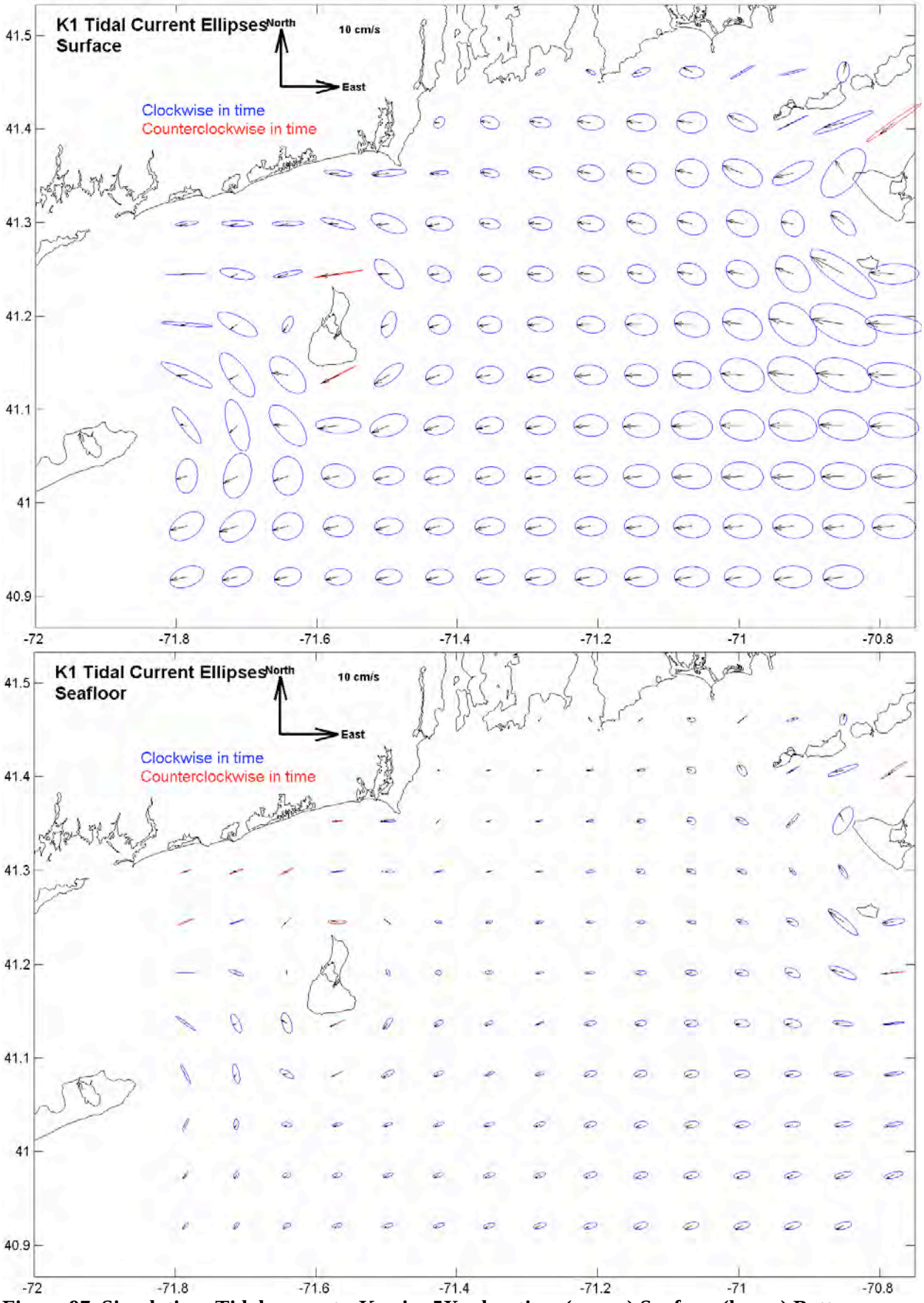

Figure 97. Simulation: Tidal currents, K_1, size 5X advection. (upper) Surface. (lower) Bottom.

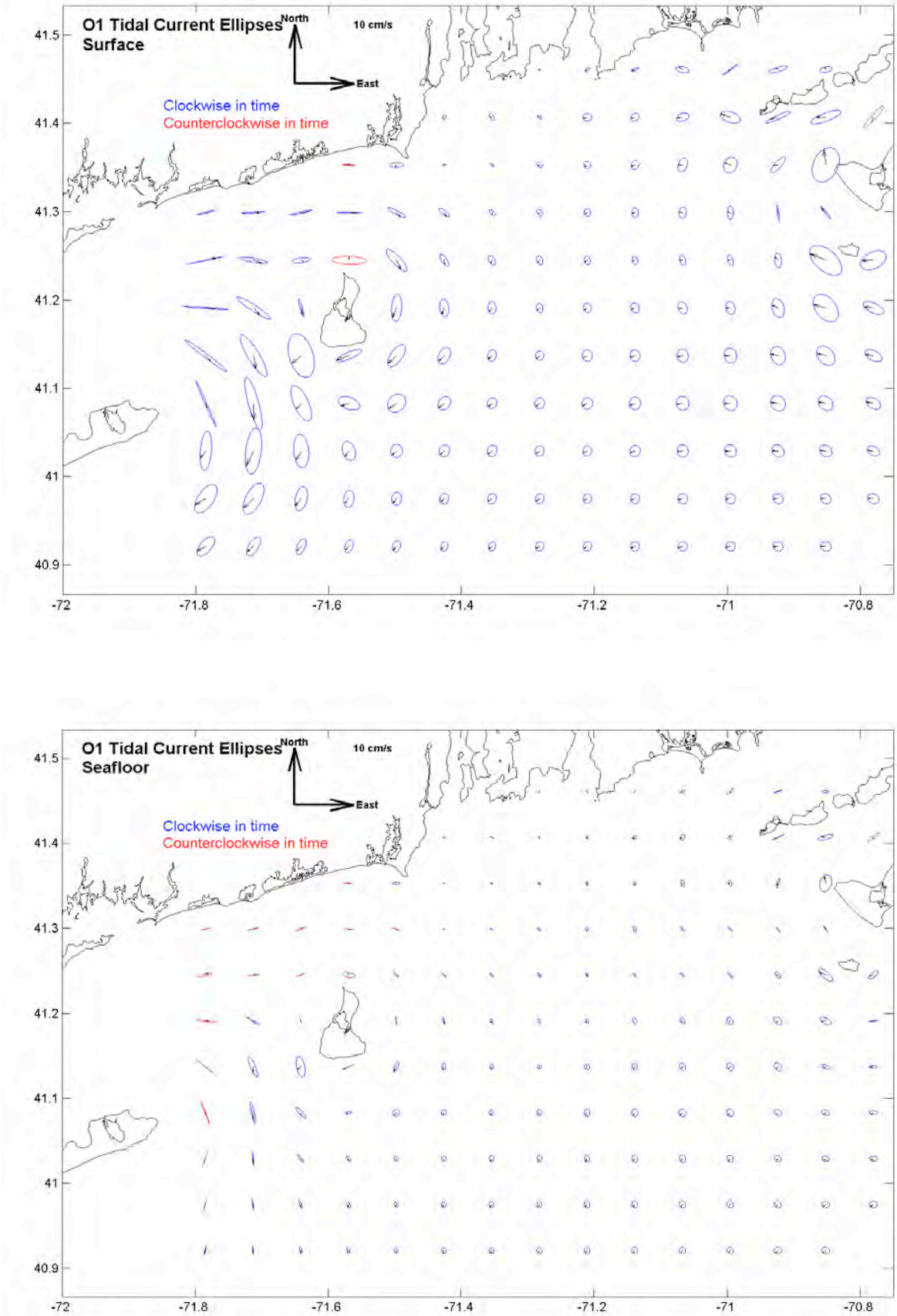

Figure 98. Simulation: Tidal currents, O_1, size 5X advection. (upper) Surface. (lower) Bottom.

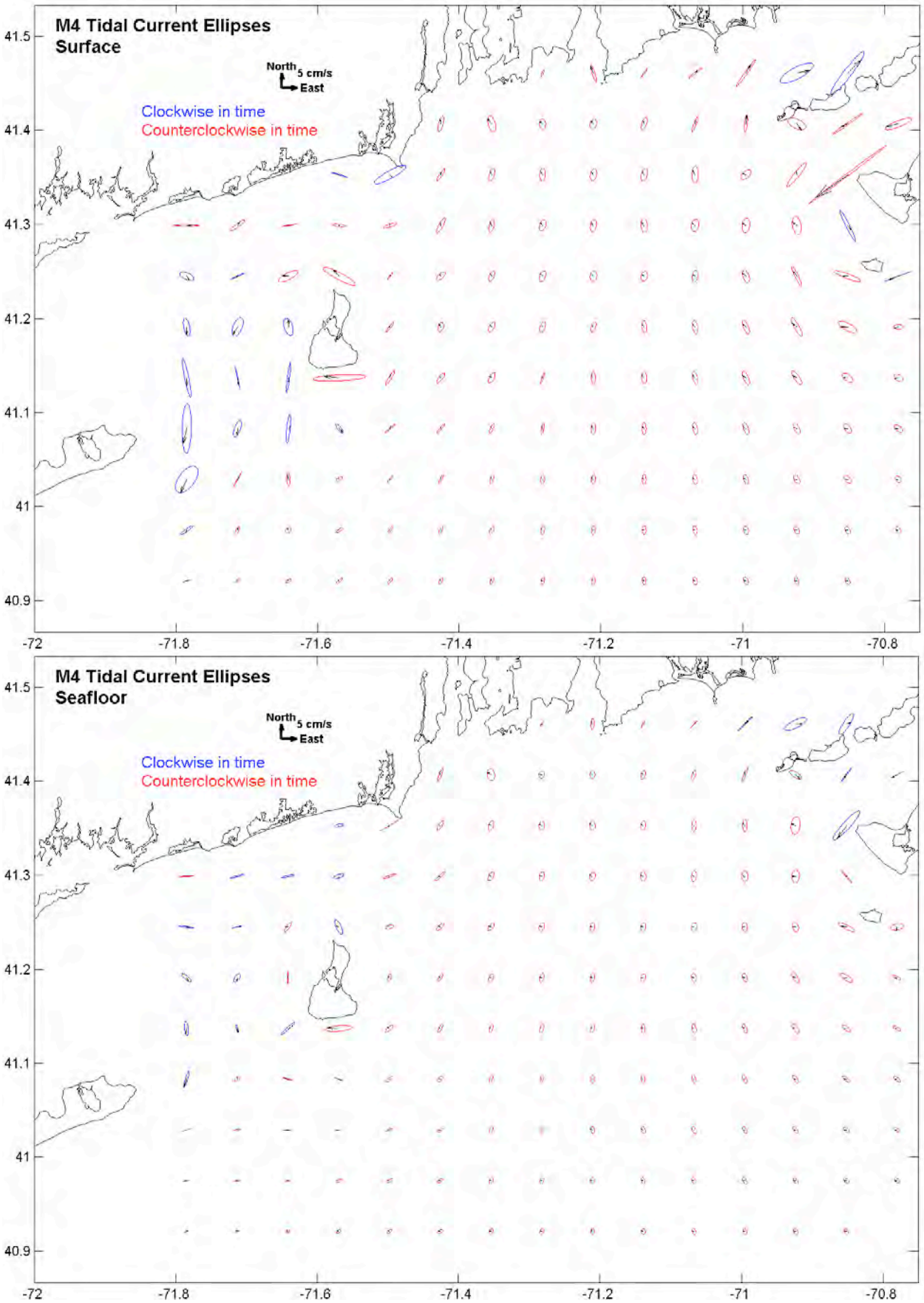

Figure 99. Simulation: Tidal currents, M_4, size 10X advection. (upper) Surface. (lower) Bottom.

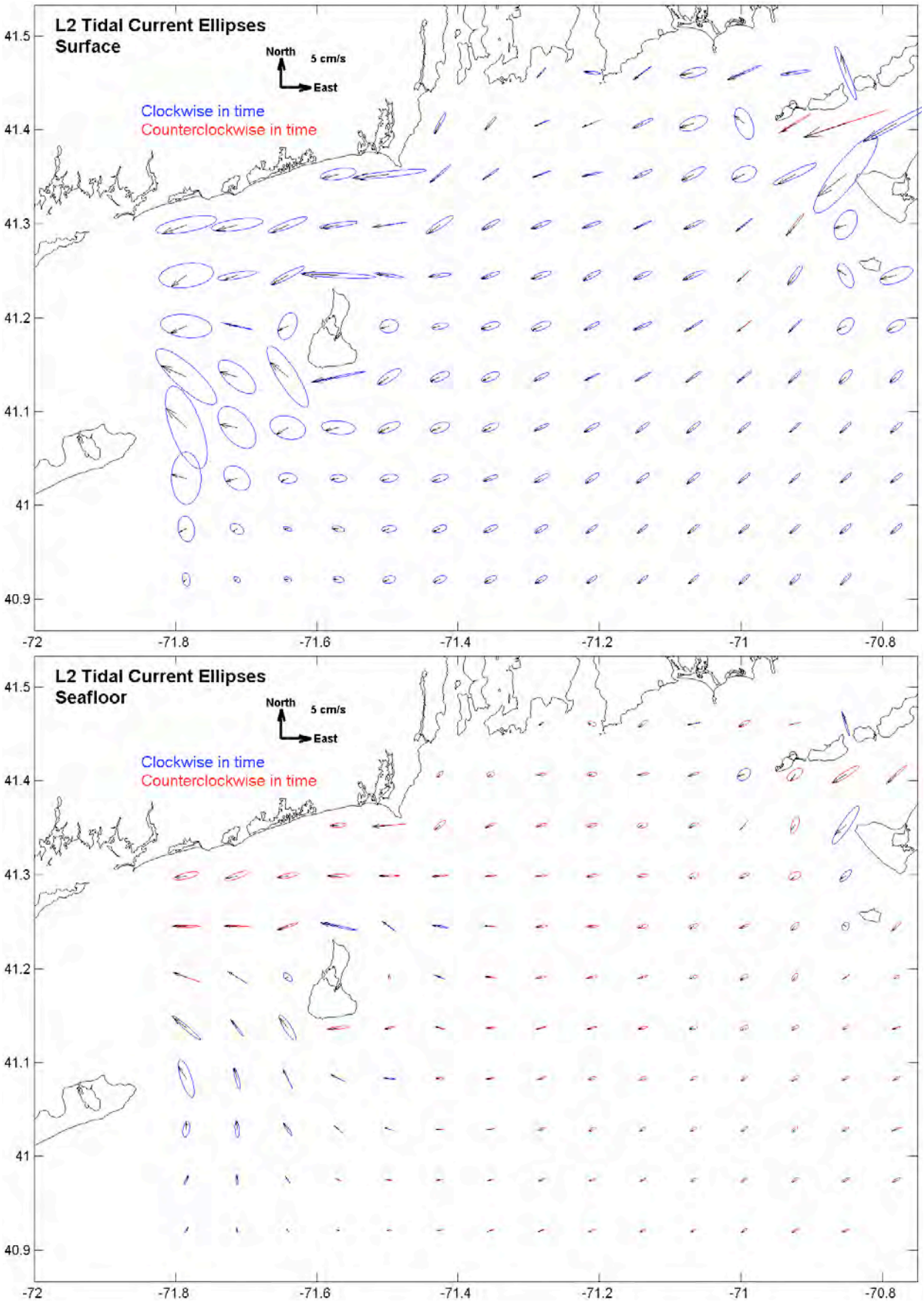

Figure 100. Simulation: Tidal currents, L_2, size 10X advection. (upper) Surface. (lower) Bottom.

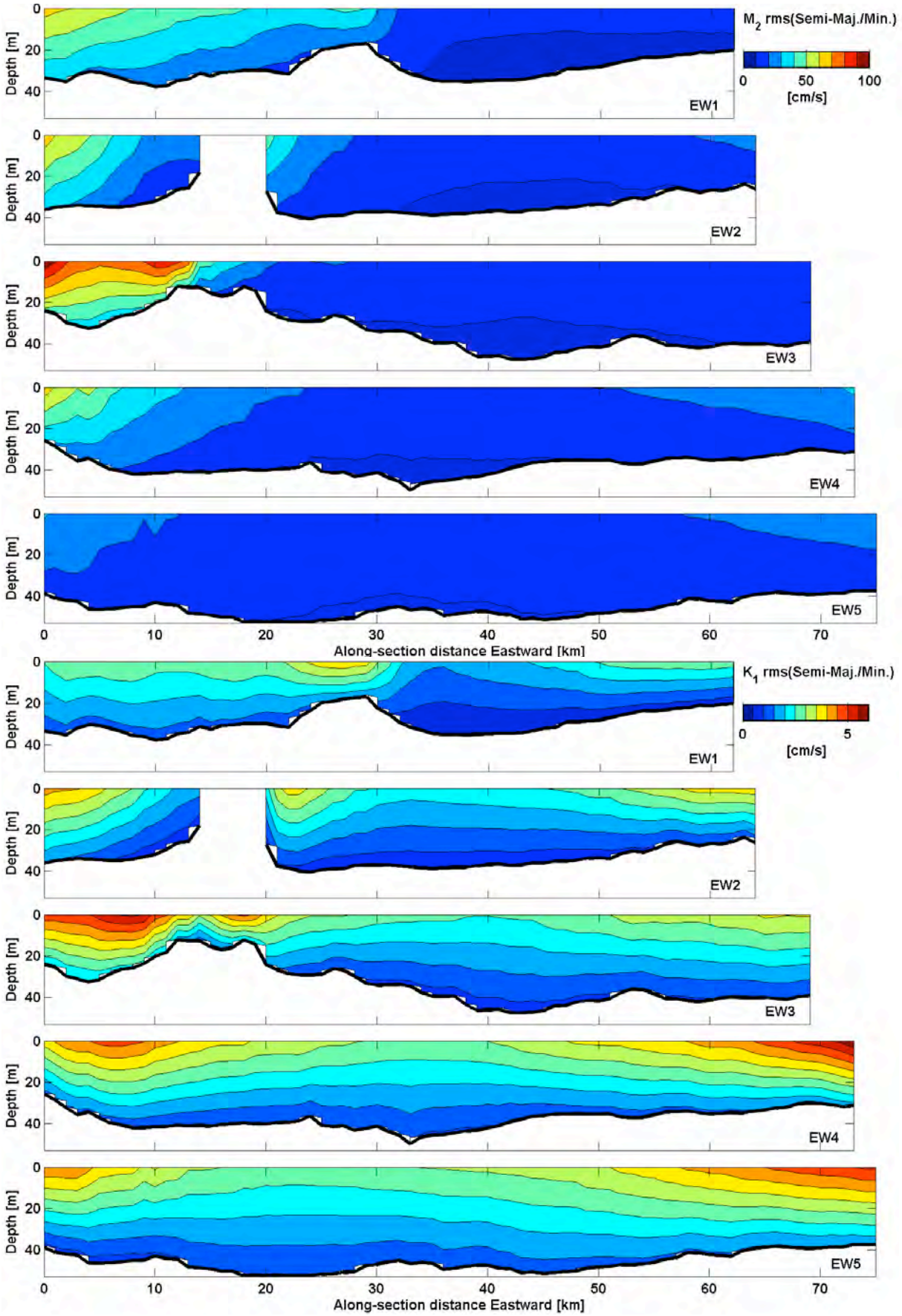

Figure 101. Simulation: Tidal currents, RMS ellipse semi-axes, EW. (upper) M_2. (lower) K_1.

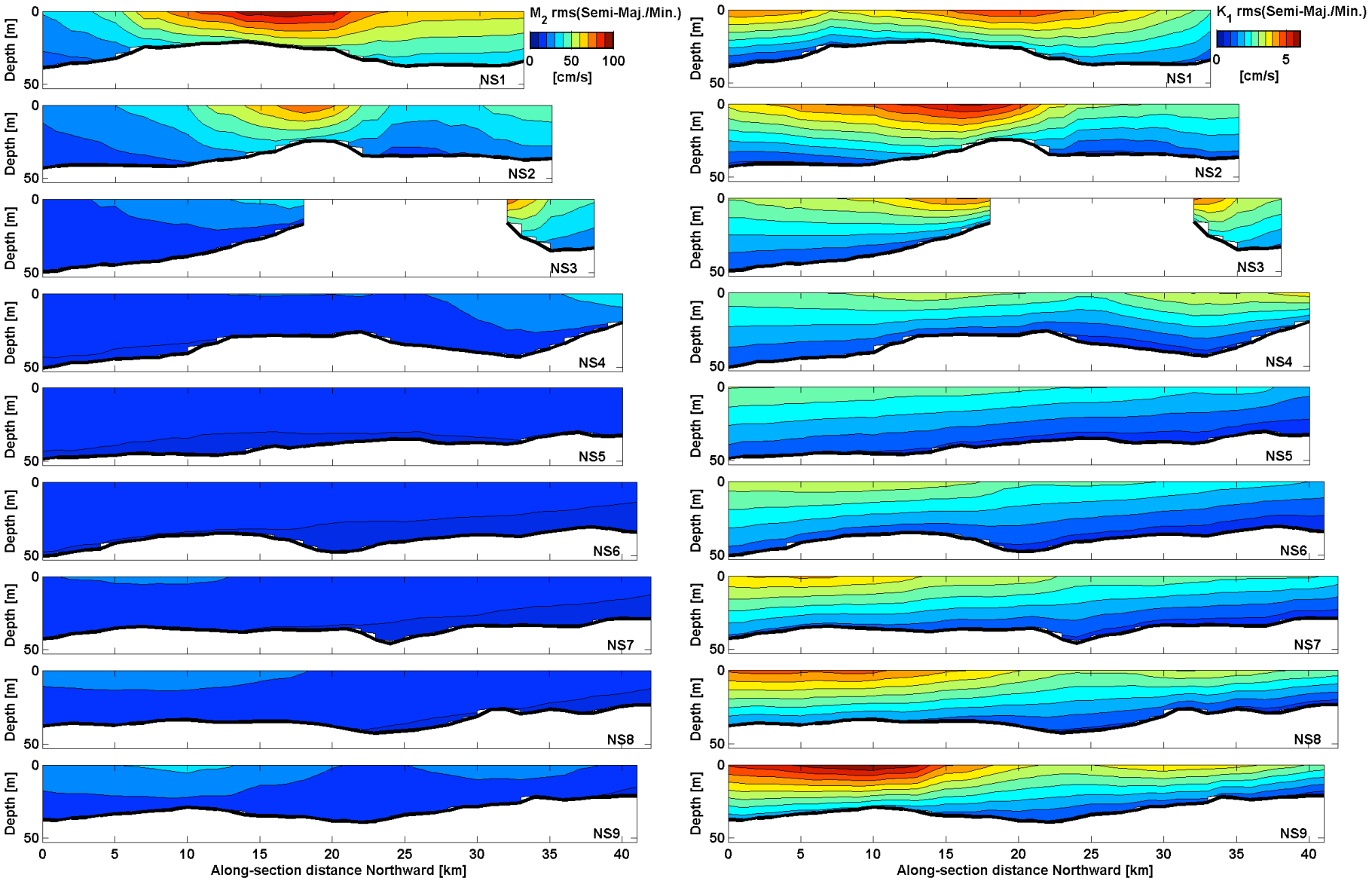

Figure 102. Simulation: Tidal currents, RMS ellipse semi-axes, NS. (left) M_2. (right) K_1.

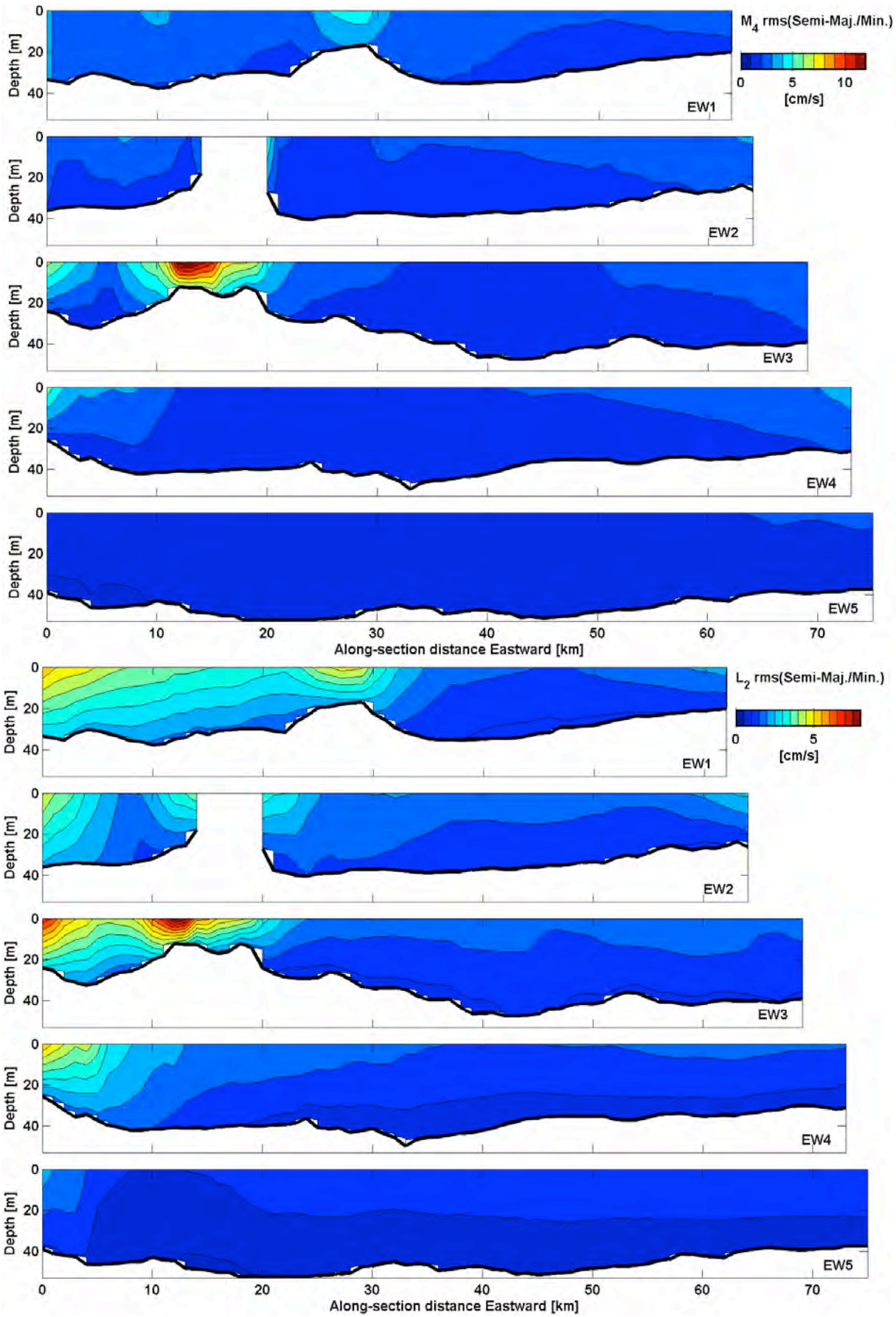

Figure 103. Simulation: Tidal currents, RMS ellipse semi-axes, EW. (upper) M_4. (lower) L_2.

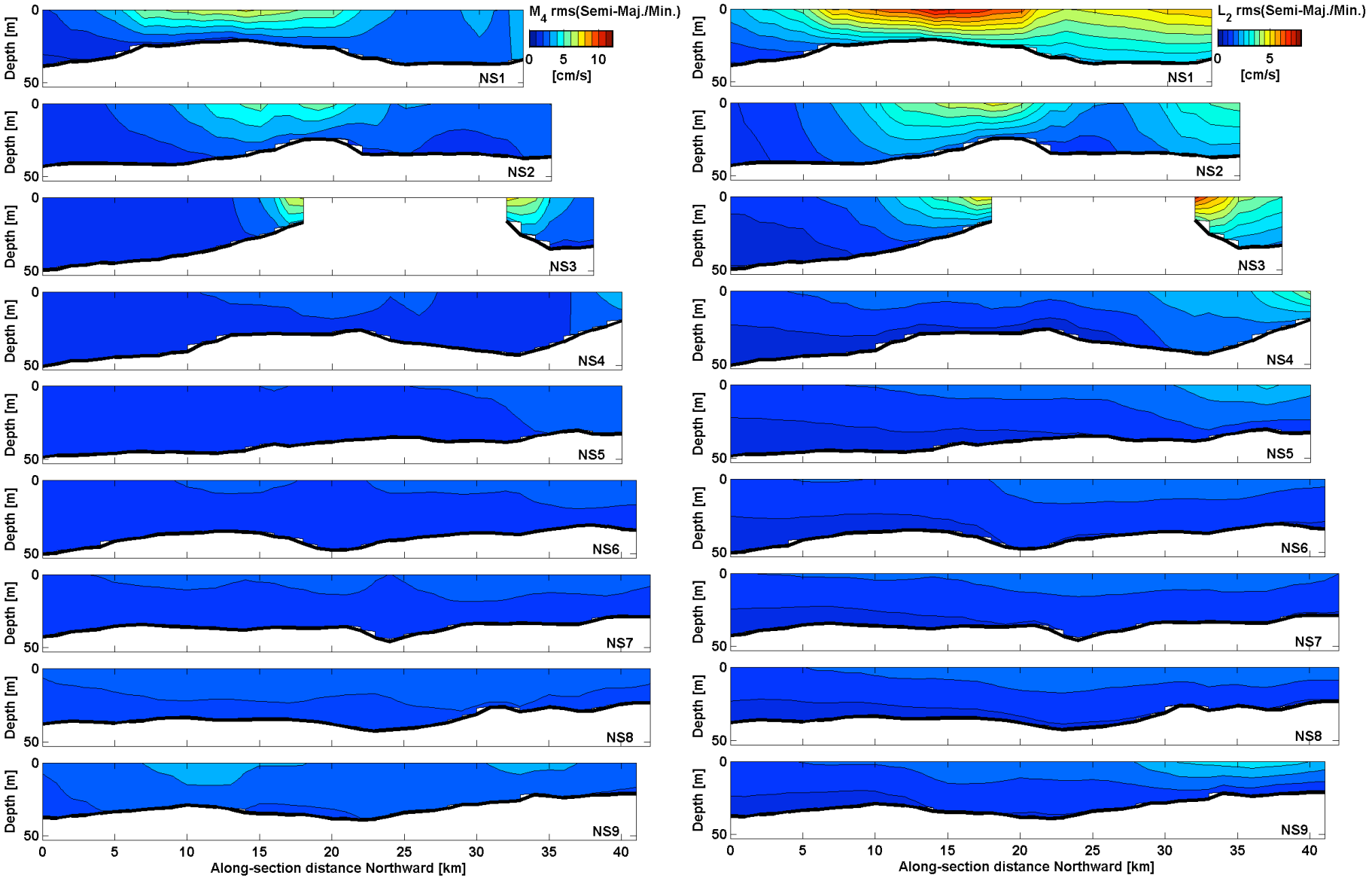

Figure 104. Simulation: Tidal currents, RMS ellipse semi-axes, NS. (left) M_4. (right) L_2.

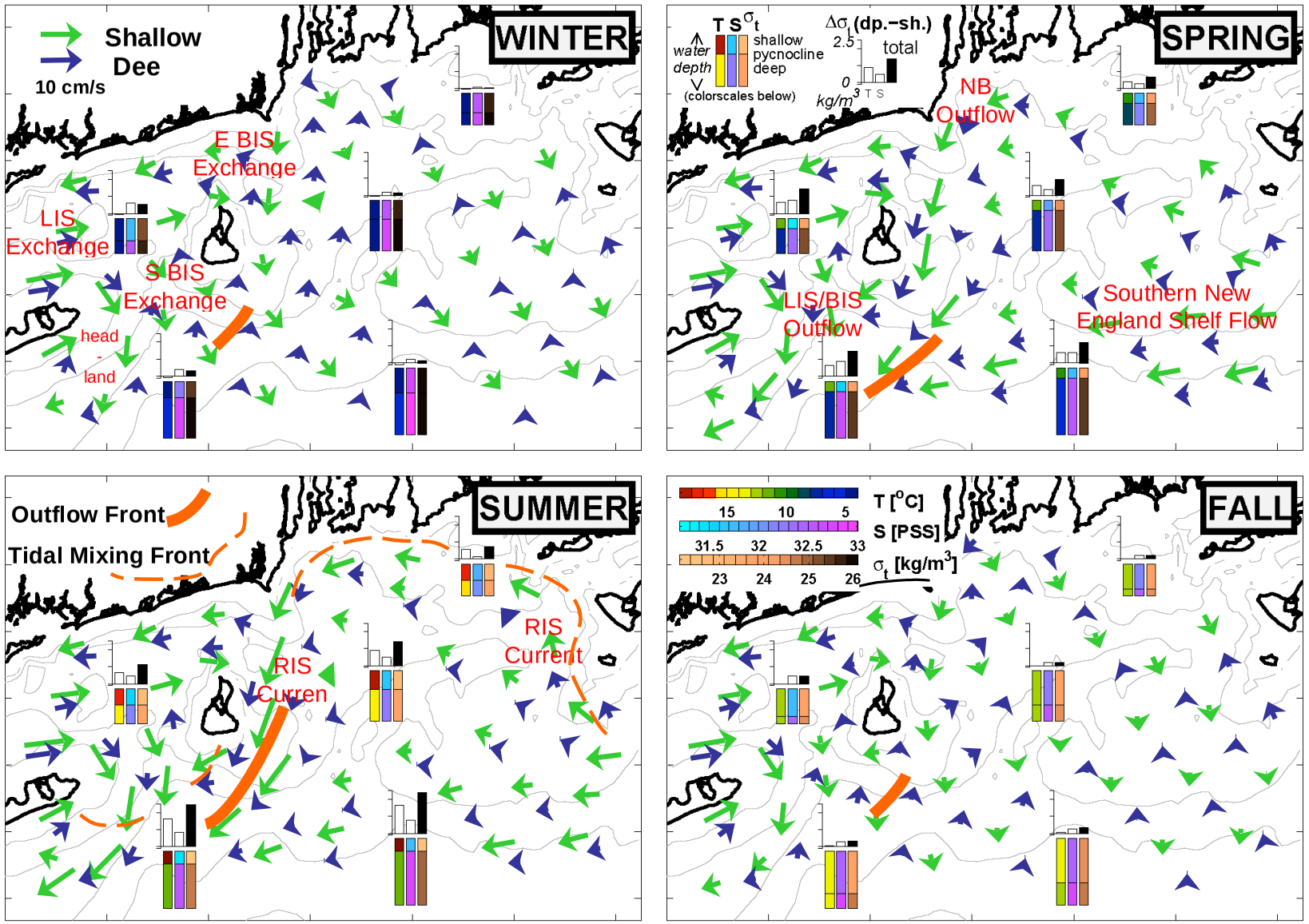

Figure 105. Summary schematic, seasonal-mean hydrography & circulation (explained in text).

Appendix A. Catalogue of Observational Studies

Below is a compilation of published studies that report on observations of hydrographic fields (temperature, salinity) or currents from locations within Rhode Island Sound and Block Island Sound, listed in chronological order by publication year. While this listing may not be absolutely comprehensive, to the best of our knowledge the primary content of any references that do not appear is represented well by one of the references listed.

The following is a key to abbreviations in the table:

Measurements: U = currents; T = temperature; S= salinity; FR = flushing rates; KED = kinetic energy dissipation

Where: sh = shallow or near-surface; dp = deep or near-bottom; N/S/E/W = North/South/East/West; BIS = Block Island Sound; RIS = Rhode Island Sound; MP = Shelf off Montauk Point

Method: CTD = vessel-based hydrographic casts or bathythermograph; MT/MS = moored thermistor/salinity sensor; CM = moored current meters; SD = surface drifters; BD = seabed drifters; VC = vessel-based current sampling; TB = towed-body sampling; SAT = satellite radiometer; HFR = high-frequency radar; AUV = autonomous underwater vehicle

Table A1. Catalogue of published observational studies.

Citation	Msmt	Where	When	Method
LeLacheur & Sammons 1932	U	BIS	Pre-1930s	VC
Haight, 1938	U	E RIS	1930s & before	VC
Riley 1952	TS, U	BIS, RIS	1946-47	CTD, CM
Powers, 1953	TS	BIS, RIS	1951	CTD
Bumpus 1965	U	RIS, BIS	1961-64	BD
Cook 1966	U	RIS	1962-63	SD, BD
Shonting et al 1966	TS	RIS	1963-64	CTD
Ichiye 1967	TS	BIS	Aug 1965	CTD
Shonting 1969	U	RIS	Aug 1967, 13 d	CM
Williams 1969	U	BIS	May 1965	CM
Hardy 1970	TS	BIS	Jan-Apr 1970	CTD
Shonting and Cook, 1970	TS	RIS	1963-64	CTD
Meguire 1971	U	BIS, sh	1965-67	VC
Hollman & Sandberg 1972	U	BIS	1970-71	SD, BD
Saila et al 1972	U	E RIS, dp	Jul 1970, 4 d	CM
Collins 1974	U	N/W RIS	Feb 1973	BD
Hollman 1974	TS	BIS	1972-73	CTD
Pratt et al 1975	U	E RIS, dp	May/Jun 1974	CM

Citation	Msmt	Where	When	Method
Raytheon, 1975	TS, U	BIS	1974-75	CTD, CM, MT/MS, SD
Griscom 1977	U	E RIS, dp	Sep-Oct 1976	CM
Krabach & Snooks 1977	FR	NE BIS	Aug 1974	Dye
Snooks et al 1977	TS	NE BIS	1975-76	CTD
Long, 1978	U	BIS	1965-67	VC, CM
Snooks and Jacobsen 1979	U	NE BIS	Feb-Dec 1977	CM, SD, BD
Bowman and Esais, 1981	TS	BIS	1978	CTD
Armstrong 1998	T	RIS	1974-83	CTD
Fox et al 2000	T	RIS, BIS	1997	SAT
Ullman & Cornillon, 1999, 2001	TS	RIS, BIS	1985-96	SAT
Kincaid et al 2003	U, TS	N RIS	1998-99	VC, CTD
Codiga and Rear 2004	U, TS	MP	2001-02	CM, MT/MS
Ullman and Codiga 2004	U, TS	BIS, WRIS, MP	2000-01	HFR, CM
Codiga 2005	U	MP	1999-2002	CM
Kirincich & Hebert 2005	U, TS	MP	Apr 2002, 2 d	TB-CTD, VC
SAIC 2005	U, TS	RIS	2004	VC, CTD
Ullman et al. 2006	U	BIS	2002 & 03; 3 d	SD
Mau et al. 2006, 2007	U	BIS, W RIS	2001	HFR
Kincaid et al 2008	U	N RIS	2000-01	CM
O'Donnell & Houk, 2009	TS	BIS, MP	2000-2001	CTD
Levine et al 2009	TS,U, KED	MP	2000-01	CTD, VC, AUV

Appendix B. Catalogue of Modeling Studies

This is a compilation of published, modern numerical/computational hydrodynamic model studies that focus on hydrodynamic fields (temperature, salinity) and/or currents and are configured with the aim of realistic simulation of at least some of the RI Ocean SAMP region, presented in chronological order. Spaulding and Gordon (1982) includes a table listing previous (1970s) modeling studies. The site abbreviations are the same as in Appendix A.

Table B1. Catalogue of published modeling studies.

Citation	***Where***	***Period modeled***	***Emphasis***
URI, 1979	BIS, RIS	--	Barotropic tidal flow
Spaulding and Gordon, 1982	BIS, RIS	--	Barotropic tidal flow
Edwards et al 2004a,b	BIS, W RIS, MP	2000	Frontogenesis, MP area
He and Wilkin 2006	E RIS	--	Barotropic tidal flow
Wilkin 2006	E RIS	2001-2003	Summer heat budget
Mau et al, 2007, 2008	BIS, RIS, MP	2001	Tidal flow (2007), MP outflow (2008)
Cowles et al, 2008	BIS, RIS, MP	1996-1997	Low-frequency flow and hydrography

Appendix C. List of GIS Layers

The following is a list of GIS layers that have been produced for the RI Ocean SAMP project. Each is listed with the number of the figure which it appears as in this report.

See the RI Ocean SAMP Supplement for these figures.